UNIVERSITAT DE BARCELONA

Selective killing of RAS-malignant tissues by exploiting oncogene-induced DNA damage

Eliminación selectiva de tejidos malignos dependientes de RAS mediante la explotación del daño en el ADN inducido por oncogenes

Lada Murcia Rosero

UNIVERSITAT DE BARCELONA

Facultat de Biologia

Programa de Doctorado del Departamento de Genética
Facultad de Biología
Universidad de Barcelona

Selective killing of RAS-malignant tissues by exploiting oncogene-induced DNA damage

Eliminación selectiva de tejidos malignos dependientes de RAS mediante la explotación del daño en el ADN inducido por oncogenes

Memoria presentada por
Lada Murcia Rosero
para optar al grado de Doctor por la Universidad de Barcelona

Development and Growth Control Laboratory
Institute for Research in Biomedicine (IRB)
Parc científic Barcelona

Barcelona, Julio de 2019

Marco Milán	Lada Murcia	Florenci Serras
(Director)	(Alumna)	(Tutor)

Acknowledgements

In the first place, I would like to thank Marco for accepting me as a master student and giving me the opportunity to pursue a PhD with these amazing people. Marco has been an excellent mentor, he has encouraged me and supported during the past 6 years and for that I am grateful.

I would also like to thank my tutor Florenci, and the members of my thesis advisory committee, Angel and Ferran for our interesting discussions over the years.

To the members of the lab, all of you, past and present. You have become my family in these years. We have shared the good and the bad moments and you have ALWAYS been there for me. My only hope is that I have supported you all in the same way you did and that I have risen to the occasion of what you deserve.

A special thanks to Marta, my rock in the lab. You have been a great part of this project, it wouldn't have been possible without you. Not only for all of your ideas and the experiments that you have performed, but also because you have always had my back and you have always believed in me, even when I didn't do it myself. For that, I will be forever grateful.

To my beloved Noies al lab! This has been a great experience, one that I have enjoyed (and will continue to enjoy) sharing with you. Taking science to the younger generations has helped me to constantly remember what it was that made me fall in love with science when I was a kid myself.

Alba, Eva, Albert, Ignacio, thanks for all these years of fun and for making me stay sane throughout my thesis.

Tania and Sandra, since that second year in university, our lives have gone separate ways, however, we have managed to stay together and you have been a great support during my thesis. Tania, I loved our long conversations in your office in the basement.

Escolano, a fellow of sorrows. I am very grateful for your support and your constant looking out for me. This process wouldn't have been this fun without you.

A mi familia, un enorme GRACIAS. No solo por su apoyo durante estos años de tesis sino por todo su esfuerzo a lo largo de toda mi vida. Por dejarse la piel para que no me faltara de nada y por brindarme todas las oportunidades que me han permitido llegar hasta aquí.

A mi pareja, mi compañero muchísimas gracias por estar ahí, por aguantarme, por apoyarme, por motivarme, por quererme, por divertirme, por ser mi mayor fan. Se que no han sido años fáciles (siento haberte dejado sin vacaciones, sin fines de semana y sin tantas cosas...) pero aun así siempre me has apoyado y has creído en mi. Estoy muy orgullosa de lo que has conseguido en los últimos años y se que lo mejor aun está por llegar,

Table of contents

Table of contents:

Abstract

Abstract

Most human solid tumors present signs of genomic instability. Activated oncogenes have been proposed to induce genomic instability through the generation of replicative stress. In this thesis, we have sown that the expression of a constitutively active form of RAS oncogene promotes accelerated G1/S transition which leads to replicative stress and genomic instability. The resulting DNA damage present in these cells should activate the DDR response, however, RasV12 cells impair DNA damage signaling. Furthermore, RasV12 expression inhibits apoptosis through ERK.

RAS is one of the most commonly mutated oncogenes, yet efficient therapies to treat RAS dependent tumors are still lacking. With this in mind, and based on our previous results, we decided to try to exploit the DNA damage present in these cells to selectively target them. In order to do so, we induced extra DNA damage with ionizing radiation and depleted ERK to promote the death of the cells. We used this strategy on RAS dependent tumors both benign and malignant tumors, and successfully targeted and killed tumor cells. We propose that MEK inhibitors, that are being used in the treatment of metastatic melanomas, could be combined with radiation to improve the therapeutic outcomes.

Aside from the previously described autonomous effects, we have also observed that RasV12 expression in the wing imaginal discs induces a non-autonomous phenotype. Wild type cells adjacent to RAS cells display signs of DNA damage, apoptosis and autophagy. The role of these non-autonomous effects is not clear; however, we hypothesize that they may play a role in metabolically supporting tumor growth.

Introduction

1. Cancer

According to the National Cancer Institute and the World Health Organization, cancer is the name given to a series of related diseases where cells start to continuously proliferate and expand into surrounding tissues. Cancer is a disease of genetic origin as it arises as a consequence of mutations in oncogenes and tumor suppressor genes. This process can originate practically in any part of the body and in many cases metastasize to distant organs. One of the most common classifications is the one that subdivides tumors according to the tissue of origin: carcinomas being of epithelial origin, sarcomas of bone and soft tissues, leukemias of blood cells, etc.

GLOBOCAN 2018, a yearly global cancer study, stated that cancer is the first or second cause of death in 91 of the 172 countries analyzed worldwide. In 2018 there will have been an estimated of 18,1 million new cases and 9,6 million cancer-related deaths. In both sexes, lung cancer is the most diagnosed and the leading cause of cancer-related death followed by breast, prostate and colorectal cancer. Cancer incidence and mortality are increasing worldwide due to different reasons like the aging of the population or the increased prevalence of risk factors (smoking, alcohol intake, obesity, physical inactivity...) associated with socioeconomic development.

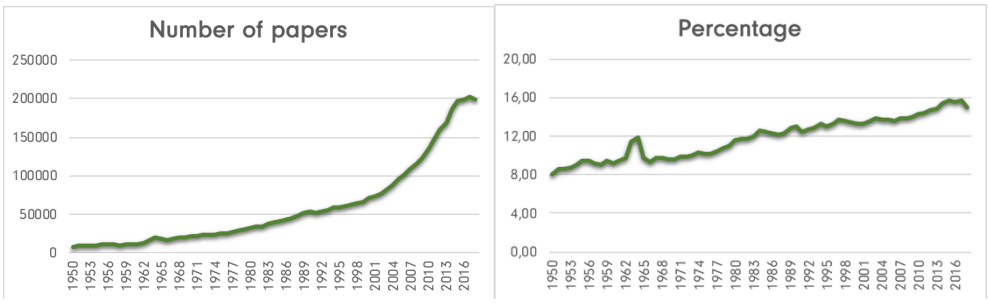

Figure 1. Cancer research in numbers. Number of entries in PubMed containing the word "cancer" every year since 1950 and the percentage they represent with respect to the total number of entries each year. Representation of data obtained from (Medline trends A. D. Corlan, 2004).

With its increasing incidence, also interest in cancer research has peaked. The amount of papers containing the word cancer indexed in PubMed has exponentially increased in the past ten years, accompanied by an increase in the percentage that these papers represent over the total publications (Fig 1).

1.1. The hallmarks of cancer

In the years of modern cancer research, knowledge of how tumor cells behave at a cellular and organismal level has been piling up. In the year 2000, Hanahan and Weinberg used all this information to propose that, although cancers are very heterogeneous and can arise from different types of cells and carry different oncogenic mutations, most of them are characterized by a series of traits that are shared and that direct malignant growth which they termed the hallmarks of cancer (Hanahan & Weinberg, 2000).

- **Self-sufficiency in growth signals.** Normal cells depend on the presence of growth signals in order to proliferate. However, cancer cells become independent of these signals and continuously proliferate. This independence can be achieved by different mechanisms such as the tumor-induced production of mitogenic molecules, the deregulation of cell surface receptors or the constitutive activation of the signal transducers.

- **Insensitivity to growth-inhibitory signals.** Normal cells need to respond to signaling cues that tell them to differentiate or become quiescent when proliferation is no longer necessary. However, cancer cells can evade or ignore those signals in order to continue to divide.

- **Evasion of programmed cell death.** Apoptosis is induced in response to external signals as well as internal signals that monitor the wellbeing of the cell. Once it is

activated, a signaling cascade will lead to the activation of effector caspases (proteases that will carry out the death program). Apoptosis is generally seen as an anticancer barrier that needs to be circumvented in order to give rise to full-blown tumors. In fact, mutations in the master apoptosis regulator p53 are very commonly found in cancer.

- **Limitless replicative potential.** This hallmark refers to the intrinsic capacity of cells to proliferate. Cellular senescence is a mechanism by which cells quit dividing. Senescence can be triggered as a consequence of the DNA damage response that is caused by the shortening of the telomeres with each cell cycle but can also arise as a consequence of reactive oxygen species (ROS) or other sources of damage. Furthermore, activated oncogenes can also lead to senescence (oncogene-induced senescence) that is why, like apoptosis, it can be seen as a cancer barrier that needs to be overridden in order for cancer to progress.

- **Sustained angiogenesis.** Oxygen and nutrients are crucial for normal cell function. Both are provided through the bloodstream forcing cells to stay close enough to a blood vessel. In cancer, there is a very rapid proliferation of tumor cells which in turn induce angiogenesis, the proliferation of vascular cells in order to provide the tumor with the necessary nutrients.

- **Tissue invasion and metastasis.** Many tumors invade neighboring tissues and eventually move out and metastasize into distant sites. In order to do so, tumor cells have to undergo an epithelial to mesenchymal transition, intravasate into the bloodstream and extravasate in the target site where it has to go back to an epithelial phenotype in order to survive and form a new tumor. Metastasis is the main cause of cancer deaths.

At the time, all of these general hallmarks seemed to describe the behavior of most human cancers. However, how these features were acquired was not clear yet. A few years later Hanahan and Weinberg expanded on their original review and added two new hallmarks, the reprogramming of energy metabolism and the evasion of the immune system. But more importantly, they also included the fields proposal that genomic instability and inflammation are the ones behind the acquisition of all the hallmarks (Hanahan & Weinberg, 2011). In normal cells, DNA surveillance mechanisms keep mutation rates at minimum levels ensuring the correct transmission of the genetic information. However, in cancer cells, the mutation rates are much higher giving rise to the accumulation of mutations in oncogenes and tumors suppressors that drive the different hallmarks of cancer.

1.2. Oncogene-induced DNA damage model for cancer development.

Genomic instability, defined as the high rate of mutations within the genome, is considered as one of the enabling characteristics of cancer due to its capacity to promote the acquisition of the rest of characteristics that compose the so-called hallmarks of cancer.

Genomic instability is present from early stages of tumorigenesis (Bartkova et al., 2005; Gorgoulis et al., 2005) in both hereditary and sporadic tumors, however, the way by which genomic instability arises in these two cases seems to be different. Many hereditary tumors are associated with mutations in caretaker genes, that is genes involved in the repair of DNA damage. This is the case for Lynch syndrome, Bloom syndrome or Fanconi anemia (Kaseb & Hozayen, 2019). Germline mutations in caretaker genes predispose to cancer given that a single mutational event is needed to deplete the gene function. Once this happens, it can directly lead to

genomic instability as a consequence of the lack of repair of naturally occurring damage events. However, in sporadic tumors, mutations in caretaker genes are not that common, and if present they tend to appear at late stages. After genome-wide analysis of the mutational signature of different tumor stages, it was found that the most common mutations in cancer are in growth-regulating genes in the form of oncogenic gains such as EGFR or RAS and loss of tumor suppressors such as PTEN, and that these mutations arise early on during tumor progression (Negrini, Gorgoulis, & Halazonetis, 2010). These two observations make it highly improbable that mutations in caretaker genes can account for the genomic instability present in most sporadic tumors from very early stages of tumor development (precancerous lesions). Some years before these genome-wide analyses it had been shown both in vitro and in animal models that oncogene activation leads to DNA damage and activation of the DNA damage response (Abulaiti et al., 2006; Bartkova et al., 2006; Denko et al., 1994; Di Micco et al., 2006; Ray et al., 2006). Altogether, these data lead to the formulation of the oncogene-induced DNA damage model for cancer development (Fig 2). This model proposed that the first event of tumor development is the acquisition of an oncogenic mutation, which would lead to increased cell growth and proliferation promoting the appearance of precancerous lesions. The aberrant proliferation induced by oncogenes leads to replicative stress and DNA damage, thus activating the antitumorigenic activity of the DNA damage response and inducing apoptosis and senescence. However, the continuous induction of DNA damage promotes genomic instability favoring the acquisition of additional mutations that drive tumor progression releasing the cells from the DDR-imposed senescence and apoptosis (Halazonetis, 2009; Halazonetis, Gorgoulis, & Bartek, 2008).

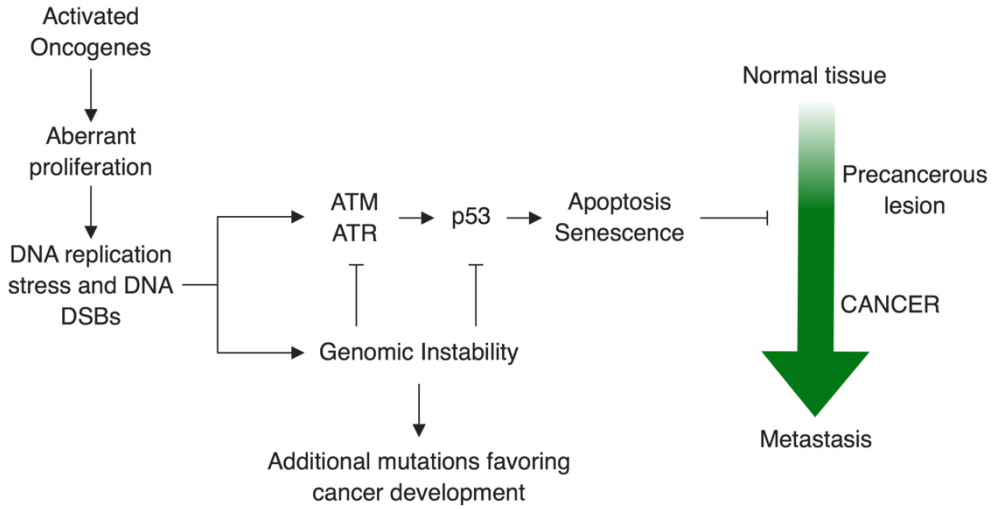

Figure 2. Oncogene-induced DNA damage model for cancer development. Scheme depicting the main event in tumor development according to the oncogene induced DNA damage model for cancer development. Adapted from (Halazonetis et al., 2008).

1.3. Oncogene-induced replication stress.

The oncogene-induced DNA damage model for cancer development is based on the capacity of activated oncogenes to induce replication stress and generate DNA damage, but how do oncogenes actually lead to replicative stress?

Replication stress is a complex phenomenon characterized by the presence of stalled, collapsed or other aberrant fork structures and a replication slowdown. It arises when the tight replication regulation, that ensures correct duplication of the DNA, is disrupted (Zeman & Cimprich, 2014).

In order to ensure the correct replication of the DNA, this process has to be coordinated with cell cycle progression (Gaillard, García-Muse, & Aguilera, 2015). The first step of replication is origin licensing which consists of the assembly of pre-replicative complexes (pre-RC) onto replication origins. The main component of the pre-RC is the minichromosome maintenance helicase (MCM), which is recruited,

along with other factors, during the G1 phase of the cell cycle. At G1/S transition high cyclin-dependent kinase 2 (CDK2) activity will activate the MCM triggering the replisome loading and origin firing. Through different CDK-dependent mechanisms, it is also ensured that origins can only be licensed once in each cell cycle.

The presence of activated oncogenes has been shown to interfere with this regulation by different means (Hills & Diffley, 2014) (Fig 3).

- **Origin under-usage:** origin licensing depends on a window of low CDK2 activity during G1 phase. However, several oncogenes induce cyclin E, a positive regulator of CDK2, overexpression. This causes a reduction in MCM helicase complex assembly, which leads to fewer origin firing. The replication checkpoint would normally prevent the entry into S phase of cells with reduced origin licensing but it is commonly compromised in cancer cells with deregulated E2F and p53 pathways.

- **Origin over-usage:** the increased firing of dormant origins can promote genomic instability through the exhaustion of replication factors as deoxynucleotides. This leads to a reduction of replication speed and fork stalling. RPA exhaustion also promotes double strand break formation by leaving single-stranded DNA unprotected. Furthermore, an increased number of replicons can lead to the collision between transcription and replication inducing fork stalling and collapse.

- **Origin re-usage:** Many of the factors that form the pre-replication complex are E2F targets, which is commonly upregulated in cancer. The upregulation of these pre-RC components may be the cause of the re-replication observed in human cells upon Ras or CycE overexpression. Origin re-usage may lead to increased active origin number leading to fork collision. Alternatively, excessive origins can cause the depletion of replication factors and cause fork slowdown or stalling.

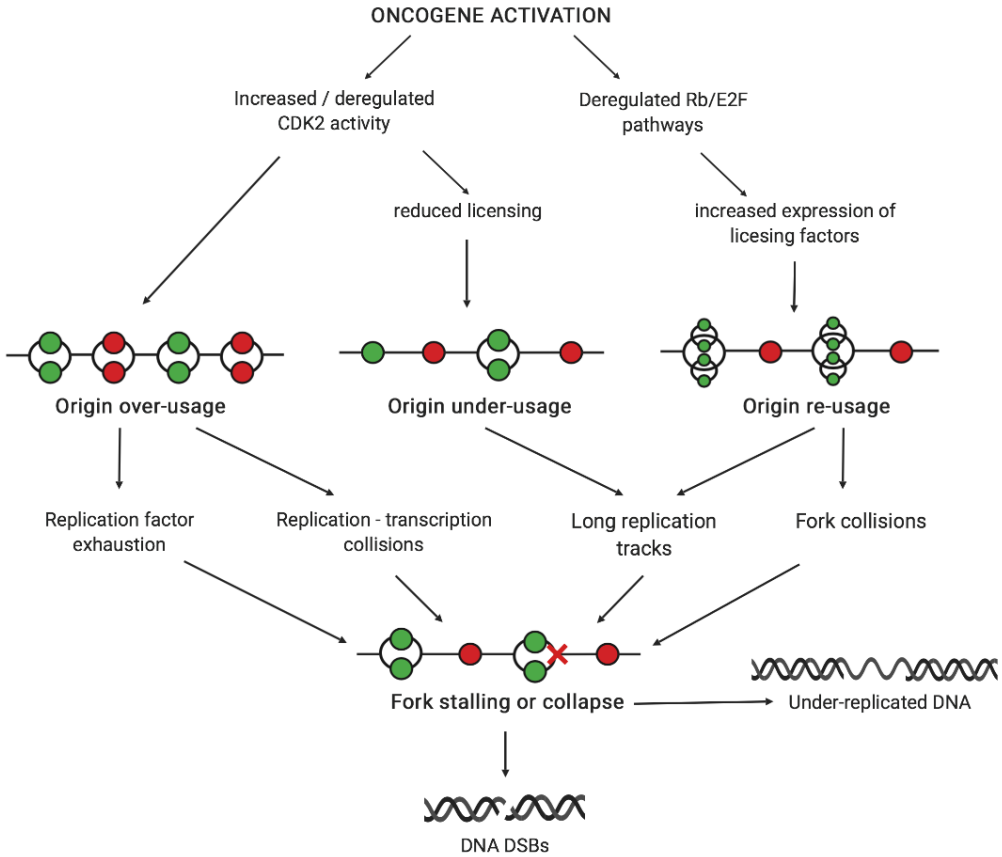

Figure 3. Summary of oncogene induced DNA replication stress (Adapted from Hills & Diffley, 2014) . Oncogene activation can interfere with the regulation of DNA replication in various ways leading to origin over-usage, under-usage or re-usage causing the stalling or collapse of the replication forks thus promoting DNA damage and genomic instability.

2. The DNA damage response pathway

2.1. The DNA damage response.

Genomes are constantly subjected to sources of DNA damage both external as UV light or tobacco smoke and internal as replicative stress or ROS. In order to maintain genome stability and maximize organismal fitness, different mechanisms have evolved in order to cope with DNA damage.

The DNA damage response is the group of cellular processes and pathways that aim to detect, signal and repair DNA damage or eliminate damaged cells. The way all of these events unfold will depend on the type of damage that is present (Fig 4).

Upon single strand DNA breaks, the remaining strand is coated by the replication protein A (RPA) complexes, composed by 3 subunits RPA3, RPA70 and RPA2, protecting it from the action of nucleases that might further damage the DNA. RPA also promotes the ATRIP/mus304 mediated recruitment an activation of the ataxia telangiectasia related (ATR/mei41) protein kinase to ssDNA (Zou & Elledge, 2003). ATR becomes activated by autophosphorylation and goes on to phosphorylate the histone 2A variant (H2Av) (Ward & Chen, 2001; Dekanty, Barrio, & Milán, 2015; Joyce et al., 2011) in order to amplify the damage signal to the DNA surrounding the original lesion, and to recruit the necessary proteins involved in DNA repair. Furthermore, ATR will phosphorylate and activate its downstream target Chk1 in order to induce a G2 cell cycle arrest (Bayer et al., 2018; de Vries et al., 2005) and allow time for DNA damage repair before cells enter into mitosis.

In the presence of double strand breaks, the MRN complex composed of the meiotic recombination homolog (Mre11), the DNA repair protein Rad50 and the Nijmegen breakage syndrome protein 1 (Nbs1) binds to the DNA and acts as a damage

sensor. Subsequently, the MRN complex will recruit and activate the ataxia telangiectasia mutated (ATM/ Tefu) protein kinase through its interaction with the Nbs1 subunit (Syed & Tainer, 2018). Once activated, ATM will phosphorylate H2Av in order to amplify the damage signal and recruit the necessary factors for DNA repair (Joyce et al., 2011). ATM will also phosphorylate its downstream target Chk2 / Loki in order to promote p53 mediated apoptosis and DNA repair (Brodsky et al., 2004; Peters et al., 2002).

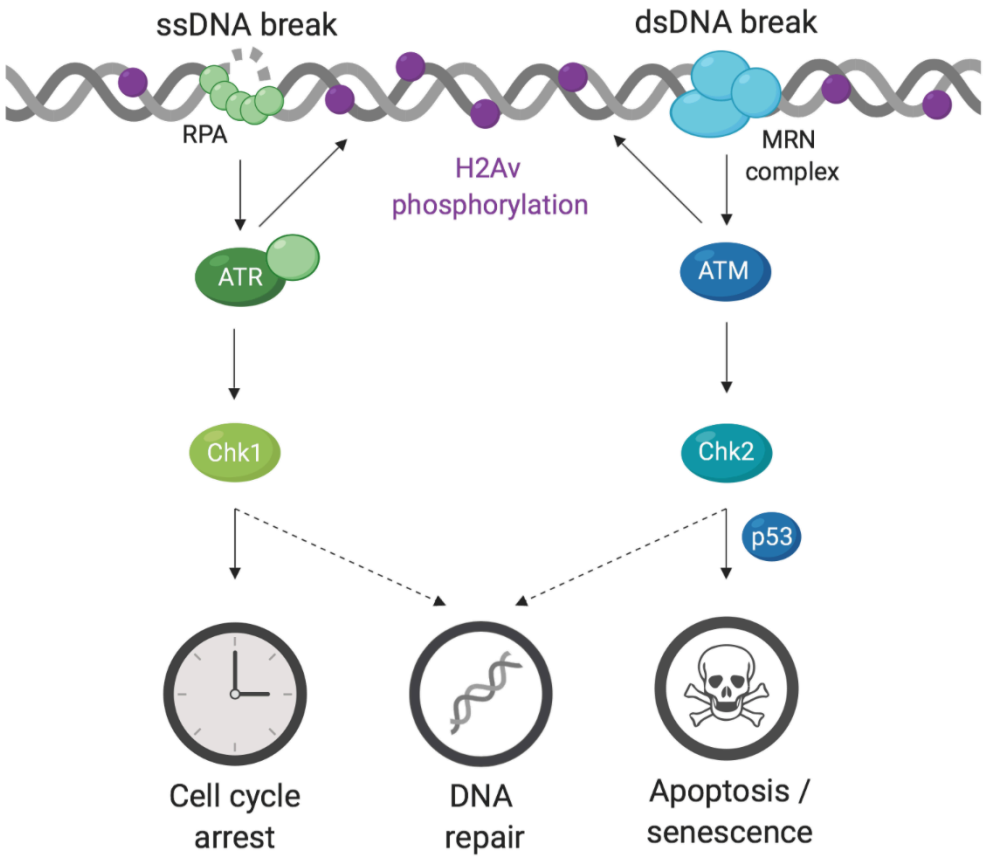

Figure 4. Summary of the DNA damage response pathway. The DDR is responsible for detecting, signaling and repairing DNA damage as well as inducing apoptosis or senescence of severely damaged cells in order to maintain organismal fitness. It does so by the activation of a kinase cascade that leads to the activation and recruitment of all the necessary factors to promote the above-mentioned effects.

These two pathways that seem to be completely independent commonly act together. This is due to the fact that unrepaired ssDNA breaks can lead to the formation of dsDNA breaks through degradation of the DNA, fork collapse, mitotic segregation of under replicated DNA, etc. On the other hand, the presence of dsDNA breaks often leads to ssDNA as a repair intermediate after end resection.

2.1.1. DNA damage repair pathways.

After the damage has been detected, several DNA repair pathways come into play in order to repair the damage. Each repair pathways will deal with a different type of DNA damage and can be subdivided depending on whether they act to repair single or double strand damage (Chatterjee & Walker, 2017) (Fig 5).

Double strand damage repair:

- **Homologous recombination.** This pathway is used in order to repair double strand DNA breaks in the presence of a template DNA. This means that this mechanism can only be used during S and G2 phases of the cell cycle, where the genome has already been duplicated. This is a conservative mechanism that implies the resection of the damaged ends, a homology-directed strand invasion and finally DNA synthesis of the missing areas.

- **Non-homologous end-joining.** This is an error prone pathway that is used to repair dsDNA breaks when a DNA template is missing. In this case, there will be a simple processing and re-ligation of the ends which can usually lead to inaccurate repair and short deletions.

Single strand damage repair:

- **Base excision repair.** It is involved in the repair of lesions that arise from the modification of DNA bases by mechanisms such as oxidation or alkylation. The damaged base is removed by a glycosylase and the remaining abasic site is removed by endonucleases and replaced by DNA synthesis.

- **Nucleotide excision repair.** This is a very important DNA repair mechanism since it is the one responsible for the repair of the bulky lesions induced by UV light. Once the damage is recognized, a segment containing the lesion is removed and the remaining strand serves as a template for DNA synthesis, and, finally, the ends are ligated. There are two forms of NER, global NER - that can act throughout the genome, and transcription-coupled NER - that is activated when the transcription machinery is blocked by the presence of a lesion

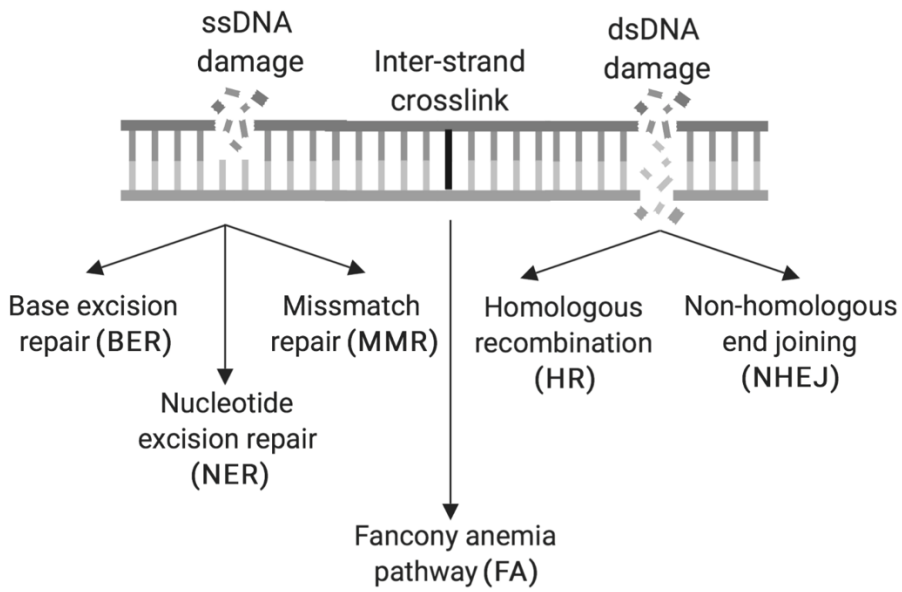

Figure 5. Summary of DNA damage repair pathways. Adapted from (Corcoran et al., 2016). dsDNA breaks are repaired via HR or NHEJ depending on the presence of a template or not. ssDNA breaks are repaired by different mechanisms depending on the type of damage that has been generated. Fanconi anemia pathway acts to repair inter-strand crosslinks.

- **Mismatch repair.** It is the mechanism in charge of repairing the erroneous pairings of bases that can happen during replication. This mechanism is capable of detecting the parental strand and after resection of the incorrect base use it to repair the damage.

- **Fanconi anemia pathway.** It is necessary for the repair of inter-strand crosslinks; these lesions cause a covalent bond between the two DNA strands leading to a blockade in replication and translation.

2.2. The DDR and its implications in cancer.

The DNA damage response (DDR) pathway has been shown to be activated early on in the tumorigenic process at precancerous stages and to act as an anticancer barrier, preventing the accumulation of mutations and the progression into more aggressive stages. In order for tumors to progress from benign to malignant, the DDR has to be inactivated and many times cells acquire mutations in key DDR genes. At the same time, tumor cells have a very highly proliferative which leads to replication stress and DNA damage. In these conditions, cells depend on the residual DDR activity in order to repair the damage and survive, leaving tumor cells hanging in a very tight equilibrium depending on the right amount of DDR pathway activity (Halazonetis et al., 2008).

2.2.1. Exploiting the DDR to target cancer cells.

Given the fragile situation of cancer cells, their dependency on the DDR and DNA repair in advanced stages could be used to selectively target cancer cells, either as a monotherapy in tumors deficient for some DDR proteins or in combination with radio- or chemotherapy as a sensitizer to DNA damage (Weber & Ryan, 2015).

A successful example of the use of this strategy is the use of PARP inhibitors to treat BRCA1 deficient tumors, which have impaired homologous recombination DNA repair. PARP proteins are involved in DNA repair via base excision repair. Their inhibition will lead to unrepaired DNA and subsequently, dsDNA breaks, which will not be repaired or not efficiently given that the cells lack proper homologous recombination thus leading to cell death (Tangutoori, Baldwin, & Sridhar, 2015).

Even nowadays, the main treatment option for many tumors is the use of chemo- and radiotherapy as therapeutic agents that target rapidly dividing cells. An increasing number of studies are focusing on the search of synthetic lethal interactions between the generation of DNA damage by the use of genotoxic agents and the depletion of DNA damage repair genes (Helleday et al., 2008; O'Connor, 2015; Toulany, 2019).

3. Ras oncogene

3.1. Discovery and function of Ras proteins.

Ras research dates back to the '70s when rat sarcoma viruses were discovered. Shortly after they were shown to promote tumorigenesis through the presence, in the viral sequence, of rat genes, they were named Ras genes after rat sarcoma virus. In the early '80s first human Ras genes were found and shown to transform cells and to play a role in human pathogenesis (Malumbres & Barbacid, 2003).

In mammals, there are three different Ras genes: H-Ras and K-Ras - identified from Harvey and Kirsten sarcoma viruses - and N-Ras -identified in neuroblastoma cell lines. Each of these genes seems to have slightly different activities and to be majoritarian in different tissues (Tsuchida et al., 2016). However, in *Drosophila* melanogaster there is only one Ras gene named Ras1 which shares a 75% homology with H-Ras (Neuman-Silberberg et al., 1984).

Ras is one of the most commonly mutated oncogenes with Ras mutations being present in about one third of all human cancers. Different Ras oncogenes present a unique mutational signature; K-Ras mutations are most commonly found in pancreatic and colorectal tumors, while H-Ras and N-Ras are most common in salivary gland and skin tumors, respectively (Table 1).

Table 1. Frequency of Ras mutation in human cancer.

TISSUE	KRAS	HRAS	NRAS	Incidence	Mortality
Biliary tract	20%	1%	3%		
Cervix	6%	3%	1%	15	8,2
Endometrium	15%	0%	2%		
Genital tract	7%	1%	2%		
Haematopoietic and lymphoid	5%	1%	9%		
Large intestine	33%	1%	4%	24	11,5

Lung	16%	0%	1%	27	23,1
Ovary	13%	0%	1%	8	
Pancreas	55%	0%	1%	6	5,7
Penis	8%	8%	3%	1	0,39
Peritoneum	46%	0%	1%		
Salivary gland	2%	12%	1%	1	0,29
Skin	3%	10%	15%	4	0,8
Small intestine	24%	0%	1%		
Stomach	6%	1%	1%		
Thyroid	2%	4%	8%	7	0,54
Upper aerodigestive tract	2%	5%	1%		
Urinary tract	6%	9%	2%		

Data on mutation frequency for the different Ras oncogenes comes from the COSMIC database. Data on mortality and incidence of each cancer type comes from the Global cancer observatory (GCO) an initiative of the international agency for research on cancer (WHO) and represents the rate per 100.000 cases.

3.1.1. Ras activation and regulation.

Ras proteins are small G proteins (guanine nucleotide binding proteins) that act as molecular switches conveying information from external stimuli into the cell. Ras proteins have two conformations: ON, when they are bound to GTP, and OFF, when they are bound to GDP (Simanshu, Nissley, & McCormick, 2017). Upon ligand binding to receptor tyrosine kinases such as EGF to the EGF receptor, the receptor dimerizes and becomes phosphorylated. This phosphorylation leads to the recruitment to the membrane of Son of sevenless (Sos), a guanine nucleotide exchange factor (GEF) that was originally discovered in *Drosophila* genetic screens (Rojas, Oliva, & Santos, 2011). GEFs promote the ejection of GDP and its replacement with GTP, that is much more abundant in the cytosol, thus leading to Ras activation. On the other hand, Ras inactivation is mediated by GTPase activating proteins (GAP) which accelerate Ras-mediated GTP hydrolysis (Fig 6).

The most common oncogenic Ras mutations are those found in the position 12 and 13 of the protein and consist on aminoacid substitutions that prevent the proper interaction between Ras and GAP proteins, thus rendering Ras in a GTP bound state that is constitutively active. Also common are mutations in position 61 in the catalytic site of Ras resulting in impaired GTP hydrolysis (Pylayeva-Gupta, Grabocka, & Bar-Sagi, 2011).

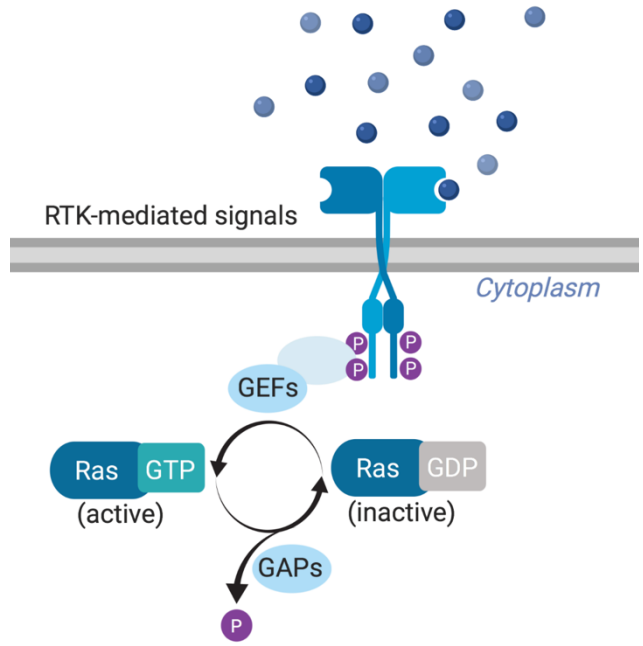

Figure 6. Regulation of Ras activation and inactivation. Upon ligand binding the RTK receptor dimerizes and autophosphorylates recruiting the GEFs responsible of Ras activation. GAP proteins promote GTP hydrolysis and inactivation.

3.1.2. Ras effectors and signaling pathways.

Once Ras has been activated, several effectors can be recruited and activated leading to multiple outcomes ranging from proliferation, growth, differentiation to apoptosis among many others (Karnoub & Weinberg, 2008).

RAF kinase (Rapidly accelerated fibrosarcoma) was the first Ras effector to be identified. RAF activation is induced by its association to activated Ras, that recruits RAF to the membrane where it becomes phosphorylated and activated. RAF activation elicits a MAPK (mitogen activated protein kinase) kinase cascade where RAF phosphorylates and activates MEK which in turn activates ERK. ERK will phosphorylate several targets among which ETS and Fos transcription factors that will give rise to a plethora of cellular responses (Fig 7).

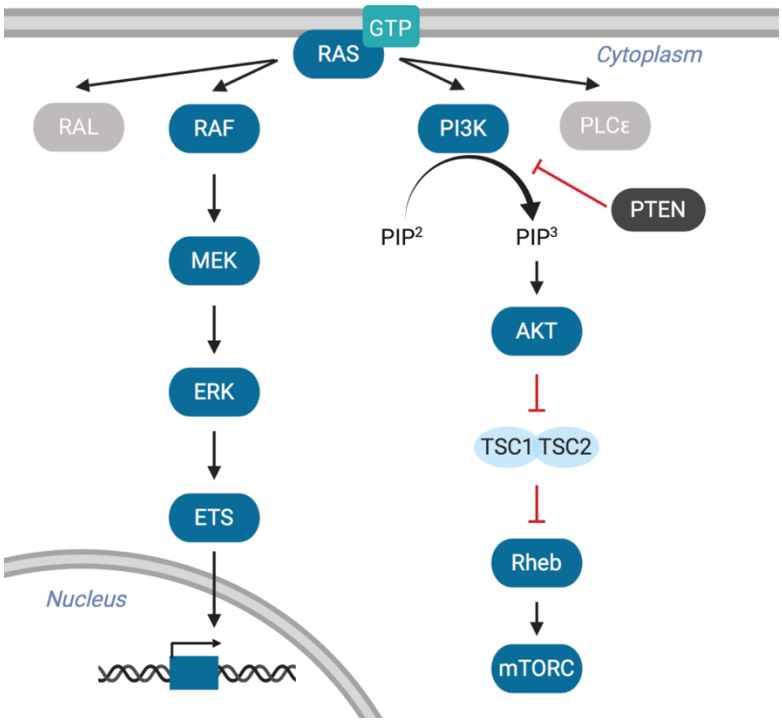

Figure 7. Summary of the MAPK-ERK and PI3K signaling pathways. Downstream of Ras activation several effector pathways will be activated in order to give rise a diverse response. The main effector pathways are the ERK and the PI3K pathways.

A year after RAF identification, PI3K (phosphoinositide 3 kinase) was found to drive responses downstream of Ras. PI3K can be directly activated via interaction with a phosphorylated RTK receptor but also it can become phosphorylated and activated

through its interaction with Ras. Once PI3K is activated, it phosphorylates phosphatidylinositol 4,5- bisphosphate (PIP_2) into phosphatidylinositol 3,4,5-triphosphate (PIP_3) which will activate AKT kinase. AKT, in turn, phosphorylates and induce the dissociation of the repressor complex TSC1-TSC2, thus leading to mTORC activation (Fig 7).

Ral (Ras like) and several other effectors have also been described. However, their implications on Ras malignancy and the mechanistic details of their downstream pathways are less clear than for the other two.

3.2. Ras and the Hallmarks of cancer

Oncogenic Ras activation has been shown to recapitulate many of the hallmarks of cancer. Among them Ras has been shown to have a prominent role in the induction of proliferation and the inhibition of apoptosis. Ras also promotes a metabolic shift from oxidative phosphorylation to aerobic glycolysis in order to more effectively produce the building blocks necessary for cell growth and division. This change is induced via the upregulation of the hypoxia inducible factor 1α mediated by mTOR. Ras can also participate in the remodeling of the microenvironment and the induction of angiogenesis via the expression of different cytokines and the vascular endothelial growth factor A (VEGFA). Also, Ras expression reduces the immunogenicity of cancer leading to the evasion of the immune response (Pylayeva-Gupta et al., 2011).

3.2.1. Ras and cell cycle regulation.

One of the main features of cancer is the promotion of proliferation independently of the presence of mitotic signals, as Ras is a key mediator of these signals it is not surprising that Ras activating mutations can drive proliferation. In mammals, it has been shown that Ras can promote the entry into the cell cycle of G0 arrested cells

by promoting the expression of the G1 cyclin D1 through the RAF and PI3K pathways. Cyclin D1 expression will lead to CDK2 activation and the phosphorylation of retinoblastoma that will then release E2F. Once E2F is activated, it will go to the nucleus and drive the expression of genes involved in G1/S transition such as cyclin E or PCNA (Downward, 1997). In *Drosophila* a similar mechanism takes place; however, in this case, Cyclin D1 doesn't seem to play a central role (Datar et al. 2000). Instead, it is cyclin E the one upregulated to bind CDK2 in order to phosphorylate and inactivate retinoblastoma.

3.2.2. Ras and apoptosis suppression.

Ras has been shown to prevent proper apoptotic response and to promote cell death evasion, one of the main hallmarks of cancer. In mammals, this is accomplished by the upregulation of antiapoptotic genes and the downregulation of proapoptotic genes through both PI3K and RAF pathways (Cox & Der, 2003). Besides its prominent pro-survival function, Ras has also been shown to elicit some proapoptotic responses for example through the MAPK-mediated activation of the JUN N-terminal kinase signaling. The capacity of Ras to induce tumorigenesis suggests that its pro-survival role prevails. In *Drosophila*, Ras prevents apoptosis via the inhibition of the pro-apoptotic gene hid. Hid (Smac/Diablo in mammals) is blocked downstream of the RAF-MAPK signaling pathway and two mechanisms of inhibition have been proposed. On the one hand, it was proposed that ERK can directly phosphorylate and inhibit hid (Bergmann et al., 1998); on the other hand, it was suggested that ERK through an ETS transcription factor can downregulate hid expression (Kurada & White, 1998).

3.4. Ras drug strategies

Given the prevalence of Ras mutations in cancer, many efforts have been made in order to find ways to target Ras mutant cancer cells. However, although many strategies were promising, none of them has proven clinically relevant. This has led to the general conception that Ras is an undruggable oncogene. Over the years, several approaches were used in order to tackle this problem (Cox et al., 2014) (Fig 8).

- **Direct Ras inhibition.** The main problem of this approach is the fact that most Ras mutations destroy Ras enzymatic activity as a GTPase, and bringing and enzymatic activity back is practically impossible. To circumvent this problem, several groups have worked in the design of small molecules that can interfere with Ras binding to GTP, SOS1, RAF, etc. Unfortunately, none of them has made it into the clinic so far.

- **Blocking Ras membrane localization.** Ras proteins need to localize to the membrane in order to exert their function. Several posttranslational modifications allow the membrane localization of Ras. Inhibitors of the enzymes responsible for such modifications exist and have been tested, however in the cases they do work they have many other target proteins that complicate their therapeutic use.

- **Inhibiting Ras effectors.** RAF-MEK-ERK cascade is one of the main effector pathways of Ras. This is a complex pathway that has negative feedback loops in order to shut down the pathway. Thus, a negative effect of the inactivation of the kinases might be an upregulation of the upstream signaling thus rendering the inhibitor useless. Nevertheless, two RAF inhibitors (Vemurafenib and Dabrafenib) and one MEK inhibitor (Trametinib) are efficient enough and have been FDA approved for the treatment of BRAF mutant metastatic melanomas. Another issue with these inhibitors is the emergence of resistance by upregulating the pathway downstream. PI3K

inhibitors are also under clinical evaluation however they have rendered rather disappointing results against Ras mutant tumors.

- **Synthetic lethal interactions.** This strategy is particularly interesting for cases like the Ras oncogene that cannot be directly targeted. Synthetic lethal screens are based on the identification of genes that are essential for the survival of tumor cells but not for normal cells. Original screens were performed by short hairpin mediated depletion and lead to the identification of several therapeutic targets (Downward, 2015). However, in the past few years, the approval of MEK inhibitors has prompted the implementation of chemical-based screens in which combinations of drugs are tested. This method has been successful in identifying synthetic lethal drug combinations that are now under clinical evaluation (Pang & Liu, 2017).

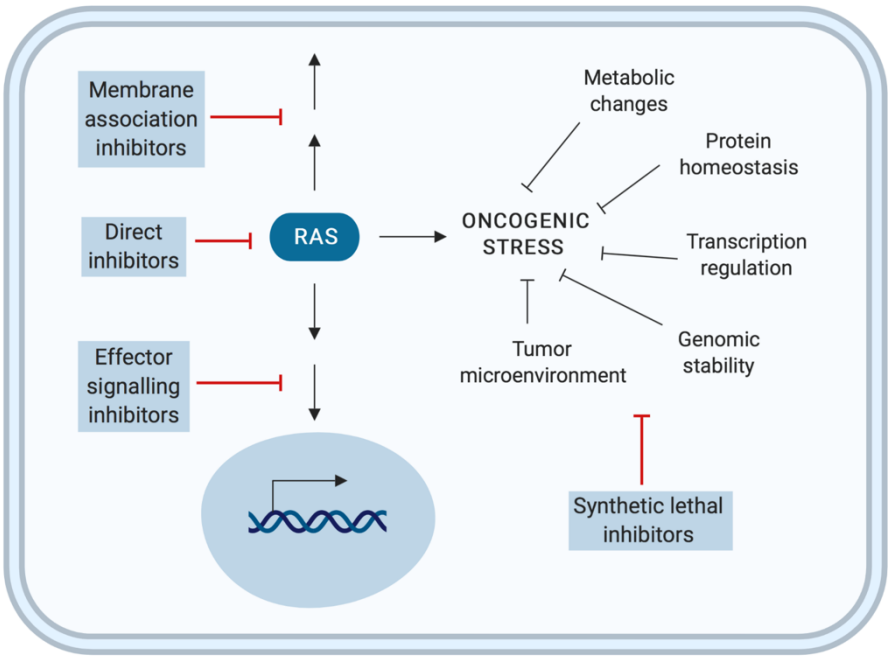

Figure 8. Strategies for targeting Ras mutant tumors. Different approaches have been used in the search for therapies that selectively target Ras mutant tumors. On the one hand inhibitors that affect Ras signaling at different levels. On the other hand, the search for synthetic lethal interaction that impinge on cellular mechanisms that help cells cope with oncogenic stress, thus offering a selective target. Adapted from (Cox et al., 2014).

4. *Drosophila* as a model organism

4.1. *Drosophila melanogaster* in research.

Drosophila melanogaster is a versatile model organism that has been used for over a century in very diverse areas of study. At the beginning of the20th century, Thomas Hunt Morgan introduced *Drosophila* into his laboratory making seminal contributions to the genetics field. Among them, improving Mendel's inheritance theories, demonstrating that genes were found in chromosomes (Bellen, Tong, & Tsuda, 2010).

Although for the first part of the century *Drosophila* was primarily used in genetic studies, its worth as a model organism has not been limited to it, as shown by the six novel prices in physiology that have been awarded to investigations conducted with this organism (Fig 9). This is due to the fact that genes involved in basic cellular processes and signaling pathways are conserved throughout evolution. Indeed, After the sequencing of its genome in the year 2000, it was found that 75% of disease-related genes in humans are conserved in *Drosophila*, consolidating it as a model for biomedical research. This together with the fact that it is a much simpler, yet *in vivo* model makes *Drosophila* the perfect system in which to study gene function.

Drosophila is a highly amenable organism for genetic manipulation, which for many years has been one of the main advantages of its use over other model organisms. The capacity to generate and maintain new mutant stocks combined with protein expression systems that allow for a tissue specific and temporally controlled expression of desired genes and constructs has made *Drosophila* a great organism to study basic gene functions (Hales et al., 2015). In fact, many genes involved in the most relevant signaling pathways were first identified in *Drosophila*.

Other, more general, characteristics that make of *Drosophila* the perfect model organism are its high breeding capacity and short life cycle, its simple genome with only 4 chromosomes and low redundancy, the relatively low maintenance cost or the capacity to perform *in vivo* studies.

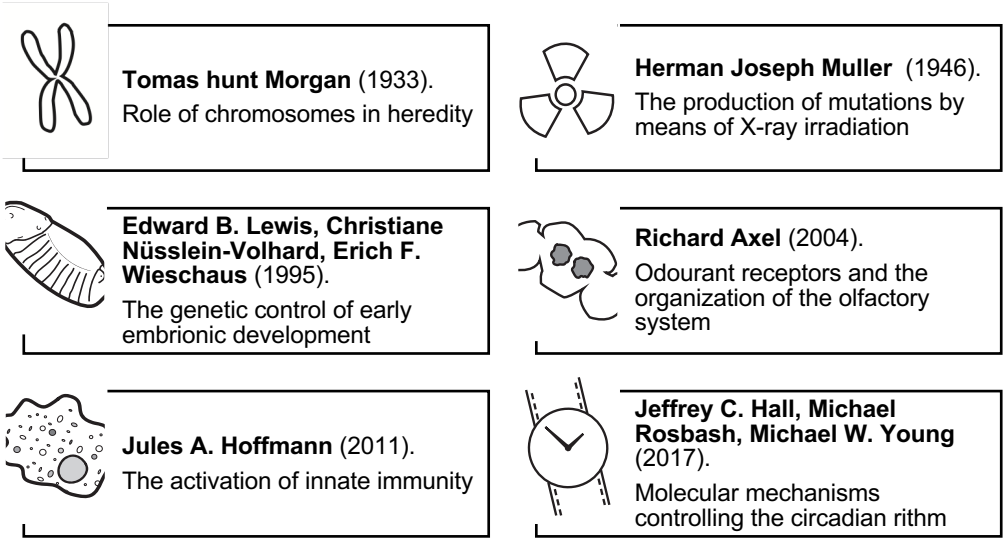

Figure 9. Nobel prizes in medicine and physiology awarded to *Drosophila* research. For many years researchers have worked in *Drosophila* genetics and the production of new mutants and tools to investigate gene function. More recently the *Drosophila* genetic toolkit has been used to discover new genes involved in physiologically relevant cellular and organismal processes.

4.2. *Drosophila* development

Drosophila is a holometabolous insect: it presents 4 different life stages (egg, larva, pupa and imago) and goes through a metamorphosis process during its development. At 25ºC the entire development of a fly takes around 10 days. For the first day, the embryo develops inside the egg before hatching in the form of a first instar larvae. For the next four days, the larvae eat and grow through three different

molds until they reach the appropriate size, pupariate and enter into metamorphosis (Fig 10). During this process, most of the larval tissues are destroyed while the so-called imaginal tissues are remodeled in order to give rise to the proper adult structures (Jennings, 2011).

During larval stages, we can find two types of tissues. On the one hand, larval tissues, that grow by endoreplication giving rise to polyploid tissues that form the biggest part of the larvae. On the other hand, imaginal tissues, which are specified during embryonic development, start out as very small groups of cells and rapidly divide during larval stages. After metamorphosis, imaginal tissues give rise to the structures of the adult body.

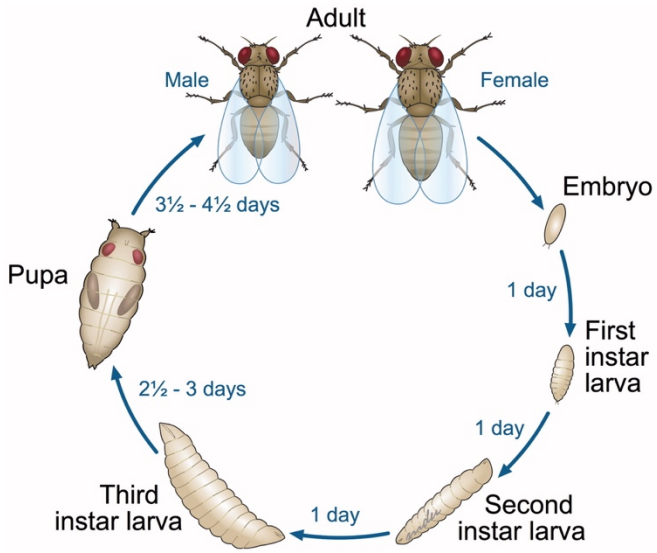

Figure 10: Schematic of *Drosophila* life cycle. During its life cycle *Drosophila* goes through different stages. First the embryo develops for one day before it hatches into a first instar larva after two more larval stages, the pupae is formed and metamorphosis take place before new adults arise. Extracted from (Ong et al., 2015).

In this work, I have used both wing and eye-antenna imaginal discs. The wing imaginal disc is subdivided along the anterior-posterior and dorsal-ventral axis into different compartments, which are comprised by cells that will not intermingle and

that have specific expression patterns of developmental genes that can be used as tissue specific drivers for gene expression.

During this work, I have taken advantage of the dual GAL4/UAS transactivation system. Coming, originally, from yeast, it was introduced in *Drosophila* by Andrea Brand and Norbert Perrimon (Brand & Perrimon, 1993). This system allows us to express any gene or RNAi of interest in specific areas of the wing disc. Together with the temperature sensitive repressor GAL80ts, it also allows for a temporally controlled expression of the transgene. I have also used the MARCM technique in order to induce labelled mitotic clones were we can control gene expression (Lee & Luo, 1999) .

4.3. *Drosophila* cancer models

The first report of *Drosophila* being used to study a cancer related phenotype dates as back as 1916, when Mary Stark, a PhD student in Morgan's lab, described the black granules that were caused by the lethal 7 factor. Years later it was discovered that the granules were actually melanotic tumors. Since then, many oncogenes and their molecular functions have been discovered by using this model organism. This happened even before their link to cancer was known, making a strong point for the need of basic research. It is the case of some of the most preeminent oncogenes in cancer such as Notch, hedgehog, hippo or JAK/STAT. For other oncogenes that were not discovered in *Drosophila*, such as Ras, research performed in *Drosophila* has been crucial to delineate its signaling pathways (Beira & Paro, 2016).

Based on this knowledge and despite the limitations of *Drosophila* (lack of some human tissues and organs, open circulatory system, lack of adaptive immunity), several cancer models have been established that recapitulate many of the hallmarks of cancer, such as: resistance to cell death, sustained proliferative

signaling, genome instability and mutation, invasion and metastasis, reprogramming cellular metabolism and inflammation (Gonzalez, 2013; Rudrapatna, Cagan, & Das, 2012).

4.3.1. Ras oncogene dependent *Drosophila* cancer models

Among the *Drosophila* cancer models that exist, some of the most commonly used are those based on the presence of a constitutively active version of the Ras oncogene.

The first ones to evaluate the effects of RasV12 constitutively active mutant expression in the wing imaginal discs were Karim and Rubin in 1998. They showed that RasV12 expression in the eye and wing imaginal discs was capable of inducing proliferation and tissue hyperplasia and that MAPK signaling was necessary but not sufficient to induce this effect (Karim & Rubin, 1998). Two years later, Edgar and Prober went deeper into the regulation of RasV12-induced proliferation. By using RasV12 clones, they showed that RasV12 induces cell growth and G1/S transition by upregulating the proto-oncogene dMyc and CycE (Prober & Edgar, 2000). Furthermore, they showed that RasV12 can also activate PI3K signaling and that PI3K activity promotes cell growth and G1/S transition (Prober & Edgar, 2002).

Rarely, tumors arise from a single mutation. More commonly, they are the result of a multistep process in which cells accumulate mutations that provide the cells with the necessary characteristics to induce tumor formation. In 2003, Brumby and Richardson showed the first example of cooperative tumorigenesis in *Drosophila*. They took advantage of the MARCM system to induce scribble mutant clones that also express RasV12. While scribble mutant clones die by JNK induced apoptosis, in RasV12, scribble mutant clones cell death is prevented and the clones overgrow to a much larger extent than RasV12 alone clones (Brumby & Richardson, 2003). In that same

year, Pagliarini and Xu introduced *Drosophila* as a model to study metastatic behavior. They performed a genetic screen and identified the cooperation between RasV12 and scribble mutation to induce invasion of adjacent organs and migration to distant sites. Both behaviors depend on the decrease in E-cadherin levels. Furthermore, they observed that RasV12, scribble mutant cells degrade the basement membrane and upregulate the actin cytoskeleton at the migration sites (Pagliarini & Xu, 2003). The same group demonstrated that the JNK proapoptotic signal, induced by the loss of the polarity determinant scribble, is switched to a pro-tumorigenic role in the presence of RasV12 and that this signal is necessary and sufficient to induce the invasion and migration of the RasV12 cells (Igaki, Pagliarini, & Xu, 2006). At the same time, it was shown that the pro-tumorigenic role of JNK needs of a dFos dependent transcriptional activation of the matrix metalloprotease MMP1 (Uhlirova & Bohmann, 2006).

Tumors are comprised of heterogeneous cell populations both genetically and functionally. *Drosophila* Ras models have been used to monitor the tumorigenic interactions between different clonal populations. In 2010, it was shown that RasV12 and scribble mutant clones could cooperate to promote tumor growth and invasion (Wu, Pastor-Pareja, & Xu, 2010). It was also shown that RasV12 clones carrying mitochondrial defects can non-autonomously induce the growth and invasion of RasV12 clones through the expression of mitogenic molecules (Ohsawa et al., 2012). Another example on intratumor cooperation is that shown by Marco Milan's lab in which we demonstrated that delaminated cells from the tumor express mitogenic molecules in order to drive the unlimited growth of the non-delaminated cells of the same tumor (Muzzopappa, Murcia, & Milán, 2017).

Tumor growth can also be affected by the interactions with its microenvironment. A very nice example of this crosstalk between the tumor and its microenvironment is

that of autophagy. While it was shown that tumor autonomous autophagy could suppress tumorigenesis by preventing the accumulation of reactive oxygen species (Manent et al., 2017), it was also shown that non-autonomous autophagy had the opposite role and was fueling tumor growth by providing nutrients to the tumor (Katheder et al., 2017). Understanding this type of interactions is crucial when considering possible therapeutic cancer targets.

Tumors have been shown to interact with the immune system. However, the role of immune cells in tumor growth is not clear yet. *Drosophila* RasV12, Scribble mutant tumors have been used to study the role of the immune system in tumor growth. First, it was proposed that hemocytes (*Drosophila* macrophages) are recruited to tumor sites in order to prevent growth and invasion by depositing collagen to counteract the basement membrane degradation (Pastor-Pareja, Wu, & Xu, 2008). Hemocytes were also proposed to promote tumor growth by inducing JNK signaling through the ligand TNF (Eiger In *Drosophila*, (Cordero et al., 2010)). However, later on, it was demonstrated that while they are recruited, hemocytes do not seem to play a major role in tumor growth (Muzzopappa et al., 2017).

Not only short range microenvironmental interactions are relevant for tumor progression but also less understood long-range systemic interactions play a role. Cachexia is a phenomenon that leads to weight loss and muscular atrophy and is an indicator of poor prognosis in cancer. Flies carrying RasV12 scribble mutant tumors have been used to study cachexia since they present similar wasting phenotypes. It was shown that the tumors secreted Impl, an antagonist of insulin signaling thus promoting insulin resistance in peripheral tissues (Figueroa-Clarevega & Bilder, 2015).

In the era of genomic data and personalized medicine, *Drosophila* is being used as a screening platform for the search of new treatment opportunities for RasV12 dependent tumors (Kasai & Cagan, 2010; Levine & Cagan; 2016; Willoughby et al., 2013).

RasV12-dependent tumors in *Drosophila* have been shown to present several hallmarks of human cancer such as sustained proliferative signaling, resistance to cell death or invasion and metastasis (Fig 11). Furthermore, except for angiogenesis, all other hallmarks of cancer can be studied in these *Drosophila* models.

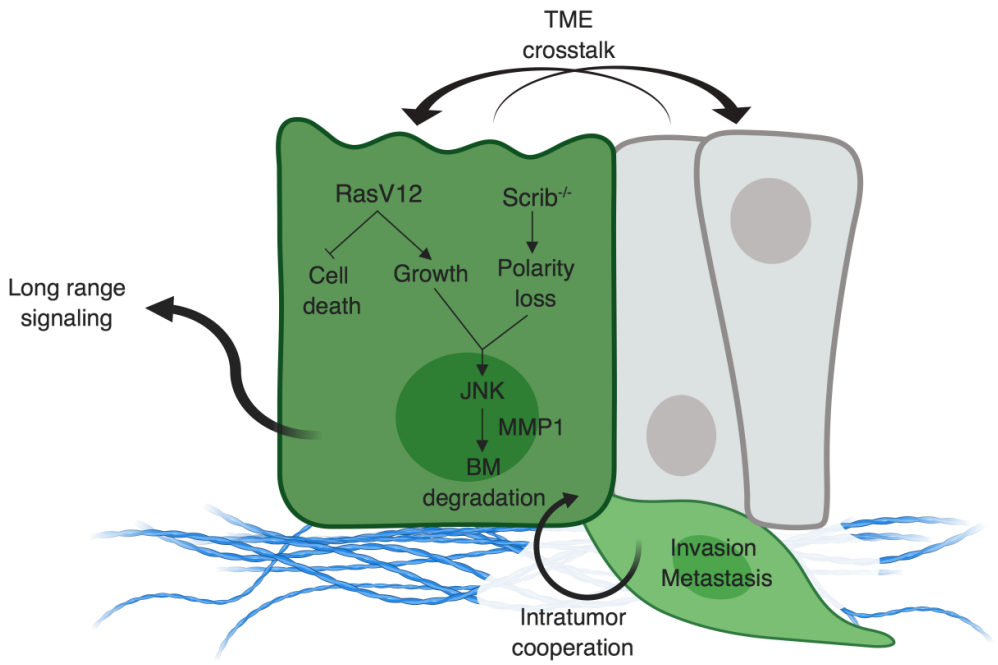

Figure 11. Schematic summary of the characteristics of RasV12 and RasV12, scrib-/- tumors. In green tumor cells, in gray adjacent epithelial wild type cells and in blue the basement membrane of the epithelium. Thick arrows represent the different interactions that the tumor cells can engage. Thin arrows represent the tumor intrinsic behavior.

Objectives

Objectives

Despite our increasing understanding of the biology of cancer cells, Ras has been nicknamed as the undruggable oncogene due to the difficulty of finding therapies that are both safe and effective. Oncogenes have been proposed, through the induction of aberrant proliferation, to induce replicative stress which in turn can lead to genomic instability and mutation, a driving force for tumor progression. In that regard, we took advantage of *Drosophila*, as a well-established model organism, to accomplish the following objectives:

- To reanalyze the capacity of Ras oncogene to promote cell cycle progression.
- To evaluate the induction of DNA damage and replicative stress caused by Ras.
- To study the relationship between Ras and the DNA damage response (DDR) pathway.
- To investigate the role of MAPK-ERK pathway in blocking apoptosis in tumors and homeostatic situations.
- To use the previous results to design and test genetic as well as chemo- and radiotherapies to selectively target Ras-expressing cells.

Tumors are formed by heterogeneous cancer cell populations but also by other cells like fibroblasts, immune cells or normal tissue cells that communicate with the tumor and contribute to tumor growth. Tumor microenvironment has emerged as a very crucial regulator of tumor growth and for that reason, we decided to set the following objectives.

- To analyze the effect of Ras on adjacent wild type epithelial cells.

- To evaluate the contribution of these cells to tumor growth.

Results

1. Characterization of RasV12 effects on tissue growth and cell cycle.

As has been described in the introduction, one of the main functions of Ras oncogenes is to promote cellular proliferation. In this chapter, we have analyzed the impact of the expression of a constitutively active form of Ras, RasV12, in promoting proliferation and tissue growth. We have also analyzed the cell cycle changes derived from this expression. In order to do that we have used the Gal4/UAS system to express RasV12 in specific compartments of the wing disc. Given the lethality of early expression of RasV12, we used the Gal80ts repressor and kept the larvae for 6 days at the restrictive temperature of 18ºC and then shifted them to 29ºC to allow transgene expression for three days, unless stated otherwise.

1.1 RasV12 expression promotes G1/S transition and tissue overgrowth.

Expression of RasV12 in the dorsal compartment of *Drosophila* wing imaginal discs leads to overgrowth and folding of the tissue (Karim & Rubin, 1998) and (Fig 1 A, B and quantification in C). The apico-basal polarity of the tissue is not lost and E-Cadherin is not miss-localized (Fig 1A', B'). Moreover, there is only a weak expression of MMP1 (fig 1 B), a matrix metalloprotease that has been linked to epithelial to mesenchymal transition and malignancy (Uhlirova & Bohmann, 2006). This growth is considered hyperplasic since there are no signs of malignancy.

RasV12 expression has been shown to drive G1/S transition in order to promote proliferation (Prober & Edgar, 2000). We confirmed previous reports by performing a DNA content analysis by FACS (fluorescence associated cell sorting) coupled with EdU (5-ethynyl-2´-deoxyuridine) staining to label S phase cells. We observed a shift in the DNA content profile from G1 towards G2/M. In control discs, 28% of the cells

are in G1, 23% in S and 49% in G2/M. Upon RasV12 expression, the number of cells in G1 drops to 17% while the cells in G2/M increase to 77% (Fig 2A).

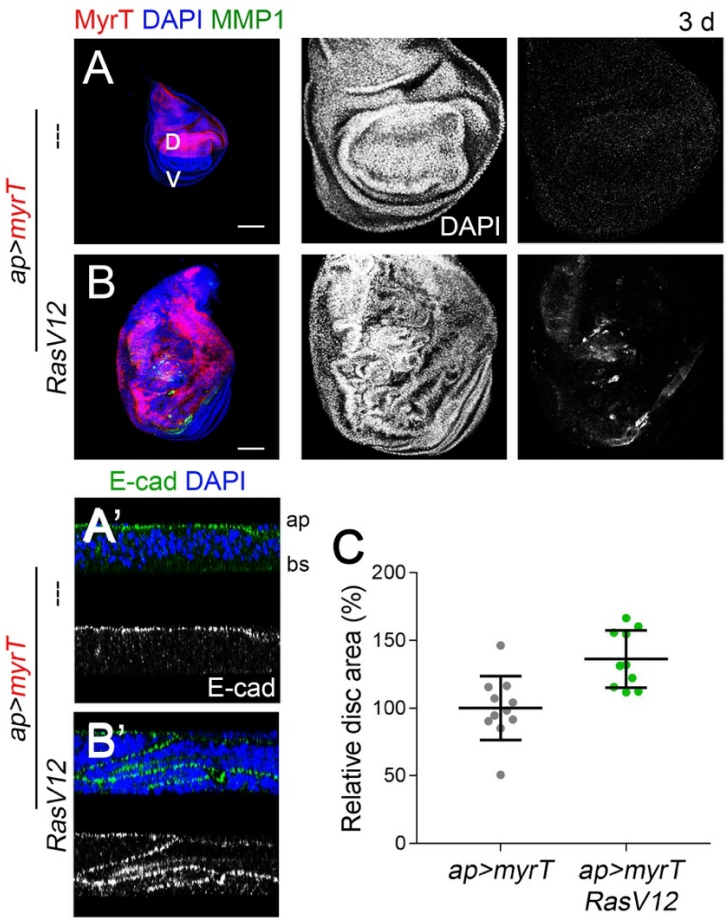

Figure 1. RasV12 promotes tissue overgrowth. (A,B) *Drosophila* wing imaginal discs expressing the *UAS-myrT* and *UAS-RasV12* transgenes under the control of the ap>gal4 driver and stained for DAPI (Blue) and MMP1 (Green). Magnifications of this same discs show DAPI and MMP1 in gray. (C) Quantification of the disc area relative to the mean control size. (A',B') Cross-sections of RasV12 and wild type discs showing E-cadherin (green and gray) and DAPI (Blue).

We obtained similar results when we analyzed the cell cycle by Fly-FUCCI, a fluorescently tagged degron based technique that allows for visualization of the different phases of the cell cycle. It depends on the degradation or not of the E2F

and CycB degrons tagged to GFP and RFP respectively (Zielke et al., 2014). As a proof of principle, in wild type discs, we can capture the developmentally programmed G1 and G2 arrest that occurs in the zone of non-proliferating cells (O'Brochta & Bryant, 1985). When we quantified the asynchronously dividing wild type cells, 33% of the cells were in G1. However, when we expressed RasV12 this percentage dropped to 13%. This was accompanied by an increase in the amount of G2 cells that went from 40% in wild type to 79% in RasV12 cells (Fig 2B).

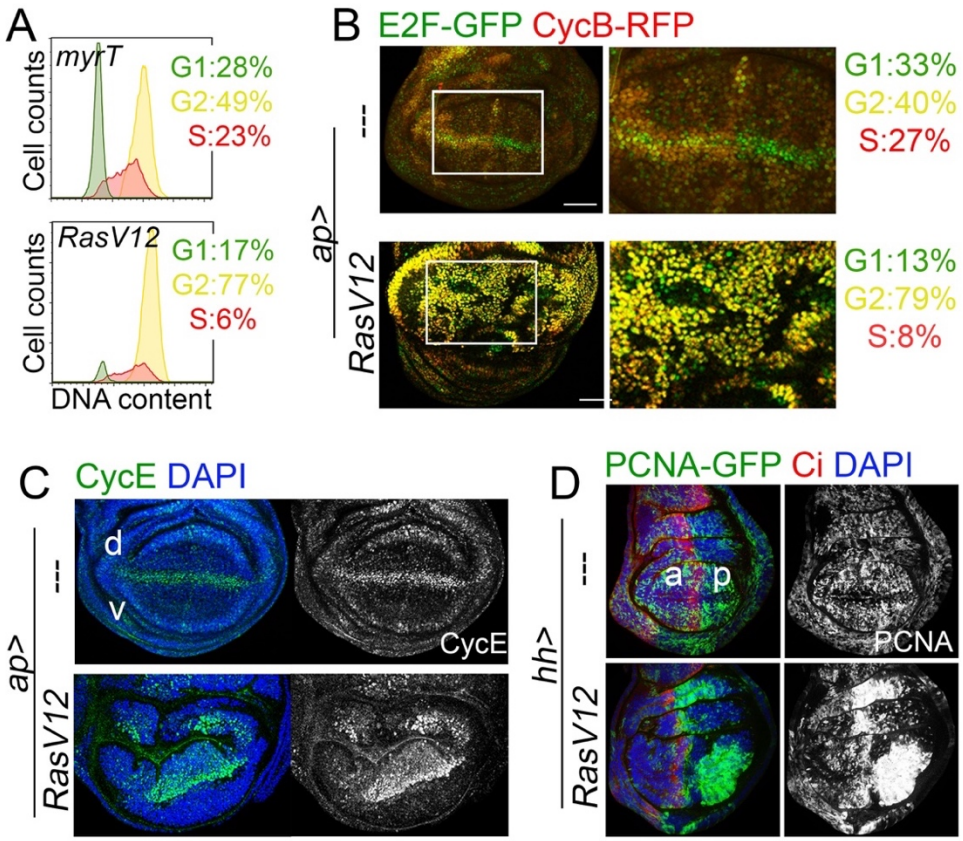

Figure 2. RasV12 expression promotes G1/S transition. (A) EdU labelled FACS sorted cells expressing the myrT and RasV12 transgenes under the control of the apterous gal4 driver to visualize the different phases of the cell cycle based on the DNA content, G1 (green), S (red) and G2/M (yellow). (B,C,D) third instar wing imaginal discs expressing different transgenes under the control of the ap or hh gal4 drivers. B wing discs carrying the fly-FUCCI construct (ub-GFP-E2F11-230 and ub-mRFP1-NLS-CycB1-266) labelling the different phases of the cell cycle G1 (green), S (red) and G2/M (yellow). (C-D) Discs stained for cyclin E (C) and the E2F reporter PCNA-GFP (D) both in green and white.

Concomitantly, we observed an increase in the levels of the G1 cyclin E (Fig 2C) and the E2F target PCNA (Fig 2D), both involved in the induction of G1/S transition. We also observed increased levels of the mitotic cyclins E and A (Fig 3A-B), consistent with the increased amount of G2 cells and a possible G2 arrest.

1.2 RasV12 and senescence.

In mammals, it has been shown that oncogene induction can lead to replicative senescence (Di Micco et al., 2006). Furthermore, previous reports in *Drosophila* have shown that RasV12 expressing cells, in the eye-antenna imaginal discs, show some senescence features (Nakamura, Ohsawa, & Igaki, 2014) such as increased cell size, increased B-galactosidase activity and cell cycle arrest.

In agreement with a senescent phenotype, during our analysis of the cell cycle, we noticed not only a shift from G1 to G2 but also a decrease in the number of replicating cells marked by EdU staining in the FACS analysis (Fig 2A in red). We observed a similar decrease when analyzing the Fly-FUCCI results (Fig 2B in red). Consistent with this, we observed low levels of replicating cells after 3 days of RasV12 expression (Fig 3C), but not after 15 hours (Fig 3D) of expression. 15 hours of RasV12 expression were sufficient to induce ERK phosphorylation (Fig 3 E, F). These results indicate that, somehow, RasV12 cells accumulate problems over time that hinder their replication and promotes a G2 arrest or elongation.

Furthermore, we performed a gene set enrichment analysis on RNA-seq data of wild type and RasV12 wing discs. We found an expected positive enrichment in receptor tyrosine kinase (RTK) signaling that serves as a positive control of Ras signaling.

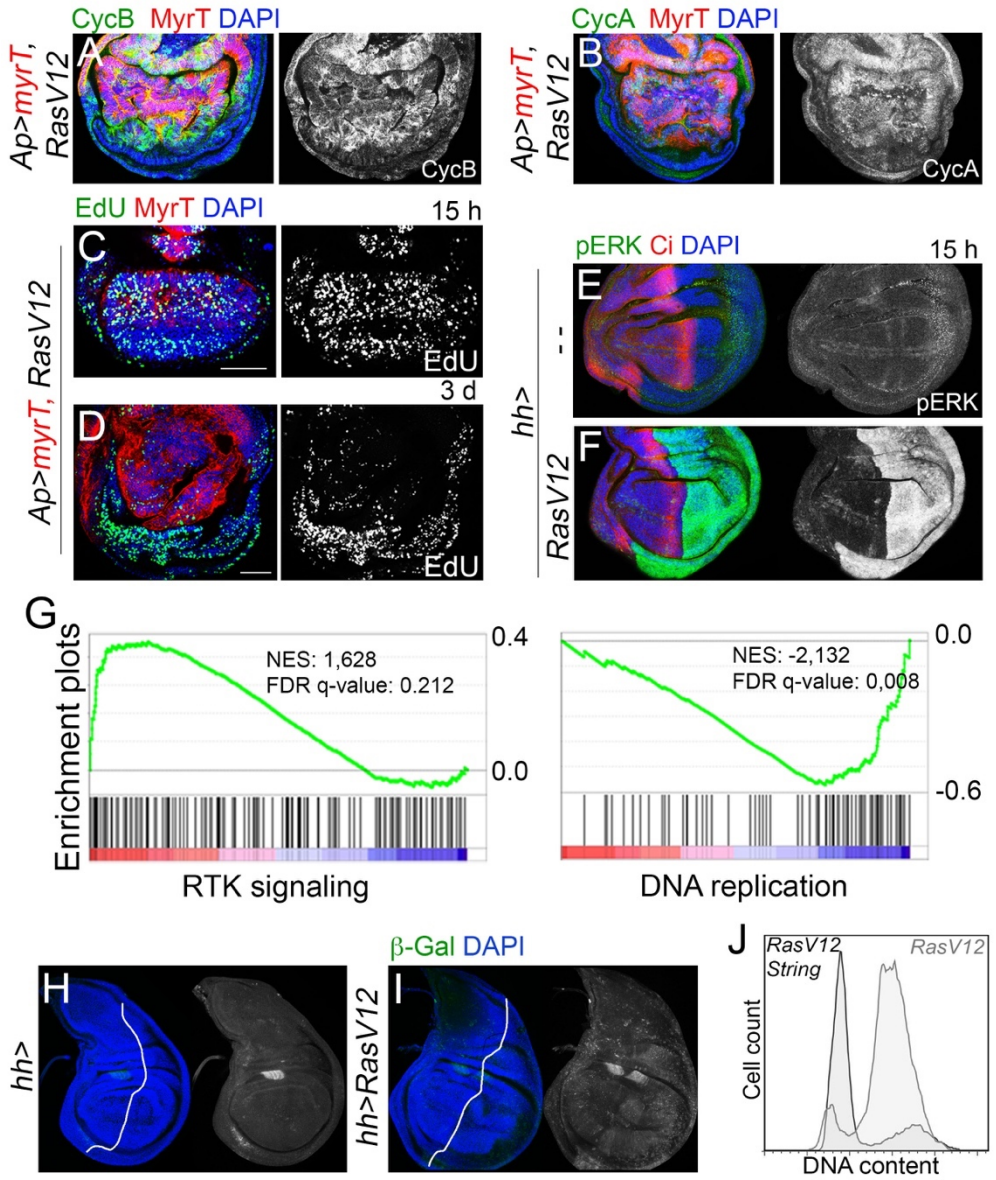

Figure 3. Oncogenic Ras and senescent phenotype. (A-F, H-I) wing imaginal discs expressing the indicated transgenes under the control of the ap-gal4 driver (A-D) or the en-gal4 driver (E-F, H-I) during 3 days (A,B,D,H,I) or 15h (C,E,F). Discs were stained for DAPI in blue, cycB in green and white (A), cycA in green and white (B), Edu in green and white (C-D), pERK in green and white (E-F), ß-gal in green and white (A), myrTomato (A-D) and Ci (E-F, H-I) both in red. (G) Enrichment plots for two significant GO terms ,positively enriched(RTK signaling) and negatively enriched (DNA replication). (J) (A) FACS sorted cells expressing the myrT, RasV12 (gray) and myrT, RasV12, String (black) transgenes under the control of the ap-gal4 driver to visualize the different phases of the cell cycle based on the DNA content.

More importantly, we also found a negative enrichment in the DNA replication class (Fig 3G). These results agree with the possibility that sustained RasV12 expression leads to DNA replication stress and senescence. Accordingly, we found slightly increased ß-gal activity in RasV12 expressing cells (Fig 3H, I).

Finally, the G2 arrest induced by RasV12 expression could be rescued by String phosphatase (Cdc25) overexpression (Fig 3J), suggesting that these cells are, indeed, arrested in G2 by a String-dependent mechanism.

2. Evaluation of the RasV12 effects on the DNA damage response.

The presence of activated oncogenes, as a response to the deregulated entry into S phase, has been shown to induce replicative stress which is one of the main sources of DNA damage and genomic instability (Hills & Diffley, 2014). In response to DNA damage, either single or double strand breaks, the DNA damage response pathway becomes activated in order to maintain the integrity of the DNA. It does so by eliciting different responses like the repair of the damage, the induction of a G2 arrest or the induction of senescence and apoptosis of the severely damaged cells (Song, 2005).

2.1 RasV12 expression generates DNA damage.

In mammals, it has been shown that RasV12 cells suffer from replicative stress and present signs of DNA damage due to the role of Ras in inducing G1/S transition. Previous reports in *Drosophila* suggested the opposite (Nakamura et al., 2014). Therefore, we decided to investigate the presence of replicative stress and DNA damage in *Drosophila* wing imaginal discs.

We analyzed RPA3:RFP fusion protein, known to bind single stranded DNA and widely used as a replicative stress marker. We observed an increase in the intensity of the signal as well as foci formation at the sites of damage (Fig 4A), indicating that RasV12 cells suffer from replicative stress.

Moreover, we analyzed Mre11 and Rad50, components of the MRN complex known to bind to and signal double stranded DNA breaks. Again, we observed an increase in the intensity as well as the formation of Mre11 and Rad50 foci at the sites of damage (Fig 4B, C). This double stranded DNA breaks may be a consequence of

the resolution of stalled replication forks or of miss segregation of the chromosomes due to under-replicated DNA.

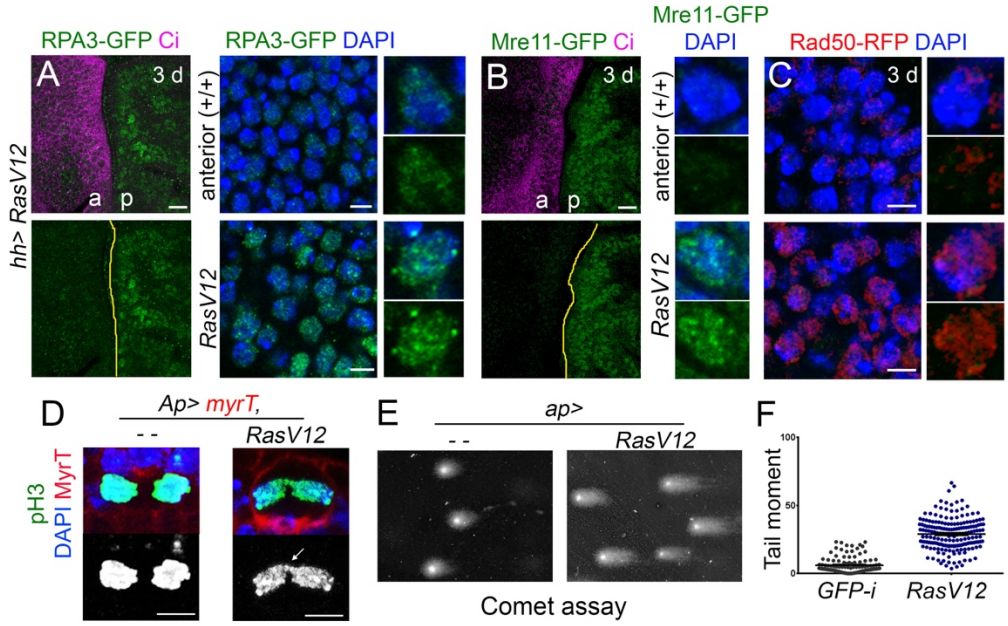

Figure 4. RasV12 expression generates DNA damage. (A-C) Third instar wing imaginal discs expressing RasV12 under the control of the hh-gal4 driver and carrying different dna damage fusion proteins, (A) RPA-GFP in green, (B) Mre11-GFP in green and (C) Rad50-GFP in red. Discs were stained for DAPI in blue and Ci in magenta, cells from the anterior compartment were used as a wild type control. (D) Mitotic pH3 (green or white) labelled cells from wing discs expressing GFP-i and RasV12 under the control of the ap-gal4 driver showing DNA bridges in RasV12 (white arrow). The percentage of chromosome bridges in RasV12 expressing cells (0,82±0,13; n=38) is significantly higher ($p<0,001$) than the one observed in wild type cells (0,096± 0,03; n=34). (E) Individual cells expressing GFP-i or RasV12 under the control of the ap-gal4 driver and subjected to comet assay. (F) scatter plot shows the tail moment (%Tail DNA x Tail Length) of over 200 cells per condition, GFP-I in black and RasV12 in blue.

Furthermore, we used the comet assay, a single cell electrophoresis technique that allows for direct DNA breaks visualization. We performed the comet assay in alkaline conditions thus detecting both single and double strand breaks. We observed an increase in the comet tail moment in RasV12 cells, reflecting increased DNA damage

(Fig 4E, F). This measurement is a combination of the length of the DNA tail that is formed, as well as the intensity of the tail which is a proxy of the amount of DNA.

In RasV12 expressing discs, we found a range of mitotic defects from lagging chromosomes, DNA bridges to uncondensed DNA, all of them signs of DNA damage and replicative stress. We closely monitored the presence of DNA bridges (Fig 4D) which is 10 times higher in RasV12 cells than in wild type although its frequency is still relatively low.

2.2 RasV12 blocks DNA damage signaling.

The most commonly used way to mark DNA damage is the phosphorylation of the histone 2 variant (H2Av), the only homologue in *Drosophila* of the mammalian histone variants H2AX and H2AZ.

Although we have seen that RasV12 cells carry high amounts of DNA damage (Fig 4), we couldn't detect any increase in H2Av phosphorylation in these cells (Fig 5A). Given this surprising result, we decided to challenge the cells with ionizing radiation, which is known to induce DNA double strand breaks and pH2Av marks. When we irradiated RasV12-expressing discs we could not detect any increase in H2Av phosphorylation (Fig 5B). These data, together with the fact that we observe recruitment of the early sensors of damage (Fig 4A-C), suggest that RasV12 might be acting at the level of the ATM and ATR kinases to impair the DNA damage response.

In *Drosophila* ovary cells, both ATM and ATR kinases have been shown to phosphorylate H2Av upon activation (Joyce et al., 2011). Indeed, when we deplete ATM or ATR in otherwise wild type wing imaginal discs and we irradiate them, producing DSBs, there is a decrease in H2Av phosphorylation (Fig 5D) similar to that observed in RasV12 cells (Fig 5B).

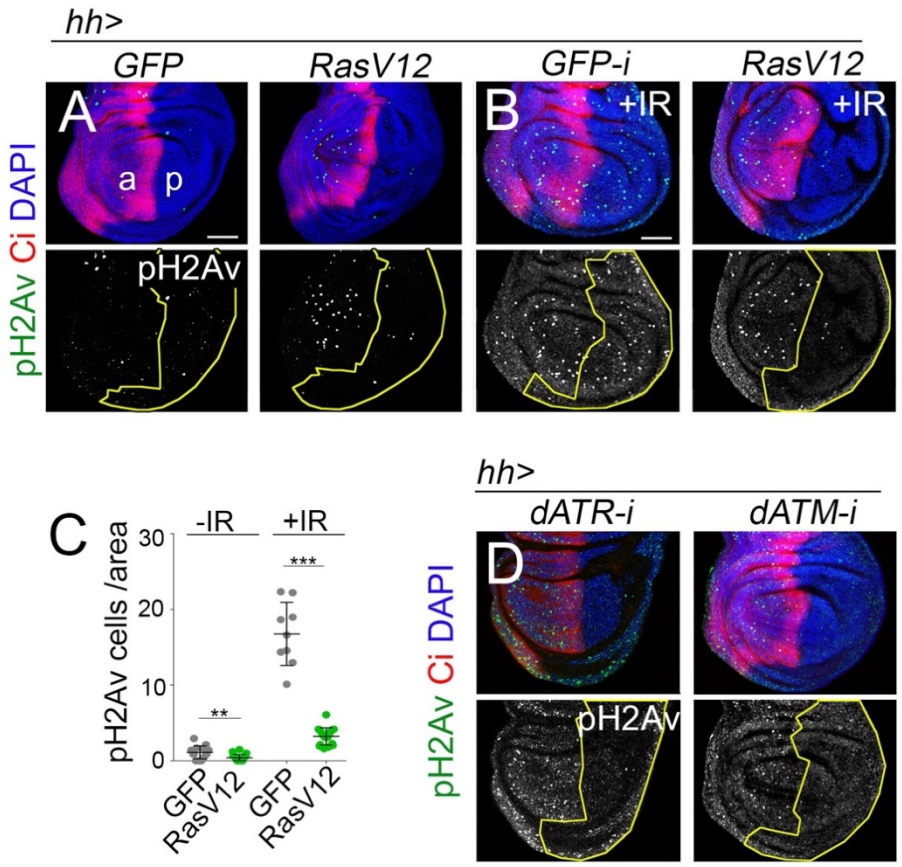

Figure 5. RasV12 and H2Av phosphorylation. (A,B,D) *Drosophila* wing imaginal discs expressing the different transgenes under the control of the hh-gal4 driver. Discs were stained with DAPI (blue), Ci (red) and pH2Av (green and white). (B,D) Discs were X-ray irradiated with a 40Gy dose and dissected 5 hours afterwards. (C) Quantification of A and depicting the amount of pH2Av positive cells per area, GFP-I in grey and RasV12 in green.

Then we decided to test if the lack of H2Av phosphorylation could be a trivial consequence of the depletion in H2Av levels. In order to do that, we overexpressed H2AV under its endogenous promoter or under the control of the GAL4/UAS system. In RasV12 discs co-expressing H2Av we did not observe any increase in pH2Av cells (Fig 6A, C). Upon irradiation of these discs, we could only detect a slight increase in H2Av phosphorylation in the case of the GAL4 driven expression of H2Av (Fig 6B, C).

Excluding the possibility of a general H2Av downregulation, the mechanism by which RasV12 cells regulate ATM and/or ATR activity remains still unresolved.

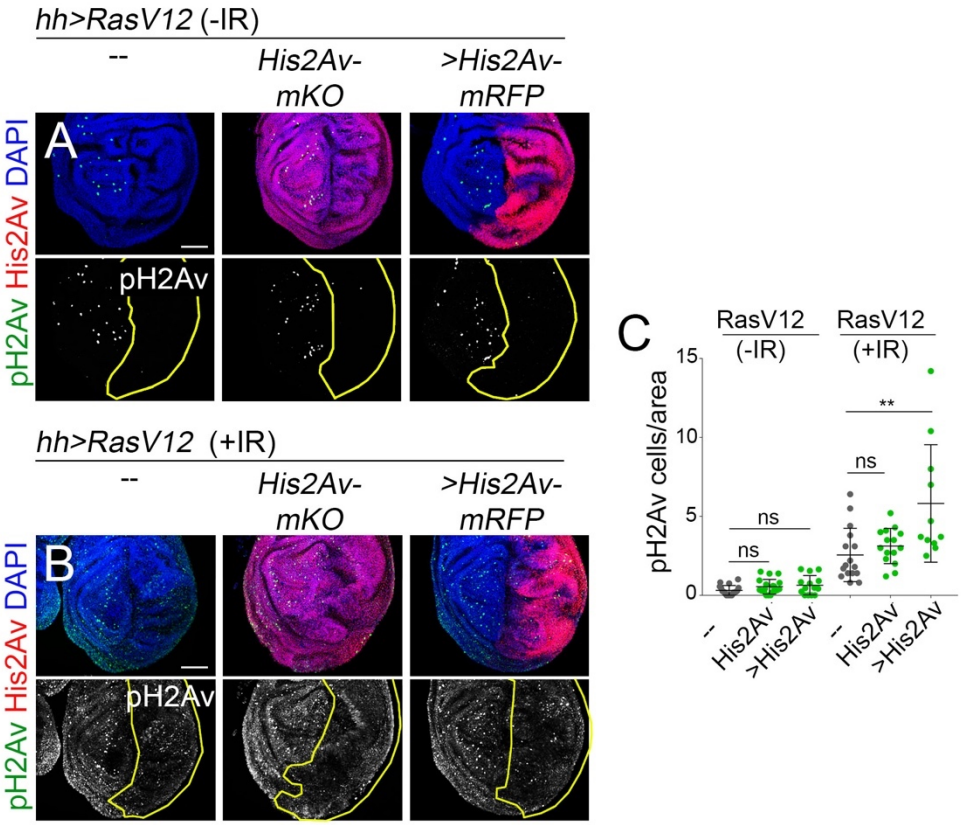

Figure 6. Histone 2A variant levels and phosphorylation. (A,B) Third instar wing discs expressing the indicated transgenes under the control of the hh-gal4 driver. His2Av transgenes are labelled in red with either mKO or mRFP, discs were stained for DAPI (Blue) and pH2AV (green and white). (B) Discs were X-ray irradiated with a 40Gy dose and dissected 5 hours afterwards. (C) Quantification of A and B depicting the amount of pH2Av positive cells per area, RasV12 controls in grey and RasV12 together with the his2Av transgenes in green.

2.2.1. RasV12 effects on checkpoint recovery.

After the DNA damage response has been activated, and it has fulfilled its function to block the cell cycle and allow for DNA repair, it has to be switched off in order to resume normal cell dynamics. This is a tightly regulated mechanism that depends on

the expression of different phosphatases that will dephosphorylate and inactivate several DDR proteins such as ATM, ATR or H2AV. However, it has also been shown that tumor cells can undergo checkpoint adaptation and resume cell cycle without resolving the DNA damage (Wang et al., 2015).

It is possible that RasV12 cells are undergoing a checkpoint adaptation process, thus explaining the lack of H2Av phosphorylation. In order to test this possibility, we depleted several known checkpoint phosphatases in RasV12 discs and analyzed its effect on H2Av phosphorylation. When we removed different subunits of protein

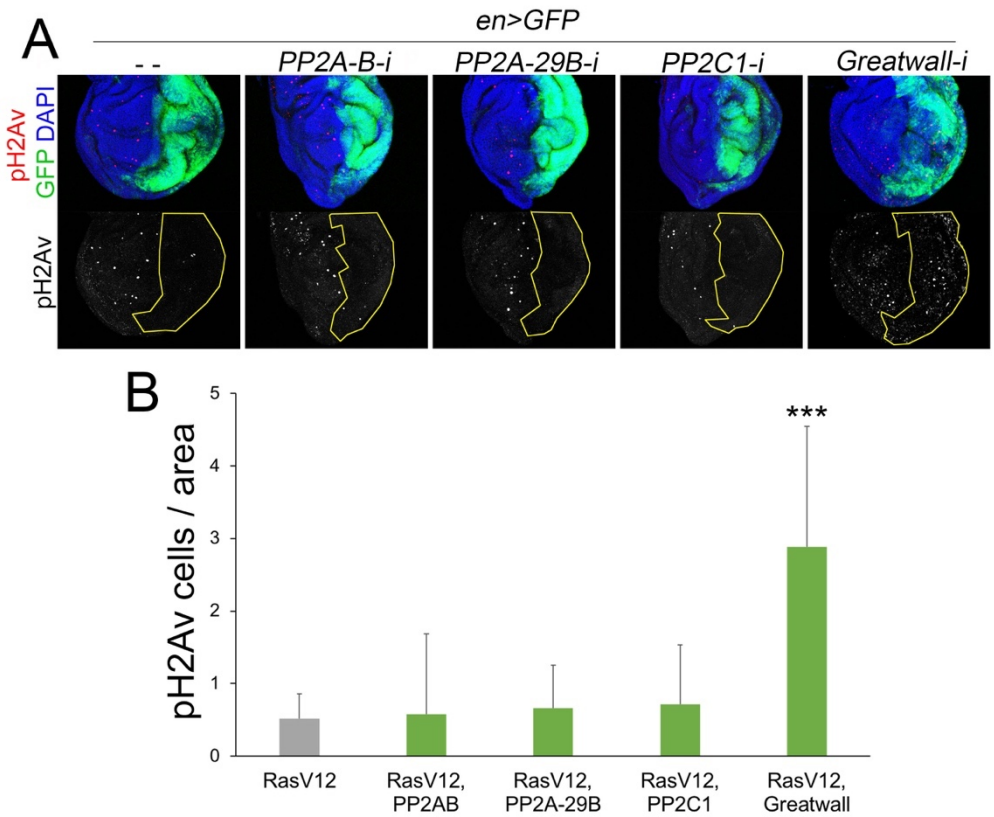

Figure 7. RasV12 and Checkpoint recovery kinases. (A) Third instar wing imaginal discs expressing the indicated transgenes under the control of the en-gal4 driver and stained for GFP (green), DAPI (blue) and pH2AV (red and white). Yellow lines outline the area of the posterior compartment. (B) Bar graph showing the quantification of the number of pH2Av positive cells in the posterior area.

phosphatase 2A or protein phosphatase 2C, we could not find any increase in H2AV phosphorylation (Fig 7A-B), suggesting that if there is checkpoint adaptation in RasV12 cells, it is not happening through any of these phosphatases. Depletion of Greatwall, a kinase involved in checkpoint adaptation, did give rise to increased pH2Av marks (Fig 7A-B). Unfortunately, that same effect was observed in wild type discs, discarding that the effect is specific for RasV12 cells.

2.3 RasV12 impairs the DNA damage response function.

Upon single stranded DNA breaks, RPA is recruited and ATR becomes phosphorylated and activated. Upon ATR activation, its target Chk1 is phosphorylated and activated to promote a G2 cell cycle arrest and allow for DNA repair (Bayer et al., 2018a).

Given the lack of ATM/ATR dependent H2Av phosphorylation, we decided to check for the activation status of ATR in RasV12 expressing tissues. In order to do that, we irradiated RasV12 and wild type tissues and measured the extent of the cell cycle arrest by counting the number of mitotic cells 5 hours after irradiation. The mitotic index in wildtype irradiated wing discs was clearly reduced when compared to non-irradiated wild type tissues (Fig 8A, C). However, in the case of RasV12 discs, this reduction in the mitotic index did not happen (Fig 8B, C), suggesting that the ATR mediated cell cycle arrest is impaired in RasV12 tissues.

Furthermore, when we expressed RNAi against ATR and Chk1 and irradiated the tissues, we observed a lack of an arrest in G2 similar to what we observe in RasV12 (Fig 8D).

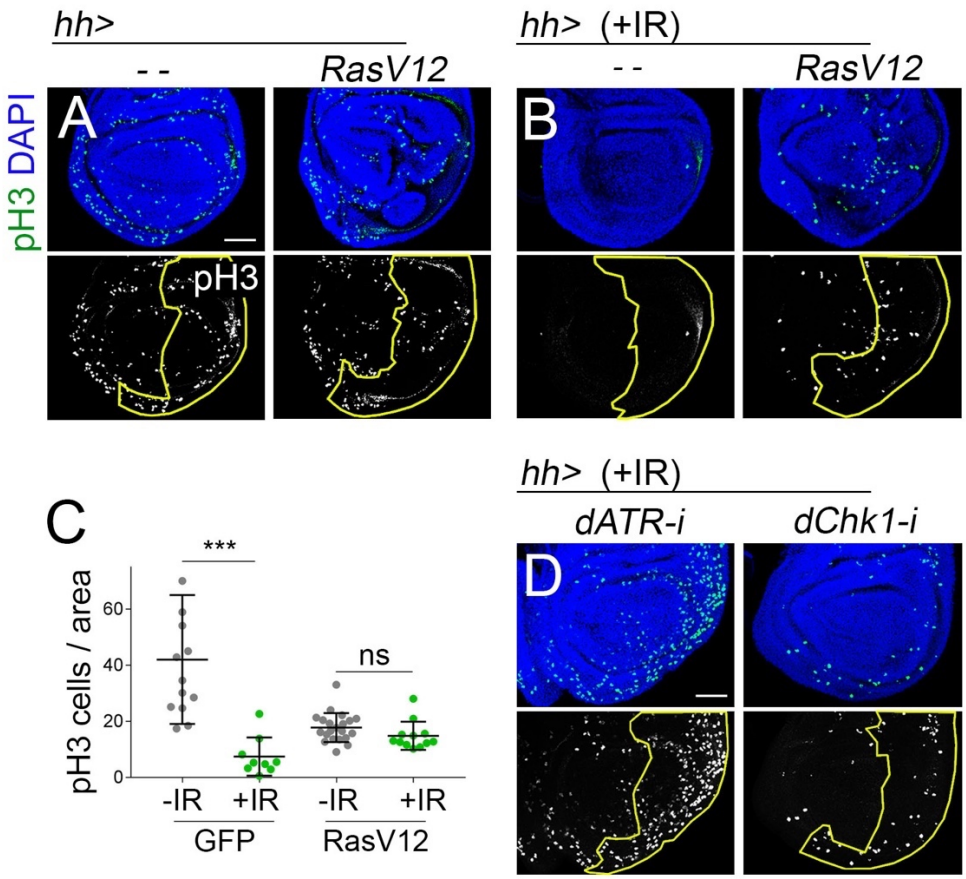

Figure 8. RasV12 and DNA damage induced cell cycle arrest. (A,B,D) Third instar lave wing discs expressing the indicated transgenes under the control of the hh-gal4 driver. Discs were stained for DAPI (blue) and pH3 (green and white). Discs in B and D were irradiated with a 40Gy dose and dissected 5h after. (C) Quantification of the amount of pH3 positive cells per area of A and B. Non-irradiated controls in gray and irradiated discs in green.

Given the fact that many of the RasV12 expressing cells are already in the G2 phase of the cell cycle, we wanted to discard the possibility that this arrest is a consequence of DNA damage and ATR/Chk1 activation. In order to do that, we expressed RNAi against mei-41/ATR and grapes/Chk1 together with RasV12, we dissociated the cells and FACS sorted them to analyze the cell cycle by DNA content analysis. In none of the cases did we observe an alleviation of the G2 arrest (Fig 9), indicating that it is

not dependent on ATR/Chk1. This is consistent with the previous results that indicate that ATR is blocked in RasV12 cells.

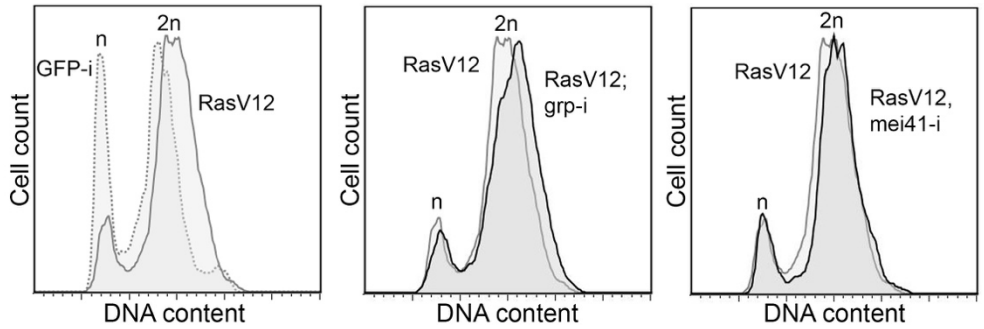

GFP-i	
G1	28,4
G2	64,6

RasV12	
G1	11,5
G2	87,7

RasV12;grp-i	
G1	10,2
G2	87,1

RasV12;mei41-i	
G1	11,7
G2	84,9

Figure 9. RasV12 G2 arrest is not dependent on ATR/Ch1 signaling. FACS sorted cells expressing the indicated transgenes under the control of the ap-gal4 driver, cells were selected based on myrTomato expression. Cell cycle analysis was performed according to DNA content labelled with DAPI.

2.5 Interaction between RasV12 and the DNA repair pathways.

We have shown that RasV12 cells have high levels of DNA damage derived from the replicative stress they suffer. We have observed both single and double strand breaks. DNA double strand breaks are normally recognized by the DDR and repaired by homologous recombination or non-homologous end joining depending on the phase of the cell cycle and the presence of a homologous template. However, we have observed that RasV12 cells present a deficient DNA damage response which leads to a deficient DNA repair. Considering the amount of damage that they carry, we wondered whether RasV12 cells may be dependent on other DNA damage repair pathways in order to cope with the presence of unresolved DNA breaks.

In order to test this possibility, we performed an RNAi screen for genes involved in the main DNA repair pathways, homologous recombination, non-homologous end joining, base excision repair, nucleotide excision repair, mismatch repair and the Fanconi anemia pathway each one of them involved in the repair of different types of DNA damage. Since H2Av phosphorylation is not a good proxy to DNA damage in our case, we decided to evaluate the growth of the RasV12 tissues depleted for different DNA repair proteins as a measure of the dependency of those tissues to the specific DNA repair pathways.

In most of the cases, we did not observe a significant difference in the growth capacity of the RasV12 tissue. However, for some genes we did find an increased growth, suggesting that, contrary to what we thought, different DNA repair pathways are slowing down tissue growth. Maybe these DNA repair pathways act by preventing the acquisition of new mutations that allow RasV12 cells to overcome their G2 arrest. Only in one case did we find a significant reduction in tissue growth, discouragingly another gene in the same pathway showed the opposite effect (Fig 10A).

Then, we evaluated the effects on tissue growth at the level of pathways instead of at the level of individual genes as before, to see if we could find any statistically significant trend. We found that the depletion of the FA, NER and NHEJ gave rise to an increase in tumor growth (Fig 10B), suggesting that, in general, the presence and activity of the different DNA repair pathways contribute to the stability of the tumor genome, thus imposing a break on tumor growth. The only exception was the mismatched repair pathway which shows a small although significant decrease in tissue size. The depletion of Homologous recombination or BER did not produce any effect. The lack of response to the depletion of homologous recombination genes, which should be the main repair pathway given the fact that most of the RasV12 cells

are in G2 phase, may be a consequence of the lack of ATR activity and consequent lack of HR repair.

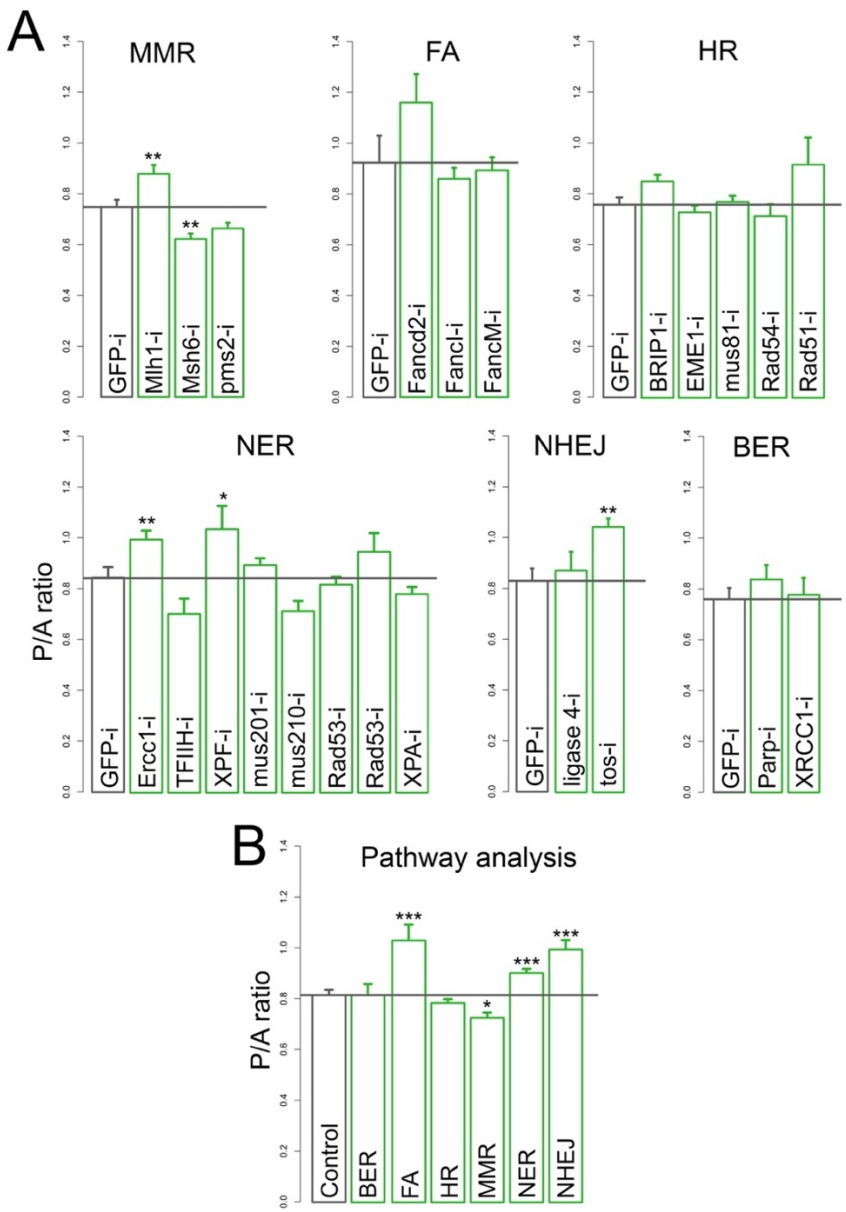

Figure 10. Interaction between RasV12 and different DNA damage repair pathways. (A) Graphs representing the growth of wing discs expressing RasV12 together with RNA-i for genes involved in different DNA repair pathways under the control of the hh-gal4 driver. The growth is expressed as the posterior to anterior size ratio. (B) Summary of the results grouped by repair pathway.

3. RasV12 and cell death.

The promotion of survival is one of the main downstream functions of Ras proteins. In *Drosophila* eye discs it has been shown that RasV12 can block apoptosis at the level of pro-apoptotic protein Hid through MAP kinase signaling (Bergmann et al., 1998; Kurada & White, 1998). Given the amount of DNA damage present on RasV12 tissues, we decided to investigate whether apoptosis was being induced in such tissues and whether Ras expression had an antiapoptotic role in our system.

3.1 RasV12 blocks cell death downstream of p53.

First, we monitored cell death upon cell cycle induction by overexpressing E2F, CycE, and RasV12 or depleting Rbf.

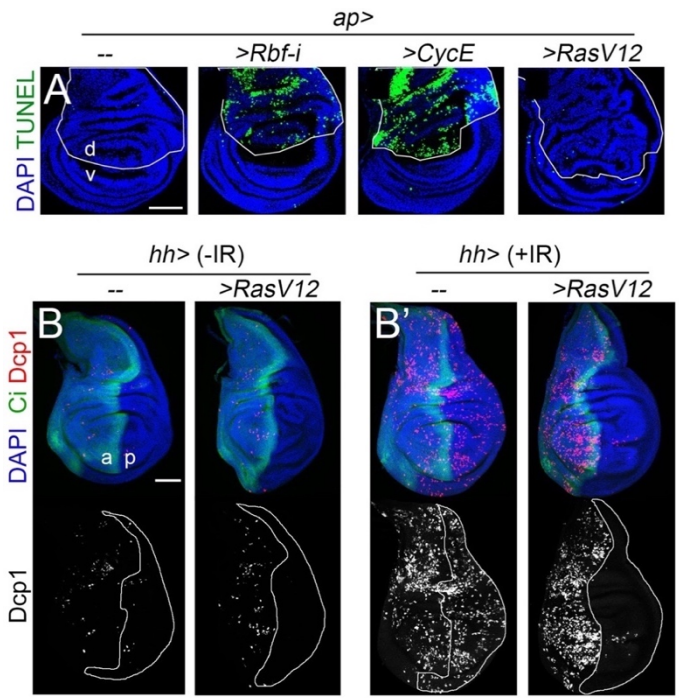

Figure 11. Cell cycle and IR induced apoptosis blocked in RasV12 discs. Wing imaginal discs expressing the indicated transgenes under the control of the ap-gal4 (A) or hh-gal4 driver (B, B'). Discs were stained for DAPI in blue (A-B') TUNEL in green (A) Ci in green (B,B') and Dcp1 in red and white (B,B'). Discs in B' were subjected to a 40Gy

dose of irradiation and dissected 5h after. (A-B') White lines indicate he are of transgene expression.

In all cases, except for RasV12 expressing cells, there was a significant induction of apoptosis as seen by TUNEL assay (Fig 11A), suggesting that RasV12 is indeed capable of blocking apoptosis induced by an accelerated G1/S transition. In order to see if this was a general response, we analyzed cell death by staining for the effector caspase Dcp-1 after irradiation of RasV12 tissues (Fig 11B-B'). Again, RasV12 is capable of completely blocking IR induced apoptosis.

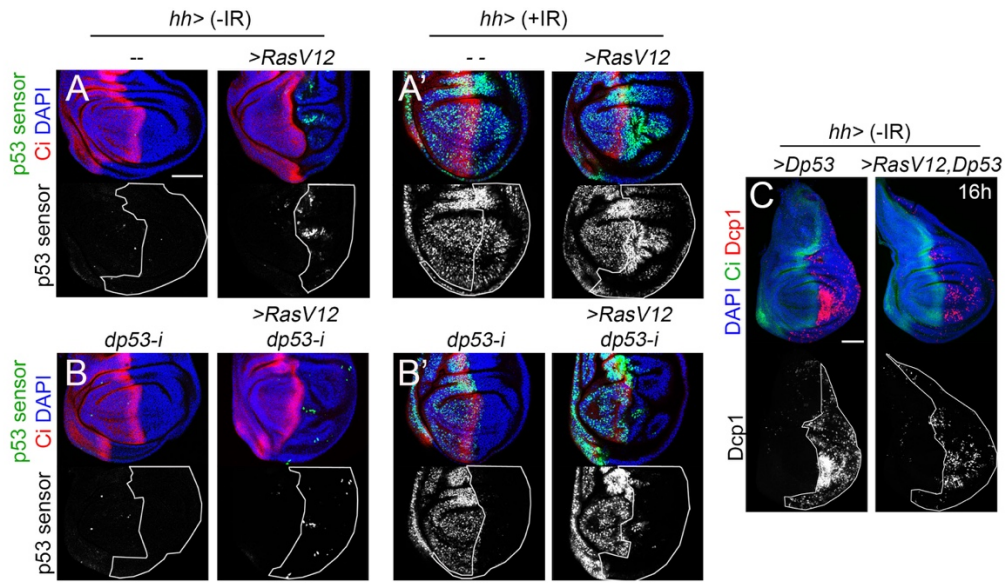

Figure 12. p53 activation in RasV12 discs. Third wing imaginal discs expressing the indicated transgenes under the control of the hh-gal4 driver for 3 days (A-B') or 16 hours (C). Discs were stained for Ci in red (A-B') and in green (C), for DAPI in blue (A-B') and dcp1 in red (C). Discs in A-B' were labelled in green with the expression of a p53 activity sensor based on the 5'hid regulatory region fused to GFP. Discs in A' and B' were subjected to 40Gy irradiation and dissected 5 hours after.

At this point, we wondered whether Dp53 was being activated by RasV12 expression. In order to test that, we used a Dp53 activity reporter that consists of the 5' region of the hid gene (Tanaka-Matakatsu et al., 2009) that responds to Dp53 (Fig 12 B-B'). Although the levels were not very high, we observed increased expression of the

Dp53 reporter upon RasV12 expression (Fig 12 A). Furthermore, when we irradiated these discs, there was a consistent upregulation of the reporter throughout the tissue, with the levels being higher in RasV12 cells (Fig 12 A'). Finally, we showed that RasV12 cells reduce cell death induced by Dp53 overexpression (Fig 12 C), indicating that RasV12 is blocking cell death downstream of Dp53.

3.2 ERK depletion in RasV12 tissues promotes cell death.

One of the main functions downstream of Ras is to promote cell survival. In the developing eye of *Drosophila,* it has been previously shown that RasV12 has an antiapoptotic role in preventing Eiger or Reaper induced cell death and that this antiapoptotic role depends on MAPK/ ERK signaling. Therefore, we wondered whether RasV12 was also blocking DNA damage-induced cell death through ERK signaling.

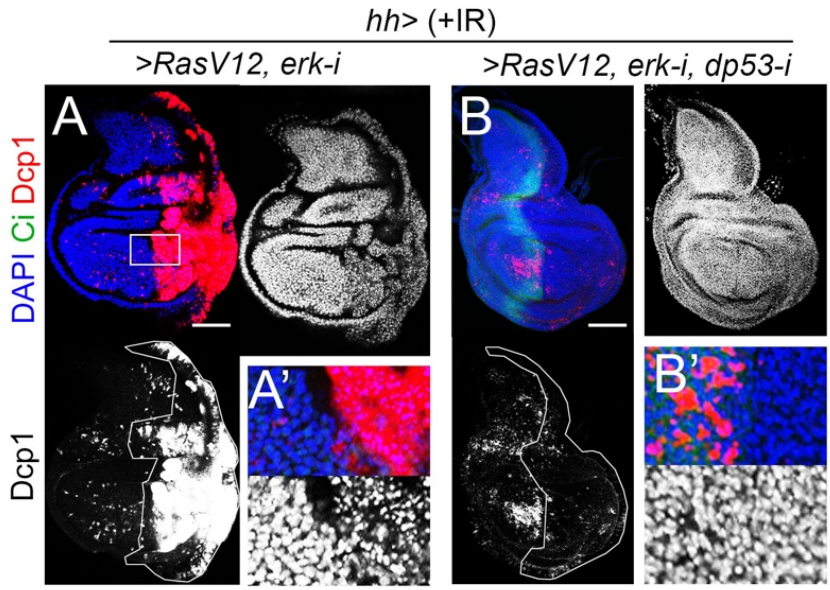

Figure 13. ERK prevents p53 induced cell death. (A-B) Wing imaginal discs expressing the indicated transgenes under the control of the hh-gal4 driver. (A', B') Magnification of the imaginal discs depicted in A and B respectively. Discs were irradiated with a 40Gy dosage, dissected 5 hours after and stained for DAPI (blue), Ci (green) and Dcp1 (red and white).

In order to test that, we depleted ERK in RasV12 expressing cells and irradiated them with a 40Gy dose to induce DNA damage. Unlike RasV12 cells, RasV12 cells depleted for ERK are extremely sensitive to irradiation-induced DNA damage and massively die by apoptosis (Fig 13 A-A'). Moreover, this IR-induced cell death is dependent on p53 activity, since co-depletion of ERK and p53 eliminates cell death in RasV12 discs (Fig 13 B-B').

3.3 RasV12 blocks apoptosis by transcriptional and post-transcriptional mechanisms.

Previous contrasting reports suggest that the RasV12-induced blockage of apoptosis can be achieved by either transcriptional regulation of the gene hid or by the ERK-mediated phosphorylation of hid protein (Bergmann et al., 1998; Kurada & White, 1998).

In order to elucidate if either of these two mechanisms applies in our case, we first depleted the Ets transcription factor Pointed which acts downstream of ERK. Upon depletion of pointed alone or in combination with RasV12 expression, we did not detect any increase in cell death (Fig 14 A). However, when we irradiated those discs we observed an increase in Dcp1 labelled cells specially in RasV12 tissues when compared to pointed-i irradiated cells (Fig 14 A') but not as high as in RasV12 ERK depleted cells (Fig 13 A). These results suggest that ERK can act through activation of pointed in order to regulate gene expression and promote survival of the cells. Whether this effect is mediated by hid or not remains to be explored.

To test the possible posttranscriptional regulation of apoptosis by ERK, we depleted KSR, a scaffolding protein that is responsible for sustaining ERK cytoplasmic activity (Casar, Pinto, & Crespo, 2008). Upon KSR depletion we did not observe any increase in cell death (Fig 14 B). However, upon irradiation, there was an increase in the

amount of dcp1 labelled cells both in wild type and RasV12 expressing cells (Fig 14 B'). These results indicate that ERK cytoplasmic activity plays a role in posttranscriptional modifications that inhibit apoptosis and promote survival. Again, we have not explored whether this effect is mediated by hid or not.

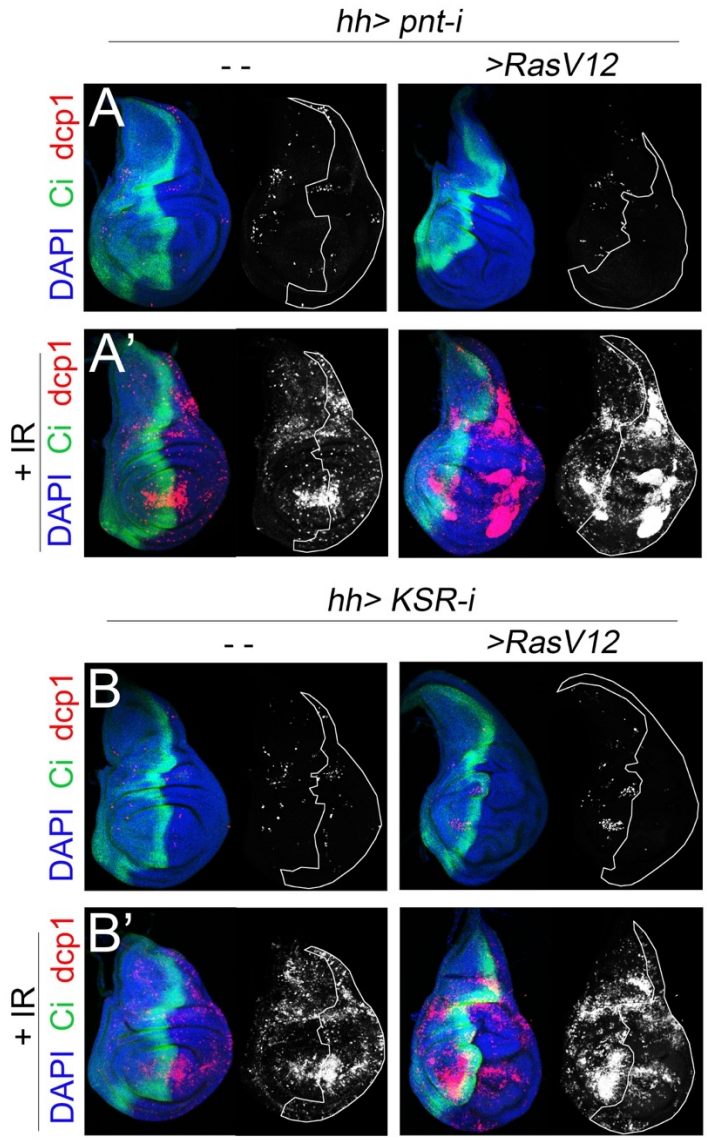

Figure 14. Mechanisms of ERK dependent apoptosis inhibition. (A-B') Third instar wing imaginal discs expressing the indicated transgenes under the control of the hh-gal4 driver. Discs in A' and B' were subjected to a 40Gy irradiation and dissected 5 hours after. All wing discs were stained for DAPI (blue), Ci (green) and Dcp1 (red and white).

Together, both results indicate that upon *RasV12* expression and ERK activation apoptosis can be blocked by different means involving both transcriptional and posttranscriptional changes.

4. Homeostatic effects of ERK signaling in response to irradiation.

We observed that RasV12 tissues promote survival to irradiation via the activation of ERK signaling. We wondered whether this mechanism was also acting in wild type tissues to promote survival of irradiated cells and to maintain tissue homeostasis.

4.1 ERK activation in response to irradiation.

First, we wondered if ERK was activated upon irradiation. To test that, we subjected wild type discs to irradiation and measured the mean intensity of pERK, the active form of ERK.

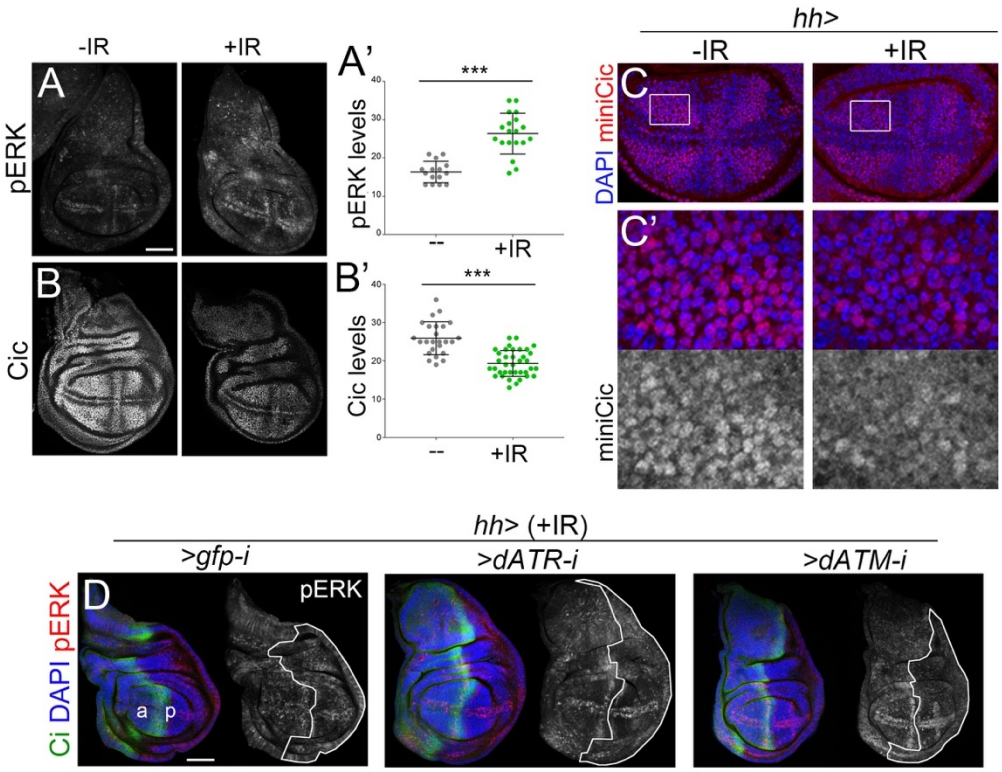

Figure 15. IR induced ERK activation. (A,B,C-D)Third instar wing discs stained for pERK (A,D, white), Capicua (B, white), DAPI (C-D, blue) and Ci (D, green). (C) Discs carry the mini-cic reporter of ERK activity which gets delocalized from the nucleus upon ERK

activation. Discs in A,B,C (right panel) and D were irradiated with a 40Gy dose. (A', B') quantification of the mean intensity levels of pERK (A') and Cic (B') throughout the disc.

We observed a significant increase in pERK mean intensity upon irradiation compared to non-irradiated discs (Fig 15 A-A'). We also measured the mean intensity of Capicua, a transcriptional repressor that is targeted for degradation upon ERK activation. Consistent with an ERK activation, the levels of Capicua were significantly decreased upon irradiation (Fig 15 B-B'). We used a mini-cic reporter that gets delocalized from the nucleus upon ERK activation (Moreno et al., 2019) to further confirm ERK activation upon irradiation (Fig 15 C-C'). Then we decided to test if the irradiation induced ERK activation is dependent on the activity of the DNA damage response. We depleted ATM and

ATR in the posterior compartment of the discs and then irradiated them; we used the anterior compartment as an internal wild type control. In doing so, we did not find any difference in pERK levels between anterior and posterior compartments of depleted discs and neither with mock GFP depleted discs (Fig 15 D) indicating that ERK activation is independent of the DDR.

On the other hand, we tested whether ERK activation had any role in the DNA damage response. We did not find any difference in H2Av phosphorylation between wild type and ERK depleted cells upon irradiation (Fig 16 A). Similarly, we could not detect any difference in the induction of G2 arrest (Fig 16 B, C), indicating that endogenous ERK levels do not play a role in the activation of the DDR upon irradiation.

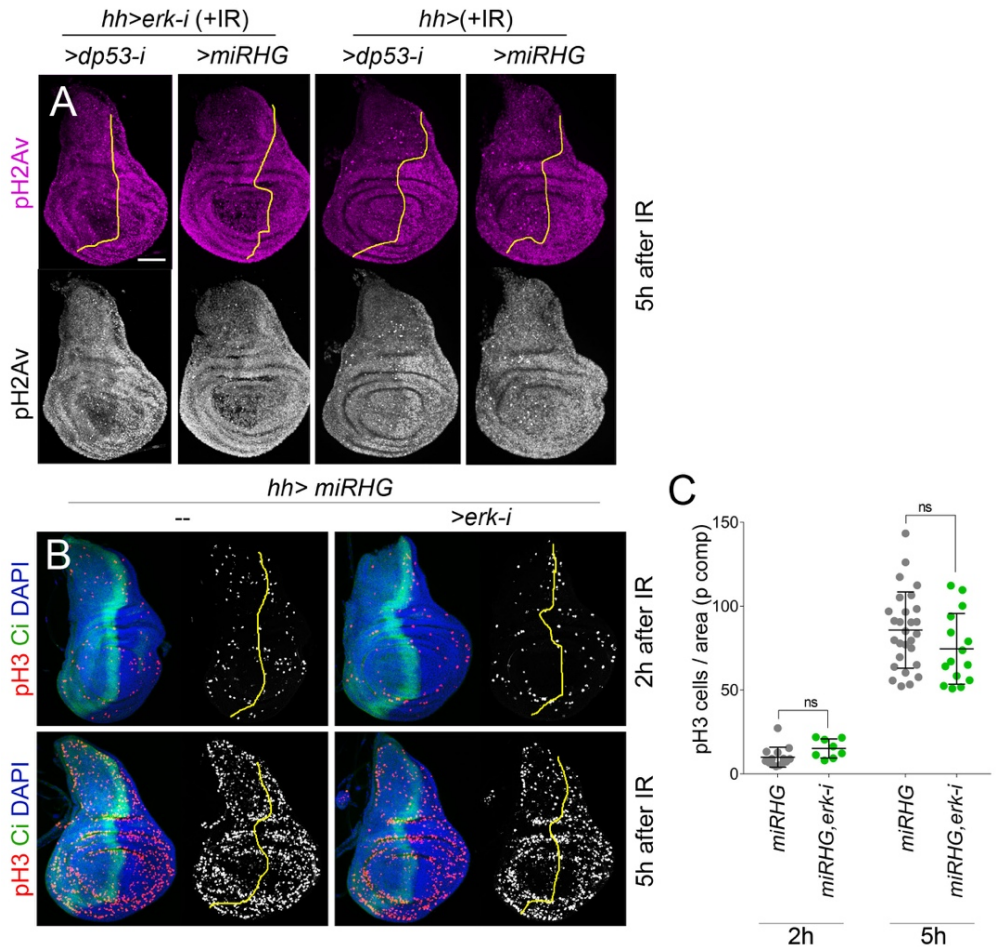

Figure 16. Role of ERK on the DNA damage response. (A, B) Third instar wing imaginal discs expressing the indicated transgenes under the control of the hh-gal4 driver. Discs in A (left panels) and B were irradiated at 40 Gy and dissected 2 or 5 hours after irradiation. (A) discs stained for pH2Av in magenta and white. (B) Discs stained for pH3 in red, Ci in green and DAPI in blue. (C) Scatter plot showing the mitotic pH3 positive cells per area. Individual values, mean and standard deviation are represented

Once we saw that ERK is activated by irradiation, we checked whether ERK depletion would promote cell death with and without irradiation. In both cases, there was increased apoptosis. However, the number of apoptotic cells marked by Dcp1 staining was much higher upon irradiation treatment (Fig 17 A-B). Furthermore, cell death could be rescued by Dp53 depletion (Fig 17 C) or the expression of a microRNA that targets the three *Drosophila* proapoptotic genes hid, reaper and grim

(Fig 17 D). Moreover, we found that p53 activity was not affected by ERK depletion suggesting that ERK is acting downstream of p53 (Fig 17 E).

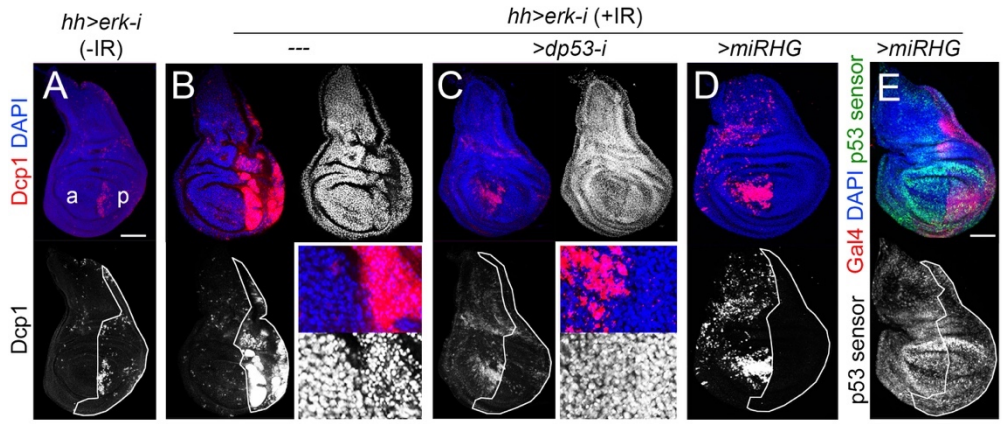

Figure 17. ERK antiapoptotic signaling. (A-D) Third instar wing imaginal discs expressing the indicated transgenes under the control of the hh-gal4 driver. Discs were stained for DAPI (Blue and white) and dcp1 (red and white). (E) Discs labelled with DAPI (blue), Gal4 (red) and p53 activity sensor (green and white). (B-E) Discs were irradiated at 40Gy and dissected 5 h after.

Given the homeostatic role of ERK in response to irradiation, we decided to check if ERK activation could have a role in a developmentally controlled setting. We used the elav-Gal4, Tub-Gal80ts driver in order to express the transgenes in the differentiated photoreceptor cells of the eye disc. Upon ERK depletion, we found a quite strong reduction in the eye size, uncovering a pro-survival role of ERK during a developmentally regulated process. In order to quantitatively compare different phenotypes, we elaborated a phenotypic classification that allowed us to quantify the percentage of each phenotype according to their severity, ranging from strong to normal/ wild type like (Fig 18 A). As previously shown, Dp53 depletion and miRHG expression lead to a rescue of the eye ERK reduced size even back to normal proportions (Fig 18 B). However, we never get a 100% rescue reflecting the role of MAPK-ERK signaling in photoreceptor development.

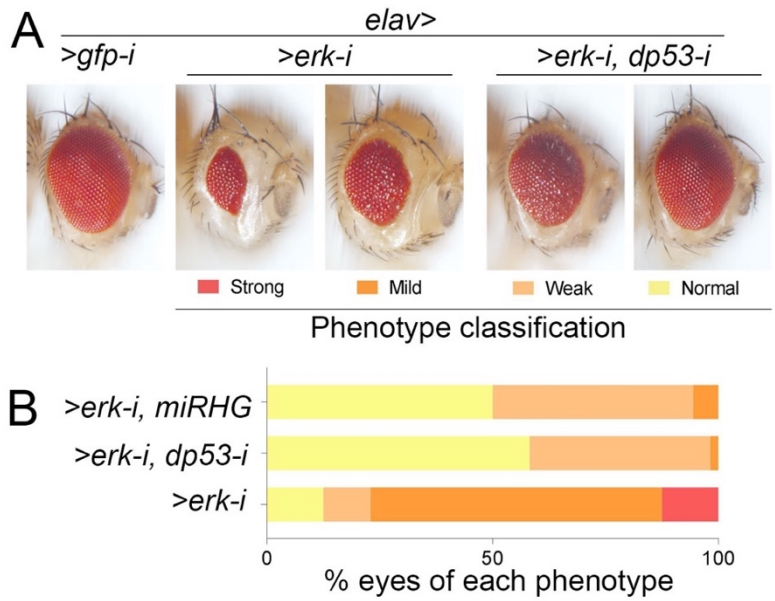

Figure 18. Endogenous role of ERK in preventing apoptosis. (A) Adult eyes of male flies expressing the indicated transgenes under the control of the elav-gal4 driver. Each fly is a representative image of the phenotypic divisions that we made in order to quantify the degree of the effect. (B) Quantification of the % of each eye phenotype in the given genotype with the following n: erk-i (n=60) , erk-i, p53-i (n=312), erk-I, miRHG (n=136).

5. Selective killing of RasV12 cells.

Given its unique nature, Ras is known as the undruggable oncogene. Most common oncogenic Ras mutations actually interfere with its enzymatic activity, inhibiting its capacity to hydrolyze GTP, thus rendering them in a constitutively active state (Pylayeva-Gupta et al., 2011). Directly blocking Ras has proven very challenging, therefore many of the strategies to block Ras have been to directed to target the downstream signaling pathways such as MAPK and PI3K. Unfortunately, many of these have failed due to the capacity of these cells to bypass this blockade and become resistant to therapy. Another strategy has been to try to exploit tumor cell dependencies in order to find synthetic lethal interactions that can specifically affect and kill tumor cells rather than wild type ones. On that note, we wondered whether we could take advantage of the intrinsic replicative stress and DNA damage found in RasV12 cells and their dependency on ERK signaling to survive, in order to selectively kill these cells.

5.1 Genetic ERK inhibition.

Our first strategy consisted of the combination of genetic ERK depletion together with ionizing irradiation. Given the fact that ERK has a homeostatic role in radioresistance of wild type cells as well, we had to establish a selective range of irradiation. To do that, we decided to test different doses of irradiation in order to find one that would synergize with the endogenous to RasV12-induced DNA damage but would not affect the wild type cells.

We found that upon ERK depletion, RasV12 cells were sensitized to all the different doses of irradiation (Fig 19 A, quantification in B, blue lines). However, only at intermediate (16Gy) and high (24Gy) levels of irradiation RasV12 cells showed higher levels of apoptosis than wild type ERK depleted cells (Fig 19 A, quantification in B,

red lines). These results suggest that there might be a therapeutic opportunity for the combination of ERK depletion and irradiation to treat Ras activated tumors.

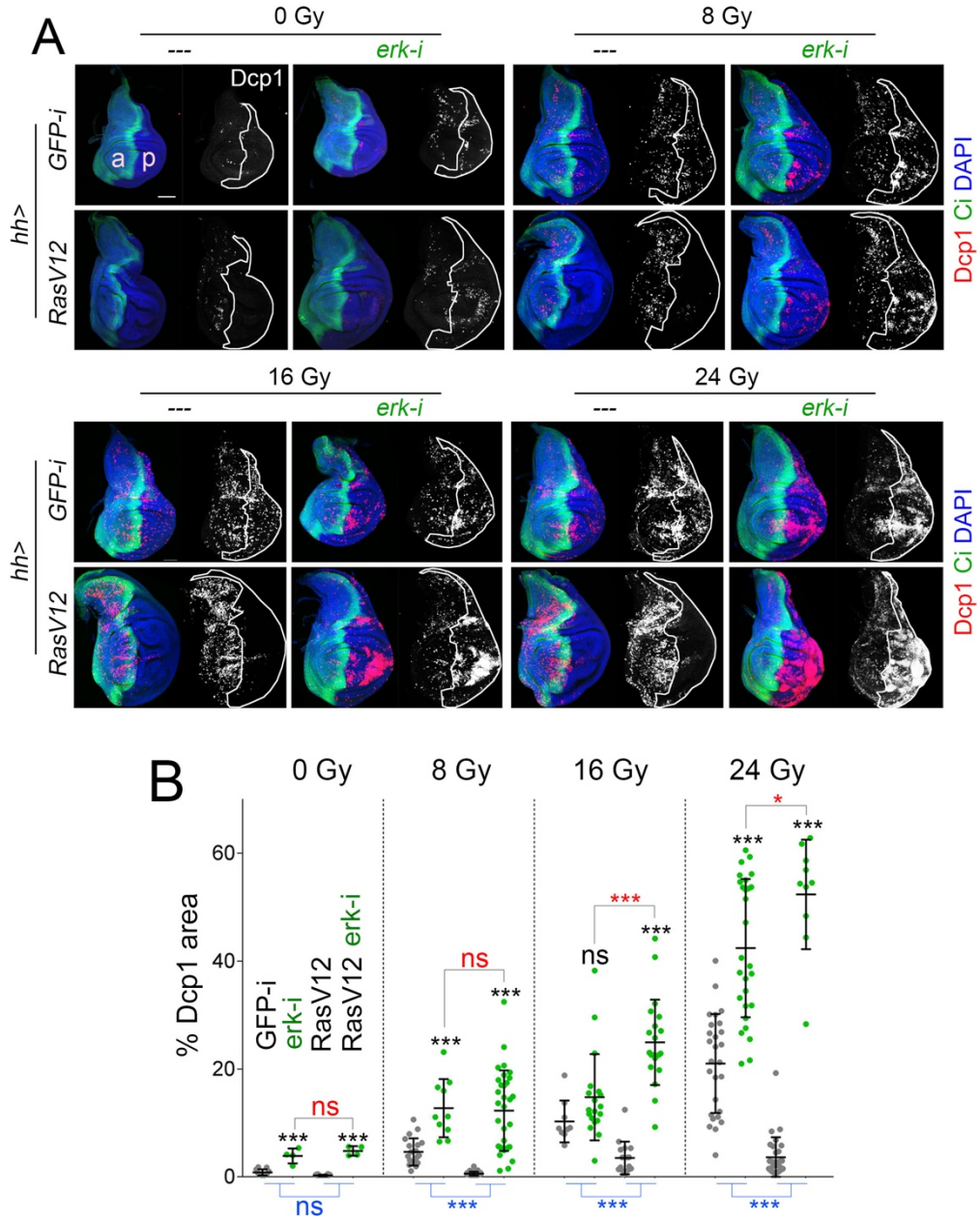

Figure 19. Radiosensitivty of ERK depleted RasV12 cells. (A) Wing imaginal discs expressing the indicated transgenes under the control of the hh-gal4 driver and subjected to different doses of irradiation. Discs were stained for DAPI (blue), Ci (green) and Dcp1 (red and white). (B) Scatter plot showing the quantification of the percentage of posterior

area that is covered by Dcp1 of the discs in A. Average, SD and individual wig disc measurements are shown. Statistically significant differences based on Student's t-test are indicated in black and red. Comparisons of differences (in blue) were performed to quantify the differences in the radiosensitivity of RasV12 vs wild type tissues upon ERK depletion.

We propose that the sensitivity of ERK depleted RasV12 cells to irradiation is due to the high levels of DNA damage that they carry as a consequence of their aberrant cell cycle progression. Both MAPK and Pi3K signaling pathways have been shown to promote cell proliferation via induction of G1/S transition (David A Prober & Edgar, 2002). After ERK depletion the MAPK pathway would be shut down leaving Pi3K signaling to promote proliferation. We wondered whether Pi3K signaling was necessary for the sensitivity of RasV12 cells to ERK depletion. Indeed, when we co-depleted ERK and Pi3K at the same time, there was a significant rescue of the cell death induced after a 16 Gy dose of irradiation (Fig 20 A-B).

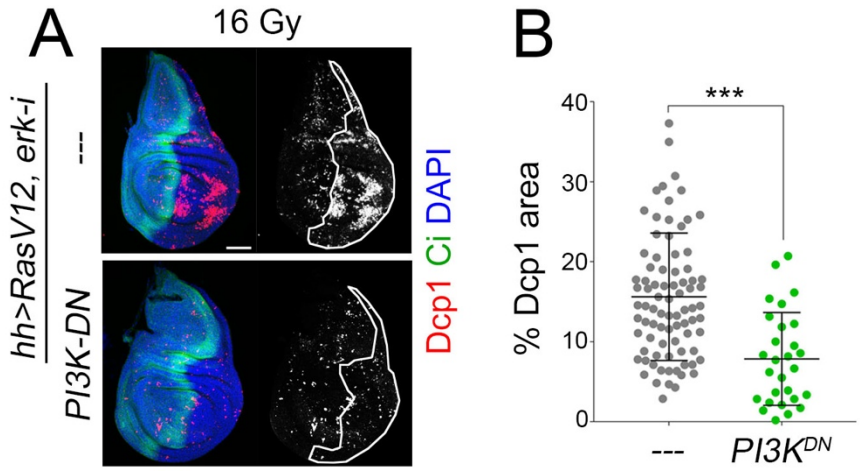

Figure 20. PI3K in RasV12 radiosensitivity. (A) Wing imaginal discs expressing the indicated transgenes under the control of the hh-gal4 driver, stained for DApI (blue), Ci (green) and Dcp1 (red and white) and dissected 5 hours after a 16 Gy irradiation dosage. (B) Scatter plot quantifying the percentage of posterior area that is covered by Dcp1; Mean, SD and individual values are represented. Student's t-test was used to test for statistical significance.

As a control, we checked that both ERK and AKT phosphorylation are actually increased upon RasV12 expression (Fig 21 C, C'). The ERK RNAi used to deplete ERK was capable of reducing pERK staining both in wild type and RasV12 cells when compared to control discs (Fig 21 A, B, D) but not pAKT (Fig 21 A', B', D'). In discs expressing ERK-i and a dominant negative form of PI3K there was a decrease in both pERK and pAKT.

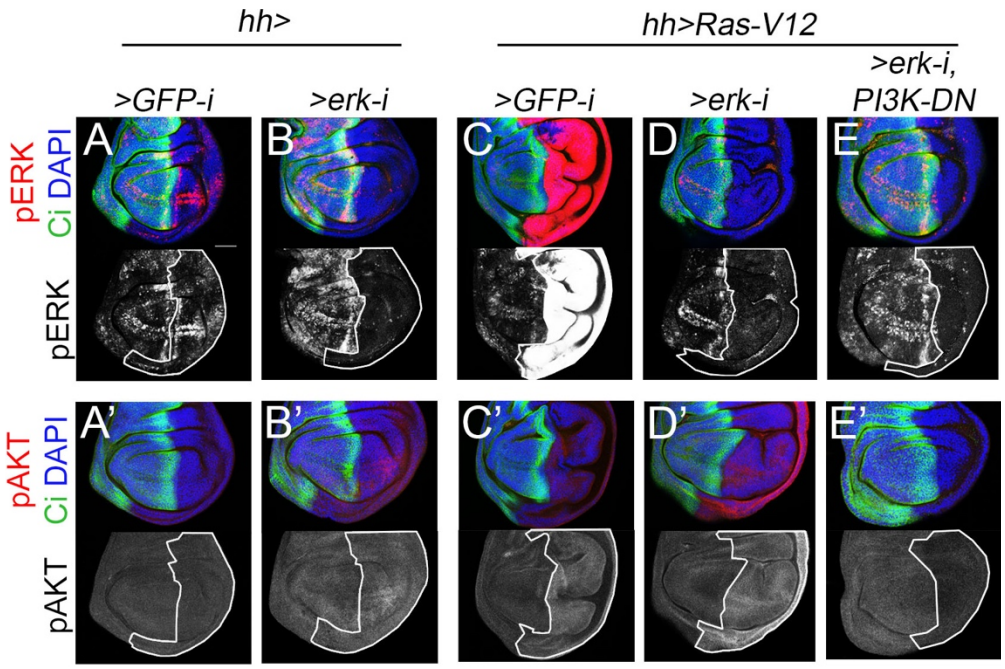

Figure 21. ERK-i and PI3K-DN deplete ERK and PI3K levels. (A-E') Wing imaginal discs expressing the indicated transgenes under the control of the hh-gal4 driver. Discs were stained for DAPI in blue and (A-E'), Ci in green (A-E'), pERK in red and white (A-E) and pAKT in red and white (A'-E'). White lines indicate the area of transgene expression.

Given the success in radiosensitizing RasV12 cells by genetic ERK depletion, we decided to try this same strategy against a more aggressive RasV12 driven tumor model. In order to do that, we took advantage of the already established and well-known RasV12, Scribble model. These tumors rely on the overexpression of RasV12 together with the depletion of the polarity determinant Scribble, producing highly

proliferative tissues presenting malignant characteristics such as developmental delay and invasive capacity (Brumby & Richardson, 2003; Pagliarini & Xu, 2003).

Excitingly, we were capable of inducing apoptosis of the *RasV12, scrib-i* cells by genetically depleting ERK in combination with different doses of ionizing radiation (Fig 22 A, quantification in B, comparison in black). However, the extent of this apoptosis is always lower than in wild type ERK depleted cells (Fig 22 B, comparison in red) making *RasV12, scrib-i* cells less radiosensitive than wild type (Fig 22 B, comparison in blue).

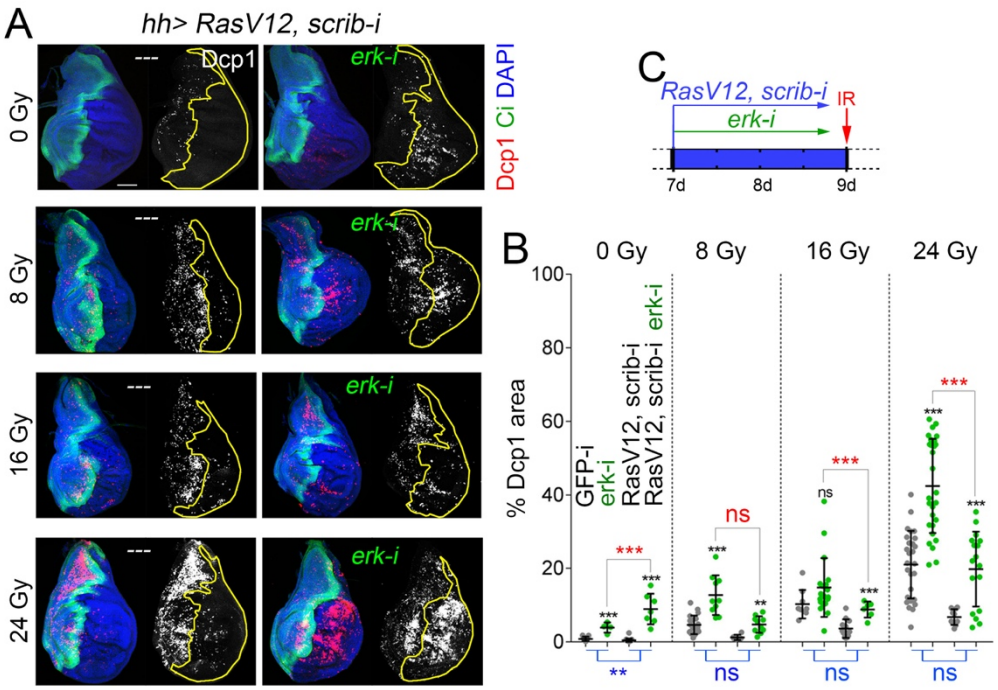

Figure 22. Genetic ERK depletion in Ras,scrib-i neoplasic tumors. (A) Third instar wing imaginal discs expressing the indicated transgenes under the control of the hh-gal4 driver, control (left panels) and ERK depleted (right panels). (B) Scatter plot showing the quantification of the percentage of posterior area that is covered by Dcp1 of the discs in A. Average, SD and individual wig disc measurements are shown. Statistically significant differences based on Student's t-test are indicated in black and red. Comparisons of differences (in blue) were performed to quantify the differences in the radiosensitivity of RasV12, scrib-i vs wild type tissues upon RNAi mediated ERK depletion.

This lack of specific radiosensitivity could be explained in different ways. On the one hand, it is possible that emerging properties of RasV12, scrib-i tumors make them more resistant to cell death than RasV12 tumors. On the other hand, it could be a consequence of the timing of transgene expression. We induce the tumor and deplete ERK at the same time without giving time for the tumors to form (Fig 22 C). In order to avoid this second possibility, we decided to move to a chemical method of ERK inhibition, that allows us to uncouple tumor formation and ERK depletion.

5.2 Chemical ERK inhibition.

Trametinib is a highly selective allosteric inhibitor of MEK1 and MEK2 proteins. It prevents RAF-mediated MEK phosphorylation and activation, thus blocking ERK activation (Gilmartin et al., 2011; Sakai et al., 2011). We chose Trametinib as ERK inhibitor because it is an already FDA approved drug for the treatment of metastatic melanoma (Flaherty et al., 2012) and is currently under clinical trial for its use in other types of cancer.

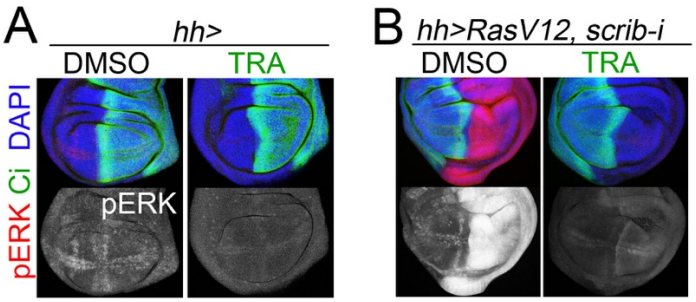

Figure 23. Trametinib is efficient in inhibiting ERK activation both in wild type and RasV12, scrib-i discs. (A-B) third instar wing imaginal discs expressing the indicated transgenes under the control of the hh-gal4 driver. Discs were treated with either DMSO or trametinib at 2μM concentrations and stained for DAPI (blue), Ci (green) and pERK (red and white).

Although previous reports showed the efficacy of trametinib in inhibiting ERK phosphorylation and activation, via western blot, at similar concentrations as we use, the exposure time was much longer (Levine & Cagan, 2016; Song et al., 2019). Therefore, we decided to test the efficacy of trametinib in our model. When we subjected *wild type* and *RasV12, scrib-i* larvae to 2 days of Trametinib treatment, we observed a vast reduction in pERK levels detected by immunostaining (Fig 23 A, B).

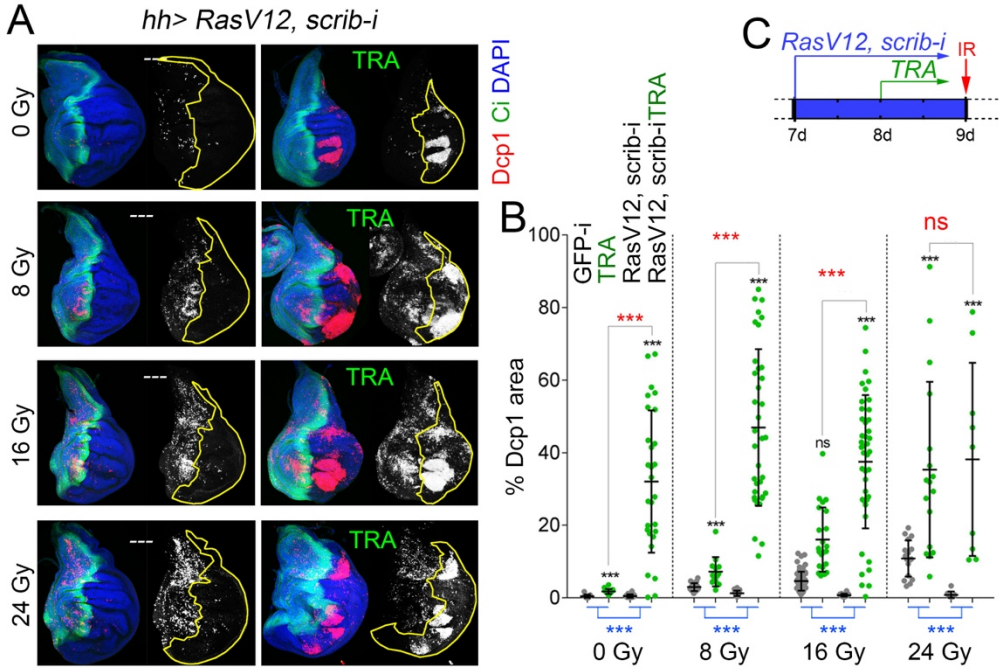

Figure 24. Chemical ERK depletion in Ras,scrib-i neoplasic tumors. (A) Third instar wing imaginal discs expressing the indicated transgenes under the control of the hh-gal4 driver, DMSO control (left panels) or trametinib treated (right panels). (B) Scatter plot showing the quantification of the percentage of posterior area that is covered by Dcp1 of the discs in A. Average, SD and individual wig disc measurements are shown. Statistically significant differences based on Student's t-test are indicated in black and red. Comparisons of differences (in blue) were performed to quantify the differences in the radiosensitivity of RasV12, scrib-i vs wild type tissues upon chemical ERK depletion.

We fed RasV12, scrib-i larvae with food containing either DMSO or Trametinib at a 2μM concentration 1 day after the initiation of transgene expression (Fig 24 C). In

order to assess the interaction between Trametinib treatment and irradiation, larvae were exposed to different doses of ionizing radiation two days after the initiation of Trametinib treatment. Wing discs expressing *RasV12, scrib-i* and treated with Trametinib were more sensitive to low and intermediate doses of irradiation that wild type cells but not at high doses (Fig 24 A, B comparisons in red).

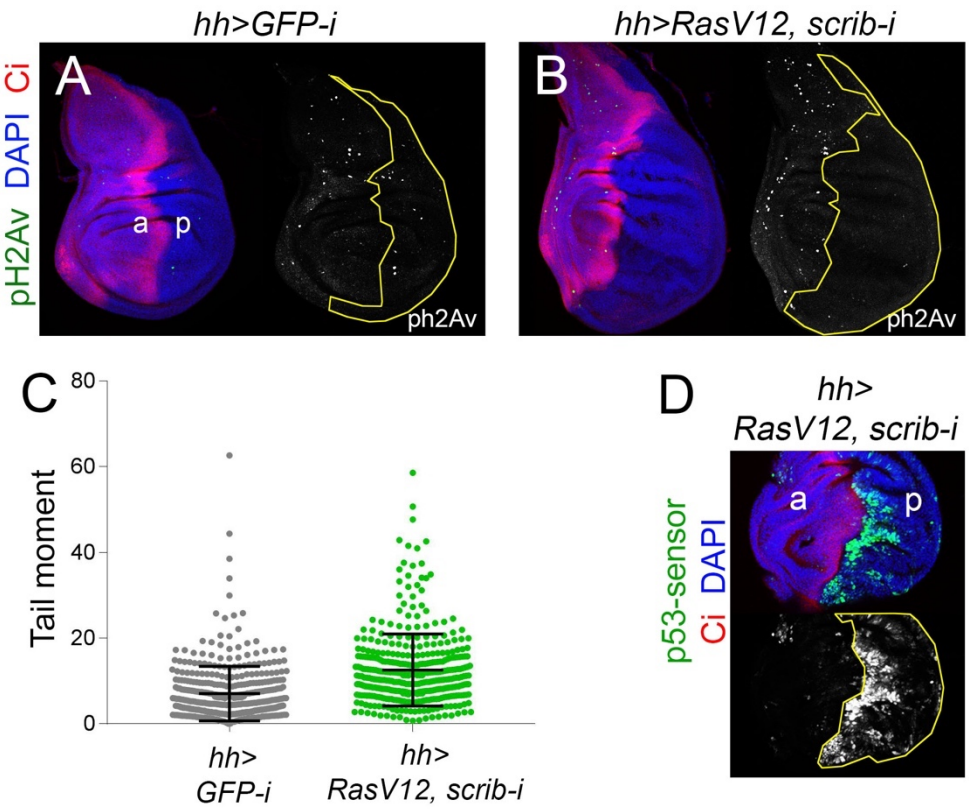

Figure 25. p53 activity and DNA damage in RasV2,scrib-i wing imaginal discs. (A,B,D) Third instar wing imaginal discs expressing the indicated transgenes under the control of the hh-gal4 driver and stained for (A,B,D) DAPI in blue, Ci in red and (A,B) pH2AV in green and white. Discs in D are labelled in green and white by a p53 activity sensor. (C) Scatter plot shows comet assay quantification in terms of the tail moment (%Tail DNA x Tail Length) of over 200 cells per condition, GFP-i in gray and RasV12,scrib-i in green.

Surprisingly, the sole action of Trametinib was also capable of inducing cell death in *RasV12, scrib-i* discs (Fig 24 A, B comparisons in black). It has been shown that these tumors activate proapoptotic Jun kinase signaling (Igaki et al., 2006). Furthermore,

these cells present high levels of DNA damage (Fig 25 C) but fail to induce H2Av phosphorylation (Fig 25 A-B). We also observed an increased p53 activity (Fig 25 D) when compared to RasV12 alone wing discs (Fig 12 A). Altogether these data point to the possibility that *RasV12, scrib-i* discs are under much higher apoptotic pressure, making them very sensitive to chemical inhibition of ERK signaling once the tumor has been formed.

5.3 Targeting malignant Ras dependent tumors.

Clonal induction of tumor growth is a more accurate representation of the tumorigenic process where most probably a single cell acquires a mutation that makes it highly proliferative leading to tumor initiation.

In that regard, clonal expression of RasV12 together with scribble homozygous mutations has extensively been used to model different characteristics of tumor growth, such as the capacity of these tumors to invade neighboring tissues (Uhlirova & Bohmann, 2006b), the induction of systemic effects such as cachexia (Figueroa-Clarevega & Bilder, 2015) or developmental delay of pupariation. We have taken advantage of this clonal model to evaluate, not only, the proapoptotic effects of Trametinib treatment, but also, its effects on tumor growth and at the whole larva level.

In order to evaluate the effect of Trametinib in tumor growth, 4 days old early L3 *RasV12, scrib*$^{-/-}$ larvae were fed with 2μM DMSO or Trametinib. Then, 2, 4, 6 or 8 days after Trametinib treatment initiation, larvae were removed from the food (Fig 26 A) and imaged to evaluate tumor burden (Fig 26 B). DMSO treated larvae showed a rapid increase in tumor burden over time while Trametinib treated larvae showed a very much reduced and more constant tumor burden.

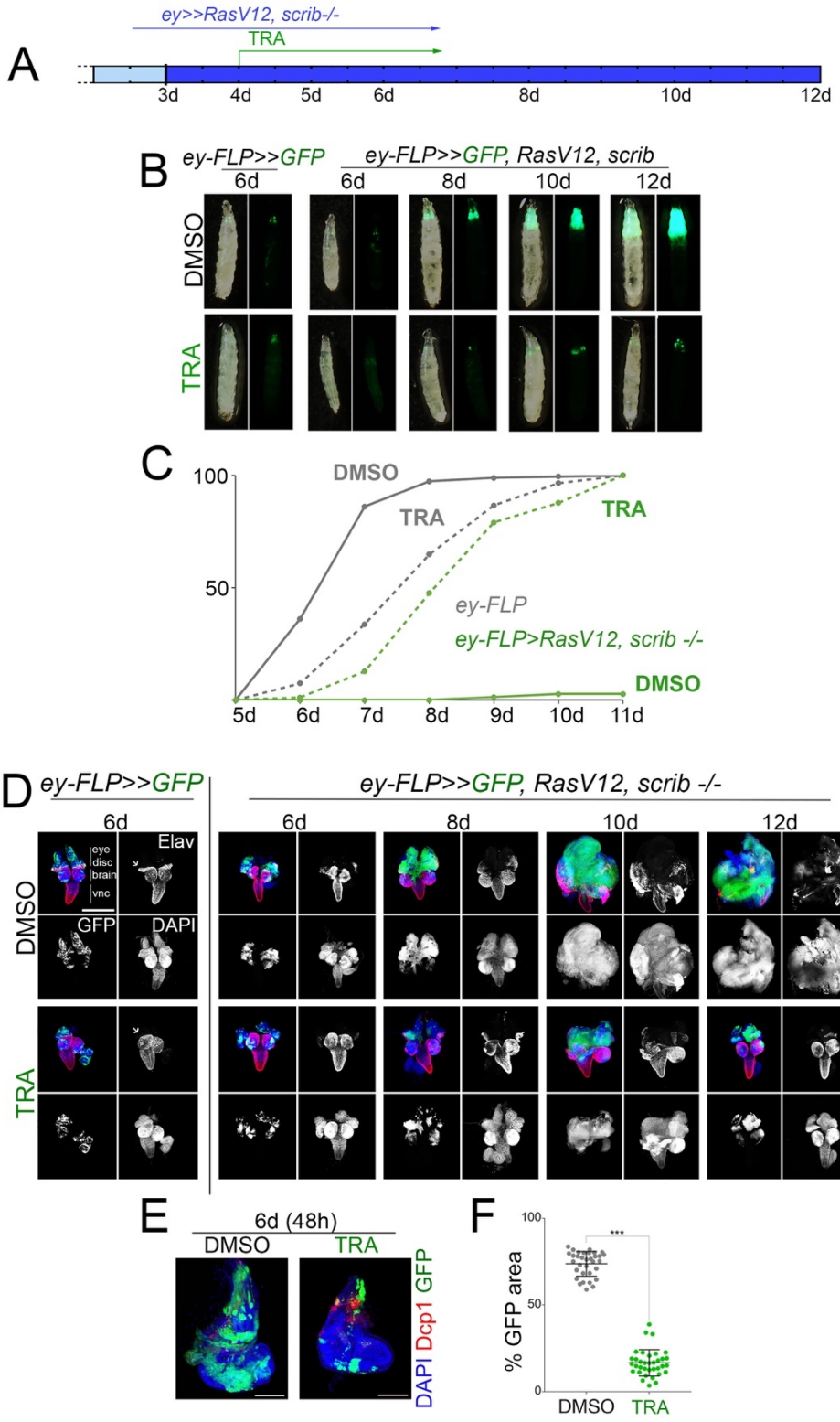
A
ey>>RasV12, scrib-/-
TRA
3d
4d
5d
6d
8d
10d
12d
B
ey-FLP>>GFP
ey-FLP>>GFP, RasV12, scrib
6d
6d
8d
10d
12d
DMSO
TRA
C
100
50
DMSO
TRA
TRA
ey-FLP
ey-FLP>RasV12, scrib -/-
DMSO
5d
6d
7d
8d
9d
10d
11d
D
ey-FLP>>GFP
ey-FLP>>GFP, RasV12, scrib -/-
6d
6d
8d
10d
12d
DMSO
TRA
eye disc
brain
vnc
Elav
GFP
DAPI
DAPI Elav GFP
DAPI Elav GFP
E
6d (48h)
DMSO
TRA
DAPI Dcp1 GFP
F
100
50
0
% GFP area
***
DMSO
TRA

Figure 26. Trametinib treatment for reducing tumor burden and developmental delay through specific induction of apoptosis. (A) Diagram showing the transgene induction time and the trametinib administration period at day 4 after egg laying. (B) Third instar larvae carrying eye GFP clones, either wild type or RasV12, Scribble mutant. Upper row larvae are mock treated with DMSO and lower row larvae are treated with 2uM Trametinib. Larvae were treated from day 4 onwards and collected at day 6, 8, 10 and 12 after egg laying. Clones are shown in green. (C) Graph showing the progression of pupariation of larvae carrying wild type clones (gray) or *RasV12, scrib*$^{-/-}$ clones (green) and treated with DMSO (solid line) or 2uM Trametinib (dashed line). n (*wild-type* + DMSO)= 188; n (*wild-type* + TRA)= 293; n (*RasV12 scrib* + DMSO)= 217; n (*RasV12 scrib* + TRA)= 172. The percentages were calculated based on the total number of larvae. (D) Cephalic complexes (Brain, ventral nerve cord and eye-antenna discs) of larvae carrying either wild type or *RasV12, scrib*$^{-/-}$ GFP expressing clones. Treated with DMSO (upper panel) or Trametinib 2uM (lower panel) at day 4 ael and dissected at day 6,8,10 and 12 ael. Cephalic complexes are labelled by GFP (green) and stained for DAPI (blue) and Elav (red). (E) Eye-antenna imaginal discs with GFP labelled (green) RasV12, Scrib$^{-/-}$ clones treated with DMSO or Trametinib 2uM and stained for DAPI (blue) and Dcp1 (red). (F) Scatter plot showing the percentage of GFP area over the total area of the discs in E. Individual values, mean and standard deviation are shown. Student's T-test was used to compare the two populations with a p>0.0001.

Regarding developmental timing, *RasV12,scrib*$^{-/-}$ larvae stay in the food as larvae way past the normal pupariation time, around day 6 after egg laying (Fig 26 C solid grey line). Indeed, very few pupae are formed and most larvae eventually die without entering into pupariation (Fig 26 C solid green line). However, after Trametinib treatment there is a significant rescue of *RasV12,scrib*$^{-/-}$ larvae pupariation (Fig 26 C dashed green line), with 50% of the pupas being formed at day 8, very much alike wild type Trametinib treated larvae (Fig 26C dashed grey line).

Then we evaluated the effects of trametinib treatment on tumor growth, invasion and organization of cephalic complexes. While DMSO treated eye imaginal discs showed an exponential increase in clone growth, Trametinib treated eye discs showed a much slower increase in clonal area (Fig 26 D, upper panel). Furthermore, at late stages, DMSO tumors grew over the ventral nerve cord and completely disorganized brain structure, both effects were mostly rescued by Trametinib treatment (Fig 26 D, lower panel). Meanwhile, Trametinib treatment did not have any

major impact on the growth of wild type eye-antenna discs, although there was a defect in the differentiation of photoreceptor cells labelled with elav, consistent with the role of MAPK signaling in that process (Fig 26 D white arrows).

Taking a closer look at day 6 eye discs, we observe a significant decrease in the clone area (measured as the percentage of the disc that is covered by GFP) (Fig 26 E, F). In many cases, these clones colocalize with Dcp1 staining (Fig 26 E).

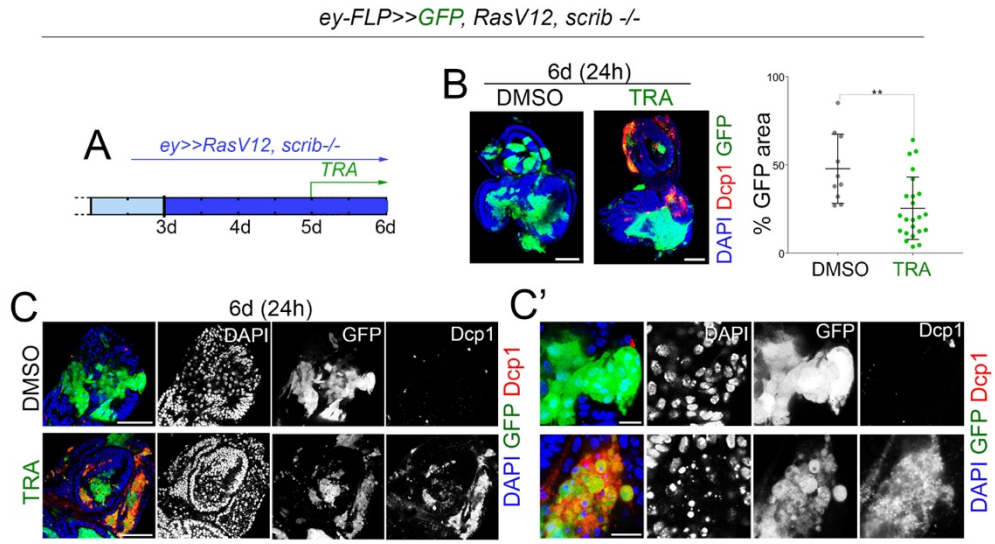

Figure 27. Effects on tumor burden of short trametinib treatment. (A) Diagram showing the time of transgene induction and the trametinib administration period at day 5 after egg laying. (B) Eye-antenna imaginal discs with GFP labelled (green) RasV12, Scrib$^{-/-}$ clones treated with DMSO or Trametinib 2uM and stained for DAPI (blue) and Dcp1 (red). Scatter plot showing the percentage of GFP area over the total area of the discs. Individual values, mean and standard deviation are shown. Student's T-test was used to compare the two populations with a p>0.0001. (C) GFP labelled RasV12, Scrib$^{-/-}$ clones of 6 days larvae treated with DMSO or trametinib (2uM) for 1 day. Stained for DAPI (blue) and Dcp1 (red). (C') Magnifications of the clones shown in C.

Pulsatile trametinib treatment has previously been shown to be useful for cancer treatment (Choi et al., 2019), therefore we tested the effect of a short, 1 day, Trametinib treatment (Fig 27 A). In these conditions, we also observed a significant

decrease in clone area, although less pronounced than with longer exposures (Fig 27 B). Again, most of the clones colocalized with Dcp1 staining and showed apoptosis marks such as the presence of pyknotic nuclei (Fig 27 C, C').

These results indicate that the effect of Trametinib on *RasV12, scrib* mutant cells is mainly to promote apoptosis of these cells rather than preventing their growth.

6. Transcriptional response of RasV12 cells.

We evaluated the transcriptional response induced by RasV12 expression in wing imaginal discs. To do that, we expressed *RasV12* under the control of the *ap-gal4* driver for 3 days, we dissected the discs and FACS sorted RasV12 cells according to myristolated Tomato levels. We extracted mRNA and performed a QUANT-seq analysis. This technique allows the measurement of the expression levels of each mRNA and is based on the use of oligo dT primers for mRNA amplification and sequencing. IRB Barcelona bioinformatics facility analyzed the data, and we obtained a list of up and downregulated genes. Then, they performed a gene set enrichment analysis based on the gene ontology biological processes lists (GOBP).

Table 2. Gene set enrichment analysis of RasV12 expressing cells. Representative up and downregulated gene sets in RasV12 cells compared to wild type cells. All data can be found under the following ID: GSE127228 at the Gene Expression omnibus web page.

	DEREGULATED GENE SETS	SIZE	NES	FDR q-val
UP	Epidermal growth factor receptor signaling pathways	58	1,868	0,189
	Photoreceptor cell development	92	1,624	0,218
	Sensory organ development	419	1,619	0,218
DOWN	DNA replication	80	-2,132	0,009
	Chromatin assembly or disassembly	32	-1,866	0,056
	DNA damage checkpoint	71	-1,768	0,087
	Regulation of cell cycle process	173	-1,649	0,109

Among the upregulated gene sets we find several RTK signaling dependent processes (Table 1, for full GOBP see supplementary table 1) which makes us confident that the detected genes and gene sets are actually a consequence of RasV12 expression. Among the downregulated gene sets we find very interesting ontologies. Consistent with the low EdU incorporation and the G2 arrest present in RasV12 cells, we find DNA replication is downregulated, we can also find gene sets related to DNA and cell cycle regulation (Table 1, for full GOBP see supplementary

table 2). Interestingly, also gene sets related to DNA damage checkpoints are downregulated. Although many of the genes are not significantly downregulated, when evaluated as a whole there is a solid tendency (supplementary table 3 and 4).

Several micro RNAs have been shown to target different DNA damage related genes, specifically ATM and ATR (He et al., 2016). Since we were interested in the regulation of the DNA damage response by RasV12, and given the fact that we do not find any specific genes downregulated that could explain the inhibition of H2Av phosphorylation, we decided to perform a microarray to evaluate the expression of the different microRNAs present in *Drosophila*.

Table 3. List of up and downregulated microRNAs in cells expressing RasV12. Up and downregulated microRNAs upon RasV12 expression based on microarray analysis.

	miRNA	FOLD CHANGE	P.Value
UP	dme-miR-10-3p	8,426	0,017
	dme-miR-263b-5p	5,702	0,020
	dme-miR-34-3p	5,129	0,020
	dme-miR-92a-5p	5,049	0,023
	dme-miR-277-3p	4,682	0,095
	dme-miR-34-5p	3,512	0,018
	dme-miR-2a-3p	2,786	0,218
	dme-miR-7-5p	2,698	0,290
	dme-miR-998-3p	2,411	0,238
	dme-miR-9a-5p	2,372	0,548
	dme-miR-92b-3p	2,322	0,184
	dme-miR-317-3p	2,190	0,213
DOWN	dme-miR-306-5p	-2,001	0,339
	dme-miR-4970-5p	-2,080	0,079
	dme-miR-285-3p	-2,581	0,548
	dme-let-7-5p	-2,656	0,519
	dme-miR-989-3p	-4,150	0,015
	dme-miR-989-5p	-4,179	0,073

We found a total of 12 miRNAs that were upregulated (Table 2). We used target scan fly (Agarwal et al., 2018) to look for predicted miRNAs targeting our proteins of

interest ATM and ATR. Then we crossed the list of putative miRNAs offered by target scan fly with the results of our microarray. We found no upregulated microRNA that was predicted to target ATM, however, we did find mir-277-3p as a putative ATR binding microRNA.

Based on the identification of ATR as a putative target of mir-277-3p, we decided to express the sponge for this miRNA in RasV12 expressing discs. When we checked H2Av phosphorylation as a read out of ATR activity, we were disappointed to find that mir-277 sponge had no effect in RasV12 expressing discs (Fig 28A), suggesting that the inhibition of ATR function is not dependent on this micro RNA.

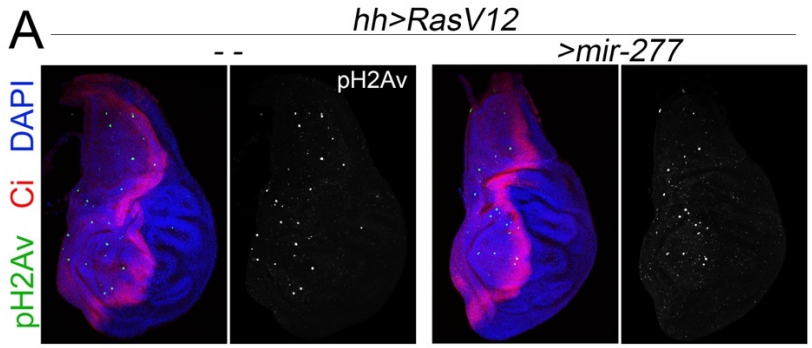

Figure 28. mir-277 sponge expression in RasV12 discs. Third instar wing imaginal discs expressing the indicated transgenes under the control of the hh-gal4 driver. Discs were stained for DAPI (blue), ci (red) and pH2Av (green and white).

7. Non-autonomous effects induced by RasV12 expression.

In the last few years, *Drosophila* has been used to assess the interactions between different tumor populations, as well as the relationship between the tumor and the surrounding wild type cells that conform the tumor microenvironment (Herranz, Weng, & Cohen, 2014; Katheder et al., 2017; Muzzopappa et al., 2017). This is due to the plethora of genetic tools that allow us to induce gene expression in specific organs and tissues and evaluate the effect of this expression in surrounding tissues.

7.1 Non-autonomous cell death and DNA damage.

During the course of our experiments to evaluate the role of RasV12 in DNA damage response and apoptosis, we realized that while there was no autonomous effect (Fig 29 A-D), there was an increase in pH2AV (Fig 29 A-B green line) and in apoptosis (Fig 29 C-D green line) in the neighboring anterior compartment.

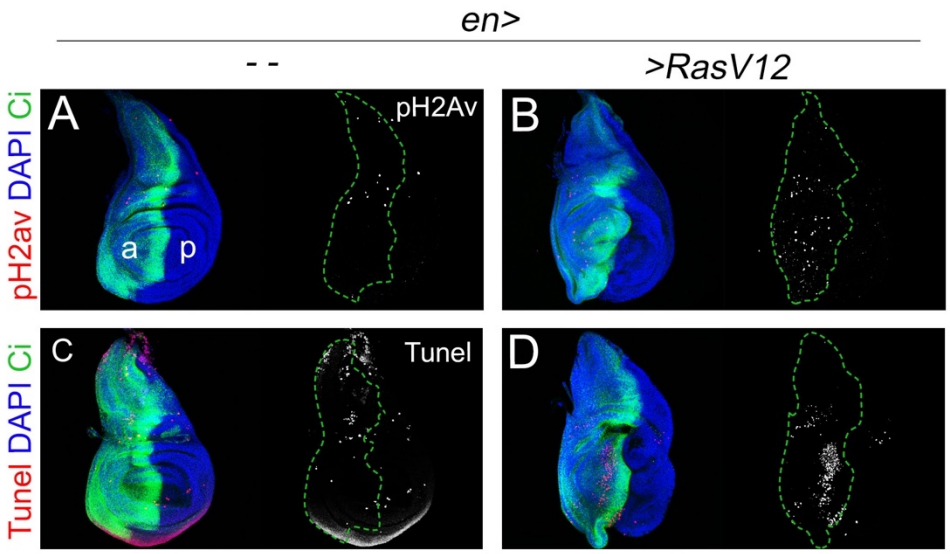

Figure 29. Non-autonomous DNA damage and apoptosis after RasV12 expression. (A-D) Third instar wing imaginal discs expressing the indicated transgenes in the posterior compartment under the control of the en-gal4 driver. Discs were stained for DAPI (blue), Ci (green) marking the anterior compartment and ph2Av (A,B) and TUNEL (C,D) in red

and white. Green dashed lines outline the area of the anterior non-autonomous compartment.

Furthermore, this non-autonomous phenotype was only found in RasV12 expressing discs but not when we induced G1/S transition by other means as CycE and E2F overexpression or Rbf downregulation (Fig 30 A-D green area), suggesting that this non-autonomous effect is Rasv12 specific. However, it is also possible that the lack of non-autonomous phenotype in these cases is due to the fact that a big amount of this cells die (Fig 11 A) and the discs do not overgrow or induce any type of tumor formation.

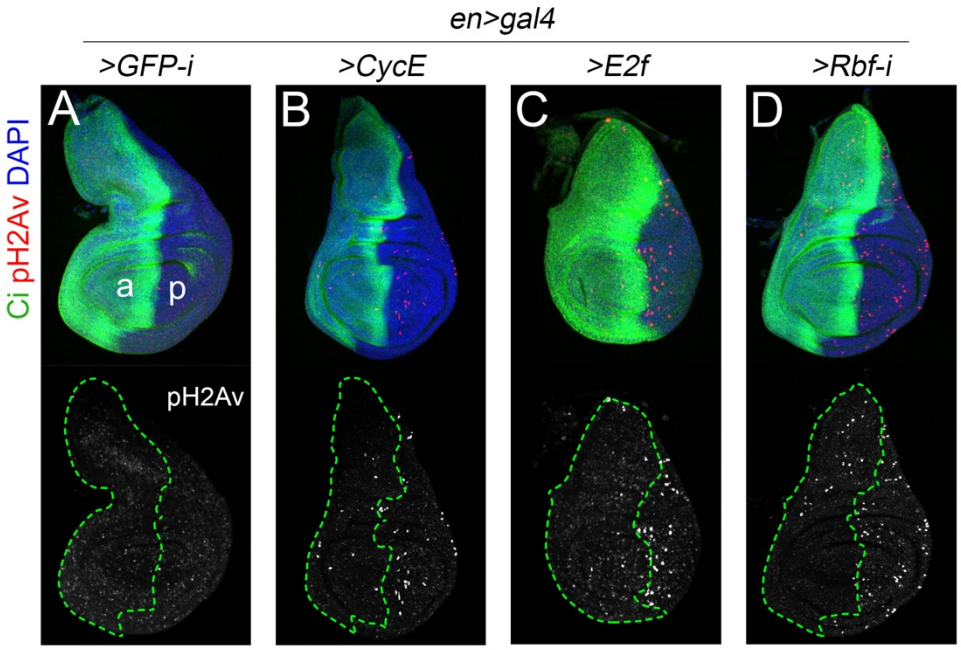

Figure 30. RasV12 induced non-autonomous DNA damage is not recapitulated by induction of G1/S transition. (A-D) Third instar wing imaginal discs expressing the indicated transgenes under the control of the en-gal4 driver. Discs were stained for DAPI (blue), Ci (green) and pH2Av (red and white). Non-autonomous compartment is marked with dashed green lines.

7.2 Non-autonomous DNA damage and nucleoside competition.

We have shown that RasV12 cells present replicative stress and replication defects. Furthermore, we have seen in our RNA-seq that the Ribonucleotide reductase, the enzyme responsible for the late steps of deoxynucleotide biosynthesis, is downregulated.

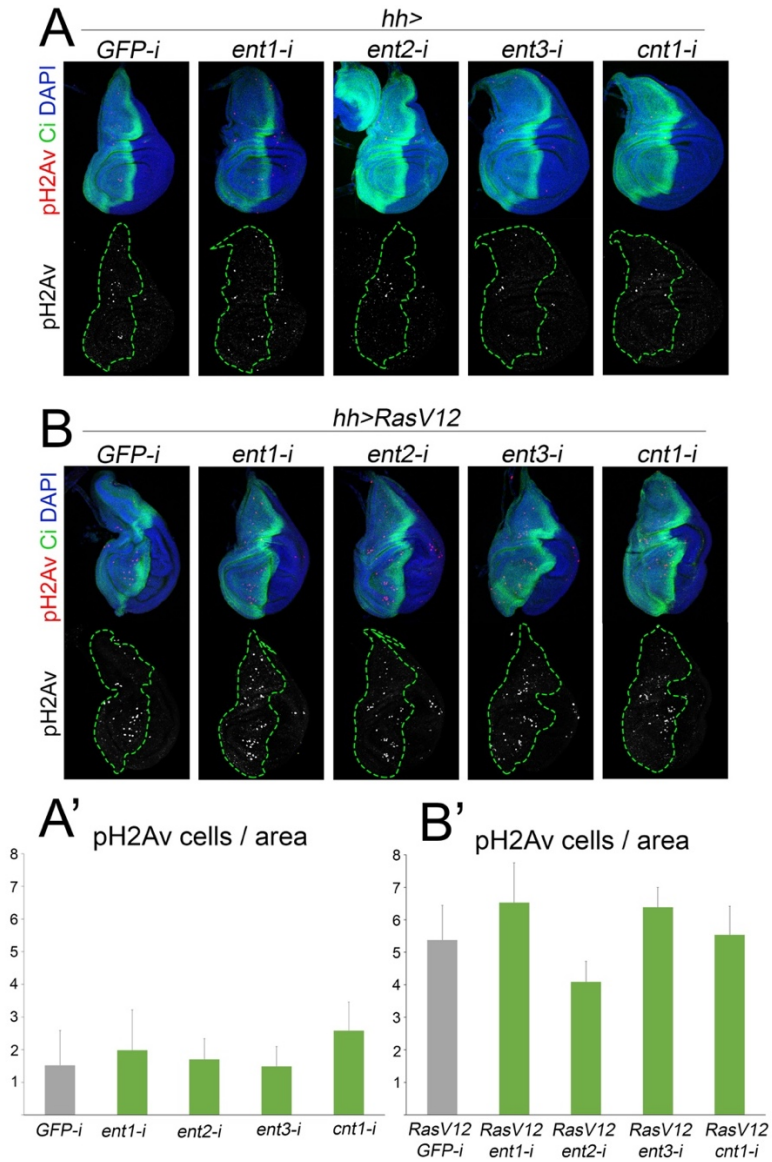

Figure 31. RasV12 induced non-autonomous effects and nucleoside transporters. (A-B) third instar wing imaginal discs expressing the indicated transgenes under the control of

the hh-gal4 driver. (A, B) Discs were stained for Ci in green, DAPI in blue and pH2Av in red and white. Dashed green lines outline the non-autonomous area. (A', B') Bar graph representing the amount of pH2Av positive cells per anterior area. Mean value and standard deviation are shown.

There are two pathways for nucleotide synthesis: the de novo pathway involving the ribonucleotide reductase and the salvage pathway that aims to recycle bases and nucleosides for nucleotide synthesis.

Given that the de novo pathway is hindered by the lack of ribonucleotide reductase, we hypothesize that RasV12 cells may strongly depend on the salvage pathways and compete with the cells in the anterior compartment for the uptake of nucleosides. This lack of nucleosides in the anterior compartment could lead to replication stress, DNA damage and apoptosis. In order to test this possibility, we decided to deplete the different nucleoside transporters present in *Drosophila* and evaluate the effect on non-autonomous DNA damage. Unfortunately, we did not observe any significant change in pH2Av upon depletion of the different transporters neither in wild type discs (Fig 31 A, A') nor in RasV12 expressing discs (Fig 31 B, B'). We only depleted the transporters individually, and it is thus possible that the rest of them can compensate for the loss of one transporter.

7.3 Non-autonomous effects and ROS.

Another possibility to explain the presence of a non-autonomous effect relays on the presence of a secreted molecule that, even though is expressed by RasV12 cells, can reach the anterior wild type cells. We turned to the RNA-seq in order to look for upregulated secreted molecules that could be related to the non-autonomous role of RasV12. The first upregulated gene that came to our attention was the Glutation S transferase D3 (GstD3). This gene is upregulated in response to ROS via the activity of the Nrf2 transcription factor. (Sykiotis, & Bohmann , 2008). We hypothesized that

ROS signaling could induce the oxidation of the DNA, thus causing DNA damage and cell death. In order to confirm the results of the RNA-seq, we used a GstD reporter to evaluate its expression in RasV12 wing discs. We observe high levels of GstD-GFP in the posterior autonomous compartment but also at the anterior-posterior boundary between compartments (Fig 32 A). Then we decided to overexpress different antioxidant enzymes in order to reduce the levels of ROS. When we overexpressed catalase or superoxide dismutase in combination with RasV12, we did not observe any reduction in the non-autonomous levels of either pH2Av (Fig 32 B, C) or cell death, (Fig 32 D, E) when compared to RasV12 alone (Fig 28 A-D).

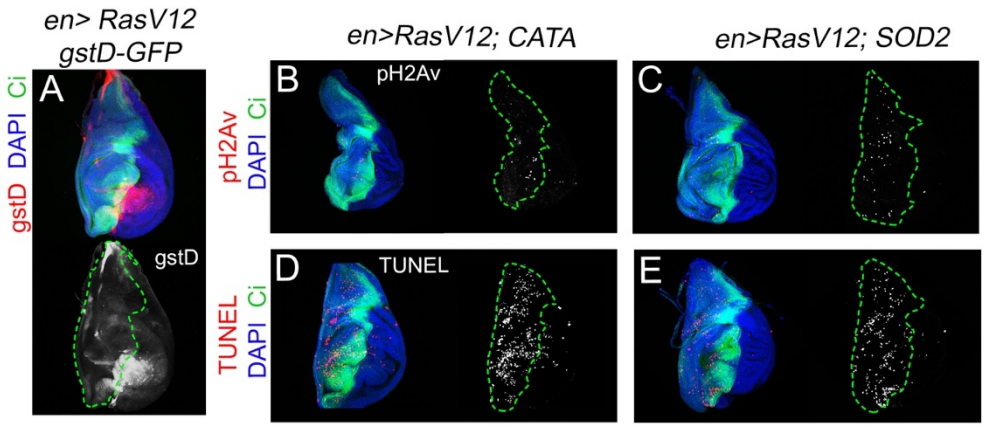

Figure 32. ROS present in RasV12 tumors and non-autonomous effects. (A-E) third instar wing imaginal discs expressing the indicated transgenes under the control of the en-gal4 driver. Discs were labelled with gstD-GFP in red and white (A) and stained for DAPI in blue (A-E), Ci in green (A-E), pH2AV in red and white (B,C) and TUNEL in red and white (D,E). Autonomous compartment is marked by dashed green lines.

7.3 Role of stat signaling in non-autonomous DNA damage and apoptosis.

RasV12 has been shown to induce non-autonomous autophagy, as a way to provide building blocks for cellular growth, thus promoting tumor growth both in mammals and *Drosophila* (Guo et al., 2016; Katheder et al., 2017). Furthermore, increasing

evidence shows that autophagy may play a role in the regulation of DNA damage and apoptosis (Hewitt & Korolchuk, 2017). We wondered whether autophagy induction could be the cause of the non-autonomous DNA damage and apoptosis.

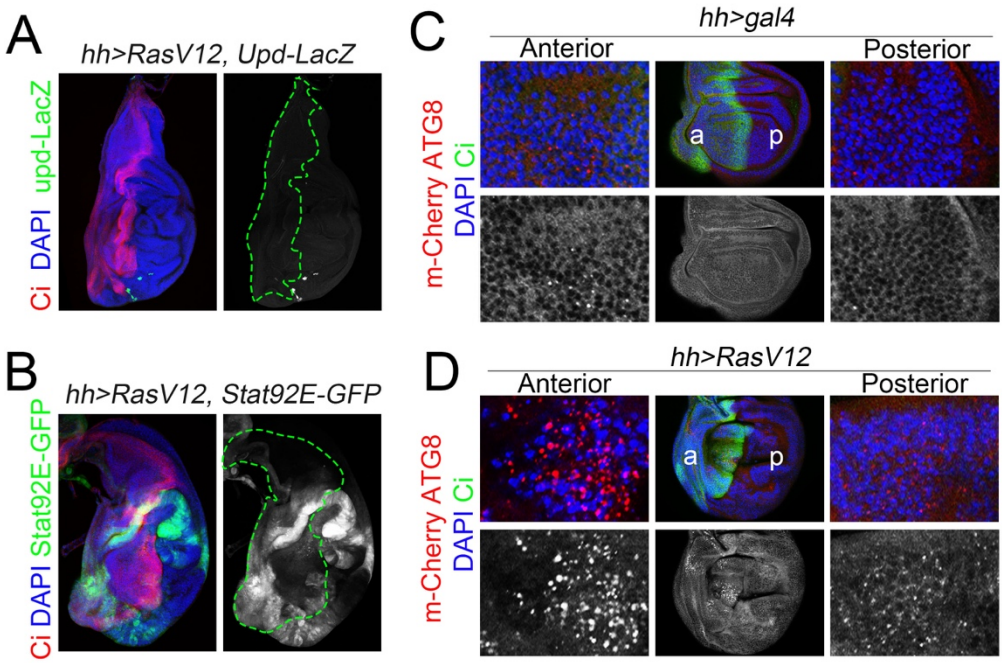

Figure 33. RasV12 induced non-autonomous autophagy. (A-D) Third instar wing imaginal discs expressing the indicated transgenes under the control of the hh-gal4 driver. Discs were stained for DAPI in blue (A-C), Ci in green (A) and red (B,C), mCherry-ATG8 in red and white (C-D), Upd-LacZ in green and white (A) and STAT92E-GFP in green and white (B). (C-D) magnifications of representative areas of the anterior and posterior compartments.

It has also been shown that JAK/STAT signaling may play a role in the induction of non-autonomous autophagy (Katheder et al., 2017). Since Upd3 and Upd2 (JAK/STAT ligands) were upregulated in our RNA-seq, we decided to confirm those results. Although we could not detect high levels of Upd expression by using an Upd3-LacZ reporter (Fig 33 A), we could detect extended STAT activity (Fig 33 B) according to the STAT92E-GFP reporter. Then, we checked for non-autonomous autophagy, by using a mCherry-ATG8 fusion protein, which can be found coating the autophagic vesicles. We observed induction of non-autonomous autophagy in RasV12 discs (Fig

33 D anterior) when compared to wild type discs (Fig 33 C anterior). We also observed an increase in autonomous autophagy although much lighter than the non-autonomous (Fig 33 D posterior).

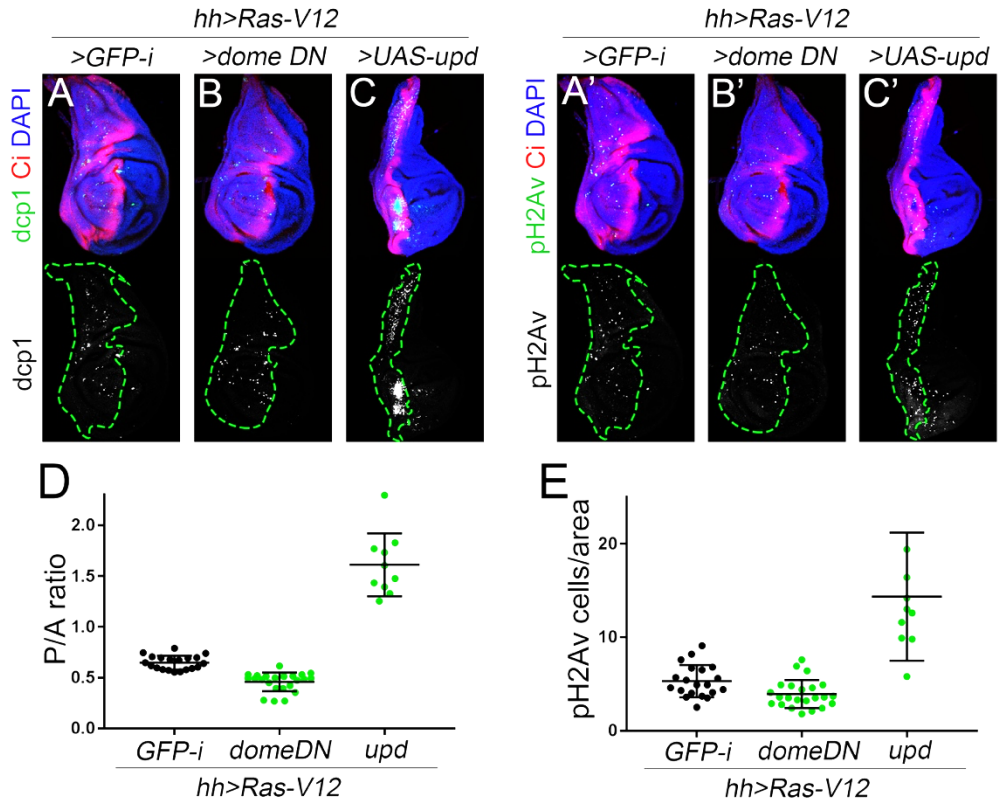

Figure 34. Role of JAK/STAT in non-autonomous DNA damage and apoptosis. (A-C') Third instar wing imaginal discs expressing the indicated transgenes under the control of the hh-gal4 driver. Discs were stained for DAPI in blue, Ci in red dcp1 in green and white (A-C) and pH2Av in green and white (A'-C'). Anterior compartment is outlined by dashed green lines. (D) Scatter plot of the ratio of the posterior to anterior area, (E) Scatter plot of the amount of pH2Av positive cells relative to the anterior area. (D, E) single values, average and standard deviation are shown in both graphs. Controls in black and experiment in green.

Then, we decided to analyze whether JAK/STAT signaling could have a role in the non-autonomous DNA damage and apoptosis. In order to do so, we expressed a dominant negative form of the receptor Domeless that acts not only by inhibiting the autonomous signaling but also by trapping the Upd ligands and preventing their

diffusion. In *RasV12, domeDN* discs, we observed a decrease in the amount of non-autonomous DNA damage (Fig 34 B',E) and cell death (Fig 34 B) as well as a reduction of the tumor growth (Fig 34 C). Furthermore, we overexpressed the ligand Upd in RasV12 discs and found a significant increase both in non-autonomous DNA damage (Fig 34 C') and apoptosis (Fig 34 C), as well as an increase in tumor growth (Fig 34 D). Due to the experimental set up is impossible to say whether JAK/STAT signaling promotes a non-autonomous effect that then impinges on tumor growth or if, on the contrary, JAK/STAT autonomously promotes tumor growth which then increases the non-autonomous effects.

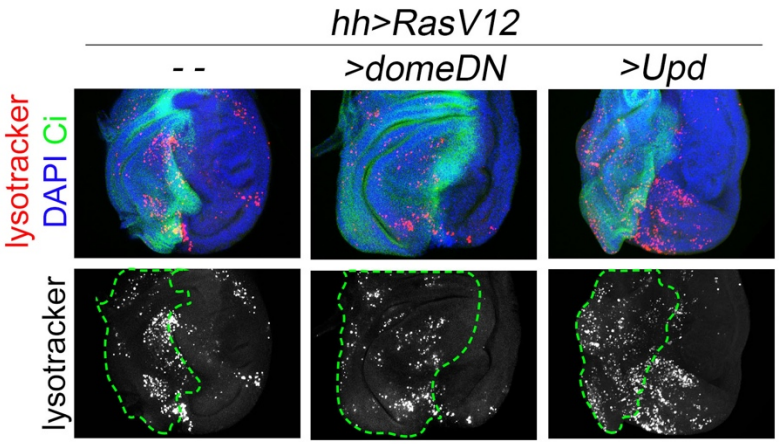

Figure 35. JAK/STAT signaling and autophagy. Third instar wing imaginal discs expressing the indicated transgenes under the control of the hh-gal4 driver. Discs were stained for lysotracker (red and white), ci (green) and DAPI (blue).

Seen that JAK/STAT signaling plays a role in, directly or indirectly, promoting non-autonomous DNA damage and apoptosis, we wondered whether it could be doing so by inducing autophagy. In order to monitor autophagy, we used the lysotracker probe which is highly selective for acidic organelles and can be used to label lysosomes and autophagolysosomes. In RasV12 discs, we observed high lysotracker staining non-autonomously, similarly to Atg8. This signal is reduced by the expression of *dome*^{DN} and increased by *Upd* overexpression both autonomously and non-

autonomously (Fig 35). Altogether, these results suggest that RasV12 cells through unpaired and JAK/STAT signaling induce both autonomous and non-autonomous autophagy as well as tumor growth.

Discussion

1. RasV12 growth and cell cycle

1.1. RasV12, G2 arrest and senescence.

We and others have shown that the capacity of RasV12 overexpression, in wing imaginal discs, to promote tumorigenesis and growth is somehow limited. It has been proposed that RasV12 overexpression can lead to the acquisition of some senescence features (Nakamura et al., 2014) such as ß-Gal activity, H3K9 trimethylation or increased cell size. However, these cells do not recapitulate a fully developed senescent phenotype. In this regard, the most interesting aspect to us is the tendency of these cells to arrest in the G2 phase of the cell cycle, which agrees with the presence of replication stress. It is curious that these cells are arrested in G2 while their levels of the mitotic cyclin B are high, suggesting that something is imposing a brake on the progression of these cells through mitosis. We have shown that this arrest is independent of the DNA damage response pathway and of ATR and ATM activity. On the contrary, we found that the G2 arrest can be rescued by String overexpression. String (Cdc25) is the phosphatase responsible for the dephosphorylation of CDK1, and therefore, activation of mitotic CyclinB-CDK1 complexes that are necessary for G2/M transition. Activation of the DDR can lead to G2 arrest by phosphorylation and inhibition of String. However, in our case ,the inactivation of String seems to be independent of the DDR. Moreover, we found that *string* mRNA levels were downregulated in *RasV12* expressing cells according to our Quant-seq results (Fig 1). Although these results were never

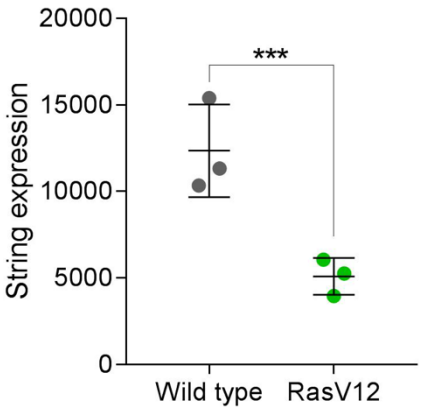

Figure 1. String expression in RasV12 vs wild type cells. Levels of string mRNA according to the three replicates of our Quant-seq. Adjusted p-value $1{,}62 \cdot e^{-12}$.

confirmed by qRT-PCR, and we did not check for the levels of phosphorylated String, we believe that in our case *string* is transcriptionally regulated by an unknown mechanism, rather than post-transcriptionally regulated by the DDR.

String downregulation has been shown to play a role in the acquisition of resistance to ATR inhibitors in murine tumors (Ruiz et al., 2016). Thus, we wonder whether String depletion in RasV12 cells could be a mechanism to cope with the DNA damage and ATR inhibition that we observe in these cells. We wonder whether, when String is upregulated, these cells resume the cell cycle, prematurely enter into mitosis and accumulate more DNA damage. If that were the case, the prevention of G2 arrest could be used to increase the DNA damage present in RasV12 cells, and in combination with ERK depletion, to selectively target Ras cells. This may be accomplished by using Wee1 inhibitors. Wee1 is a CDK1 inhibitory kinase that is usually antagonized by the phosphatase activity of String. In the absence of String, Wee1 maintains CDK1 inhibited. By using Wee1 inhibitors, we could prevent the inhibition of CDK1 and therefore allow the resumption of cell cycle progression, which may lead to mitotic catastrophe in the presence of DNA damage. Wee1 inhibitors are currently undergoing clinical trials, and the combination of ATR and Wee1 inhibitors has been shown to be synthetically lethal in breast cancer models (Bukhari et al., 2019).

1.2. RasV12 and replication stress.

In 1998 Karim and Rubin found that RasV12 expression led to an increase in EdU positive cells. However, we have observed the opposite, a reduction in the number of EdU positive cells upon RasV12 expression. But not only that, we have shown, through the use of an RPA reporter, that RasV12 expression in the wing imaginal disc leads to DNA replication stress. Furthermore, many of the RasV12 cells show aberrant

mitoses with DNA bridges, which are a feature of mitosis entry with an under-replicated genome (Wise & Brinkley, 1997). These seemingly contradictory results may be explained by the differences in the induction protocol. They used a dpp-Gal4 driver to constitutively drive RasV12 expression to the wing discs, and raised the flies at 25ºC leading to a rather mild expression of RasV12, where they even obtained viable adults. In our case we used the hh-Gal4 driver to induce RasV12 expression in the whole posterior compartment of the wing disc, we used the Gal80^{ts} repressor to prevent early transgene expression, and then, transferred the flies to 29ºC for maximal expression. It is possible that low levels of RasV12 expression lead to a proliferative phenotype without producing too much DNA damage and without eliciting a cell cycle arrest. We found that RasV12 expression drove a decrease in the amount of EdU positive cells but only after 3 days of expression. Although it is possible that we missed the first wave of Ras-induced proliferation, we could not observe an increase in EdU cells even examining the initial response after 15 hours of induction. We could try to test different induction times to capture this moment.

Another element that suggested the presence of replicative stress is the downregulation of the gene ontology group of DNA replication. Among the genes downregulated in this group were the Ribonucleotide reductase, necessary for the production of nucleotides, and several MCM and Orc components, indispensable for origin licensing. However, whether this downregulation is a cause of the replication stress or a simple consequence of the overrepresentation of G2 arrested cells, we do not know.

1.1. RasV12 and malignancy.

The oncogene-induced DNA replication stress model proposed that, initially, oncogenic activation will lead to aberrant proliferation and activation of the DDR to

act as an antitumoral barrier (Halazonetis, Gorgoulis, & Bartek, 2008b). Our Ras model mimics a premalignant state where there is DNA damage and cells become arrested, in our case, independently of the DDR. Normally, RasV12 larvae pupariate with about one day delay with respect to wild type larvae. However, we believe that this is not enough time for RasV12 cells to overcome their senescence-like phenotype and to give rise to a malignant tumor. From time to time, we would get escapers that stayed longer in the food, even for two or three extra days. When dissected, the tumors were bigger, disorganized and presented MMP1 staining (Data not shown). This suggested that, if given enough time, RasV12 tumors would eventually overcome the cell cycle arrest and give rise to malignant tumors. It would be interesting to deeply evaluate the senescence and malignant status of these escaper larvae in order to prove our hypothesis. It would also be possible to implement a system in which we can induce the developmental delay of RasV12 larvae and analyze the tumor evolution in time.

On the contrary, RasV12, scribble-i larvae have tumors with a high proliferation capacity, that are developmentally delayed, and show signs of malignancy as MMP1 upregulation. How Scribble depletion induces the bypass of the G2 arrest, observed in RasV12 cells, to give rise to a malignant tumor is not completely clear. It has previously been shown that Scribble depletion in RasV12 expressing cells induces the delamination of some of the cells that activate JNK leading to a pro-tumorigenic transcriptional program (Uhlirova & Bohmann, 2006a). Previous work in Marco Milan's group has shown that the Wingless and Unpaired molecules secreted from the delaminated cells are necessary for the growth and proliferation of the cells remaining in the epithelium (Muzzopappa et al., 2017). How these two molecules override the G2 arrest or if it is through a direct or indirect mechanism remains still to be explored. A full evaluation of the cell cycle status of the two tumor populations that

are formed in RasV12, scribble-i tumors would be interesting. Maybe understanding this mechanism would point towards a therapy to prevent the malignant transformation of RasV12 dependent adenomas.

2. Ras V12 inhibition of the DDR

2.1 ATR inhibition by Ras.

Genetically, we have shown that RasV12 expression in the *Drosophila* wing imaginal disc leads to a decrease in H2Av phosphorylation in response to DNA damage and that this is due to the impairment of ATR function. How this ATR inhibition happens and whether it is transcriptional or post-transcriptional is still unresolved.

With regard to the effectors of ATR regulation downstream of Ras, we do not know either. In order to find out, we could express RasV12 and block the downstream effectors of the different pathways and analyze the recovery in H2Av phosphorylation. However, it is possible that by blocking them we are eliminating the source of the damage itself. Therefore, negative results in these experiments would not exclude the involvement of these pathways in ATR regulation. Alternatively, mutations in Ras effector loop that specifically activate ERK, PI3K or Ral pathways were identified in mammals in 1995 (White et al., 1995). Given the conservation of this region of the Ras protein, these mutant forms were also generated in flies in 1998 (F. D. Karim & Rubin, 1998). We could express these mutant forms and see if any of them recapitulates RasV12 effects in terms of ATR inhibition, at least in response to irradiation.

2.1.1. Transcriptional regulation.

The activation of the DNA damage response pathway is a rapid process that needs to happen immediately after the induction of the damage. Therefore, and although

ATR can be transcriptionally regulated by different proteins (Beesetti et al., 2017; Sethy et al., 2018), this does not seem to be the main regulatory element of ATR activity. We have not found an ATR downregulation in our transcriptomic analysis of RasV12 cells. Furthermore, overexpression of ATR/mei41, which induces ATR activation (Bayer et al., 2018), does not result in an increase in H2Av phosphorylation in RasV12 (Fig 2), suggesting that there is an alternative mechanism to prevent its activation. All in all, we do not think that ATR transcriptional regulation is playing a major role in our model.

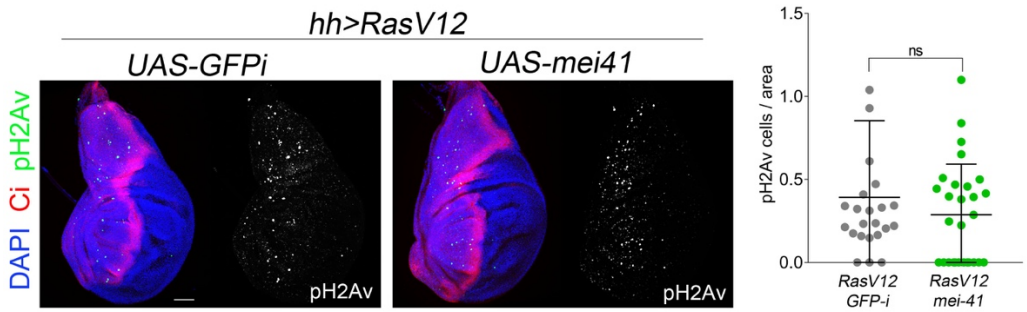

Figure 2. ATR overexpression in RasV12 cells. Third instar wing imaginal discs expression the indicated transgenes under the control of the hh-gal4 driver. Discs were stained with DAPI (blue), Ci (red) and pH2AV (green and white). Quantification of the number of pH2Av positive cells per area.

2.1.2. Post-transcriptional regulation.

Phosphorylation (activation) and dephosphorylation (inactivation) is the main way to rapidly regulate ATR activity in response to damage. In mammals, the most common way to check for the activation of ATR is to use phospho-specific antibodies which detect the phosphorylation of different residues on ATR and its target Chk1. However, in *Drosophila* we are lacking such antibodies, and, although there is conservation in ATR proteins, the mammalian antibodies have not been tested either. In order to confirm a possible posttranscriptional regulation of ATR downstream of RasV12, we could test the existing mammalian antibodies in the fly. Or even more interestingly,

we would like to evaluate if RasV12 causes ATR inhibition in mammalian cells. Disappointingly, although many reports link ATR regulation and Ras, they propose the opposite, that Ras, through ERK, promotes the activation of ATR signaling rather than its inactivation (Grabocka et al., 2014; Lee et al., 2017; Wei, Yan, & Tang, 2011).

The Ras-induced ATR inactivation does not seem to depend on checkpoint phosphatases or microRNAs, and we do not have any putative target to be responsible for this regulation. In this context, a phospho-proteomic analysis of RasV12 expressing cells might help to define the phosphorylation status of ATR and its targets and also to identify possible mediators of this ATR inhibition.

2.2 DDR inhibitors for cancer treatment.

Studies in human cultured fibroblasts have shown that RasV12 overexpression induces DNA damage and oncogene-induced senescence, that is abolished by ATM depletion (Bartkova et al., 2006b; Di Micco et al., 2006). However similar experiments in mouse have shown that RasV12 overexpression leads to senescence in the absence of any DNA damage signaling (Efeyan et al., 2009). In this last report, they never actually looked into the DNA damage itself. Therefore, we do not know whether RasV12 expression in mouse induces DNA damage or not. In our model, we have found that RasV12 expression is capable of generating DNA damage while at the same time blocking the DNA damage signaling.

It has been proposed that high levels of DNA damage response activation act as a barrier for tumor progression, and that this needs to be overcome in order to allow cell cycle reentry and tumorigenesis. However, at this stage low levels of DNA damage response are still necessary for the survival of these cells. Based on this notion, ATR and Chk1 inhibitors have been developed in order to target cells that harbor replication stress. Although they were shown to work for Myc-induced tumors,

the inhibitors were found to be totally ineffective in Ras-dependent tumors (Murga et al., 2011). The fact that we observe that RasV12 can impair ATR activity could explain why ATR inhibitors fail as a treatment to Ras-induced tumors.

Irrespective of the DDR activation, RasV12 cells still carry large amounts of DNA damage that they have to cope with. We have shown that these cells do not depend on DNA damage repair pathways for their growth. However, it has been shown that extra Chk1 can limit replication stress and promote transformation (López-Contreras, et al., 2012). We decided to overexpress Chk1 in RasV12 wing discs and we observed increased tissue growth and folding (Fig 3). Although we have not carefully analyzed this phenotype, and we do not know whether the cells have less damage or are no longer G2 arrested, we believe this is the case. All these results suggest that we need to be extremely careful in using DDR inhibitors as therapeutics targets in different types of tumors, considering whether the DDR is activated or not and at which stage of the tumor progression is the treatment administered.

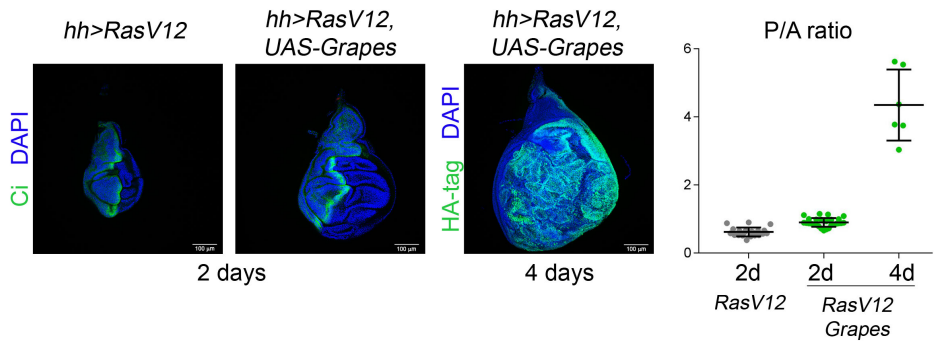

Figure 3. Grapes overexpression promotes RasV12 tissue growth. Third instar wing imaginal discs expressing the indicated transgenes under the control of the hh-Gal4 driver. Discs were stained for DAPI (Blue), Ci and HA (Green). Quantification of tissue growth in terms of posterior / anterior ratio at different induction times.

3. Role of ERK in apoptosis inhibition

3.1. Homeostatic role of ERK in blocking apoptosis.

Besides its very well-known role in patterning and differentiation, we have shown that endogenous levels of ERK protein play a role in protecting cells from apoptosis, both in the case of developmental and irradiation induced apoptosis. ERK is commonly activated after mitogenic signaling. This will induce proliferation, that will very provably generate some replication problems that could elicit a DDR response. We believe that ERK plays a role in buffering the apoptotic response induced by this damage in order to maintain the integrity of the tissue.

In the case of an irradiation response, we and others (Mogila, Xia, & Li, 2006) have shown that ERK becomes phosphorylated and activated upon irradiation. However, the mechanism of ERK activation is not clear yet. We thought that the main suspect should be the DNA damage response since it is rapidly activated after damage. However, we have shown that ERK phosphorylation in *Drosophila* is not dependent on the activation of neither ATR nor ATM. Different mechanisms for ERK activation have been proposed. A possibility is a ROS dependent activation of the EGFR receptor (Yan et al., 2015). Another possible mechanism is that IR can generate mitochondrial damage and fission and this in turn, can activate AMPK that phosphorylates ERK (J. Wu, Zhang, Wuu, Davidson, & Hei, 2017). We do not have any data that points into any of the possibilities, yet it would be interesting and relatively manageable to study if any of these proposed mechanisms apply to our case. It is also possible that given the relevance of ERK activation in maintaining tissue homeostasis, not only one mechanism applies but rather a series of redundant signals give rise to the activation of ERK in response to IR.

3.2 Pro-tumoral role of ERK in blocking apoptosis.

In our model, we have shown that RasV12 cells become addicted to ERK oncogenic signaling in order to maintain tumor cells alive. Whether these cells have sequestered the homeostatic role of ERK to promote their survival or this is a newly acquired characteristic of cells with very high levels of ERK we do not know.

In mammals, there is still some controversy about whether ERK signaling plays a pro-survival or pro-apoptotic role. Dependent on the cellular context, both effects have been observed. However, it is generally accepted that it has a pro-survival function in response to irradiation (Dent et al., 2003; Hein, Ouellette, & Yan, 2014; Munshi & Ramesh, 2013). In *Drosophila,* ERK has been proposed to mediate a pro-survival role through the inhibition of the proapoptotic gene *hid*. And not only this, the existence of an ERK-dependent G2 checkpoint in response to DNA damage has been proposed (Mogila et al., 2006). This checkpoint is supposed to induce the arrest of damaged cells in G2 independently of ATR and Chk1 and might be a relevant copying mechanism of RasV12 cells.

However, to us more important than the mediators of this effect, was how could we exploit this ERK dependency as a weakness of tumor cells for cancer treatment.

4. Exploiting oncogene induced replication stress as a therapeutic opportunity

The ability of oncogenes to promote replicative stress and DNA damage has been exploited as a way to induce the selective elimination of cancer cells by targeting the DDR and different repair mechanisms (Lecona & Fernandez-Capetillo, 2018; Puigvert, Sanjiv, & Helleday, 2016). However. some of these approaches have been

ineffective in targeting RasV12-tissues (Murga et al., 2011), possibly due to inhibition of ATR in these tissues.

4.1 ERK inhibition to selectively target Ras tissues.

Given the lack of response of Ras cells to ATR inhibitors, we decided to test an alternative approach, where we can exploit the intrinsic characteristics of RasV12 cells to make them more sensitive to irradiation. We have shown that the combination of the endogenous replicative stress and the inhibition of the capacity of ERK to block cell death can be exploited to selectively radiosensitize RasV12 cells when compared to wild type cells.

4.1.1 Genetic ERK inhibition.

We used genetic ERK depletion as a proof of concept. We showed that genetic ERK inhibition radiosensitizes RasV12 cells producing cell death of the tissue. We measured the amount of apoptosis rather than the growth of the tissue to separate the effects of ERK inhibition on tissue growth from its capacity to prevent apoptosis.

Unfortunately, in most cases ,when tumors are detected in patients they are no longer benign. Therefore, we changed our model for a well-established Ras-dependent model of transformed neoplastic growth. Unfortunately, in this case genetic ERK depletion was not capable of radiosensitizing the cells. At first, we thought that this was due to some emergent feature of this new model, that somehow made the neoplastic cells resistant. However, we are inducing tumor formation at the same time as depleting ERK which may directly interfere with the tumor formation.

4.1.2 Chemical ERK inhibition.

Chemical ERK depletion, by Trametinib, in RasV12, Scribble-i cells could radiosensitize the cells. This suggested that the lack of response to genetic ERK inhibition was a

problem of induction timing rather than resistance of these cells. Importantly, we observed that Trametinib treatment alone was capable of inducing cell death in this malignant model. RasV12, Scribble-i discs grow more that RasV12 discs, suggesting that they may have overcome the G2 arrest induced by Ras expression. This could increase replication stress and DNA damage and lower the time available for DNA damage repair, thus making RasV12, Scribble-i cells more sensitive to Trametinib treatment. Alternatively, and as mentioned in the results, RasV12, Scribble-i discs induce known pro-apoptotic JNK signaling (Igaki et al., 2006). We have also shown that they induce high levels of p53 activity. This double pro-apoptotic signaling might make them more dependent on ERK signaling for cell survival than RasV12 cells.

After testing the effects of chemical inhibition in the wing discs, we shifted to a clonal model which recapitulates more faithfully the steps of tumor initiation and progression. Previous reports had used Trametinib to prevent Ras-dependent tumor initiation (Levine & Cagan, 2016). By using this model, we were able to show that Trametinib treatment after the tumor has already been established can also prevent tumor growth, but more importantly that it promotes apoptosis of the tumor cells. This is particularly relevant since ERK inhibition treatments are generally considered to be cytostatic rather than cytotoxic. It would be interesting to evaluate whether after interruption of Trametinib treatment the remaining tumor cells can reconstitute the tumor or not. Latest reports suggest that inhibition of ERK signaling can present a complete response even after months of treatment cessation (Brugnara et al., 2018).

4.1.3 MEK inhibitors in cancer treatment.

Trametinib has been approved for the treatment of metastatic melanoma mutant for BRAF. These tumors are originally treated with BRAF inhibitors, however, they usually become resistant to this treatment by activating ERK signaling downstream of RAF (Chapman, 2013; Griffin et al., 2017). In order to prevent this effect, the combination

of MEK and BRAF inhibitors is used (Flaherty et al., 2012). Currently, Trametinib is being clinically tested for the treatment of other types of tumors (Planchard et al., 2016; Subbiah et al., 2018). However, in these trials, the role of MAPK-ERK signaling in preventing irradiation induced cell death is not taken into consideration. Our results pave the way for radiotherapy to be considered as a treatment option in order to increase the DNA damage induced by the oncogene, in combination with MEK and BRAF inhibitors (Fig 4).

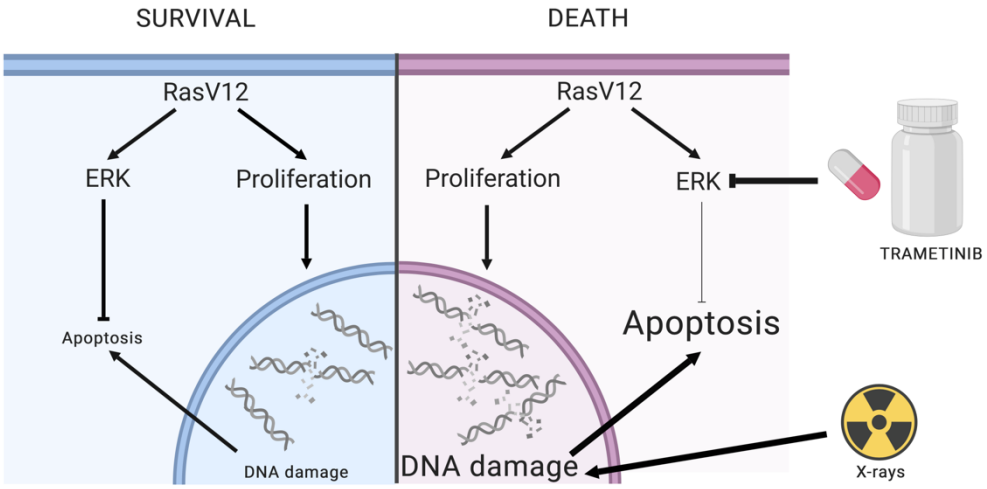

Figure 4. Combined MEK inhibitor and IR therapy selectively kills Ras cells. RasV12 expressing cells reach a balanced state, in which the apoptosis induced by endogenous DNA damage is blocked by the high levels of ERK activation. Upon ERK inhibition by Trametinib treatment and the induction of DNA damage by irradiation, there is a perturbation of the balance towards apoptosis induction which leads to the selective killing of RasV12 cells.

We have not analyzed the effect of the combination of MEK inhibitors with other DNA damaging drugs. However, the fact that ERK has been shown to be upregulated in response to not only IR, but also UV light, Hydroxyurea and other damaging agents (Razidlo et al., 2009; Tang et al., 2002; Wu et al., 2006; Yan, Black, & Cowan, 2007), suggests that MEK inhibition should be effective irrespective of the type of damage generated.

Ideally, we would like to test our model and the combination of Trametinib and irradiation in mouse models or human cell lines in order to further the possible applicability of this treatment option.

5. Relevance of non-autonomous autophagy

The role of autophagy in tumor progression is still under discussion, many reports show that autophagy is necessary for tumor growth while others demonstrate that it plays the opposite role (Yun & Lee, 2018). This has made people very cautious about the use of autophagy as a possible therapeutic target.

Here we have shown a possible role of autophagy in driving tumor growth. Similarly to that observed by (Katheder et al., 2017), autophagy seems to be dependent on JAK/STAT signaling. In this pape,r it was shown that the role of JAK/STAT was mediated by ROS production. However, in our case, ROS do not seem to play the expected role.

Another paper published in the same year showed a role of autonomous autophagy in protecting cells from ROS accumulation thus preventing tumor growth (Manent et al., 2017). This led us to think that maybe some of the differences that are observed in the role of autophagy could be due to differentiated functions of autonomous and non-autonomous autophagy. If this were true it would certainly complicate the use of autophagy inhibitors as a treatment option.

Conclusions

Conclusions

Based on the experiments carried out during the past five years and exposed in this thesis, we can extract the following conclusions.

1. RasV12 expression in *Drosophila* wing imaginal discs induces a benign tissue overgrowth.

2. RasV12 expression promotes G1/S transition and G2 arrest. The later can be rescued by String overexpression.

3. RasV12 cells exhibit characteristics of senescent cells.

4. RasV12 expression induces replicative stress and DNA damage.

5. The mechanisms of DNA damage signaling are impaired by RasV12 expression.

6. RasV12 expressing cells block Dp53-dependent apoptosis in an ERK dependent manner.

7. In wild type tissues, ERK is upregulated, independently of the DDR, upon irradiation.

8. Homeostatic ERK levels prevent developmental and irradiation-induced apoptosis.

9. A combination of irradiation and genetic depletion of ERK can be used to selectively kill RasV12 cells.

10. The previous combination is not effective in killing RasV12, scribble malignant tissues.

11. MEK inhibitors can be combined with irradiation to kill RasV12, scribble cells.

12. Clonally induced RasV12, scribble mutant tumors can be treated with MEK inhibitors to achieve a reduction in tumor burden, a rescue of developmental delay and to selectively induce the death of malignant tumor cells.

13. RasV12 expression causes a non-autonomous induction of DNA damage, apoptosis and autophagy.

Materials and methods

1. Materials

1.1 *Drosophila* Strains:

The following strains were provided by the following sources: (1) Bloomington *Drosophila* Stock Center (BDSC): (2) Vienna *Drosophila* RNAi Center (VDRC):

Table 4. List of *Drosophila* stocks

ap-GAL4	3041	BDSC
elav-gal4	8765	BDSC
en-gal4	30564	BDSC
hid-EGFP.5'F-WT	50750	BDSC
hid-EGFP.5'F-WT	50751	BDSC
Hid-GFP	50750	BDSC
His2Av-mRFP1	23650	BDSC
mCherry-atg8	37749	BDSC
mir277- sponge	61408	BDSC
PCNA-GFP	25749	BDSC
Tub-gal80t^{ts}	41598	BDSC
UAS- His2Av-mKO	53731	BDSC
UAS- Mlh1^{RNAi}	32940	BDSC
UAS-cat A^{RNAi}	24621	BDSC
UAS-CycE	4781	BDSC
UAS-dATM^{RNAi}	108074	BDSC
UAS-dp53-2.1	6584	BDSC
UAS-ERCC1^{1RNAi}	52929	BDSC
UAS-erk^{RNAi}	34855	BDSC
UAS-FamcM^{RNAi}	32889	BDSC
UAS-FancD2^{RNAi}	56141	BDSC
UAS-FancI^{RNAi}	32972	BDSC
UAS-gfp^{RNAi}	35786	BDSC
UAS-Greatwall^{RNAiv}	34525	BDSC
UAS-ksr^{RNAi}	41698	BDSC
UAS-Msh6^{RNAi}	35737	BDSC
UAS-mus201^{RNAi}	35652	BDSC
UAS-myristoylated-Tomato	32222	BDSC
UAS-PARP^{RNAi}	57265	BDSC
UAS-Pms2^{RNAi}	55614	BDSC
UAS-pnt^{RNAi}	31936	BDSC
UAS-PP2A-B^{RNAi}	30512	BDSC
UAS-PP2AB-29B^{RNAi}	43283	BDSC
UAS-PP2C1^{RNAi}	40827	BDSC
UAS-Rad23^{RNAi}	51434	BDSC
UAS-Ras-V12	64196	BDSC

UAS-Ras23^{RNAi}	44031	BDSC
UAS-sod2	24494	BDSC
UAS-TFIIH^{RNAi}	53345	BDSC
UAS-tos^{RNAi}	33934	BDSC
UAS-XPA^{RNAi}	51806	BDSC
UAS-XPF^{RNAi}	55313	BDSC
UAS-XRCC1^{RNAi}	61359	BDSC
ub-EGFP-E2F1$^{1-230}$, ub-RFP-CycB$^{1-266}$	55123	BDSC
ub-EGFP-E2F1$^{1-230}$, ub-RFP-CycB$^{1-266}$	55124	BDSC
UAS-Rad54^{RNAi}	104323	VDRC
UAS-scrib^{RNAi}	105412	VDRC
UAS-scrib^{RNAi}	105412	VDRC
UAS-lig4^{RNAi}	107044	VDRC
UAS-mei-41^{RNAi} (*UAS-dATR^{RNAi}*)	11251	VDRC
UAS-grp^{RNAi} (*UAS-dChk1^{RNAi}*)	12680	VDRC
UAS-rad51^{RNAi}	13362	VDRC
UAS-mus210^{RNAi}	15696	VDRC
UAS-mus81^{RNAi}	33688	VDRC
UAS–dp53^{RNAi}	38235	VDRC
UAS-EME1^{RNAi}	38750	VDRC
UAS-erk^{RNAi}	43123	VDRC
UAS-ent2^{RNAi}	47536	VDRC
UAS-ent3^{RNAi}	47536	VDRC
UAS-ent1^{RNAi}	51055	VDRC
UAS-cnt^{RNAi}	7374	VDRC
DomeDN		(Brown et al., 2001)
Mini-cic		(Moreno et al., 2019)
Upd-lacZ		(Jiang et al., 2011)
Stat92E-GFP		(Bach et al., 2007)
UAS-dE2F1 UAS-DP		(Neufeld et al., 1998)
gstD-GFP		(Sykiotis & Bohmann, 2008)
UAS-RasV12;FTR82B scrib-1		(Cordero et al., 2010)
UAS-Pi3K DN		(Leevers et al.,1996)
ey flp; Act>y+>Gal4, UAS-GFP; FRT82B TubGal80		(Pagliarini & Xu, 2003)
UAS-miRHG		(Siegrist et al., 2010)
UAS-upd^{RNAi}		(Ayala-Camargo et al., 2013)
Tub-RPA-GFP		(Murcia et al., 2019)
Tub-Mre11-GFP		(Murcia et al., 2019)
Tub-Rad50- RFP		(Murcia et al., 2019)

1.2 Antibodies

Table 5. List of primary and secondary antibodies

Mouse anti-dMMP1	14A3D2	DSHB
Rat anti-E-cadherin	DCAD2	DSHB
Mouse anti-P-H2Av	UNC93-5.2.1	DSHB
Rabbit anti-P-H2Av	S137	Rockland Immunochemicals
Rat anti-Ci	2A1	DSHB
Rabbit anti-CycE	Sc-481	Santa Cruz Biotechnology
Rabbit anti-Gal4	Sc-577	Santa Cruz Biotechnology
Rabbit polyclonal anti-p-ERK	4370	Cell Signaling Technology
Rabbit anti-cleaved Dcp1	9578-s	Cell Signaling Technology
Rabbit anti-pAkt	Ser 505	Cell Signaling Technology
Rabbit anti-PH3	Ser 10	Merck
Rabbit anti-Capicua		(Fores et al., 2017)
Mouse anti-CycB	F2F4	DSHB
Mouse anti- Cyc A	A12	DSHB
Mouse anti-ß-gal	40.1A	DSHB
Rabbit anti-dsRed	632496	Clonetech
Alexa fluor 488-conjugated AffiniPure Donkey Anti-Mouse IgG (H+L)		Jackson ImmunoResearch
Cy2 AffiniPure Donkey Anti-Rabbit IgG (H+L)		Jackson ImmunoResearch
Cy3 AffiniPure Donkey Anti-Mouse IgG (H+L)		Jackson ImmunoResearch
Cy3 AffiniPure Donkey Anti-Rabbit IgG (H+L)		Jackson ImmunoResearch
Cy5 AffiniPure Donkey Anti-Rat IgG (H+L)		Jackson ImmunoResearch

Developmental Studies Hybridoma bank (DSBH)

1.3 Other reagents

Table 6. List of reagents

In Situ Cell Death Detection Kit, Fluorescein (TUNEL)	11684 795910	Roche
Click-iT™ Plus EdU Alexa Fluor™ 647 Imaging Kit	C10640	Invitrogen
Click-iT™ Plus EdU Alexa Fluor™ 488 Flow Cytometry Assay Kit	C10632	Invitrogen
Comet Assay Kit	4250-050K	Trevigen
DAPI	28718-90-3	Sigma Aldrich
Trametinib	HY-10999A	MedChem Express
CellEvent™ Senescence Green detection kit	C10850	Invitrogen

2. Methods

2.1 Fly husbandry.

Generally, flies were allowed to lay eggs on standard fly food for 24 hours at 18°C, larvae were maintained at 18°C for 6 days and switched to 29ºC 3 days before dissection (Fig 1). For 15h inductions flies were kept at 18ºC for 9 days and switched at 29ºC 15h prior to dissection. If necessary Trametinib as administered 1 day after transgene expression and 2 days prior to dissection. Irradiation treatment was implemented between 2 and 5 hours prior to dissection (Fig 1).

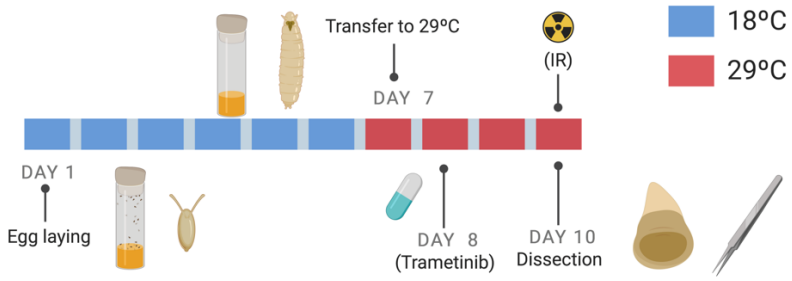

Figure 1. Transgene expression protocol

To generate *RasV12, scrib-/-* clones, flies carrying the *MARCM 82B* green tester (*eyFLP1; act>y+>Gal4, UAS-GFP; FRT82B tub-Gal80* (Pagliarini & Xu, 2003) were crossed with flies of the following genotype *UAS-RasV12; FRT82B scrib*^{1} flies as described in (Mundorf & Uhlirova, 2016). Flies were allowed to lay eggs during 24 h at 25ºC and to develop at this same temperature. As in (Willoughby et al., 2013), Trametinib was added 4 days after egg laying to the food at a 2µM final concentration. Larvae were analyzed 6, 8, 10 and 12 days after egg laying (Fig 2). For pupariation measurements, the same induction protocol was used but flies were allowed to lay eggs for 4 hours. Trametinib treatment was administered ad least one

day after clone induction and flies were evaluated2, 4, 6 or 8 days after treatment (Fig 2).

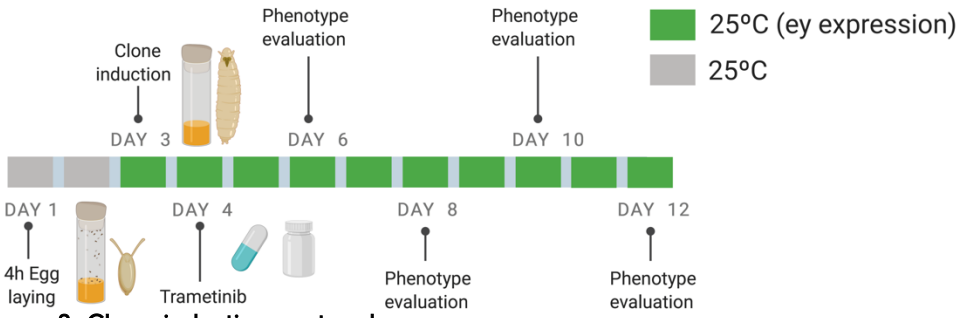

Figure 2. Clone induction protocol

2.2 Treatments

2.2.1 Ionizing Radiation (IR) treatments and quantifications.

Irradiations were carried out in an YXLON MaxiShot X-ray system at the standard dose of 40Gy and at lower doses of 8, 12, 16 and 24 Gy. Number of pH2Av foci, mitotic (pH3-positive) cells and apoptotic (Dcp1-positive) cells were analysed 5 hours after the IR treatment and these numbers were normalized to the area. Measurements in control untreated wing discs grown in parallel were carried out in every experiment. .

2.2.2 Trametinib treatment

Flies were allowed to lay eggs on fly food for 24h and resulting larvae were maintained at 18°C for 6 days. Trametinib (1µM final concentration) was added to vials 1 day after transgene induction. 1,5µl of Trametinib (MedchemExpress) 10 mM (or 1.5 µl DMSO as a control) was diluted in 200 µl of H_2O and added to vials. Trametinib was diluted in DMSO and used at concentrations that ensured that the final DMSO concentration was lower than 0.05%. The final concentration of DMSO was 0.01%.

2.3 Immunostaining and labeling

2.3.1 Immunostaining

Wing imaginal discs of third instar larvae were dissected in cold PBS, fixed with formaldehyde 4% for 20 minutes, rinsed three times in PBT (PBS + 0.1% Triton) and blocked for 1 hour in BBT (PBS + 0.1% Triton+ 0,3% BSA + 250mM NaCl). Then discs were incubated with primary antibodies overnight, rinsed with BBT and incubated with secondary antibodies for 2 hours. After 3 PBT washes, discs were kept on mounting media (80ml glycerol + 10ml PBS 10x + 0,8 ml N-propyl-gallate 50%).

Zeiss LSM780 and Zeiss LSM 880 with airyscan confocal microscopes were used to take high resolution images.

2.3.2 TUNEL assay

TUNEL analysis was performed as described in (Milan et al., 1997) used to label the DNA breaks produced in apoptotic cells (Cat. No. 11 684 795 910, Roche).

2.3.3 EdU labelling

Click-iT™ Plus EdU Alexa Fluor™ 647 Imaging Kit from Invitrogen (C10640) was performed, following the manufacturer's indications, to measure DNA synthesis (S phase) in proliferating cells. EdU (5-ethynyl-2´-deoxyuridine) provided in the kit is a nucleoside analog of thymidine and is incorporated into DNA during active DNA synthesis. Detection is based on a click reaction.

2.3.4 Senescence labelling

CellEvent™ senescence green detection kit from Invitrogen (C10850) was used to detect senescence-associated β-galactosidase (SA-β-gal) activity following the manufacturer's instructions. Wing discs were fixed with 4% PFA, washed (1% BSA in

PBS) and then incubated in working solution for 2h at 37°C. Discs were then washed in PBS and mounted for confocal imaging.

2.4 Image processing and analysis

Fiji [National Institute of Health (NIH) Bethesda, MD] was used to measure the size of the Anterior (A), Dorsal (D) compartments (based on Ci and MyrT expression respectively), or the whole wing discs (based on DAPI staining), and to manually count mitotic cells (PH3 positive cells) or DDR active cells (pH2Av positive cells). Image stacks were obtained using a Zeiss LSM780 confocal microscope, 25X glycerol immersion objective with 4 µm per optical section to cover the entire thickness of each disc, maximum intensity Z-projection was performed on the stacks prior to quantification. Control wing discs grown in parallel and subjected to the same experimental conditions (temperature and time of transgene induction) were always quantified in parallel. At least 10 wing discs per genotype were scored.

2.4.1 Fly-FUCCI quantification:

Images were taken using a Zeiss LSM780 confocal microscope with a 25X glycerol immersion objective. Apical sections of the wing discs where imaged under identical confocal settings. A region of interest was delimited within the asynchronously dividing cells of the wing pouch area, carefully avoiding the zone of non-proliferating cells (ZNC) both in wild type and RasV12-expressing discs. Red, green or red and green cells were manually quantified. RasV12 and control wing discs were grown in parallel and subjected to the same experimental conditions. At least 10 wing discs per genotype were scored.

2.4.2 Measurement of pERK and Cic levels

All samples to be compared were processed in parallel. Apical images were obtained using identical settings in a ZEISS LSM780 confocal microscope. Mean pERK or Capicua intensity was analyzed by FIJI software (NIH, USA). Confocal settings were adjusted to avoid any saturated pixels with maximal intensity.

2.4.3 Comet assay

The Comet Assay Kit (Trevigen, Catalog #4250-050K) was performed as described in (Rimkus & Wassarman, 2018) to detect Double Strand Breaks (DSBs) in the molecule of DNA at a single cell level. Comets were imaged using an ECLIPSE E800 + OLYMPUS DP72 upright microscope with a 10X objective. For each sample, >200 comets were imaged and analyzed using CaspLab Software. Damage was quantified as the comet tail moment, which is defined as the product of the tail length and the fraction of total DNA in the tail (Tail moment=tail length x % of DNA in the tail). Unpaired equal-variance two-tail t-test was performed using GraphPad Prism 7 Project to compare comet tail moment between pairs of samples. The experiment was conducted 3 times with similar results.

2.5 Flow Cytometry analysis

Third instar larvae of each genotype were dissected in cold PBS. To label S-phase cells we used Click-iT™ Plus EdU Alexa Fluor™ 488 Flow Cytometry Assay Kit (C10632), following the manufacturer´s indications with some modifications. After incubating larvae with 10μM EdU in PBS for 5 min, tissues were trypsinized in the presence of EDTA at 32ºC for 45 min as described in (Neufeld et al., 1998). Once Click-iT™ reaction was performed, permeabilized cells were stained with DAPI 1mg/ml and RNase 100 mg/ml and incubated for 1h at RT. Fluorescence was determined by flow cytometry using a FacsAria I SORP sorter (Beckton Dickinson, San

Jose, California). Excitation with the blue line of the laser (488 nm) permits the acquisition of scatter parameters, green (530 nm) fluorescence from GFP and red (635 nm) fluorescence from Tomato. A UV laser (350nm) was used for DAPI excitation. Doublets were discriminated using an integral/peak dotplot of DAPI fluorescence. Optical alignment was on optimized signal from 10 μm fluorescent beads (Flowcheck,Coulter Corporation, Miami, FL). DNA analysis (cell cycle) on single fluorescence histograms was done using FlowJo, LLC Software.

2.6 QuantSeq

Wing imaginal discs expressing MyrT and RasV12 or MyrT and GFP-i under the control of the ap-Gal4 driver were dissected and FACS sorted to isolate the transgene expressing cells. 150.000 cells per replicate were collected in in Lysis Buffer (20 mM DTT, 10 mM Tris.HCl ph 7.4, 0.5% SDS, 1μg/μl proteinase K), incubated 15 min at 65ºC and stored at -80ºC. RNA extraction and library preparation was performed by the Functional Genomic Core Facility at IRB Barcelona. RNA was extracted using RNA Clean XP bead suspension (Agencourt Bioscience), digested with DNAse-I, cleaned-up by a 2nd pull-down and eluted in water. Library preparation was performed from a 150 ng total RNA using the kit Quant Seq 3' mRNA-Seq Library Prep for Illumina (Lexogen) following the manufacturer's instructions. 100 bp SE sequencing was performed in an Illumina HiSeq 2500 by the VBCF NGS Unit. Data was analyzed at IRB Barcelona's Biostatistics and Bioinformatics Unit. Unaligned bam files were converted to FastQ files using Bedtools 2.17. Original 100bp reads were trimmed down to 50bp with trimmomatic 0.33 to reduce trailing PolyA contamination. FastQ files were aligned against the dm6 genome using STAR 2.3.0e, using default options. Aligned reads were imported in R using RSamtools to perform further quality control steps. Only reads with MapQ>0 (aligning to 10 sites or less) were kept for downstream procedures. To obtain per-sample expression estimates we used the

summarize Overlaps function from the Genomic Alignments package, using the Intersection Not Empty mode and single end strand specific options. Counts were used to perform a differential expression analysis using the DESeq2 package, previously removing genes without reads in any of the analyzed samples, and using the default options. Output results were filtered to consider differentially expressed genes with |FC|>2 and Benjamini-Hochberg adjusted pvalue < 0.05. FastQC v011 was used to perform a quality control overview of FastQ files and aligned BAM files. Binary tracks in BigWig format were generated with the tracklayer package, both for individual and pooled samples by group. The log2FC information was used to rank all genes in the genome with n reads>0 and a Gene Set Enrichment Analysis (Subramanian et al., 2005)was performed with Gene Ontology Biological Processes (Gene Ontology Consortium, 2015), GOSLIM and KEGG collections.

2.7 Statistical Analysis

Statistical analysis was generally performed by Students t-test. Differences were considered significant when p values were less than 0.001 (***), 0.01 (**), or 0.05 (*). All genotypes included in each histogram were analyzed in parallel. For comparisons of differences, Wald test derived from the linear model after quadratic root transformation was used to perform pairwise comparisons and to assess the significance of the interaction. Results for pairwise comparisons were adjusted by multiple comparisons using Shaffer's method. A 5% level was chosen as significance threshold. All data points were graphed in Prism 7.0 (Graphpad) statistical software.

Bibliography

Abulaiti, A., Fikaris, A. J., Tsygankova, O. M., & Meinkoth, J. L. (2006). Ras induces chromosome instability and abrogation of the DNA damage response. *Cancer Research*, *66*(21), 10505–10512. https://doi.org/10.1158/0008-5472.CAN-06-2351

Agarwal, V., Subtelny, A. O., Thiru, P., Ulitsky, I., & Bartel, D. P. (2018). Predicting microRNA targeting efficacy in Drosophila. *Genome Biology*, *19*(1), 152. https://doi.org/10.1186/s13059-018-1504-3

Alexandru Dan Corlan. (2004). Medline trend: automated yearly statistics of PubMed results for any query. Retrieved June 6, 2019, from http://dan.corlan.net/medline-trend.html

Ayala-Camargo, A., Anderson, A. M., Amoyel, M., Rodrigues, A. B., Flaherty, M. S., & Bach, E. A. (2013). JAK/STAT signaling is required for hinge growth and patterning in the Drosophila wing disc. *Developmental Biology*, *382*(2), 413–426. https://doi.org/10.1016/j.ydbio.2013.08.016

Bach, E. A., Ekas, L. A., Ayala-Camargo, A., Flaherty, M. S., Lee, H., Perrimon, N., & Baeg, G.-H. (2007). GFP reporters detect the activation of the Drosophila JAK/STAT pathway in vivo. *Gene Expression Patterns*, *7*(3), 323–331. https://doi.org/10.1016/j.modgep.2006.08.003

Bartkova, J., Horejsí, Z., Koed, K., Krämer, A., Tort, F., Zieger, K., … Bartek, J. (2005). DNA damage response as a candidate anti-cancer barrier in early human tumorigenesis. *Nature*, *434*(7035), 864–870. https://doi.org/10.1038/nature03482

Bartkova, J., Rezaei, N., Liontos, M., Karakaidos, P., Kletsas, D., Issaeva, N., … Gorgoulis, V. G. (2006a). Oncogene-induced senescence is part of the tumorigenesis barrier imposed by DNA damage checkpoints. *Nature*, *444*(7119), 633–637. https://doi.org/10.1038/nature05268

Bartkova, J., Rezaei, N., Liontos, M., Karakaidos, P., Kletsas, D., Issaeva, N., … Gorgoulis, V. G. (2006b). Oncogene-induced senescence is part of the tumorigenesis barrier imposed by DNA damage checkpoints. *Nature*, *444*(7119), 633–637. https://doi.org/10.1038/nature05268

Bayer, F. E., Zimmermann, M., Preiss, A., & Nagel, A. C. (2018a). Overexpression of the Drosophila ATR homologous checkpoint kinase Mei-41 induces a G2/M checkpoint in Drosophila imaginal tissue. *Hereditas*, *155*(1), 27. https://doi.org/10.1186/s41065-018-0066-4

Bayer, F. E., Zimmermann, M., Preiss, A., & Nagel, A. C. (2018b). Overexpression of the Drosophila ATR homologous checkpoint kinase Mei-41 induces a G2/M

checkpoint in Drosophila imaginal tissue. *Hereditas*, *155*(1), 27. https://doi.org/10.1186/s41065-018-0066-4

Beesetti, S., Mavuluri, J., Surabhi, R. P., Oberyszyn, T. M., Tober, K., Pitani, R. S., … Rayala, S. K. (2017). Transcriptional regulation of ataxia-telangiectasia and Rad3-related protein by activated p21-activated kinase-1 protects keratinocytes in UV-B-induced premalignant skin lesions. *Oncogene*, *36*(44), 6154–6163. https://doi.org/10.1038/onc.2017.218

Beira, J. V., & Paro, R. (2016). The legacy of Drosophila imaginal discs. *Chromosoma*, *125*(4), 573–592. https://doi.org/10.1007/s00412-016-0595-4

Bellen, H. J., Tong, C., & Tsuda, H. (2010). 100 years of Drosophila research and its impact on vertebrate neuroscience: a history lesson for the future. *Nature Reviews. Neuroscience*, *11*(7), 514–522. https://doi.org/10.1038/nrn2839

Bergmann, A., Agapite, J., McCall, K., & Steller, H. (1998). The Drosophila gene hid is a direct molecular target of Ras-dependent survival signaling. *Cell*, *95*(3), 331–341. Retrieved from http://www.ncbi.nlm.nih.gov/pubmed/9814704

Brand, A. H., & Perrimon, N. (1993). Targeted gene expression as a means of altering cell fates and generating dominant phenotypes. *Development (Cambridge, England)*, *118*(2), 401–415. Retrieved from http://www.ncbi.nlm.nih.gov/pubmed/8223268

Brodsky, M. H., Weinert, B. T., Tsang, G., Rong, Y. S., McGinnis, N. M., Golic, K. G., … Rubin, G. M. (2004). Drosophila melanogaster MNK/Chk2 and p53 regulate multiple DNA repair and apoptotic pathways following DNA damage. *Molecular and Cellular Biology*, *24*(3), 1219–1231. https://doi.org/10.1128/mcb.24.3.1219-1231.2004

Brown, S., Hu, N., & Hombría, J. C. (2001). Identification of the first invertebrate interleukin JAK/STAT receptor, the Drosophila gene domeless. *Current Biology : CB*, *11*(21), 1700–1705. Retrieved from http://www.ncbi.nlm.nih.gov/pubmed/11696329

Brugnara, S., Sicher, M., Bonandini, E. M., Donner, D., Chierichetti, F., Barbareschi, M., … Caffo, O. (2018). Treatment with combined dabrafenib and trametinib in BRAFV600E-mutated metastatic malignant melanoma: a case of long-term complete response after treatment cessation. *Drugs in Context*, *7*, 212515. https://doi.org/10.7573/dic.212515

Brumby, A. M., & Richardson, H. E. (2003). scribble mutants cooperate with oncogenic Ras or Notch to cause neoplastic overgrowth in Drosophila. *The EMBO Journal*, *22*(21), 5769–5779. https://doi.org/10.1093/emboj/cdg548

Bukhari, A. B., Lewis, C. W., Pearce, J. J., Luong, D., Chan, G. K., & Gamper, A. M. (2019). Inhibiting Wee1 and ATR kinases produces tumor-selective synthetic lethality and suppresses metastasis. *The Journal of Clinical Investigation*, *129*(3), 1329–1344. https://doi.org/10.1172/JCI122622

Casar, B., Pinto, A., & Crespo, P. (2008). Essential Role of ERK Dimers in the Activation of Cytoplasmic but Not Nuclear Substrates by ERK-Scaffold Complexes. *Molecular Cell*, *31*(5), 708–721. https://doi.org/10.1016/J.MOLCEL.2008.07.024

Chapman, P. B. (2013). Mechanisms of resistance to RAF inhibition in melanomas harboring a BRAF mutation. *American Society of Clinical Oncology Educational Book. American Society of Clinical Oncology. Annual Meeting*. https://doi.org/10.1200/EdBook_AM.2013.33.e80

Chatterjee, N., & Walker, G. C. (2017). Mechanisms of DNA damage, repair, and mutagenesis. *Environmental and Molecular Mutagenesis*, *58*(5), 235–263. https://doi.org/10.1002/em.22087

Choi, H., Deng, J., Li, S., Silk, T., Dong, L., Brea, E. J., … Wolchok, J. D. (2019). Pulsatile MEK Inhibition Improves Anti-tumor Immunity and T Cell Function in Murine Kras Mutant Lung Cancer. *Cell Reports*, *27*(3), 806–819.e5. https://doi.org/10.1016/j.celrep.2019.03.066

Corcoran, N. M., Clarkson, M. J., Stuchbery, R., & Hovens, C. M. (2016). Molecular Pathways: Targeting DNA Repair Pathway Defects Enriched in Metastasis. *Clinical Cancer Research*, *22*(13), 3132–3137. https://doi.org/10.1158/1078-0432.CCR-15-1050

Cordero, J. B., Macagno, J. P., Stefanatos, R. K., Strathdee, K. E., Cagan, R. L., & Vidal, M. (2010). Oncogenic Ras diverts a host TNF tumor suppressor activity into tumor promoter. *Developmental Cell*, *18*(6), 999–1011. https://doi.org/10.1016/j.devcel.2010.05.014

Cox, A. D., & Der, C. J. (2003). The dark side of Ras: regulation of apoptosis. *Oncogene*, *22*(56), 8999–9006. https://doi.org/10.1038/sj.onc.1207111

Cox, A. D., Fesik, S. W., Kimmelman, A. C., Luo, J., & Der, C. J. (2014). Drugging the undruggable RAS: Mission Possible? *Nature Reviews Drug Discovery*, *13*(11), 828–851. https://doi.org/10.1038/nrd4389

Datar, S. A., Jacobs, H. W., de la Cruz, A. F., Lehner, C. F., & Edgar, B. A. (2000). The Drosophila cyclin D-Cdk4 complex promotes cellular growth. *The EMBO Journal*, *19*(17), 4543–4554. https://doi.org/10.1093/emboj/19.17.4543

de Vries, H. I., Uyetake, L., Lemstra, W., Brunsting, J. F., Su, T. T., Kampinga, H. H., & Sibon, O. C. M. (2005). Grp/DChk1 is required for G2-M checkpoint activation in Drosophila S2 cells, whereas Dmnk/DChk2 is dispensable. *Journal of Cell Science*, *118*(9), 1833–1842. https://doi.org/10.1242/jcs.02309

Dekanty, A., Barrio, L., & Milán, M. (2015). Contributions of DNA repair, cell cycle checkpoints and cell death to suppressing the DNA damage-induced tumorigenic behavior of Drosophila epithelial cells. *Oncogene*, *34*(8), 978–985. https://doi.org/10.1038/onc.2014.42

Denko, N. C., Giaccia, A. J., Stringer, J. R., & Stambrook, P. J. (1994). The human Ha-ras oncogene induces genomic instability in murine fibroblasts within one cell cycle. *Proceedings of the National Academy of Sciences of the United States of America*, *91*(11), 5124–5128. Retrieved from http://www.pubmedcentral.nih.gov/articlerender.fcgi?artid=43944&tool=pmcentrez&rendertype=abstract

Dent, P., Yacoub, A., Fisher, P. B., Hagan, M. P., & Grant, S. (2003). MAPK pathways in radiation responses. *Oncogene*, *22*(37), 5885–5896. https://doi.org/10.1038/sj.onc.1206701

Di Micco, R., Fumagalli, M., Cicalese, A., Piccinin, S., Gasparini, P., Luise, C., … d'Adda di Fagagna, F. (2006). Oncogene-induced senescence is a DNA damage response triggered by DNA hyper-replication. *Nature*, *444*(7119), 638–642. https://doi.org/10.1038/nature05327

Downward, J. (1997). Cell cycle: Routine role for Ras. *Current Biology*, *7*(4), R258–R260. https://doi.org/10.1016/S0960-9822(06)00116-3

Downward, J. (2015). RAS Synthetic Lethal Screens Revisited: Still Seeking the Elusive Prize? *Clinical Cancer Research : An Official Journal of the American Association for Cancer Research*, *21*(8), 1802–1809. https://doi.org/10.1158/1078-0432.CCR-14-2180

Efeyan, A., Murga, M., Martinez-Pastor, B., Ortega-Molina, A., Soria, R., Collado, M., … Serrano, M. (2009). Limited role of murine ATM in oncogene-induced senescence and p53-dependent tumor suppression. *PloS One*, *4*(5), e5475. https://doi.org/10.1371/journal.pone.0005475

Figueroa-Clarevega, A., & Bilder, D. (2015). Malignant Drosophila tumors interrupt insulin signaling to induce cachexia-like wasting. *Developmental Cell*, *33*(1), 47–55. https://doi.org/10.1016/j.devcel.2015.03.001

Flaherty, K. T., Robert, C., Hersey, P., Nathan, P., Garbe, C., Milhem, M., … Schadendorf, D. (2012). Improved Survival with MEK Inhibition in BRAF-Mutated

Melanoma. *New England Journal of Medicine*, *367*(2), 107–114. https://doi.org/10.1056/NEJMoa1203421

Fores, M., Simon-Carrasco, L., Ajuria, L., Samper, N., Gonzalez-Crespo, S., Drosten, M., … Jimenez, G. (2017). A new mode of DNA binding distinguishes Capicua from other HMG-box factors and explains its mutation patterns in cancer. *PLoS Genet*, *13*(3), e1006622. https://doi.org/10.1371/journal.pgen.1006622

Gaillard, H., García-Muse, T., & Aguilera, A. (2015). Replication stress and cancer. *Nature Reviews Cancer*, *15*(5), 276–289. https://doi.org/10.1038/nrc3916

Gene Ontology Consortium. (2015). Gene Ontology Consortium: going forward. *Nucleic Acids Research*, *43*(D1), D1049–D1056. https://doi.org/10.1093/nar/gku1179

Gilmartin, A. G., Bleam, M. R., Groy, A., Moss, K. G., Minthorn, E. A., Kulkarni, S. G., … Laquerre, S. G. (2011). GSK1120212 (JTP-74057) Is an Inhibitor of MEK Activity and Activation with Favorable Pharmacokinetic Properties for Sustained In Vivo Pathway Inhibition. *Clinical Cancer Research*, *17*(5), 989–1000. https://doi.org/10.1158/1078-0432.CCR-10-2200

Gonzalez, C. (2013). Drosophila melanogaster: a model and a tool to investigate malignancy and identify new therapeutics. *Nature Reviews. Cancer*, *13*(3), 172–183. https://doi.org/10.1038/nrc3461

Gorgoulis, V. G., Vassiliou, L.-V. F., Karakaidos, P., Zacharatos, P., Kotsinas, A., Liloglou, T., … Halazonetis, T. D. (2005). Activation of the DNA damage checkpoint and genomic instability in human precancerous lesions. *Nature*, *434*(7035), 907–913. https://doi.org/10.1038/nature03485

Grabocka, E., Pylayeva-Gupta, Y., Jones, M. J. K., Lubkov, V., Yemanaberhan, E., Taylor, L., … Bar-Sagi, D. (2014). Wild-Type H- and N-Ras Promote Mutant K-Ras-Driven Tumorigenesis by Modulating the DNA Damage Response. *Cancer Cell*, *25*(2), 243–256. https://doi.org/10.1016/j.ccr.2014.01.005

Griffin, M., Scotto, D., Josephs, D. H., Mele, S., Crescioli, S., Bax, H. J., … Karagiannis, S. N. (2017). BRAF inhibitors: resistance and the promise of combination treatments for melanoma. *Oncotarget*, *8*(44), 78174–78192. https://doi.org/10.18632/oncotarget.19836

Guo, J. Y., Teng, X., Laddha, S. V., Ma, S., Van Nostrand, S. C., Yang, Y., … White, E. (2016). Autophagy provides metabolic substrates to maintain energy charge and nucleotide pools in Ras-driven lung cancer cells. *Genes & Development*, *30*(15), 1704–1717. https://doi.org/10.1101/gad.283416.116

Halazonetis, T. D. (2009). An Oncogene-Induced DNA Replication Stress Model for Cancer Development. In *The DNA Damage Response: Implications on Cancer Formation and Treatment* (pp. 47–63). Dordrecht: Springer Netherlands. https://doi.org/10.1007/978-90-481-2561-6_3

Halazonetis, T. D., Gorgoulis, V. G., & Bartek, J. (2008a). An oncogene-induced DNA damage model for cancer development. *Science (New York, N.Y.)*, *319*(5868), 1352–1355. https://doi.org/10.1126/science.1140735

Halazonetis, T. D., Gorgoulis, V. G., & Bartek, J. (2008b). An oncogene-induced DNA damage model for cancer development. *Science (New York, N.Y.)*, *319*(5868), 1352–1355. https://doi.org/10.1126/science.1140735

Hales, K. G., Korey, C. A., Larracuente, A. M., & Roberts, D. M. (2015). Genetics on the fly: A primer on the drosophila model system. *Genetics*, *201*(3), 815–842. https://doi.org/10.1534/genetics.115.183392

Hanahan, D., & Weinberg, R. A. (2000). The hallmarks of cancer. *Cell*, *100*(1), 57–70. https://doi.org/10.1016/S0092-8674(00)81683-9

Hanahan, D., & Weinberg, R. A. (2011). Hallmarks of cancer: the next generation. *Cell*, *144*(5), 646–674. https://doi.org/10.1016/j.cell.2011.02.013

He, M., Zhou, W., Li, C., & Guo, M. (2016). MicroRNAs, DNA Damage Response, and Cancer Treatment. *International Journal of Molecular Sciences*, *17*(12). https://doi.org/10.3390/ijms17122087

Hein, A. L., Ouellette, M. M., & Yan, Y. (2014). Radiation-induced signaling pathways that promote cancer cell survival (review). *International Journal of Oncology*, *45*(5), 1813–1819. https://doi.org/10.3892/ijo.2014.2614

Helleday, T., Petermann, E., Lundin, C., Hodgson, B., & Sharma, R. A. (2008). DNA repair pathways as targets for cancer therapy. *Nature Reviews Cancer*, *8*(3), 193–204. https://doi.org/10.1038/nrc2342

Herranz, H., Weng, R., & Cohen, S. M. (2014). Crosstalk between epithelial and mesenchymal tissues in tumorigenesis and imaginal disc development. *Current Biology : CB*, *24*(13), 1476–1484. https://doi.org/10.1016/j.cub.2014.05.043

Hewitt, G., & Korolchuk, V. I. (2017). Repair, Reuse, Recycle: The Expanding Role of Autophagy in Genome Maintenance. *Trends in Cell Biology*, *27*, 340–351. https://doi.org/10.1016/j.tcb.2016.11.011

Hills, S. A., & Diffley, J. F. X. (2014a). DNA replication and oncogene-induced

replicative stress. *Current Biology : CB*, *24*(10), R435-44. https://doi.org/10.1016/j.cub.2014.04.012

Hills, S. A., & Diffley, J. F. X. (2014b). DNA Replication and Oncogene-Induced Replicative Stress. *Current Biology*, *24*(10), R435–R444. https://doi.org/10.1016/J.CUB.2014.04.012

Igaki, T., Pagliarini, R. A., & Xu, T. (2006). Loss of cell polarity drives tumor growth and invasion through JNK activation in Drosophila. *Current Biology : CB*, *16*(11), 1139–1146. https://doi.org/10.1016/j.cub.2006.04.042

Jennings, B. H. (2011). Drosophila-a versatile model in biology & medicine. *Materials Today*, *14*(5), 190–195. https://doi.org/10.1016/S1369-7021(11)70113-4

Jiang, H., Grenley, M. O., Bravo, M.-J., Blumhagen, R. Z., & Edgar, B. A. (2011). EGFR/Ras/MAPK signaling mediates adult midgut epithelial homeostasis and regeneration in Drosophila. *Cell Stem Cell*, *8*(1), 84–95. https://doi.org/10.1016/j.stem.2010.11.026

Joyce, E. F., Pedersen, M., Tiong, S., White-Brown, S. K., Paul, A., Campbell, S. D., & McKim, K. S. (2011). Drosophila ATM and ATR have distinct activities in the regulation of meiotic DNA damage and repair. *The Journal of Cell Biology*, *195*(3), 359–367. https://doi.org/10.1083/jcb.201104121

Karim, F. D., & Rubin, G. M. (1998). Ectopic expression of activated Ras1 induces hyperplastic growth and increased cell death in Drosophila imaginal tissues. *Development (Cambridge, England)*, *125*(1), 1–9. Retrieved from http://www.ncbi.nlm.nih.gov/pubmed/9389658

Karim, F., & Rubin, G. (1998). Ectopic expression of activated Ras1 induces hyperplastic growth and increased cell death in Drosophila imaginal tissues. *Development*, *125*(1), 1–9. Retrieved from http://dev.biologists.org/content/125/1/1.abstract?ijkey=d2c5b19688b7534a05e1c959e4de442b2277255d&keytype2=tf_ipsecsha

Karnoub, A. E., & Weinberg, R. A. (2008). Ras oncogenes: split personalities. *Nature Reviews. Molecular Cell Biology*, *9*(7), 517–531. https://doi.org/10.1038/nrm2438

Kasai, Y., & Cagan, R. (2010). Drosophila as a tool for personalized medicine: a primer. *Personalized Medicine*, *7*(6), 621–632. https://doi.org/10.2217/pme.10.65

Kaseb, H., & Hozayen, S. (2019). *Chromosome Instability Syndromes*. *StatPearls*.

Retrieved from http://www.ncbi.nlm.nih.gov/pubmed/30725883

Katheder, N. S., Khezri, R., O'Farrell, F., Schultz, S. W., Jain, A., Rahman, M. M., … Rusten, T. E. (2017). Microenvironmental autophagy promotes tumour growth. *Nature*, *541*(7637), 417. https://doi.org/10.1038/NATURE20815

Kurada, P., & White, K. (1998). Ras promotes cell survival in Drosophila by downregulating hid expression. *Cell*, *95*(3), 319–329. https://doi.org/10.1016/S0092-8674(00)81764-X

Lecona, E., & Fernandez-Capetillo, O. (2018). Targeting ATR in cancer. *Nature Reviews Cancer*, *18*(9), 586–595. https://doi.org/10.1038/s41568-018-0034-3

Lee, H.-J., Cao, Y., Pham, V., Blackwood, E., Wilson, C., Evangelista, M., … Settleman, J. (2017). Ras-MEK Signaling Mediates a Critical Chk1-Dependent DNA Damage Response in Cancer Cells. *Molecular Cancer Therapeutics*, *16*(4), 694–704. https://doi.org/10.1158/1535-7163.MCT-16-0504

Lee, T., & Luo, L. (1999). Mosaic Analysis with a Repressible Cell Marker for Studies of Gene Function in Neuronal Morphogenesis. *Neuron*, *22*(3), 451–461. https://doi.org/10.1016/S0896-6273(00)80701-1

Leevers, S. J., Weinkove, D., MacDougall, L. K., Hafen, E., & Waterfield, M. D. (1996). The Drosophila phosphoinositide 3-kinase Dp110 promotes cell growth. *Embo J*, *15*, 6584–6594.

Levine, B. D., & Cagan, R. L. (n.d.). Drosophila Lung Cancer Models Identify Trametinib Plus Statin as Candidate Therapeutic. https://doi.org/10.1016/j.celrep.2015.12.105

Levine, B. D., & Cagan, R. L. (2016). Drosophila Lung Cancer Models Identify Trametinib plus Statin as Candidate Therapeutic. *Cell Reports*, *14*(6), 1477–1487. https://doi.org/10.1016/j.celrep.2015.12.105

López-Contreras, A. J., Gutierrez-Martinez, P., Specks, J., Rodrigo-Perez, S., & Fernandez-Capetillo, O. (2012). An extra allele of Chk1 limits oncogene-induced replicative stress and promotes transformation. *The Journal of Experimental Medicine*, *209*(3), 455–461. https://doi.org/10.1084/jem.20112147

Malumbres, M., & Barbacid, M. (2003). RAS oncogenes: the first 30 years. *Nature Reviews. Cancer*, *3*(6), 459–465. https://doi.org/10.1038/nrc1097

Manent, J., Banerjee, S., de Matos Simoes, R., Zoranovic, T., Mitsiades, C., Penninger, J. M., … Richardson, H. E. (2017). Autophagy suppresses Ras-driven

epithelial tumourigenesis by limiting the accumulation of reactive oxygen species. *Oncogene*, *36*(40), 5576–5592. https://doi.org/10.1038/onc.2017.175

Milan, M., Campuzano, S., & Garcia-Bellido, A. (1997). Developmental parameters of cell death in the wing disc of Drosophila. *Proc Natl Acad Sci U S A*, *94*(11), 5691–5696.

Mogila, V., Xia, F., & Li, W. X. (2006). An Intrinsic Cell Cycle Checkpoint Pathway Mediated by MEK and ERK in Drosophila. *Developmental Cell*, *11*(4), 575–582. https://doi.org/10.1016/j.devcel.2006.08.010

Moreno, E., Eo Valon, L., Levillayer, F., Correspondence, R. L., & Levayer, R. (2019). Competition for Space Induces Cell Elimination through Compaction-Driven ERK Downregulation. *Current Biology*, *29*, 23–34. https://doi.org/10.1016/j.cub.2018.11.007

Mundorf, J., & Uhlirova, M. (2016). The Drosophila Imaginal Disc Tumor Model: Visualization and Quantification of Gene Expression and Tumor Invasiveness Using Genetic Mosaics. *Journal of Visualized Experiments*, (116). https://doi.org/10.3791/54585

Munshi, A., & Ramesh, R. (2013). Mitogen-activated protein kinases and their role in radiation response. *Genes & Cancer*, *4*(9–10), 401–408. https://doi.org/10.1177/1947601913485414

Murcia, L., Clemente-Ruiz, M., Pierre-Elies, P., Royou, A., & Milán, M. (2019). Selective Killing of RAS-Malignant Tissues by Exploiting Oncogene-Induced DNA Damage. *Cell Reports*, *28*(1), 119–131.e4. https://doi.org/10.1016/j.celrep.2019.06.004

Murga, M., Campaner, S., Lopez-Contreras, A. J., Toledo, L. I., Soria, R., Montaña, M. F., … Fernandez-Capetillo, O. (2011). Exploiting oncogene-induced replicative stress for the selective killing of Myc-driven tumors. *Nature Structural & Molecular Biology*, *18*(12), 1331–1335. https://doi.org/10.1038/nsmb.2189

Muzzopappa, M., Murcia, L., & Milán, M. (2017). Feedback amplification loop drives malignant growth in epithelial tissues. *Proceedings of the National Academy of Sciences of the United States of America*, *114*(35). https://doi.org/10.1073/pnas.1701791114

Nakamura, M., Ohsawa, S., & Igaki, T. (2014). Mitochondrial defects trigger proliferation of neighbouring cells via a senescence-associated secretory phenotype in Drosophila. *Nature Communications*, *5*(1), 5264. https://doi.org/10.1038/ncomms6264

Negrini, S., Gorgoulis, V. G., & Halazonetis, T. D. (2010). Genomic instability–an evolving hallmark of cancer. *Nature Reviews. Molecular Cell Biology*, *11*(3), 220–228. https://doi.org/10.1038/nrm2858

Neufeld, T. P., de la Cruz, A. F., Johnston, L. A., & Edgar, B. A. (1998). Coordination of growth and cell division in the Drosophila wing. *Cell*, *93*(7), 1183–1193.

Neuman-Silberberg, F. S., Schejter, E., Hoffmann, F. M., & Shilo, B. Z. (1984). The Drosophila ras oncogenes: structure and nucleotide sequence. *Cell*, *37*(3), 1027–1033. https://doi.org/10.1016/0092-8674(84)90437-9

O'Brochta, D. A., & Bryant, P. J. (1985). A zone of non-proliferating cells at a lineage restriction boundary in Drosophila. *Nature*, *313*(5998), 138–141. https://doi.org/10.1038/313138a0

O'Connor, M. J. (2015). Targeting the DNA Damage Response in Cancer. *Molecular Cell*, *60*(4), 547–560. https://doi.org/10.1016/j.molcel.2015.10.040

Ohsawa, S., Sato, Y., Enomoto, M., Nakamura, M., Betsumiya, A., & Igaki, T. (2012). Mitochondrial defect drives non-autonomous tumour progression through Hippo signalling in Drosophila. *Nature*, *490*(7421), 547–551. https://doi.org/10.1038/nature11452

Ong, C., Yung, L.-Y. L., Cai, Y., Bay, B.-H., & Baeg, G.-H. (2015). *Drosophila melanogaster* as a model organism to study nanotoxicity. *Nanotoxicology*, *9*(3), 396–403. https://doi.org/10.3109/17435390.2014.940405

Pagliarini, R. A., & Xu, T. (2003). A genetic screen in Drosophila for metastatic behavior. *Science (New York, N.Y.)*, *302*(5648), 1227–1231. https://doi.org/10.1126/science.1088474

Pang, X., & Liu, M. (2017). Defeat mutant *KRAS* with synthetic lethality. *Small GTPases*, *8*(4), 212–219. https://doi.org/10.1080/21541248.2016.1213783

Pastor-Pareja, J. C., Wu, M., & Xu, T. (2008). An innate immune response of blood cells to tumors and tissue damage in Drosophila. *Disease Models & Mechanisms*, *1*(2–3), 144–54; discussion 153. https://doi.org/10.1242/dmm.000950

Peters, M., DeLuca, C., Hirao, A., Stambolic, V., Potter, J., Zhou, L., … Mak, T. W. (2002). Chk2 regulates irradiation-induced, p53-mediated apoptosis in Drosophila. *Proceedings of the National Academy of Sciences*, *99*(17), 11305–11310. https://doi.org/10.1073/pnas.172382899

Planchard, D., Besse, B., Groen, H. J. M., Souquet, P.-J., Quoix, E., Baik, C. S., …

Johnson, B. E. (2016). Dabrafenib plus trametinib in patients with previously treated BRAFV600E-mutant metastatic non-small cell lung cancer: an open-label, multicentre phase 2 trial. *The Lancet Oncology*, *17*(7), 984–993. https://doi.org/10.1016/S1470-2045(16)30146-2

Prober, D. A., & Edgar, B. A. (2000). Ras1 promotes cellular growth in the Drosophila wing. *Cell*, *100*(4), 435–446. Retrieved from http://www.ncbi.nlm.nih.gov/pubmed/10693760

Prober, D. A., & Edgar, B. A. (2002). Interactions between Ras1, dMyc, and dPI3K signaling in the developing Drosophila wing. *Genes & Development*, *16*(17), 2286–2299. https://doi.org/10.1101/gad.991102

Puigvert, J. C., Sanjiv, K., & Helleday, T. (2016). Targeting DNA repair, DNA metabolism and replication stress as anti-cancer strategies. *FEBS Journal*, *283*(2), 232–245. https://doi.org/10.1111/febs.13574

Pylayeva-Gupta, Y., Grabocka, E., & Bar-Sagi, D. (2011). RAS oncogenes: weaving a tumorigenic web. *Nature Reviews. Cancer*, *11*(11), 761–774. https://doi.org/10.1038/nrc3106

Ray, S., Atkuri, K. R., Deb-Basu, D., Adler, A. S., Chang, H. Y., Herzenberg, L. A., & Felsher, D. W. (2006). *MYC* Can Induce DNA Breaks *In vivo* and *In vitro* Independent of Reactive Oxygen Species. *Cancer Research*, *66*(13), 6598–6605. https://doi.org/10.1158/0008-5472.CAN-05-3115

Razidlo, G. L., Johnson, H. J., Stoeger, S. M., Cowan, K. H., Bessho, T., & Lewis, R. E. (2009). KSR1 Is Required for Cell Cycle Reinitiation Following DNA Damage. *Journal of Biological Chemistry*, *284*(11), 6705–6715. https://doi.org/10.1074/jbc.M806457200

Rimkus, S. A., & Wassarman, D. A. (2018). A pharmacological screen for compounds that rescue the developmental lethality of a Drosophila ATM mutant. *PLOS ONE*, *13*(1), e0190821. https://doi.org/10.1371/journal.pone.0190821

Rojas, J. M., Oliva, J. L., & Santos, E. (2011). Mammalian son of sevenless Guanine nucleotide exchange factors: old concepts and new perspectives. *Genes & Cancer*, *2*(3), 298–305. https://doi.org/10.1177/1947601911408078

Rudrapatna, V. A., Cagan, R. L., & Das, T. K. (2012). Drosophila cancer models. *Developmental Dynamics : An Official Publication of the American Association of Anatomists*, *241*(1), 107–118. https://doi.org/10.1002/dvdy.22771

Ruiz, S., Mayor-Ruiz, C., Lafarga, V., Murga, M., Vega-Sendino, M., Ortega, S., & Fernandez-Capetillo, O. (2016). A Genome-wide CRISPR Screen Identifies

CDC25A as a Determinant of Sensitivity to ATR Inhibitors. *Molecular Cell*, *62*(2), 307–313. https://doi.org/10.1016/J.MOLCEL.2016.03.006

Sakai, T., Yamaguchi, T., Kakefuda, R., Kakefuda, R., Tajima, N., Tajima, N., … Sakai, T. (2011). Antitumor activities of JTP-74057 (GSK1120212), a novel MEK1/2 inhibitor, on colorectal cancer cell lines in vitro and in vivo. *International Journal of Oncology*, *39*(1), 23–31. https://doi.org/10.3892/ijo.2011.1015

Sethy, R., Rakesh, R., Patne, K., Arya, V., Sharma, T., Haokip, D. T., … Muthuswami, R. (2018). Regulation of ATM and ATR by SMARCAL1 and BRG1. *Biochimica et Biophysica Acta (BBA) - Gene Regulatory Mechanisms*, *1861*(12), 1076–1092. https://doi.org/10.1016/J.BBAGRM.2018.10.004

Siegrist, S. E., Haque, N. S., Chen, C. H., Hay, B. A., & Hariharan, I. K. (2010). Inactivation of both Foxo and reaper promotes long-term adult neurogenesis in Drosophila. *Curr Biol*, *20*(7), 643–648. https://doi.org/10.1016/j.cub.2010.01.060

Simanshu, D. K., Nissley, D. V., & McCormick, F. (2017). RAS Proteins and Their Regulators in Human Disease. *Cell*, *170*(1), 17–33. https://doi.org/10.1016/j.cell.2017.06.009

Song, W., Kir, S., Hong, S., Hu, Y., Wang, X., Binari, R., … Perrimon, N. (2019). Tumor-Derived Ligands Trigger Tumor Growth and Host Wasting via Differential MEK Activation. *Developmental Cell*, *48*(2), 277–286.e6. https://doi.org/10.1016/j.devcel.2018.12.003

Song, Y.-H. (2005). Drosophila melanogaster: a model for the study of DNA damage checkpoint response. *Molecules and Cells*, *19*(2), 167–179. Retrieved from http://www.ncbi.nlm.nih.gov/pubmed/15879698

Subbiah, V., Kreitman, R. J., Wainberg, Z. A., Cho, J. Y., Schellens, J. H. M., Soria, J. C., … Keam, B. (2018). Dabrafenib and Trametinib Treatment in Patients With Locally Advanced or Metastatic BRAF V600-Mutant Anaplastic Thyroid Cancer. *Journal of Clinical Oncology : Official Journal of the American Society of Clinical Oncology*, *36*(1), 7–13. https://doi.org/10.1200/JCO.2017.73.6785

Subramanian, A., Tamayo, P., Mootha, V. K., Mukherjee, S., Ebert, B. L., Gillette, M. A., … Mesirov, J. P. (2005). Gene set enrichment analysis: a knowledge-based approach for interpreting genome-wide expression profiles. *Proc Natl Acad Sci U S A*, *102*(43), 15545–15550. https://doi.org/10.1073/pnas.0506580102

Syed, A., & Tainer, J. A. (2018). The MRE11-RAD50-NBS1 Complex Conducts the Orchestration of Damage Signaling and Outcomes to Stress in DNA Replication and Repair. https://doi.org/10.1146/annurev-biochem

Sykiotis, G. P., & Bohmann, D. (2008). Keap1/Nrf2 signaling regulates oxidative stress tolerance and lifespan in Drosophila. *Developmental Cell*, *14*(1), 76–85. https://doi.org/10.1016/j.devcel.2007.12.002

Tanaka-Matakatsu, M., Xu, J., Cheng, L., & Du, W. (2009). Regulation of apoptosis of rbf mutant cells during Drosophila development. *Dev Biol*, *326*(2), 347–356. https://doi.org/10.1016/j.ydbio.2008.11.035

Tang, D., Wu, D., Hirao, A., Lahti, J. M., Liu, L., Mazza, B., … Ingram, A. J. (2002). ERK Activation Mediates Cell Cycle Arrest and Apoptosis after DNA Damage Independently of p53. *Journal of Biological Chemistry*, *277*(15), 12710–12717. https://doi.org/10.1074/jbc.M111598200

Tangutoori, S., Baldwin, P., & Sridhar, S. (2015). PARP inhibitors: A new era of targeted therapy. *Maturitas*, *81*(1), 5–9. https://doi.org/10.1016/j.maturitas.2015.01.015

Toulany, M. (2019). Targeting DNA Double-Strand Break Repair Pathways to Improve Radiotherapy Response. *Genes*, *10*(1), 25. https://doi.org/10.3390/genes10010025

Tsuchida, N., Murugan, A. K., Grieco, M., Tsuchida, N., Kannan Murugan, A., & Grieco, M. (2016). Kirsten Ras* oncogene: Significance of its discovery in human cancer research. *Oncotarget*, *7*(29), 46717–46733. https://doi.org/10.18632/oncotarget.8773

Uhlirova, M., & Bohmann, D. (2006a). JNK- and Fos-regulated Mmp1 expression cooperates with Ras to induce invasive tumors in Drosophila. *The EMBO Journal*, *25*(22), 5294–5304. https://doi.org/10.1038/sj.emboj.7601401

Uhlirova, M., & Bohmann, D. (2006b). JNK- and Fos-regulated Mmp1 expression cooperates with Ras to induce invasive tumors in Drosophila. *The EMBO Journal*, *25*(22), 5294–5304. https://doi.org/10.1038/sj.emboj.7601401

Wang, H., Zhang, X., Teng, L., & Legerski, R. J. (2015). DNA damage checkpoint recovery and cancer development. *Experimental Cell Research*. https://doi.org/10.1016/j.yexcr.2015.03.011

Ward, I. M., & Chen, J. (2001). Histone H2AX Is Phosphorylated in an ATR-dependent Manner in Response to Replicational Stress. *Journal of Biological Chemistry*, *276*(51), 47759–47762. https://doi.org/10.1074/jbc.C100569200

Weber, A. M., & Ryan, A. J. (2015). ATM and ATR as therapeutic targets in cancer. *Pharmacology & Therapeutics*, *149*, 124–138. https://doi.org/10.1016/J.PHARMTHERA.2014.12.001

Wei, F., Yan, J., & Tang, D. (2011). Extracellular signal-regulated kinases modulate DNA damage response - a contributing factor to using MEK inhibitors in cancer therapy. *Current Medicinal Chemistry*, *18*(35), 5476–5482. Retrieved from http://www.ncbi.nlm.nih.gov/pubmed/22087839

White, M. A., Nicolette, C., Minden, A., Polverino, A., Van Aelst, L., Karin, M., & Wigler, M. H. (1995). Multiple Ras functions can contribute to mammalian cell transformation. *Cell*, *80*(4), 533–541. Retrieved from http://www.ncbi.nlm.nih.gov/pubmed/7867061

Willoughby, L. F., Schlosser, T., Manning, S. A., Parisot, J. P., Street, I. P., Richardson, H. E., … Brumby, A. M. (2013). An in vivo large-scale chemical screening platform using Drosophila for anti-cancer drug discovery. *Disease Models & Mechanisms*, *6*(2), 521–529. https://doi.org/10.1242/dmm.009985

Wise, D. A., & Brinkley, B. R. (1997). Mitosis in cells with unreplicated genomes (MUGs): Spindle assembly and behavior of centromere fragments. *Cell Motility and the Cytoskeleton*, *36*(3), 291–302. https://doi.org/10.1002/(SICI)1097-0169(1997)36:3<291::AID-CM9>3.0.CO;2-A

Wu, D., Chen, B., Parihar, K., He, L., Fan, C., Zhang, J., … Tang, D. (2006). ERK activity facilitates activation of the S-phase DNA damage checkpoint by modulating ATR function. *Oncogene*, *25*(8), 1153–1164. https://doi.org/10.1038/sj.onc.1209148

Wu, J., Zhang, B., Wuu, Y.-R., Davidson, M. M., & Hei, T. K. (2017). Targeted cytoplasmic irradiation and autophagy. *Mutation Research/Fundamental and Molecular Mechanisms of Mutagenesis*, *806*, 88–97. https://doi.org/10.1016/j.mrfmmm.2017.02.004

Wu, M., Pastor-Pareja, J. C., & Xu, T. (2010). Interaction between RasV12 and scribbled clones induces tumour growth and invasion. *Nature*, *463*(7280), 545–548. https://doi.org/10.1038/nature08702

Yan, Y., Black, C. P., & Cowan, K. H. (2007). Irradiation-induced G2/M checkpoint response requires ERK1/2 activation. *Oncogene*, *26*(32), 4689–4698. https://doi.org/10.1038/sj.onc.1210268

Yan, Y., Hein, A. L., Greer, P. M., Wang, Z., Kolb, R. H., Batra, S. K., & Cowan, K. H. (2015). A novel function of HER2/Neu in the activation of G2/M checkpoint in response to γ-irradiation. *Oncogene*, *34*(17), 2215–2226. https://doi.org/10.1038/onc.2014.167

Yun, C. W., & Lee, S. H. (2018). The Roles of Autophagy in Cancer. *International Journal of Molecular Sciences*, *19*(11). https://doi.org/10.3390/ijms19113466

Zeman, M. K., & Cimprich, K. A. (2014). Causes and consequences of replication stress. *Nature Cell Biology*, *16*(1), 2–9. https://doi.org/10.1038/ncb2897

Zielke, N., Korzelius, J., van Straaten, M., Bender, K., Schuhknecht, G. F. P., Dutta, D., … Edgar, B. A. (2014). Fly-FUCCI: A Versatile Tool for Studying Cell Proliferation in Complex Tissues. *Cell Reports*, *7*(2), 588–598. https://doi.org/10.1016/j.celrep.2014.03.020

Zou, L., & Elledge, S. J. (2003). Sensing DNA Damage Through ATRIP Recognition of RPA-ssDNA Complexes. *Science*, *300*(5625), 1542–1548. https://doi.org/10.1126/SCIENCE.1083430

Supporting information

Supporting tables

Table 1. GSEA positively regulated gene sets

POSITIVELY REGULATED GENE SETS	SIZE	NES	FDR q-val
Epithelial structure maintenance	17	1,958	0,133
ErbB signaling pathways	58	1,906	0,158
Epidermal growth factor receptor signaling pathways	58	1,868	0,189
Trachea development	21	1,674	0,212
Transmembrane receptor protein tyrosine kinase signaling pathway	137	1,628	0,212
Regulation of neurogenesis	113	1,642	0,214
Multicellular organismal homeostasis	40	1,629	0,215
Regulation of epidermal growth factor receptor signaling pathway	33	1,675	0,216
Establishment of ommatidial planar polarity	59	1,682	0,216
Torso signaling pathway	33	1,643	0,217
R3/R4 cell fate commitment	16	1,617	0,217
Photoreceptor cell development	92	1,624	0,218
Sensory organ development	419	1,619	0,218
Gastrulation with mouth forming first	35	1,621	0,218
Peripheral nervous system development	87	1,688	0,219
Actin polymerization or depolymerization	38	1,630	0,219
Response to wounding	80	1,683	0,220
Gastrulation involving germ band extension	35	1,643	0,221
Compound eye photoreceptor fate commitment	55	1,663	0,222
R7 cell differentiation	48	1,633	0,222
Neuroblast division	34	1,631	0,222
Ommatidial rotation	26	1,648	0,222
Regulation of stress-activated	38	1,603	0,223
Biological adhesion	201	1,676	0,223
Regulation of ErbB signaling pathway	33	1,645	0,224
Asymmetric neuroblast division	33	1,665	0,224
Defense response	246	1,604	0,224
Negative regulation of epidermal growth factor receptor signaling	21	1,689	0,224
Death	254	1,606	0,225
Neural precursor cell proliferation	59	1,633	0,226

Regulation of response to stress	114	1,609	0,226
Regulation of JNK cascade	37	1,607	0,227
Adherens junction organization	27	1,611	0,227
Neuroblast proliferation	58	1,648	0,228
Epithelial tube morphogenesis	90	1,598	0,229
Cell adhesion	193	1,691	0,230
Notch signaling pathway	101	1,649	0,233
Toll signaling pathway	42	1,593	0,234
Photoreceptor differentiation	165	1,589	0,235
Apoptotic process	153	1,585	0,235
Eye photoreceptor cell fate commitment	56	1,650	0,236
Response to pheromone	20	1,696	0,237
Chaeta morphogenesis	46	1,692	0,238
Cell death	251	1,590	0,238
Transition metal ion homeostasis	19	1,586	0,238
Regulation of stress-activated protein kinase signaling cascade	38	1,652	0,239
R3/R4 cell differentiation	17	1,702	0,246
Negative regulation of cell fate specification	18	1,576	0,247
Negative regulation of ErbB signaling pathway	21	1,696	0,248
Response to starvation	48	1,573	0,249

Table 2. GSEA negatively regulated gene sets

NEGATIVELY REGULATED GENE SETS	SIZE	NES	FDR q-val
DNA replication	80	-2,132	0,009
Posterior head segmentation	15	-1,970	0,028
Protein-DNA complex subunit organization	48	-1,959	0,029
Nucleosome organization	27	-1,933	0,032
DNA-dependent DNA replication	53	-1,971	0,032
Nucleosome assembly	17	-1,918	0,035
Eggshell chorion gene amplification	16	-1,935	0,035
Potassium ion transport	32	-1,974	0,039
Cell cycle DNA replication	25	-1,979	0,047
DNA integrity checkpoint	74	-1,862	0,054
Chromatin assembly or disassembly	32	-1,866	0,056
Anterior/posterior pattern specification, imaginal disc	19	-1,871	0,057
Protein-DNA complex assembly	34	-1,990	0,061
DNA amplification	18	-1,844	0,063
Mitotic G2 DNA damage checkpoint	60	-1,821	0,075
Chromatin assembly	26	-1,794	0,081
Regulation of DNA metabolic process	31	-1,797	0,083
Positive regulation of intracellular protein transport	22	-1,798	0,087
DNA damage checkpoint	71	-1,768	0,087
mRNA export from nucleus	21	-1,777	0,087
Regulation of transcription factor import into nucleus	22	-1,684	0,088
Canonical wnt receptor signaling pathway	29	-1,678	0,088
Neuropeptide signaling pathway	26	-1,686	0,088
Regulation of transcription elongation from RNA polymerase II promoter	15	-1,781	0,089
Regulation of DNA-dependent transcription, elongation	19	-1,679	0,089
RNA export from nucleus	26	-1,686	0,090
DNA conformation change	77	-1,680	0,090
Protein localization to nucleus	64	-1,761	0,090
Head segmentation	26	-1,768	0,091
Mitotic DNA integrity checkpoint	64	-1,799	0,091
DNA endoreduplication	19	-1,687	0,091
RNA splicing, via transesterification reactions with bulged adenosine as nucleophile	212	-1,689	0,091
NFAT protein import into nucleus	15	-1,671	0,093
Somatic muscle development	47	-1,751	0,093

Positive regulation of NFAT protein import into nucleus	15	-1,689	0,093
Protein targeting to nucleus	60	-1,744	0,094
Serine family amino acid metabolic process	16	-1,691	0,094
Protein import into nucleus	60	-1,695	0,094
Transcription factor import into nucleus	22	-1,698	0,094
DNA packaging	68	-1,693	0,095
Mitotic DNA damage checkpoint	63	-1,745	0,095
Regulation of chromatin silencing	24	-1,738	0,095
mRNA transport	29	-1,752	0,096
Cell cycle checkpoint	89	-1,699	0,096
Regulation of mRNA splicing, via spliceosome	57	-1,701	0,097
Nuclear import	61	-1,722	0,097
Positive regulation of protein import into nucleus	18	-1,733	0,097
RNA splicing, via transesterification reactions	213	-1,712	0,097
G2 DNA damage checkpoint	61	-1,724	0,098
Lymph gland development	29	-1,702	0,099
Regulation of mRNA processing	62	-1,704	0,100
mRNA splicing, via spliceosome	212	-1,712	0,100
Positive regulation of nucleocytoplasmic transport	18	-1,716	0,100
Head development	28	-1,706	0,100
Regulation of NFAT protein import into nucleus	15	-1,726	0,100
Transcription elongation from RNA polymerase II promoter	19	-1,654	0,106
Larval lymph gland hemocyte differentiation	15	-1,647	0,109
Regulation of cell cycle process	173	-1,649	0,109
RNA splicing	220	-1,642	0,110
Positive regulation of transcription factor import into nucleus	18	-1,644	0,111
mRNA processing	263	-1,637	0,113
Regulation of RNA splicing	61	-1,619	0,129
DNA biosynthetic process	26	-1,615	0,131
Cardiocyte differentiation	29	-1,608	0,134
Larval locomotory behavior	19	-1,610	0,134
Mitotic cell cycle checkpoint	77	-1,603	0,137
Regulation of alternative mRNA splicing, via spliceosome	50	-1,595	0,142
Regulation of gene silencing	44	-1,596	0,143
Trunk segmentation	18	-1,586	0,150
G-protein coupled receptor signaling pathway	145	-1,573	0,163
Alternative mRNA splicing, via spliceosome	51	-1,571	0,163

Nucleocytoplasmic transport	96	-1,563	0,171
Nuclear transport	96	-1,559	0,174
Regulation of intracellular protein transport	36	-1,550	0,183
Mesoderm morphogenesis	29	-1,547	0,184
mRNA metabolic process	281	-1,537	0,190
DNA metabolic process	265	-1,540	0,191
Cuticle development involved in chitin-based cuticle molting cycle	16	-1,538	0,193
Negative regulation of cell cycle phase transition	102	-1,533	0,194
Chromosome condensation	41	-1,524	0,202
Positive regulation of intracellular transport	28	-1,525	0,203
Post-embryonic hemopoiesis	18	-1,516	0,211
Larval chitin-based cuticle development	15	-1,494	0,228
Gonad development	57	-1,495	0,229
Larval lymph gland hemopoiesis	18	-1,497	0,229
Ribonucleoside monophosphate biosynthetic process	37	-1,498	0,230
RNA processing	357	-1,499	0,230
Nucleoside monophosphate biosynthetic process	38	-1,500	0,232
Negative regulation of cell cycle process	106	-1,486	0,236

Table 3. Transmembrane receptor tyrosin kinase signalling pathway

Symbol	Gene Name	Fold change (Log 2)
pnt	pointed	4,187
sty	sprouty	3,866
aos	argos	2,698
edl	ETS-domain lacking	2,618
kek1	Kekkon 1	2,081
E(spl)m8-HLH	Enhancer of split m8, helix-loop-helix	1,792
ImpL2	Ecdysone-inducible gene L2	1,704
fog	folded gastrulation	1,642
brn	brainiac	1,612
peb	pebbled	1,629
Pvf3	PDGF- and VEGF-related factor 3	1,480
Mmp2	Matrix metalloproteinase 2	1,437
Alk	Anaplastic lymphoma kinase	1,195
btl	breathless	1,082
rho	rhomboid	1,080
Pvf2	PDGF- and VEGF-related factor 2	0,994
ato	atonal	0,961
Fas2	Fasciclin 2	0,960
ru	roughoid	0,925
Rho1	Rho1	0,804
cv-c	crossveinless c	0,718
melt	melted	0,694
Sulf1	Sulfated	0,627
Ras85D	Ras oncogene at 85D	0,605
Dab	Disabled	0,585
boss	bride of sevenless	0,549
Socs36E	Suppressor of cytokine signaling at 36E	0,530
Hrs	Hepatocyte growth factor regulated tyrosine kinase substrate	0,498
Pvr	PDGF- and VEGF-receptor related	0,488
sNPF	short neuropeptide F precursor	0,465
Egfr	Epidermal growth factor receptor	0,453
spi	spitz	0,451
pum	pumilio	0,418
Nrk	Neurospecific receptor kinase	0,415
hkb	huckebein	0,411

Table 4. DNA replication class

Symbol	Gene Name	Fold change (Log 2)
dup	double parked	-1,142
RnrS	Ribonucleoside diphosphate reductase small subunit	-1,140
dpa	disc proliferation abnormal	-0,970
Caf1-180	Chromatin assembly factor 1, p180 subunit	-0,919
Mcm3	Minichromosome maintenance 3	-0,890
Mcm2	Minichromosome maintenance 2	-0,836
Mcm5	Minichromosome maintenance 5	-0,800
Orc2	Origin recognition complex subunit 2	-0,696
Mcm7	Minichromosome maintenance 7	-0,652
Mcm10	Minichromosome maintenance 10	-0,646
RnrL	Ribonucleoside diphosphate reductase large subunit	-0,642
Pdp1	PAR-domain protein 1	-0,575
hd	humpty dumpty	-0,556
Rbf	Retinoblastoma-family protein	-0,546
geminin	geminin	-0,535
RecQ4	RecQ4 helicase	-0,532
fs(1)Ya	female sterile (1) Young arrest	-0,521
cutlet	cutlet	-0,520
Mcm6	Minichromosome maintenance 6	-0,514
Gnf1	Germ line transcription factor 1	-0,512
DNA-ligI	DNA ligase 1	-0,503
DNApol-α60	DNA polymerase alfa 60	-0,484
rec	recombination-defective	-0,434
DNApol-α180	DNA polymerase alfa 180	-0,430
Cdc6	Cdc6	-0,422
RpA-70	Replication Protein A 70	-0,414
dre4	dre4	-0,406
Dref	DNA replication-related element factor	-0,400
plu	plutonium	-0,382
Mes4	Mesoderm-expressed 4	-0,359
Orc4	Origin recognition complex subunit 4	-0,343
RfC38	dILP-inhibitor	-0,339
RPA2	Replication protein A2	-0,320
CycE	Cyclin E	-0,319
DNApol-α73	DNA polymerase alfa 73	-0,297

Nfl	Nuclear factor I	-0,291
pita	pita	-0,276
DNApol-δ	DNA polymerase delta	-0,276
Orc1	Origin recognition complex subunit 1	-0,273
DNApol-ε	DNA polymerase epsilon	-0,272
Top2	Topoisomerase 2	-0,260
CDC45L	CDC45L	-0,247
Btk29A	Btk family kinase at 29A	-0,246

Figure index

Introduction

Results

Discussion

Materials and methods

Table index

Introduction

Results

Materials and methods

Supporting information

Abbreviations

AEL: after egg laying

AKT: Ak strain transforming

Ap: apterous

ATG8: autophagy related protein 8

ATM /TEFU: ataxia telangiectasia mutated / telomere fusion

ATR/MEI41: ataxia telangiectasia related / meiotic 41

ATRIP/MUS304: ATR interacting protein /mutagen sensitive 304

BER: base excision repair

BRCA1: breast cancer 1

CATA: catalase

CDK2: cyclin dependent kinase 2

CHK1/GRP: Checkpoint kinase 1 / grapes

CHK2 / LOK: Checkpoint kinase 2 / loki

CIC: capicua

CNT: concentrative nucleoside transporter

DAPI: 4′,6-diamidino-2 phenylindole

Dcp1: decaping protein 1

DDR: DNA damage response

DMSO: dimethyl sulfoxide

DNA: deoxyribonucleic acid

DOME: domeless

dsBREAK: double stranded DNA break

E-CAD: E-cadherin

EDU: 5-Ethynyl-2'-deoxyuridine

EGF: epidermal growth factor

EGFR: epidermal growth factor receptor

Elav: embryonic lethal abnormal vision

En: engrailed

ENT: equilibrative nucleoside transporter

ERK: extracellular signal-regulated kinase

ETS: E26 transformation specific

Ey: eyeless

FA: Fanconi anemia

FACS: fluorescence associated cell sorting

FDA: food and drug administration

FDR: False discovery rate

Flp: flipase

FUCCI: fluorescent ubiquitination-based cell cycle indicator

GAL4: GAL4 transcription factor

GAL80ts: thermosensitive Gal80 transcriptional repressor

GAP: GTPase activating protein

GDP: guanine di-phosphate

GEF: guanine nucleotide exchange factor

GFP: Green fluorescent protein

GI: genomic instability

GLOBOCAN: global cancer observatory

GOBP: gene ontology biological process

GSEA: gene set enrichment analysis

GstD: Glutathione S transferase D

GTP: guanine tri-phosphate

Gy: Gray. 1Gy=100 rad

H2AV: Histone 2 A variant

H3K9: Histone 3 lysin 9

Hh: hedgehog

HID: head involution defective

HIF1 α: hypoxia inducible factor 1 α

HR: homologous recombination

IR: ionizing radiation

JAK: Janus kinase

JNK: Jun kinase

KSR: kinase suppressor of Ras

MAPK: mitogen activated protein kinase

MARCM: mosaic analysis with a repressible cell marker

MCM: minichromosome maintenance

miRNA: micro RNA

miRHG: miRNA for reaper, hid and grim

mKO: monomeric kusabira orange

MMP1: matrix metaloprotease 1

MMR: mismatch repair

MRE11: meiotic recombination homolog 1

MRN: mre11 - rad50 - NBS1 complex

mRNA: messenger RNA

mTOR: mammalian target of rapamycin

MyrT: myristoylated tomato

NBS1: Nijmegen breakage syndrome protein 1

NCI: national cancer institute

NER: nucleotide excision repair

NES: normalized enrichment score

NHEJ: non-homologous end joining

NRF: nuclear respiratory factor

ORC: origin recognition complex

P/A RATIO: posterior area / anterior area

PARP: poly (ADP ribose) polymerase

PCNA: proliferating cell nuclear antigen

PH3: phosphorylated histone 3

PI3K: phosphatidylinositol 3 kinase
PIP2: Phosphatidylinositol 4,5-bisphosphate
PIP3: Phosphatidylinositol (3,4,5)-trisphosphate

PLC Ɛ: phosphoinositide phospholipase C

Pnt: pointed

PP2A-29B: protein phosphatase 2A subunit 29B

PP2A-B: protein phosphatase 2A subunit B

PP2C1: protein phosphatase 2C subunit 1

pre-RC: pre-replication complex

PTEN: phosphatase and tensin homolog

qRT-PCR: quantitative real time polymerase chain reaction

RAF: rapidly accelerated fibrosarcoma

RAL: ras like protein

RAS: rat sarcoma

RBF: retinoblastoma

RFP: red fluorescent protein

RHEB: ras homolog enriched in brain

RNAi: RNA interference

RPA: replication protein A

RTK: receptor tyrosine kinase

SCRIB: scribble

SOD2: superoxide dismutase 2

SOS: son of sevenless

ssBREAK: single stranded DNA break

ß-GAL: ß-galactosidase

STAT: signal transducer and activator of transcription

Stg: string

TRA: trametinib

TSC1/2: tuberous sclerosis complex 1 and 2

TUNEL: terminal deoxynucleotidyl transferase dUTP nick end labelling

UAS: upstream activating sequence

Upd: unpaired

UV: ultraviolet

WHO: world health organization

Resumen en Castellano

La mayoría de tumores sólidos presentan signos de inestabilidad genómica. Se ha propuesto que la activación de oncogenes puede generar inestabilidad genómica mediante la inducción de estrés replicativo. En esta tesis hemos demostrado que la expresión de una forma constitutivamente activa del oncogén RAS en células epiteliales de *Drosophila* promueve una aceleración de la transición entre las fases G1 y S del ciclo celular. Esto lleva a una inducción de estrés replicativo y deriva en inestabilidad genómica. El daño en el ADN resultante de este proceso debería de activar la respuesta al daño en el ADN, sin embargo, esta se encuentra bloqueada. Además, la expresión de RasV12 inhibe la muerte celular gracias a los altos niveles de activación de ERK.

Ras es uno de los oncogenes mas comúnmente mutados, sin embargo seguimos sin terapias para tratar tumores dependientes de Ras que sean seguras y efectivas. Con esto en mente, y basándonos en nuestros resultados anteriores, decidimos tratar de explotar en daño en el ADN presente en estas células para destruirlas de forma selectiva. A estos efectos, indujimos más daño mediante irradiación e inhibimos la expresión ERK para promover la muerte de estas células. Usamos esta estrategia tanto en tumores benignos como malignos y en ambos casos logramos destruir de forma selectiva las células tumorales. Proponemos que los inhibidores de MEK, que se usan para el tratamiento de melanomas metastáticos, podrían combinarse con radiación para mejorar los efectos terapéuticos.

A parte de los efectos autónomos descritos con anterioridad, también hemos observado que la expresión de RasV12 induce un fenotipo no autónomo. Las células normales adyacentes a las células Ras presentan signos de daño en el ADN, apoptosis y autofagia. El papel de estos efectos no autónomos no está claro,

hipotetizamos que podrían jugar un papel en sustentar metabólicamente el crecimiento del tumor.

Publications

In addition to the project addressed in this PhD thesis and that recently been published in Cell Reports **(Publication 1)**, I have also contributed to another research project that resulted in a publication in PNAS in 2017.

In collaboration with Mariana Muzzopappa, I participated in a project focused on deciphering the interactions between tumor populations and the biological relevance of this interactions. Furthermore, we studied the function of the microenvironment on tumor growth and malignancy **(Publication2)**. We described a self-amplification loop that drives tumor growth and relies on the interaction between two functionally distinct cell populations. ROS dependent JNK activation in tumor epithelial cells drives the expression of secreted molecules to delaminated cells which then promote the proliferation of the epithelial tissue. I contributed to this project by performing some of the experimental work and analyzing the data.

Publication 1

Selective killing of Ras-malignant tissues by exploiting oncogene-induced DNA damage. Lada Murcia, Marta Clemente-Ruiz, Priscilla Pierre-Ellies, Anne Royou & Marco Milán. Cell Reports 2019.

Article

Cell Reports

Selective Killing of RAS-Malignant Tissues by Exploiting Oncogene-Induced DNA Damage

Graphical Abstract

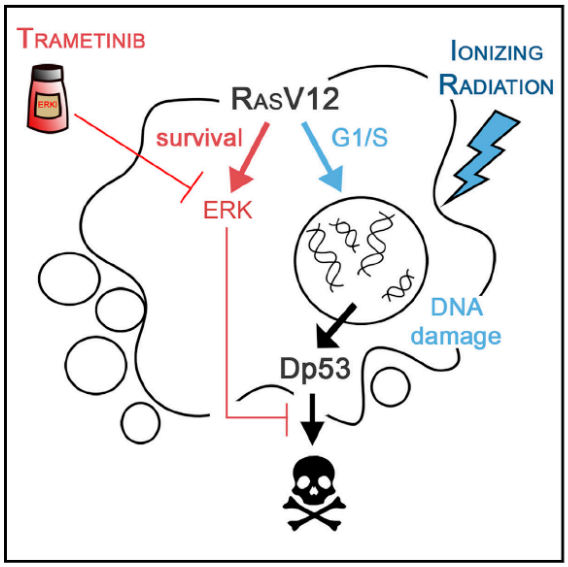

Authors

Lada Murcia, Marta Clemente-Ruiz, Priscillia Pierre-Elies, Anne Royou, Marco Milán

Correspondence

marco.milan@irbbarcelona.org

In Brief

RAS oncoproteins are virtually "undruggable" cancer targets. Murcia et al. take advantage of the inherent induction of DNA damage and additional blockade of the DDR by the RAS oncogene to show that genetic or chemical inhibition of ERK coupled to radiation can selectively eliminate RAS-malignant tumors once they are formed.

Highlights

- RAS oncogene induces DNA damage and silences the response of the DDR pathway
- RAS blocks Dp53-dependent induction of cell death through ERK
- In tissues subjected to ionizing radiation, ERK is activated to counteract Dp53 activity
- Genetic or chemical inhibition of ERK selectively eliminates RAS-malignant tissues

Murcia et al., 2019, Cell Reports *28*, 119–131
July 2, 2019
https://doi.org/10.1016/j.celrep.2019.06.004

CellPress

Cell Reports
Article

OPEN ACCESS
CellPress

Selective Killing of RAS-Malignant Tissues by Exploiting Oncogene-Induced DNA Damage

Lada Murcia,[1] Marta Clemente-Ruiz,[1] Priscillia Pierre-Elies,[3] Anne Royou,[3] and Marco Milán[1,2,4,*]
[1]Institute for Research in Biomedicine (IRB Barcelona), The Barcelona Institute of Science and Technology, Baldiri Reixac, 10-12, 08028 Barcelona, Spain
[2]Institució Catalana de Recerca i Estudis Avançats (ICREA), Pg. Lluís Companys 23, 08010 Barcelona, Spain
[3]Institut Européen de Chimie et Biologie, 2, rue Robert Escarpit, 33607 Pessac, France
[4]Lead Contact
*Correspondence: marco.milan@irbbarcelona.org
https://doi.org/10.1016/j.celrep.2019.06.004

SUMMARY

Several oncogenes induce untimely entry into S phase and alter replication timing and progression, thereby generating replicative stress, a well-known source of genomic instability and a hallmark of cancer. Using an epithelial model in *Drosophila*, we show that the RAS oncogene, which triggers G1/S transition, induces DNA damage and, at the same time, silences the DNA damage response pathway. RAS compromises ATR-mediated phosphorylation of the histone variant H2Av and ATR-mediated cell-cycle arrest in G2 and blocks, through ERK, Dp53-dependent induction of cell death. We found that ERK is also activated in normal tissues by an exogenous source of damage and that this activation is necessary to dampen the pro-apoptotic role of Dp53. We exploit the pro-survival role of ERK activation upon endogenous and exogenous sources of DNA damage to present evidence that its genetic or chemical inhibition can be used as a therapeutic opportunity to selectively eliminate RAS-malignant tissues.

INTRODUCTION

Genomic instability, defined as a high frequency of DNA alterations, is a hallmark of cancer. It can originate from several insults, of which DNA replication errors are the major source (Gaillard et al., 2015). Oncogenes produce genomic instability by promoting premature entry into S phase and by altering replication timing and progression to cause replicative stress (Hills and Diffley, 2014). More than 30% of all human tumors arise from mutations that encode a Ras protein essentially locked in a constitutively activated form (Vogelstein et al., 2013). Ras oncogene promotes both over-use and re-use of replication origins, thus causing replicative stress and genomic instability (Di Micco et al., 2006). Despite more than three decades of effort by academia and industry, only recently have effective Ras inhibitors started to be identified (Furuse et al., 2018; Janes et al., 2018). One approach to increasing therapeutic selectivity for cancer cells is to identify potential synthetic lethal interactions with the oncogene of interest, that is, genes for which the loss of function would be lethal only in the presence of the oncogene. Oncogene-induced replicative stress induces the DNA damage response (DDR) pathway. Activation of ataxia telangiectasia and Rad3-related protein (ATR) and checkpoint kinase 1 (Chk1) triggers cell-cycle arrest and DNA repair, as well as the activation, reactivation, or stabilization of replication origins or forks to dampen the amount of genomic instability in the tissue (Hills and Diffley, 2014). The presence of replicative stress in oncogene-driven tumors has been successfully exploited by targeting the ATR- and Chk1-dependent response to produce the selective elimination of cancer cells. Although this therapy was highly effective in killing lymphomas and pancreatic tumors induced by the proto-oncogene Myc in mice, Ras-driven pancreatic adenocarcinomas were unresponsive (Murga et al., 2011).

Here we used a *Drosophila* epithelial model to drive the expression of RasV12, an oncogenic version of Ras known to trigger entry into S phase (Prober and Edgar, 2000), and to analyze the impact of this expression on the stability of the genome and on the response of the DDR pathway. Given the conservation of cancer-related genes and signaling pathways between humans and *Drosophila*, flies have been widely used as an *in vivo* model to molecularly dissect Ras-mediated tumorigenesis (Brumby and Richardson, 2005; Gonzalez, 2013; Pastor-Pareja and Xu, 2013). *Drosophila* has also been instrumental in functionally demonstrating a role of ATR and Chk1 in counteracting the impact of replicative stress on genome stability (Purdy et al., 2005; Sibon et al., 1997, 1999). We first present evidence that RasV12 induces DNA damage while simultaneously silencing ATR-mediated phosphorylation of the histone variant H2Av and ATR-mediated cell-cycle arrest and blocking, through ERK, Dp53-induced cell death. We next show that ERK is also activated by exogenous sources of DNA damage and that this activation protects cells from Dp53-mediated cell death. Given the inherent induction of DNA damage and additional blockade of the DDR at different levels by the Ras oncogene, we propose that RasV12-expressing cells become dependent on the anti-apoptotic role of ERK to survive. Consistent with this notion, we present experimental evidence that genetic or chemical inhibition of ERK activity coupled to ionizing radiation (IR) can be used as a therapeutic approach to selectively eliminate RasV12-malignant tissues.

increased from 49% in wild-type to 77% in *RasV12*-expressing cells). The accumulation of cells in G2/M upon RasV12 expression was rescued by co-expression of the *Drosophila* Cdc25 ortholog String, known to drive G2-M transition (Figure S1J). To label cells in S phase, we coupled DNA content analysis of dissociated *RasV12* and wild-type cells with a 10 min pulse of EdU. Surprisingly, we observed a remarkable reduction in the number of cells in S phase in RasV12-expressing tissues (S: 6%) compared with wild-type tissues (S: 23%) (Figure 1C). A similar reduction was observed by Fly-Fucci (Figure 1B, red cells; from 27% in wild-type to 8% in *RasV12*-expressing cells) and by the labeling of RasV12-expressing wing discs exposed to a 10 min pulse of EdU (Figure 1D). We noticed, though, that the reduction in the fraction of cells in S phase was observed only upon long (3 days) inductions of RasV12 expression and was not an immediate response to exposure to the oncogene (15 h; Figure 1D). Note, in this case, that 15 h of oncogene expression was sufficient to induce high levels of ERK activation (Figures S1G and S1H). We next analyzed the transcriptional profile of wing disc cells subjected to a 3 day exposure to RasV12 expression and compared it with the profile of wild-type wing disc cells. RasV12-expressing cells were enriched in genes previously identified to be regulated by the canonical Ras/Raf/MAP kinase cascade (Figure S1I; Table S1), such as the ETS domain transcription factors Ets21C and Pointed (Jin et al., 2015), the nuclear protein Phyllopod (Dickson et al., 1995), or the EGFR/ERK antagonists Sprouty (Casci et al., 1999), Argos (Golembo et al., 1996), and Kekkon-1 (Ghiglione et al., 1999). The transcriptome dataset thus contains genes known to contribute to mediating or modulating RTK/ERK signaling. Interestingly, gene set enrichment analysis pinpointed DNA replication genes as a class of genes whose expression profile was significantly reduced in RasV12-expressing cells (Figure S1I; Table S1). Taken together, these results suggest that the capacity of RasV12-expressing cells to replicate their DNA is to a certain extent compromised, which is consistent with the previously reported role of RasV12 in promoting cellular senescence in *Drosophila* tissues (Nakamura et al., 2014; see also Figures S1K and S1L).

RasV12 Induces DNA Damage

Given the reported role of RasV12 in causing replicative stress and genomic instability as a result of over-use (dormant origin activation) and re-use (Hills and Diffley, 2014) of replication origins, we monitored whether RasV12 expression led to an increase in the amount of DNA damage in the tissue. For this purpose, we used a battery of fluorescent reporters shown to be activated upon an exogenous source of DNA damage (Figures S1M–S1O). In response to replicative stress, cells relocate and activate DNA repair proteins such as the single-stranded DNA (ssDNA)-binding protein RPA and the MRE11-RAD50-NBS1 (MRN) complex. In *Drosophila*, the conserved replication protein A (Rpa) complex consists of three subunits, RpA-70, Rpa2, and Rpa3 (Zou and Elledge, 2003). Interestingly, intense foci of Rpa3 were observed within nuclei of RasV12-expressing cells (Figure 1E). The resulting protein-coated ssDNA not only is protected but also promotes binding of the MRN complex and other DNA repair proteins that initiate damage signaling, fork protection, and repair (Syed and Tainer, 2018). Intense foci of Mre11 and Rad50 were also observed within nuclei of RasV12-expressing cells (Figures 1F and 1G). Some stalled DNA replication forks are rapidly converted into double-strand breaks (DSBs) during S phase in response to DNA replication stress. In order to measure DNA damage in RasV12-expressing tissues, we performed a Comet assay, a single-cell electrophoresis of lysed cells in low melting agarose (see STAR Methods). Fragments of damaged DNA migrate faster than intact chromosomes during electrophoresis, creating a comet. A high incidence of DNA damage was present in RasV12-expressing cells (Figure 1I). Consistent with the large amount of DNA damage observed in these cells, aberrant mitotic figures with chromosomal bridges were also found (Figure 1H).

RasV12 Silences the DDR and Blocks, through ERK, Dp53-Induced Apoptosis

In response to DSBs and stalled forks, the histone H2A variant—H2AX in mammals—is phosphorylated by the kinases ATR, ATM, and DNA-PK. Surprisingly, the levels of H2Av phosphorylation (pH2Av) in RasV12 cells were very low (Figure 2A, quantified in Figure 2C; see also Figures S2A and S2B). In contrast, wing discs overexpressing cyclin E or E2F or expressing an RNAi form of Rbf, genetic manipulations known to induce the G1-S transition in fly cells (Neufeld et al., 1998) and to cause replicative stress and genomic instability in mammals (Hills and Diffley, 2014), led to a clear increase in the number of pH2Av-positive cells (Figures S2A and S2B). RasV12 was also able to prevent pH2Av in tissues subjected to high doses (40 Gy) of IR (Figure 2B, quantified in Figure 2C). The observed effects of RasV12 on pH2Av levels were not a trivial consequence of the reduction in the levels of H2Av, as monitored by the use of two transgenes expressing H2Av either under the control of its own promoter or under the control of an UAS promoter (Figure 2D, quantified in Figure 2F). Because IR-induced pH2Av results from the activation of ATR/ATM in wing disc cells (Figure 2B; see also Dekanty et al., 2015), these results suggest that RasV12 blocks the activity of at least one of these two kinases (see below). Upon IR, ATR and its downstream effector Chk1 also drive mitotic arrest (Jaklevic and Su, 2004; Song et al., 2004; see also Figure 2I). Interestingly, the IR-induced mitotic arrest was compromised in RasV12-expressing tissues (Figures 2G and 2H, quantified in Figure 2J). Altogether, these results indicate that RasV12 induces DNA damage but that the phosphorylation of H2Av and cell-cycle arrest, two key steps regulated by the DDR, are compromised.

Despite the DNA damage caused by prolonged expression of RasV12 in wing disc cells (Figure 1), apoptosis was absent in these cells, as shown by TUNEL staining (Figure 3A) and Dcp1 (Figure 3B). As a control, we observed a strong apoptotic response in tissues subjected to overexpression of cyclin E or depletion of Rbf (Figure 3A). The blockade of the apoptotic pathway by RasV12, monitored by Dcp1 staining, also occurred in tissues subjected to IR-induced DNA damage (Figure 3B′). Exogenous and endogenous sources of DNA damage are known to activate *Drosophila* p53 (Dp53; Brodsky et al., 2000; Jin et al., 2000; Ollmann et al., 2000), which drives the expression of the pro-apoptotic gene *hid* in the wing epithelium (Fan et al., 2010). Dp53 activity, monitored by the expression of *hid-GFP*, was slightly

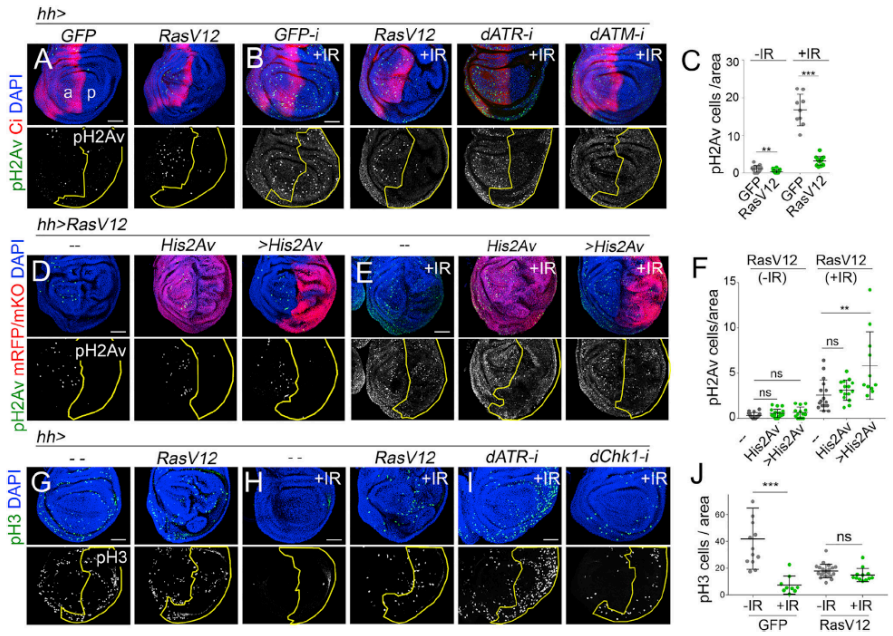

Figure 2. RasV12 Silences the DDR Pathway

(A, B, D, E, and G–I) Late third-instar wing discs expressing the indicated transgenes under the control of the *hh-gal4* driver (which is expressed in posterior [p] cells) and stained for Ci (red, A and B, to mark the anterior [a] compartment), DAPI (blue), pH2Av (green or white, A, B, D, and E), His2Av-RFP (red, D and E, middle panels), His2Av-mKO (red, D and E, right panels), and pH3 (green or white, G–I). Wing discs in (B), (E), (H), and (I) were subjected to ionizing radiation (IR; 40 Gy) and dissected 5 h later. The regions of transgene expression are marked by a yellow line. Scale bars, 50 μm.

(C, F, and J) Scatterplots showing the number of pH2Av-positive (C and F) and pH3-positive (J) cells per area of wing discs expressing the indicated transgenes under the control of the *hh-gal4* driver. Average, SD, and individual wing discs measurements are shown. Statistically significant differences based on Student's t test are indicated: $^{**}p < 0.01$ and $^{***}p < 0.001$; ns, not significant.

Samples were dissected from late third-instar larvae raised at 29°C for 3 days.

See also Figure S2.

induced in RasV12-expressing tissues (Figure 3C), and this induction, probably as a consequence of DNA damage, was reduced upon Dp53 depletion (Figure 3D). *hid-GFP* expression was also induced in wild-type and RasV12-expressing tissues subjected to IR (Figure 3C'), and this expression was also completely rescued upon Dp53 depletion (Figure 3D'). All these results indicate that RasV12 does not interfere with the activation of Dp53 and the transcriptional upregulation of the pro-apoptotic gene *hid*, and suggest that RasV12 compromises the activity of the apoptotic machinery downstream of Dp53. RasV12 has been previously reported to block the activity of Hid by direct phosphorylation through ERK (Bergmann et al., 1998). Consistently, RasV12 was able to reduce the ability of Dp53 to trigger apoptosis when overexpressed in wing disc cells (Figure 3E), RNAi-mediated depletion of ERK in RasV12-expressing tissues rescued IR-induced cell death (Figure 3F), and this cell death was also mostly dependent on the activity of Dp53 (Figure 3G). Together these results indicate that RasV12 compromises the activity of the DDR and blocks, through ERK, Dp53-induced apoptosis at the level of the pro-apoptotic gene *hid* (Figure 3H). Because ATM-mediated activation of Dp53 is not compromised in RasV12-expressing cells, the impact of this oncogene on pH2Av levels is most probably a consequence of compromised ATR activity.

Radiation-Induced ERK Dampens the Pro-apoptotic Response of Dp53 in Wild-Type Cells

We found that the IR-induced apoptotic response, in terms of Dcp1 protein levels and nuclear morphology, was clearly enhanced in RasV12 tissues expressing an RNAi form of ERK compared with irradiated control cells (Figure 3F) and that this

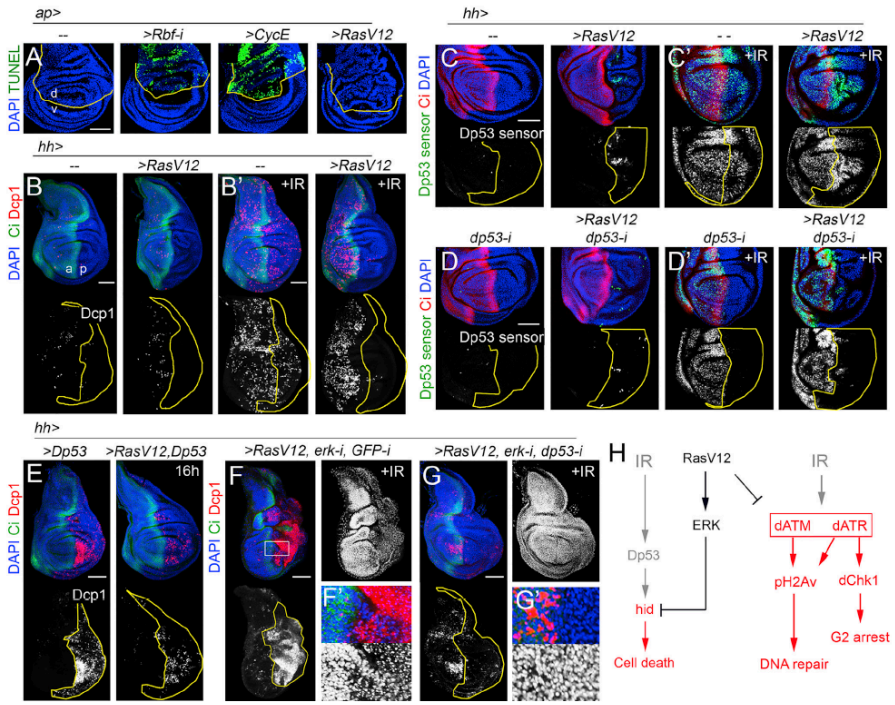

Figure 3. RasV12 Blocks, through ERK, Dp53-Induced Cell Death

(A–G) Late third-instar wing discs expressing the indicated transgenes under the control of the *ap-gal4* driver (which is expressed in dorsal [d] cells, A) or the *hh-gal4* driver (which is expressed in posterior [p] cells, B–G) and stained for DAPI (blue), TUNEL (green, A, to label apoptotic cells), Ci (green in B, B′, E, and G, red in C–D′, to mark the anterior [a] compartment), Dcp1 (red or white, B, B′, and E–G), and Dp53 sensor (*hid-GFP*, green or white, C–D′). Wing discs in (B′), (C′), (D′), (F), and (G) were subjected to IR (40 Gy) and dissected 5 h later. The regions of transgene expression are marked by a yellow line. Higher magnifications of the wing discs in (F) and (G) are shown in (F′) and (G′). Scale bars, 50 μm. Samples were dissected from late third-instar larvae raised at 29°C for 3 days.
(H) Cartoon depicting the impact of RasV12 and ERK on the DDR pathway.

response was largely rescued upon depletion of Dp53 levels (Figure 3G). Interestingly, wild-type tissues expressing an RNAi form of ERK showed a similar apoptotic response when subjected to IR (compare Figures 4A and 4B), and this response was also rescued upon depletion of Dp53 levels (Figure 4C). The same rescue was observed when expressing a synthetic microRNA (miRNA) (*miRHG*; Siegrist et al., 2010) designed to target the three pro-apoptotic genes *hid*, *reaper*, and *grim* (Figure 4D). ERK depletion did not have any impact on the activity levels of Dp53 upon IR (Figure 4E) and did not have a profound effect on apoptosis levels in non-irradiated cells (Figure 4A). These results indicate that endogenous ERK signaling has a physiological role in dampening DNA damage-induced apoptosis caused by Dp53 activation. Targeted expression of the same transgenes to the developing eye primordium reinforced the protective role of endogenous ERK against Dp53-induced apoptosis and, most interestingly, unveiled a developmental role of ERK in diminishing the deleterious effects of Dp53 (Figure 4F). Whether Dp53 is activated in this developmental context by an endogenous source of DNA damage remains to be confirmed.

We next addressed whether physiological ERK signaling is induced by an exogenous source of DNA damage and whether this induction has a widespread role in dampening the effects of the DDR pathway in terms of apoptotic induction, cell-cycle arrest, and pH2Av. Remarkably, IR-treated wing discs showed a significant increase in the levels of ERK phosphorylation (Figures 4G and 4G′, quantified in Figure 4H). Activation of the ERK pathway

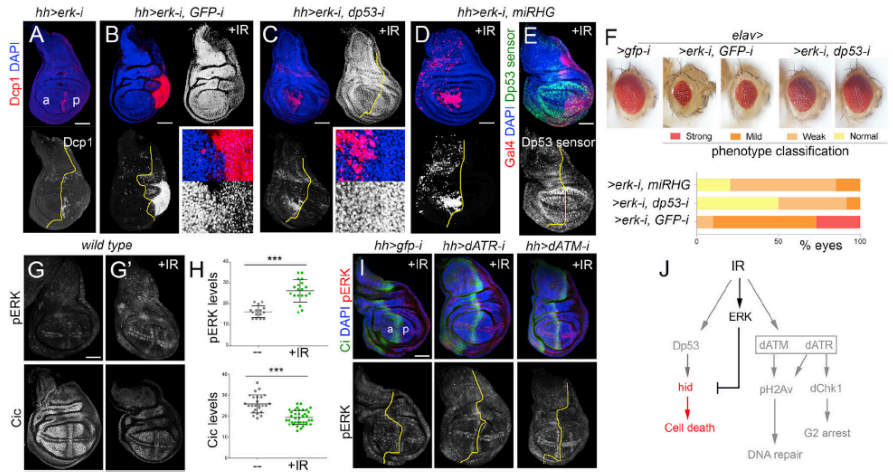

Figure 4. IR-Induced ERK Dampens the Pro-apoptotic Role of Dp53

(A–E, G, G′, and I) Late third-instar wing discs expressing the indicated transgenes under the control of the *hh-gal4* driver (A–E and I, which is expressed in posterior [p] cells) or from wild-type larvae (G and G′) and stained for DAPI (blue or white, A–E and I), Dcp1 (red or white, A–D), Dp53 sensor (*hid-GFP*, green or white, E), Gal4 (red, E), pERK (white, G and G′, upper panels, red or white, I), Cic (white, G and G′, lower panels), and Ci (green, I). Wing discs in (B)–(E), (G′), and (I) were subjected to IR (40 Gy) and dissected 5 h later. The boundaries between anterior (a) and posterior (p) compartments are marked with a yellow line. Higher magnifications of the wing discs in (B) and (C) are shown in the right lower panels. Scale bars, 50 μm.

(F) Adult eyes expressing the indicated transgenes under the control of the *elav-Gal4* driver and histogram showing the percentages of the resulting phenotypes that range from a strong to an undetectable (normal) reduction in the size of the eye. n (number of eyes per genotype) = 60 (*erk-i*, *gfp-i*), 312 (*erk-i*, *dp53-i*), and 136 (*erk-i*, *miRHG*). Note that the rescue of eye size by *dp53-RNAi* was not complete, most probably reflecting the developmental role of Erk.

(H) Scatterplots showing pERK and Cic levels per area of wing discs subjected (in green) or not (in gray) to IR (40 Gy) and dissected 5 h later. Average, SD, and individual wing disc measurements are shown. Statistically significant differences on the basis of Student's t test are indicated: ***$p < 0.001$. Samples were dissected from late third-instar larvae raised at 29°C for 3 days.

(J) Cartoon depicting the induction of ERK by IR and its role in dampening Dp53-dependent cell death and DNA repair.

See also Figure S4.

results in the proteasome-mediated degradation of Capicua (Cic), a transcriptional repressor of EGFR target genes (Jiménez et al., 2000). In wing discs subjected to IR, Cic protein levels were significantly reduced compared with untreated control wing discs (Figures 4G and 4G′, quantified in Figure 4H). IR-induced activation of ERK was independent of the DDR pathway, as depletion of ATR or ATM did not have any impact on the levels of IR-induced ERK phosphorylation (Figure 4I). The activation of ERK by IR did not have a significant effect on the activity of ATR and ATM, as the levels of pH2Av did not change in ERK-depleted cells (Figure S3A), and cell-cycle arrest was properly timed in these cells (Figures S3B and S3C). All these results indicate that IR-induced activation of physiological ERK plays a crucial role in buffering the pro-apoptotic effects of Dp53 activation.

Increased Radiosensitivity of RasV12-Expressing Tissues upon ERK Depletion

Our data indicate that the induction of physiological levels of ERK in IR-treated wild-type epithelial cells dampens Dp53-mediated cell death without affecting ATM/ATR activity. In contrast, RasV12 is shown not only to block Dp53-induced cell death, through non-physiological levels of ERK, but also to silence ATR-mediated sensing of the damage and ATR/Chk1-mediated cell-cycle arrest. These observations, together with the fact that RasV12 also induces DNA damage, most probably as a result of replicative stress, suggest that the pro-survival role of ERK is more prominent in RasV12-expressing cells than in wild-type cells upon an external source of DNA damage, such as IR. To experimentally test this proposal, we subjected wild-type and RasV12-expressing wing discs to different doses of IR (0, 8, 16, and 24 Gy) and analyzed the impact on cell death upon RNAi-mediated knockdown of ERK activity in the two genotypes. As shown in Figures 5A and 5B, ERK depletion radiosensitized at higher levels RasV12-expressing tissues than wild-type cells (Figure 5B, see comparison of differences analysis in blue), and the greatest differences in the amount of apoptosis between the two genotypes were observed upon intermediate (16 Gy) levels of IR (Figure 5B,

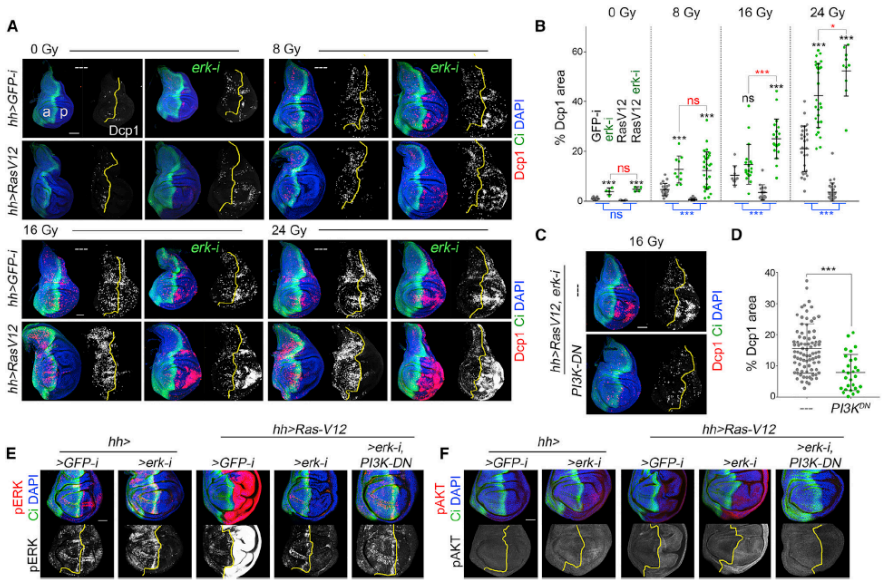

Figure 5. Selective Killing of RasV12-Expressing Tissues by Combined Therapy

(A and C) Late third-instar wing discs expressing the indicated transgenes under the control of the *hh-gal4* driver (which is expressed in posterior [p] cells), subjected to different doses of IR and stained for Dcp1 (red or white), Ci (green, to mark the anterior [a] compartment), and DAPI (blue). Expression in (C) of PI3K-DN caused a reduction in Dcp1 levels.

(B and D) Scatterplots showing the amount of cell death, measured as the percentage of the area covered by Dcp1-positive cells, of wing discs expressing the indicated transgenes under the control of the *hh-gal4* driver and subjected to the indicated doses of IR. Average, SD, and individual wing discs measurements are shown. Statistically significant differences on the basis of Student's t test are indicated: *$p < 0.05$ and ***$p < 0.001$; ns, not significant. Comparisons of differences (in blue) were performed to quantify the differences in the radiosensitivity of RasV12 versus wild-type tissues upon ERK depletion and t test (in red) to quantify the greatest differences in the amount of apoptosis between the two genotypes. Expression in (D) of PI3K-DN caused a reduction in Dcp1 levels.

(E and F) Late third-instar wing discs expressing the indicated transgenes under the control of the *hh-gal4* driver and stained for pERK (red or white, E), pAkt (red or white, F), Ci (green), and DAPI (blue). The boundaries between anterior (a) and posterior (p) compartments are marked with a yellow line.

Scale bars, 50 μm. Samples were dissected from late third-instar larvae raised at 29°C for 3 days.

see t test analysis in red). Low (8 Gy) and high (24 Gy) levels of IR did not give rise to a clear difference in the amount of death in *RasV12* and wild-type cells upon ERK depletion. RasV12 drives the G1-S transition through the ERK and Dp110/PI3K signaling pathways (Prober and Edgar, 2000, 2002). We thus questioned whether the activity of the PI3K pathway, and its role in driving G1-S transition and DNA damage, is an absolute requirement for the increased sensitivity of RasV12-expressing cells to IR when subjected to ERK depletion. Interestingly, expression of a dominant-negative form of PI3K/Dp110 (PI3K-DN) upon ERK depletion reduced the radiosensitivity levels of RasV12-expressing tissues (Figures 5C and 5D). The increase in pAkt levels observed in RasV12-expressing tissues was clearly rescued upon expression of the PI3K-DN transgene (Figure 5F), whereas the ability of erk-RNAi to deplete pERK levels was unaffected (Figure 5E). Taken together, these results indicate that ERK depletion combined with IR can provide a therapeutic approach to selectively target RasV12-expressing cells.

Chemical Targeting of RasV12-Malignant Tumors

Oncogenic cooperation between RasV12 and loss of polarity determinants Scribble or Discs large has been widely used to identify the underlying cellular and molecular events mediating the malignant and neoplastic growth of an epithelial tissue (Brumby and Richardson, 2005; Pastor-Pareja and Xu, 2013). The pro-apoptotic role of JNK, with a primary aim to remove deleterious cells from the tissue, switches to a pro-tumorigenic one through the anti-apoptotic role of RasV12 (Cordero et al., 2010; Igaki et al., 2006). These data, together with our experimental observations that RasV12 induces DNA damage and Dp53 activation, suggest that RasV12-malignant tissues are subjected to two

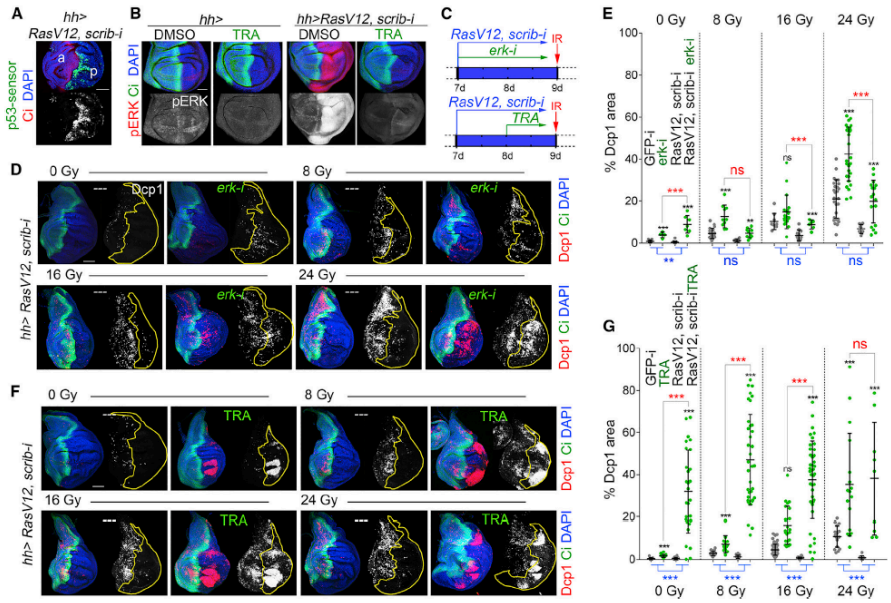

Figure 6. Selective Killing of RasV12-Malignant Tissues by Chemical Therapy

(A, B, D, and F) Late third-instar wing discs expressing the indicated transgenes under the control of the *hh-gal4* driver (which is expressed in posterior [p] cells) and stained for p53-sensor (GFP or white, A), pERK (red or white, B), Dcp1 (red or white, D and F), Ci (red in A, green in D and F, to mark the anterior [a] compartment), and DAPI (blue). In (D) and (F), larvae were subjected to different doses of IR. In (F), larvae were fed 1 μM trametinib (TRA). The p compartment is marked by a yellow line. Scale bar, 50 μm; all images are taken at the same magnification.

(C) Cartoon depicting the temporal induction of transgene expression and chemical treatment.

(E and G) Scatterplots showing the amount of cell death, measured as the percentage of the area covered by Dcp1-positive cells, of wing discs expressing the indicated transgenes under the control of the *hh-gal4* driver and subjected to the indicated doses of IR. Average, SD, and individual wing discs measurements are shown. Statistically significant differences on the basis of Student's t test are indicated: $^{**}p < 0.01$ and $^{***}p < 0.001$; ns, not significant. Comparisons of differences (in blue) were performed to quantify the differences in the radiosensitivity of *RasV12, scrib-i* versus wild-type tissues upon ERK depletion (E) or TRA treatment (G) and t test (in red) to quantify the greatest differences in the amount of apoptosis between the different genotypes.

Samples were dissected from late third-instar larvae raised at 29°C for 3 days.

independent pro-apoptotic inputs, namely, JNK and Dp53. Indeed, cells expressing RasV12 and an RNAi form of *scribble* (*scrib-RNAi*) showed elevated levels of the Dp53 activity reporter *hid-GFP* (Figure 6A), and these levels were higher than those in cells expressing RasV12 alone (compare with Figure 3C). This finding thus points to the existence of emerging sources of DNA damage as a result of the oncogenic cooperation between RasV12 and loss of *scribble*. Indeed, these tissues have been shown to present high levels of radical oxygen species (Bunker et al., 2015; Pérez et al., 2017), an endogenous source of genomic instability, high levels of DNA damage (Figure S4C), and compromised phosphorylation of H2Av (Figures S4A and S4B). Given the observations that RasV12-malignant tissues are subjected to two independent pro-apoptotic inputs and that ERK activation plays a fundamental role in promoting their survival, we decided to combine ERK depletion and IR to increase the extent of DNA damage and selectively target malignant cells. Unfortunately, ERK depletion sensitized *RasV12/scrib-RNAi*-expressing cells only to high (24 Gy) doses of IR (Figures 6D and 6E). The radiosensitivity of these cells was consistently smaller than that of wild-type tissues depleted of ERK (Figure 6E, see comparison of differences analysis in blue; compare Figures 5A and 6D). Moreover, the amount of apoptosis was always smaller in *RasV12/scrib-RNAi*-expressing tissues depleted of ERK (Figure 6E, see t test analysis in red). These results could be explained either by the presence of emerging pathways with an active role in reducing the radiosensitivity of these tissues or the experimental setup, in which chronic depletion of ERK can interfere with the development of the malignant tissue (Figure 6C). We thus switched to an alternative chemical

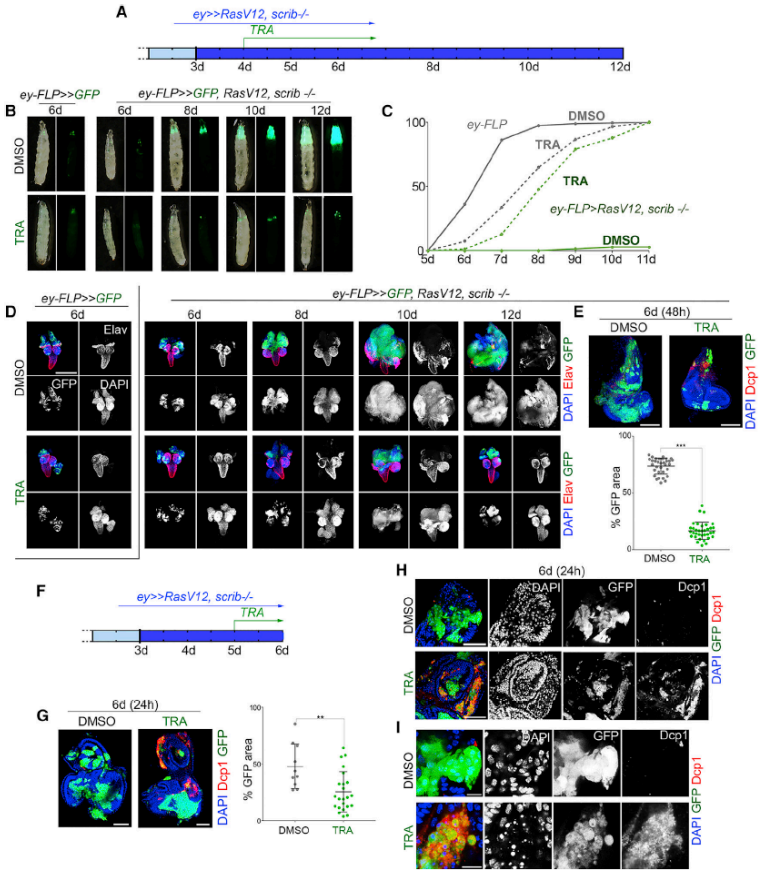

Figure 7. Chemical Targeting of Eye Malignant Tumors

(A) Cartoon depicting the timing (in days after egg laying) of clone induction and exposure to DMSO or TRA for (B)–(E).

(B) Late third-instar larvae bearing GFP-expressing clones of wild-type cells (left) or cells expressing RasV12 and mutant for *scribble* (*scrib*, right).

(C) Timing of pupariation in days after egg laying. Percentages were normalized to the final number of pupae for each genotype: larvae bearing GFP-expressing clones of wild-type cells (gray) or cells expressing RasV12 and mutant for *scribble* (green) subjected to DMSO (continuous lines) or 2 μM TRA (dashed lines). n (wild-type + DMSO) = 188; n (wild-type + TRA) = 293; n (*RasV12 scrib* + DMSO) = 217; n (*RasV12 scrib* + TRA) = 172.

(D) Larval brains and eye imaginal discs bearing GFP-expressing clones (green or white) of wild-type cells (left) or cells expressing RasV12 and mutant for *scribble* (*scrib*, right), stained for Elav (red or white) and DAPI (blue or white). All panels were taking at the same magnification.

(E) Eye imaginal discs bearing GFP-expressing clones (green) of cells expressing RasV12 and mutant for *scribble* (*scrib*, right), stained for Dcp1 (red) and DAPI (blue), and histogram plotting the percentage of the eye-antenna primordia covered by GFP-expressing clones. Number of discs: DMSO = 33, TRA = 35.

(F) Cartoon depicting the timing (in days after egg laying) of clone induction and exposure to DMSO or TRA for panels for (G)–(I).

(G–I) Eye imaginal discs bearing GFP-expressing clones (green or white) of cells expressing RasV12 and mutant for *scribble* (*scrib*, right), stained for Dcp1 (red or white) and DAPI (blue or white). In (G), histogram plotting the percentage of the eye-antenna primordia covered by GFP-expressing clones is shown. Number of

(legend continued on next page)

OPEN ACCESS
CellPress

approach in which ERK activation is depleted 24 h after initiation of the expression of the tumor-promoting transgenes (Figure 6C). Larvae bearing *RasV12, scrib-RNAi*-expressing tissues were fed food containing 1 μM trametinib (TRA), a MEK inhibitor approved for metastatic melanoma (Flaherty et al., 2012), and then subjected to different doses (8, 16, and 24 Gy) of IR. TRA was very efficient in reducing the amount of pERK signal in RasV12, *scrib-RNAi*-expressing tissues (Figure 6B) and in sensitizing these cells to low (8 Gy) and intermediate (16 Gy) doses of IR (Figure 6F). TRA radiosensitized *RasV12, scrib-RNAi*-expressing tissues at higher levels than wild-type cells (Figure 6G, see comparison of differences analysis in blue), and the greatest differences in the amount of apoptosis between the two genotypes were observed upon low (8 Gy) and intermediate (16 Gy) levels of IR (Figure 6G, see t test analysis in red). We observed that TRA was highly effective in specifically killing *RasV12, scrib-RNAi*-expressing cells even in the absence of IR (Figures 6F and 6G). In larvae bearing eye epithelial tumors consisting of *RasV12* cells mutant for the *scribble* gene, a well-established fly model of tumor neoplasia and malignancy, exposure to this MEK inhibitor 24 h after tumor initiation (Figure 7A) blocked tumor growth and tissue invasiveness (Figures 7B and 7D). The area of the eye covered by *RasV12*-malignant clones was drastically reduced (Figure 7E). This fly model is well known to delay the transition from larval to pupa as a consequence of the expression of the systemic hormone Dilp8 (Colombani et al., 2012; Garelli et al., 2012). Exposure to TRA also rescued the developmental delay produced by the tumor (Figure 7C). The effect of TRA on tumor growth, invasiveness, and developmental timing was a consequence of specific killing of malignant tumors, as revealed by careful analysis of eye primordia and neoplastic clones at the early stages of tumor initiation. Exposure for only 24 h to TRA once the tumors had been allowed to grow for at least 2 days (Figure 7F) was also able to drastically reduce the area of the eye covered by *RasV12*-malignant clones without affecting the development and size of the primordia (Figure 7G). Those clones that remained in the tissue were positive for Dcp1 staining (Figures 7H and 7I), and their nuclei were highly pyknotic (Figure 7I). Taken together, all these data indicate that RasV12-induced DNA damage can be efficiently exploited by depleting ERK to selectively target RasV12-malignant tissues and to rescue its malignant features.

DISCUSSION

The ability of oncogenes to produce genomic instability has been used to induce the selective elimination of cancer cells by targeting the DDR pathway (Lecona and Fernandez-Capetillo, 2018). Surprisingly, though, Ras-driven tumors were shown to be unresponsive to this treatment (Murga et al., 2011). To revisit the impact of a constitutively active form of Ras, RasV12, on the stability of the genome and on the activity of the DDR pathway, here we used an epithelial model of *Drosophila*, which has been successfully exploited to molecularly dissect Ras-mediated tumorigenesis (Brumby and Richardson, 2005; Gonzalez, 2013; Pastor-Pareja and Xu, 2013). We present evidence that chronic expression of RasV12, previously shown to drive G1-S transition (Prober and Edgar, 2000; see also Figure 1), not only induces DNA damage in these cells but also blocks DNA repair by compromising ATR-dependent phosphorylation of H2Av and cell-cycle arrest in G2 and Dp53-induced cell death. These observations unveil a dual role of RasV12 in producing genomic instability, on one hand by promoting DNA damage, most probably through replicative stress, and on the other by blocking the DDR. The impact of Ras on the DDR could explain the reported refractoriness of Ras-driven tumors to ATR inhibitors (Murga et al., 2011). To further investigate this lack of response, characterization of DNA damage and ATR activity in Ras murine tumors will be required. Future experiments in the fly should be able to molecularly characterize the mechanism by which Ras and its downstream signaling pathways repress ATR.

We next provide experimental evidence that oncogene-driven genomic instability and the role of ERK in blocking Dp53-mediated cell death can be successfully exploited to selectively target RasV12-expressing cells. The survival of these cells and wild-type cells after exposure to IR, an exogenous source of DNA damage, is promoted by an anti-apoptotic role of ERK that negatively regulates Dp53-mediated cell death. On the basis of the non-physiological levels of ERK activity induced in RasV12-expressing cells, their inherent DNA damage, and the additional blockade of the DDR, we show that oncogene-expressing cells become highly sensitive to IR upon genetic depletion of ERK activity compared with control wild-type cells. Consequently, low doses of IR combined with ERK depletion are very effective in preferentially killing RasV12-expressing cells. Finally, we used a well-established fly epithelial model of neoplastic transformation and malignant growth to show that exposures to TRA, a MEK inhibitor approved for metastatic melanoma, are highly efficient in targeting RasV12-malignant tumors, even in the absence of an exogenous source of IR, and once the tumor has been initiated. On the basis of these results, we propose that these tumors, which rely on oncogenic cooperation between the RasV12 oncogene and loss of polarity determinants, become addicted to the anti-apoptotic role of ERK and that this addiction can be therapeutically exploited. Future directions using our fly epithelial model include the identification of the molecular mechanism underlying IR-induced activation of ERK through the use of the powerful genetics of *Drosophila*. Interestingly, a similar pro-survival role of ERK upon IR has been recently reported in mammalian cells, in which IR-induced activation of ERK is shown to rely on the activity of EGFR (Ohm et al., 2019). All these data will certainly contribute to the successful use of radiotherapies in combination of MEK inhibitors in cancer treatment (Wei et al., 2011).

Most melanomas carry oncogenic mutations in BRAF (35%–50%) or NRAS (10%–25%), which result in constitutive

discs: DMSO = 10; TRA = 23. Larvae were fed DMSO or TRA (2 μM). Higher magnifications of the eye discs in (H) are shown in (I). Dating of larvae in days after egg laying at 25°C is shown.
Scale bars, 500 μm (D), 50 μm (E, G, and H), and 10 μm (I). In histograms in (E) and (G), average, SD, and individual wing discs measurements are shown. Statistically significant differences on the basis of Student's t test are indicated: **$p < 0.01$ and ***$p < 0.001$.

OPEN ACCESS
CellPress

activation of the ERK pathway (Akbani et al., 2015). Whereas surgical resection of early-stage melanomas is associated with excellent long-term prognosis, resection of locally advanced tumors has a high incidence of recurrence, and patients will ultimately die from metastatic melanoma. The treatment landscape for unresectable or metastatic melanoma has shifted dramatically since 2011. Before that year, metastatic melanoma was considered a devastating disease with a median patient survival of 9 months. The use of BRAF and MEK inhibitors (Flaherty et al., 2012; Robert et al., 2015) and the introduction of immunotherapies (Luke et al., 2017) has dramatically improved patient outcomes, and the median overall survival of patients has increased to 2 years. Our work indicates that radiotherapy should be considered as a treatment option to further increase the amount of DNA damage produced by the oncogene. Its combination with BRAF and MEK inhibitors in order to compromise the pro-survival role of ERK will contribute to selectively kill malignant cells.

STAR★METHODS

Detailed methods are provided in the online version of this paper and include the following:

- KEY RESOURCES TABLE
- LEAD CONTACT AND MATERIALS AVAILABILITY
- EXPERIMENTAL MODEL AND SUBJECT DETAILS
  - Fly strains
- METHOD DETAILS
  - Immunohistochemistry and confocal imaging
  - Generation of transgenic flies
  - Flow cytometry analysis
  - Fly-Fucci quantification
  - QuantSeq
  - Ionizing Radiation (IR) treatments and quantifications
  - Measurement of pERK and Cic levels
  - Trametinib treatment
  - Induction of eye-tumors
  - Comet assay
- QUANTIFICATION AND STATISTICAL ANALYSIS
  - Image Processing and Analysis
  - Statistical Analysis
- DATA AND CODE AVAILABILITY

SUPPLEMENTAL INFORMATION

Supplemental Information can be found online at https://doi.org/10.1016/j.celrep.2019.06.004.

ACKNOWLEDGMENTS

We thank C.-H. Chen, B. Edgar, H. Richardson, M. Uhlirova, the Bloomington *Drosophila* Stock Center (United States), the Vienna *Drosophila* RNAi Center (Austria), and the National Institute of Genetics (Japan) for flies, the Developmental Studies Hybridoma Bank (United States) for antibodies, the Advanced Digital Microscopy and Biostatistics Core facilities at IRB Barcelona for their help with confocal imaging and statistical analysis, and members of the lab for comments on the manuscript. L.M. was funded by a PhD fellowship from La Caixa. M.C.-R. was funded by a Juan de la Cierva post-doctoral contract from Ministerio de Ciencia, Innovación y Universidades (Government of Spain), and M.M. is an ICREA Research Professor. A.R.'s laboratory was funded by a grant from the European Commission (ERC-GA311358-NoAneuploidy). M.M.'s laboratory was funded by the SIGNAGROWTH-BFU2013-44485 and INTERGROWTH-BFU2016-77587-P grants from Ministerio de Ciencia, Innovación y Universidades (Government of Spain) and ERDF "Una Manera de Hacer Europa." M.M.'s laboratory also gratefully acknowledges institutional funding from Ministerio de Ciencia, Innovación y Universidades (Government of Spain) through the Centres of Excellence Severo Ochoa Award and from the CERCA Programme of the Catalan Government.

AUTHOR CONTRIBUTIONS

L.M., M.C.-R., and M.M. conceived and designed the experiments and analyzed the data. L.M. and M.C.-R. performed the experiments. P.P.-E. and A.R. contributed reagents. M.M. wrote the paper.

DECLARATION OF INTERESTS

The authors declare no competing interests.

Received: February 25, 2019
Revised: May 7, 2019
Accepted: May 31, 2019
Published: July 2, 2019

REFERENCES

Akbani, R., Akdemir, K.C., Aksoy, B.A., Albert, M., Ally, A., Amin, S.B., Arachchi, H., Arora, A., Auman, J.T., Ayala, B., et al. (2015). Genomic Classification of Cutaneous Melanoma. Cell *161*, 1681–1696.

Bergmann, A., Agapite, J., McCall, K., and Steller, H. (1998). The Drosophila gene hid is a direct molecular target of Ras-dependent survival signaling. Cell *95*, 331–341.

Brodsky, M.H., Nordstrom, W., Tsang, G., Kwan, E., Rubin, G.M., and Abrams, J.M. (2000). Drosophila p53 binds a damage response element at the reaper locus. Cell *101*, 103–113.

Brumby, A.M., and Richardson, H.E. (2005). Using Drosophila melanogaster to map human cancer pathways. Nat. Rev. Cancer *5*, 626–639.

Bunker, B.D., Nellimoottil, T.T., Boileau, R.M., Classen, A.K., and Bilder, D. (2015). The transcriptional response to tumorigenic polarity loss in Drosophila. eLife *4*, e03189.

Casci, T., Vinós, J., and Freeman, M. (1999). Sprouty, an intracellular inhibitor of Ras signaling. Cell *96*, 655–665.

Colombani, J., Andersen, D.S., and Léopold, P. (2012). Secreted peptide Dilp8 coordinates Drosophila tissue growth with developmental timing. Science *336*, 582–585.

Cordero, J.B., Macagno, J.P., Stefanatos, R.K., Strathdee, K.E., Cagan, R.L., and Vidal, M. (2010). Oncogenic Ras diverts a host TNF tumor suppressor activity into tumor promoter. Dev. Cell *18*, 999–1011.

Dekanty, A., Barrio, L., and Milán, M. (2015). Contributions of DNA repair, cell cycle checkpoints and cell death to suppressing the DNA damage-induced tumorigenic behavior of Drosophila epithelial cells. Oncogene *34*, 978–985.

Di Micco, R., Fumagalli, M., Cicalese, A., Piccinin, S., Gasparini, P., Luise, C., Schurra, C., Garre', M., Nuciforo, P.G., Bensimon, A., et al. (2006). Oncogene-induced senescence is a DNA damage response triggered by DNA hyper-replication. Nature *444*, 638–642.

Dickson, B.J., Dominguez, M., van der Straten, A., and Hafen, E. (1995). Control of Drosophila photoreceptor cell fates by phyllopod, a novel nuclear protein acting downstream of the Raf kinase. Cell *80*, 453–462.

Fan, Y., Lee, T.V., Xu, D., Chen, Z., Lamblin, A.-F., Steller, H., and Bergmann, A. (2010). Dual roles of Drosophila p53 in cell death and cell differentiation. Cell Death Differ. *17*, 912–921.

Flaherty, K.T., Robert, C., Hersey, P., Nathan, P., Garbe, C., Milhem, M., Demidov, L.V., Hassel, J.C., Rutkowski, P., Mohr, P., et al.; METRIC Study Group

(2012). Improved survival with MEK inhibition in BRAF-mutated melanoma. N. Engl. J. Med. *367*, 107–114.

Forés, M., Simón-Carrasco, L., Ajuria, L., Samper, N., González-Crespo, S., Drosten, M., Barbacid, M., and Jiménez, G. (2017). A new mode of DNA binding distinguishes Capicua from other HMG-box factors and explains its mutation patterns in cancer. PLoS Genet. *13*, e1006622.

Furuse, J., Kurata, T., Okano, N., Fujisaka, Y., Naruge, D., Shimizu, T., Kitamura, H., Iwasa, T., Nagashima, F., and Nakagawa, K. (2018). An early clinical trial of Salirasib, an oral RAS inhibitor, in Japanese patients with relapsed/refractory solid tumors. Cancer Chemother. Pharmacol. *82*, 511–519.

Gaillard, H., García-Muse, T., and Aguilera, A. (2015). Replication stress and cancer. Nat. Rev. Cancer *15*, 276–289.

Garelli, A., Gontijo, A.M., Miguela, V., Caparros, E., and Dominguez, M. (2012). Imaginal discs secrete insulin-like peptide 8 to mediate plasticity of growth and maturation. Science *336*, 579–582.

Gene Ontology Consortium (2015). Gene Ontology Consortium: going forward. Nucleic Acids Res. *43*, D1049–D1056.

Ghiglione, C., Carraway, K.L., 3rd, Amundadottir, L.T., Boswell, R.E., Perrimon, N., and Duffy, J.B. (1999). The transmembrane molecule kekkon 1 acts in a feedback loop to negatively regulate the activity of the Drosophila EGF receptor during oogenesis. Cell *96*, 847–856.

Golembo, M., Schweitzer, R., Freeman, M., and Shilo, B.-Z. (1996). Argos transcription is induced by the Drosophila EGF receptor pathway to form an inhibitory feedback loop. Development *122*, 223–230.

Gonzalez, C. (2013). Drosophila melanogaster: a model and a tool to investigate malignancy and identify new therapeutics. Nat. Rev. Cancer *13*, 172–183.

Hills, S.A., and Diffley, J.F. (2014). DNA replication and oncogene-induced replicative stress. Curr. Biol. *24*, R435–R444.

Igaki, T., Pagliarini, R.A., and Xu, T. (2006). Loss of cell polarity drives tumor growth and invasion through JNK activation in Drosophila. Curr. Biol. *16*, 1139–1146.

Jaklevic, B.R., and Su, T.T. (2004). Relative contribution of DNA repair, cell cycle checkpoints, and cell death to survival after DNA damage in Drosophila larvae. Curr. Biol. *14*, 23–32.

Janes, M.R., Zhang, J., Li, L.-S., Hansen, R., Peters, U., Guo, X., Chen, Y., Babbar, A., Firdaus, S.J., Darjania, L., et al. (2018). Targeting KRAS mutant cancers with a covalent G12C-specific inhibitor. Cell *172*, 578–589.e17.

Jiménez, G., Guichet, A., Ephrussi, A., and Casanova, J. (2000). Relief of gene repression by torso RTK signaling: role of capicua in Drosophila terminal and dorsoventral patterning. Genes Dev. *14*, 224–231.

Jin, S., Martinek, S., Joo, W.S., Wortman, J.R., Mirkovic, N., Sali, A., Yandell, M.D., Pavletich, N.P., Young, M.W., and Levine, A.J. (2000). Identification and characterization of a p53 homologue in Drosophila melanogaster. Proc. Natl. Acad. Sci. U S A *97*, 7301–7306.

Jin, Y., Ha, N., Forés, M., Xiang, J., Gläßer, C., Maldera, J., Jiménez, G., and Edgar, B.A. (2015). EGFR/Ras signaling controls Drosophila intestinal stem cell proliferation via capicua-regulated genes. PLoS Genet. *11*, e1005634.

Karim, F.D., and Rubin, G.M. (1998). Ectopic expression of activated Ras1 induces hyperplastic growth and increased cell death in Drosophila imaginal tissues. Development *125*, 1–9.

Lecona, E., and Fernandez-Capetillo, O. (2018). Targeting ATR in cancer. Nat. Rev. Cancer *18*, 586–595.

Leevers, S.J., Weinkove, D., MacDougall, L.K., Hafen, E., and Waterfield, M.D. (1996). The Drosophila phosphoinositide 3-kinase Dp110 promotes cell growth. Embo. J *15*, 6584–6594.

Luke, J.J., Flaherty, K.T., Ribas, A., and Long, G.V. (2017). Targeted agents and immunotherapies: optimizing outcomes in melanoma. Nat. Rev. Clin. Oncol *14*, 463–482.

Milán, M., Campuzano, S., and García-Bellido, A. (1997). Developmental parameters of cell death in the wing disc of Drosophila. Proc. Natl. Acad. Sci. U S A *94*, 5691–5696.

Mundorf, J., and Uhlirova, M. (2016). The Drosophila imaginal disc tumor model: visualization and quantification of gene expression and tumor invasiveness using genetic mosaics. J. Vis. Exp. *116*.

Murga, M., Campaner, S., Lopez-Contreras, A.J., Toledo, L.I., Soria, R., Montaña, M.F., Artista, L., Schleker, T., Guerra, C., Garcia, E., et al. (2011). Exploiting oncogene-induced replicative stress for the selective killing of Myc-driven tumors. Nat. Struct. Mol. Biol. *18*, 1331–1335.

Nakamura, M., Ohsawa, S., and Igaki, T. (2014). Mitochondrial defects trigger proliferations of neighboring cells via a senescence-associated secretory phenotype in Drosophila. Nat. Commun *5*, 5264.

Neufeld, T.P., de la Cruz, A.F., Johnston, L.A., and Edgar, B.A. (1998). Coordination of growth and cell division in the Drosophila wing. Cell *93*, 1183–1193.

Ohm, A.M., Affandi, T., and Reyland, M.E. (2019). EGF receptor and PKCδ kinase activate DNA damage-induced pro-survival and pro-apoptotic signaling via biphasic activation of ERK and MSK1 kinases. J. Biol. Chem *294*, 4488–4497.

Ollmann, M., Young, L.M., Di Como, C.J., Karim, F., Belvin, M., Robertson, S., Whittaker, K., Demsky, M., Fisher, W.W., Buchman, A., et al. (2000). Drosophila p53 is a structural and functional homolog of the tumor suppressor p53. Cell *101*, 91–101.

Pagliarini, R.A., and Xu, T. (2003). A genetic screen in Drosophila for metastatic behavior. Science *302*, 1227–1231.

Pastor-Pareja, J.C., and Xu, T. (2013). Dissecting social cell biology and tumors using Drosophila genetics. Annu. Rev. Genet. *47*, 51–74.

Pérez, E., Lindblad, J.L., and Bergmann, A. (2017). Tumor-promoting function of apoptotic caspases by an amplification loop involving ROS, macrophages and JNK in *Drosophila*. eLife *6*, e26747.

Prober, D.A., and Edgar, B.A. (2000). Ras1 promotes cellular growth in the Drosophila wing. Cell *100*, 435–446.

Prober, D.A., and Edgar, B.A. (2002). Interactions between Ras1, dMyc, and dPI3K signaling in the developing Drosophila wing. Genes Dev. *16*, 2286–2299.

Purdy, A., Uyetake, L., Cordeiro, M.G., and Su, T.T. (2005). Regulation of mitosis in response to damaged or incompletely replicated DNA require different levels of Grapes (Drosophila Chk1). J. Cell Sci. *118*, 3305–3315.

Robert, C., Karaszewska, B., Schachter, J., Rutkowski, P., Mackiewicz, A., Stroiakovski, D., Lichinitser, M., Dummer, R., Grange, F., Mortier, L., et al. (2015). Improved overall survival in melanoma with combined dabrafenib and trametinib. N. Engl. J. Med *372*, 30–39.

Rimkus, S.A., and Wassarman, D.A. (2018). A pharmacological screen for compounds that rescue the developmental lethality of a Drosophila ATM mutant. PLoS ONE *13*, e0190821.

Sibon, O.C., Stevenson, V.A., and Theurkauf, W.E. (1997). DNA-replication checkpoint control at the Drosophila midblastula transition. Nature *388*, 93–97.

Sibon, O.C., Laurençon, A., Hawley, R., and Theurkauf, W.E. (1999). The Drosophila ATM homologue Mei-41 has an essential checkpoint function at the midblastula transition. Curr. Biol. *9*, 302–312.

Siegrist, S.E., Haque, N.S., Chen, C.H., Hay, B.A., and Hariharan, I.K. (2010). Inactivation of both Foxo and reaper promotes long-term adult neurogenesis in Drosophila. Curr. Biol. *20*, 643–648.

Song, Y.H., Mirey, G., Betson, M., Haber, D.A., and Settleman, J. (2004). The Drosophila ATM ortholog, dATM, mediates the response to ionizing radiation and to spontaneous DNA damage during development. Curr. Biol. *14*, 1354–1359.

Subramanian, A., Tamayo, P., Mootha, V.K., Mukherjee, S., Ebert, B.L., Gillette, M.A., Paulovich, A., Pomeroy, S.L., Golub, T.R., Lander, E.S., and Mesirov, J.P. (2005). Gene set enrichment analysis: a knowledge-based approach for interpreting genome-wide expression profiles. Proc. Natl. Acad. Sci. U S A *102*, 15545–15550.

Syed, A., and Tainer, J.A. (2018). The MRE11-RAD50-NBS1 complex conducts the orchestration of damage signaling and outcomes to stress in DNA replication and repair. Annu. Rev. Biochem. *87*, 263–294.

Publication 2

Feedback amplification loop drives malignant growth in epithelial tisssues. Mariana Muzzopappa, Lada Murcia & Marco Milán. PNAS 2017.

Feedback amplification loop drives malignant growth in epithelial tissues

Mariana Muzzopappa[a], Lada Murcia[a], and Marco Milán[a,b,1]

[a]Institute for Research in Biomedicine (IRB Barcelona), The Barcelona Institute of Science and Technology, 08028 Barcelona, Spain; and [b]Institució Catalana de Recerca i Estudis Avançats (ICREA), 08010 Barcelona, Spain

Edited by Norbert Perrimon, Harvard Medical School, Boston, MA, and approved July 25, 2017 (received for review February 1, 2017)

Interactions between cells bearing oncogenic mutations and the surrounding microenvironment, and cooperation between clonally distinct cell populations, can contribute to the growth and malignancy of epithelial tumors. The genetic techniques available in *Drosophila* have contributed to identify important roles of the TNF-α ligand Eiger and mitogenic molecules in mediating these interactions during the early steps of tumor formation. Here we unravel the existence of a tumor-intrinsic—and microenvironment-independent—self-reinforcement mechanism that drives tumor initiation and growth in an Eiger-independent manner. This mechanism relies on cell interactions between two functionally distinct cell populations, and we present evidence that these cell populations are not necessarily genetically different. Tumor-specific and cell-autonomous activation of the tumorigenic JNK stress-activated pathway drives the expression of secreted signaling molecules and growth factors to delaminating cells, which nonautonomously promote proliferative growth of the partially transformed epithelial tissue. We present evidence that cross-feeding interactions between delaminating and nondelaminating cells increase each other's sizes and that these interactions can explain the unlimited growth potential of these tumors. Our results will open avenues toward our molecular understanding of those social cell interactions with a relevant function in tumor initiation in humans.

tumor microenvironment | chromosomal instability | epithelial tumor | Wingless | JNK

Cancer development is a multistep process that involves altered cellular signaling, resulting in limitless replicative potential of the cells, evasion of apoptosis, tissue invasion, and metastasis (1). Carcinomas, tumors of epithelial origin, are often associated with inflammatory cells and activated fibroblasts, the tumor microenvironment (TME), which plays a critical role in cancer progression and in the colonization of target tissues (reviewed in ref. 2). These tumors are genetically heterogeneous, and intratumor cooperation between different subclonal cell populations can also contribute to the growth of these tumors (reviewed in ref. 3).

In recent decades, *Drosophila* models of epithelial tumors have been shown to reproduce key aspects of cancer development and have become useful model systems to characterize the cellular and molecular determinants that initiate tumorigenesis (reviewed in ref. 4). The epithelial primordia of the adult ectoderm, the so-called imaginal discs, provide the advantage that individual cells can be tracked, and the tissue can be manipulated genetically in temporal and spatial manner. In malignant neoplastic tumors of epithelial origin, activation of the c-Jun N-terminal kinase (JNK) stress cascade plays a tumor-suppressing or a tumor-promoting role depending on the activity of the apoptotic pathway (5–7). In neoplastic tumors resulting from mutations in the tumor suppressor genes *scribbled* (*scrib*) or *discs large 1* (*dlg1*), encoding for cell polarity determinants, JNK activates the apoptotic program and induces the removal of transformed cells from the tissue, thus limiting tumor growth (6–8). By contrast, in those tumors in which the apoptotic pathway is being inhibited, thus mimicking an important hallmark of human cancer (1), sustained activation of JNK becomes tumor-promoting. Activation of a JNK-dependent transcriptional program in these tumors induces the expression of a collection of well-defined target genes that contribute to driving unlimited growth, malignancy, and metastatic behavior (8–12). The genetic techniques available in *Drosophila* have unraveled how interactions between clones of cells bearing oncogenic mutations and the surrounding WT epithelium contribute to JNK activation, tumor growth, and malignancy, and have identified a major role of the TNF-α ligand Eiger and its receptor Grindelwald (Grnd) in mediating these interactions (13–16). Moreover, intratumor cooperation between clonally distinct cell populations can also contribute to the growth of these tumors (17).

Epithelial tumors generated in larval primordia are embedded in the open circulatory system of the fly and are infiltrated by circulating immune cells [hemocytes (5, 18)] and associated with resident mesenchymal cells [myoblasts (19)]. These two cell populations are also part of the TME and are amplified by cell proliferation as a response to the expression of mitogenic molecules produced by tumor cells (18, 19). In tumors resulting from mutations in *scrib* or *dlg1*, attached hemocytes restrict growth by limiting basement membrane disruption (18) and enhancing JNK-mediated removal of transformed cells by apoptosis (5). By contrast, proliferating myoblasts promote epithelial transformation in tumors resulting from the oncogenic cooperation between the EGF receptor and loss of epigenetic factors (19).

Here we have used two well-defined JNK-driven *Drosophila* neoplastic tumor models of epithelial origin to address the relative contribution of TME-independent and tumor-intrinsic mechanisms to the unlimited growth potential of these tumors. We used the *GAL4/UAS* system to drive tumorigenesis in large

Significance

Progression of epithelial tumors and successful colonization of target tissues rely in many cases on the presence of the tumor microenvironment (TME), which acts as a niche to provide secreted signaling molecules and growth factors to tumor cells. Here we used *Drosophila* to show that the TME is not an absolute requirement for the growth of epithelial tumors caused by chromosomal instability (CIN) or compromised cell polarity. Instead, tumor growth is driven by a feedback amplification loop between two well-defined—but not necessarily genetically different—tumor cell populations. As CIN or impaired cell polarity are frequently observed in human tumors of epithelial origin, our results will provide insight to the mechanistic understanding of their unlimited growth potential.

Author contributions: M. Muzzopappa and M. Milán designed research; M. Muzzopappa and L.M. performed research; M. Muzzopappa, L.M., and M. Milán analyzed data; and M. Milán wrote the paper.

The authors declare no conflict of interest.

This article is a PNAS Direct Submission.

[1]To whom correspondence should be addressed. Email: marco.milan@irbbarcelona.org.

This article contains supporting information online at www.pnas.org/lookup/suppl/doi:10.1073/pnas.1701791114/-/DCSupplemental.

territories, thus reducing interactions with surrounding WT epithelial cells and generating genetically homogenous tumor-like structures. We combined allograft transplantations and two independent transactivation systems to demonstrate that JNK activation and tumor initiation in these models are largely unaffected by the genetic ablation of circulating immune cells and resident mesenchymal cells. Our data also indicate that JNK activation and tumor growth do not depend on the activity of Eiger, the *Drosophila* TNF-α (20, 21), and its receptor Grnd (14). We unravel the use of cell-autonomous and tumor-specific molecular mechanisms to activate a common JNK kinase (JNKK)/JNK core signaling pathway that induces a shared transcriptional program to initiate tumorigenesis. Our results support the proposal that intratumor social interactions between functionally distinct cell populations can drive unlimited growth in the absence of the TME. Remarkably, these two cell populations are not necessarily genetically different, as opposed to the cooperation between clonally distinct cell populations reported in vertebrate and invertebrate tumor models (3, 4). We propose that the previously reported roles of the TME and Eiger in tumorigenesis are mainly restricted to mediating interactions between tumor-initiating and surrounding WT epithelial cells (13–16).

Results

Two Molecularly Distinct Tumor Models, Three Cell Populations, and Eiger Expression. We selected two different epithelial tumor models that rely on the activation of JNK and the transcriptional induction of a common set of target genes responsible for their high mitotic activity and metastatic behavior and for causing malignancy to the host. The first model, the chromosomal instability (CIN) model, is based on the protumorigenic action of CIN, a high rate of gain or loss of whole chromosomes or parts of them (22). Depletion of the spindle assembly checkpoint (SAC) by means of GAL4-mediated expression of RNAi forms of the SAC genes *bub3* or *rod* causes chromosome segregation errors, and the resulting aneuploid cells, cells with extra or missing chromosomes, delaminate from the tissue and activate the JNK transcriptional program that induces apoptosis (23). Blockade of the apoptotic program by expressing the baculovirus protein P35, which binds and inhibits the activity of effector caspases Dcp1 and DrIce (24), leads to activation of JNK in aneuploid cells and to the robust transcriptional induction of JNK-regulated target genes with a role in driving tumorigenesis (25). Ectopic expression of mitogenic molecules, such as Wingless (Wg) and IL-6–like Upd cytokines, contributes to tumor growth, whereas ectopic expression of matrix metalloproteinases (MMPs; Fig. 1*B*) results in basement membrane degradation. The second model system, the polarity-impaired model, is based on the conserved oncogenic cooperation between the activated form of Ras (Ras-V12) and the loss of polarity determinants *scrib* and *dlg1* (7, 26–29). Whereas GAL4-mediated expression of Ras-V12 induces hyperplastic growth by increasing the expression of the growth-promoting proto-oncogene dMyc and driving G1-S transition (30), reduction in the expression levels of *scrib* or *dlg1* by the use of mutant alleles or RNAi forms leads to neoplasia, JNK activation, and, again, robust transcriptional induction of JNK-regulated genes with a role in driving tumorigenesis, such as Wg, Upd cytokines, and MMPs (Fig. 1*B*) (7, 12, 26). The growth potential of these two tumor models can be easily quantified and visualized in allograft experiments in

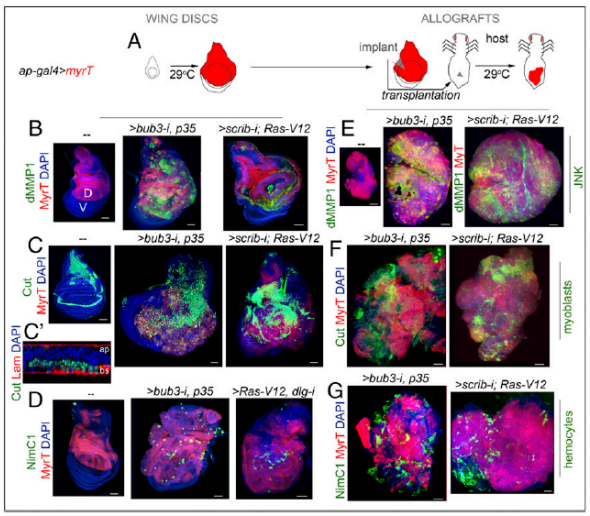

Fig. 1. *Drosophila* JNK-dependent epithelial tumor models, hemocyte recruitment, and myoblast proliferation. (*A*) Cartoon showing the expression of tumor-inducing transgenes in the dorsal (marked as "D") compartment (red) of larval wing discs (*Left*) and allograft transplantations into the abdomen of female hosts (*Right*). Fly hosts were maintained at 29 °C. (*B–G*) Larval wing primordia (*B–D*) and allograft transplants (*E–G*) expressing the indicated transgenes in the dorsal compartment under the control of the *ap-GAL4* driver and stained with DAPI (blue), MyrT (red), dMMP1 (green, *B* and *E*), Cut (green, *C*, *C'*, and *F*), NimC1 (green, *D* and *G*), and laminin (Lam; red, *C'*). In *C'*, cross-section of the proximal part of the wing disk is shown to visualize the localization of the myoblasts underneath the main epithelium. Apical (ap) and basal (bs) sides of the epithelium are marked. Transplants were extracted 5 days (*scrib-i; Ras-V12*) or 12 days (*bub3-i, p35*) after implantation. (Scale bars, 50 μm.)

which a small piece of the tumor (i.e., implant) is able to regenerate a solid tumor in the abdomen of female adult hosts several days after implantation (Fig. 1 *A* and *E*). In these allografts, the growth capacity of WT tissues is shown to be limited, and JNK is not induced (Fig. 1*E*). Remarkably, CIN and polarity-impaired tumors induce the amplification of the resident myoblast population, which can be marked by the expression of Cut (Fig. 1 *C* and *F*) (31) or Twist (Fig. S1) transcription factors. These two models also share a strong capacity to attract circulating hemocytes, labeled by the expression of Nimrod C1 [NimC1; a phagocytosis receptor used as a marker of the most abundant type of hemocytes, the plasmatocytes (32); Fig. 1 *D* and *G*]. Progression to neoplasia in CIN and polarity-impaired tumors rely on the activation of JNK and on a collection of transcription factors that induce a tumorigenic transcriptional program (10). Eiger, the unique member of the TNF superfamily of ligands in *Drosophila* (20, 21), activates the JNK signaling pathway by binding to the TNF-α receptor Grnd (14), and has been proposed to play a tumor-promoting role in the presence of Ras-V12 (5). Interestingly, expression of Eiger, visualized by the use of two different reporter constructs and an antibody (*Materials and Methods*), was observed in the myoblast population of WT and CIN and polarity-impaired wing primordia (Fig. 2 *A–C* and Fig. S1), and became ectopically expressed in tumor epithelial cells [labeled by the expression of myristoylated Tomato (MyrT); Fig. 2 *D* and *F* and Fig. S1] as well in those hemocytes attached to the tumor [Fig. 2 *E* and *G*, labeled by the expression of the hemocyte-specific transmembrane protein Hemese (He)] (33). We observed that Eiger expression was also induced in hemocytes from the host that were attached to the allografted tumors (Fig. 2*H*). Based on these observations, the potential role of TME cells in tumor initiation and the requirement of Eiger for JNK activation will be analyzed.

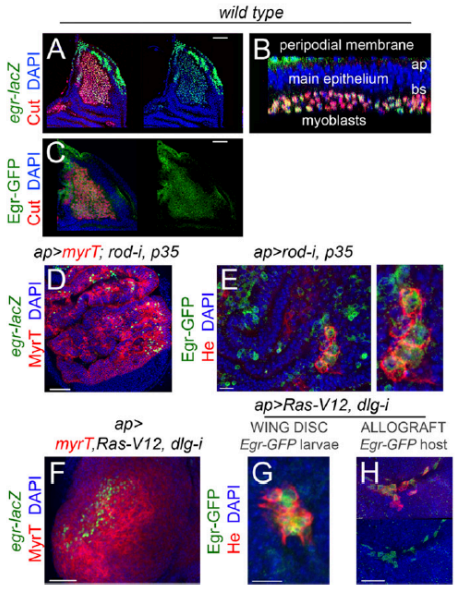

Fig. 2. Eiger expression in development and in JNK-driven epithelial tumors. (*A–H*) Larval wing primordia from WT individuals (*A–C*) or from individuals expressing the indicated transgenes under the control of the *ap-GAL4* driver (*D–H*) and stained for DAPI (blue, *A–H*), Cut (red in *A–C*), *eiger-lacZ* (green, *A, B, D,* and *F*), Eiger-GFP (green, *C, E, G,* and *H*), He (red, *E, G,* and *H*), and MyrT (red, *D* and *F*). Eiger is expressed in myoblasts (labeled by the expression of Cut) in WT wing discs (*A–C*) and becomes activated in a scattered pattern in epithelial cells (labeled by the expression of MyrT) and recruited hemocytes (labeled by the expression He) in JNK-driven tumor-like overgrowths (*D–H*). (Scale bars, *A, C, D, F,* and *H*, 50 μm; *E* and *G*, 15 μm.)

JNK Activation and Tumor Growth in the Absence of Hemocytes. We first analyzed the contribution of hemocytes to tumor initiation. For this purpose, we performed allograft transplantations into the abdomen of adult females and analyzed JNK activation and growth of these allografts upon genetic ablation of adult hemocytes. Females carrying the hemocyte-specific *hemese-GAL4* (*he-GAL4*) driver, the *tub-GAL80ts* transgene, and the *UAS-GFP* and *UAS-reaper* constructs were used as hosts. The temperature-sensitive GAL80 (GAL80ts) molecule, which represses GAL4 transcriptional activity at low temperatures (18 °C) (34), was used to control expression of the proapoptotic gene *reaper* by shifting the animals from 18 °C to 29 °C a few hours before allograft transplantation. Adult females carrying the *he-GAL4* driver and the *UAS-GFP* transgene were used as controls. We also used the GAL80ts molecule and the temperature shifts to initiate transgene expression and tumorigenesis in larval tissues when they had been transplanted into the adult abdomen. As a proof of concept, larval wing primordia raised at 18 °C and containing the *ap-GAL4* driver and the *tub-GAL80ts* and the corresponding *UAS* transgenes showed no overgrowth phenotype and no obvious effect on JNK activation, as monitored by the expression of the JNK target *Drosophila* matrix metalloproteinase 1 (dMMP1) (Fig. 3*A*; note the endogenous and JNK-independent expression of dMMP1 in the trachea marked by arrows). Very few hemocytes, if any, were observed in these wing discs (Fig. 3*A*, arrowheads). As depicted in Fig. 3*B*, a small piece of these wing discs was transplanted into the abdomen of adult hosts that were then maintained at 29 °C to initiate transgene expression. Note that the implanted piece consists mainly of cells expressing the tumor-initiating transgenes. The implanted tissues were dissected and processed for immunofluorescence after a period of 5 or 12 days for the CIN and polarity-impaired tumor models, respectively. Initiation of transgene expression in the transplanted tissues drove tumor growth (Fig. 3 *C* and *G*), induced a 1,000-fold increase in tissue size (Fig. 3*M*), and activated JNK, as monitored by the expression of dMMP1 (Fig. 3 *D′* and *H′*). Interestingly, these tumors recruited a large number of circulating hemocytes of the adult host, labeled by the expression of GFP (Fig. 3 *D* and *H*) or by the expression of NimC1 (Fig. 3 *I* and *I′*). Recruited hemocytes expressed Eiger (Fig. 2*H*), engulfed cell debris coming from the tumor (labeled by MyrT; Fig. S2), and deposited collagen IV (labeled by the Viking-GFP fusion protein), a fundamental element of epithelial basement membranes (Fig. S2). When the hemocyte cell population was ablated by the expression of *reaper* (Fig. 3 *E*, *F*, and *J–L*), initiation of transgene expression in the transplanted tissues was also able to drive tumor growth (Fig. 3 *E*, *F*, *J*, and *K*) and JNK activation (Fig. 3 *F′* and *K′*). Surprisingly, JNK activation and tumor size were both unaffected by the absence of hemocytes (quantified in Fig. 3*M*), but the amount of collagen IV deposited in the tumor was clearly reduced (Fig. S2). Altogether, our results indicate, as previously shown (18), that hemocytes deposit collagen IV in the tumor, most probably to reconstitute the basement membrane, and they engulf cellular debris. However, our data indicate that these hemocytes are not an absolute requirement for tumor initiation and JNK activation in CIN and polarity-impaired tumor models.

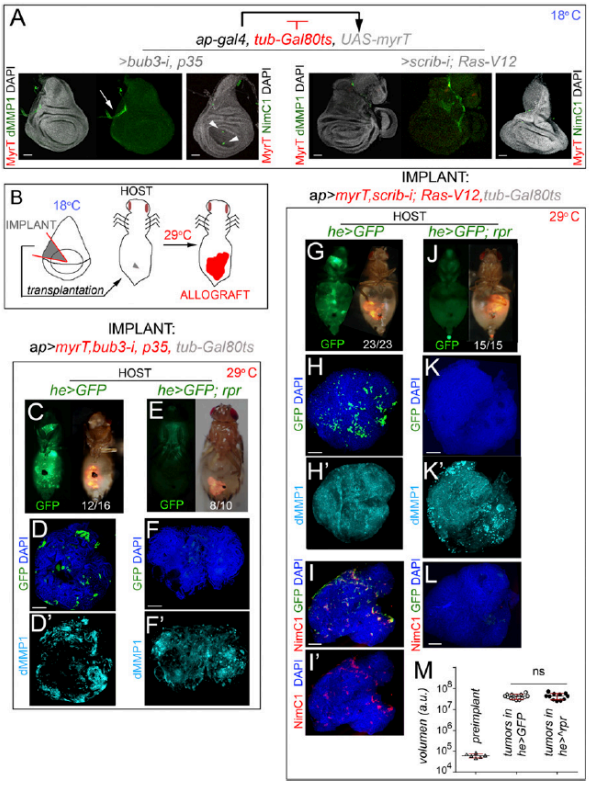

Fig. 3. JNK activation and tumor-like growth in the absence of hemocytes. (*A*) Larval wing primordia of the indicated genotypes, raised at 18 °C to turn off transgene expression in a GAL80-dependent manner, and stained for DAPI (gray), MyrT (red), and dMMP1 (green) or NimC1 (green, *Right*). (Scale bars, 50 μm.) MyrT is not expressed and dMMP1 is not induced under these circumstances. Arrow points to the endogenous expression of dMMP1 in the trachea and arrowheads point to a few hemocytes recruited to control wing primordia. (*B*) Cartoon showing the allograft-transplantation protocol. Wing primordia carrying CIN or *scrib-i*; *Ras-V12* transgenes under control of the *ap-GAL4* driver, and silenced with the GAL80ts factor, were dissected from L3 larvae raised at 18 °C, cut into small pieces, and injected into the abdomen of young adult females. Fly hosts were then transferred to a temperature of 29 °C to induce transgene expression. (*C*, *E*, *G*, and *J*) Micrographs of adult flies carrying MyrT-labeled (red) implants of the indicated genotypes and expressing GFP (green) under the *he-GAL4* driver. Host flies were maintained at 29 °C to induce transgene expression; images were taken 5 days (*G* and *I*) or 12 days (*C* and *E*) after implantation; ratios indicating the reproducibility of the phenotype are shown. In *E* and *J*, host flies expressed the proapoptotic gene *reaper* under the control of the *he-GAL4* driver. (*D*, *D*′, *F*, *F*′, and *H*–*L*) Allograft transplants of the indicated genotypes stained to visualize GFP (green, *D*, *F*, *H*, *I*, and *K*) or NimC1 (red, *I*, *I*′, and *L*), dMMP1 (cyan, *D*′, *F*′, *H*′, *K*′), and DAPI (green, *D*, *F*, *H*, *I*, *I*′, *K*, and *L*). Transplants were extracted 5 days (*H*–*L*) or 12 days (*D*–*F*′) after implantation. (Scale bars, 100 μm.) (*M*) Histogram plotting the size [in arbitrary units (a.u.)] of preimplanted wing disc pieces (*Left*) or allograft transplants expressing *scrib-i*; *Ras-V12* and implanted in adult flies expressing *GFP* (*Middle*) or *GFP* and *reaper* (*Right*) transgenes. Error bars indicate SD. No statistical difference (ns) in allograft size was observed upon induction of *reaper* expression in the adult hemocytes [$P(0.05) = 0.6007$]. Volume (preimplanted wing disc) = $6.17.10^4 \pm 1.3.10^4$ ($n = 6$). Volume (allograft in *he>GFP* hosts) = $4.18.10^7 \pm 1.13.10^7$ ($n = 14$). Volume (allograft in *he>rpr* hosts) = $4.35.10^7 \pm 1.5.10^7$ ($n = 11$).

JNK Activation and Tumor Growth in the Absence of Myoblasts. Myoblasts play a critical role in EGFR-driven epithelial tumors by providing secreted factors that enhance tumor growth (19). As we observed that this population is also the major source of Eiger expression in CIN and polarity-impaired tumors (Fig. 2), we next addressed the potential contribution of the myoblast population to JNK activation and tumor initiation. The *GAL4/UAS* and *lexA/lexO* systems were combined to induce tumor formation in epithelial cells and simultaneously ablate the myoblast population by the expression of the proapoptotic gene *reaper*. We used the myoblast-specific *15B03-lexA* driver for this purpose (Fig. 4*G*) (19). Myoblasts were marked in all experiments by the expression of the Twist transcription factor. As expression of *reaper* under the control of the *15B03-lexA* driver was not able to genetically ablate these cells in CIN and polarity-impaired tumors using the *ap-GAL4* driver (Fig. S3 and *SI Results*), we switched to the *hh-GAL4* driver, whose expression is restricted to epithelial cells. In this case, in both WT wing discs and CIN and polarity-impaired tumors,

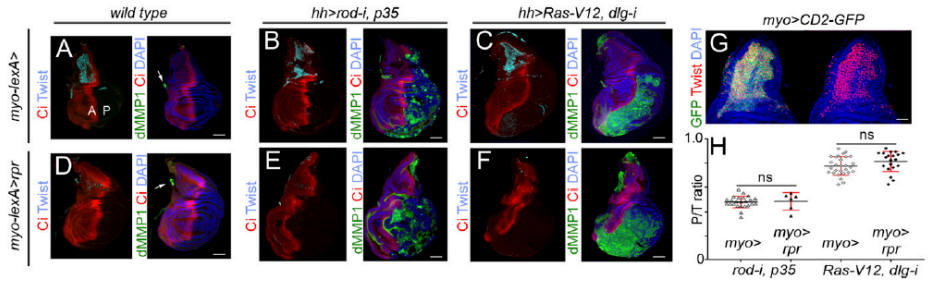

Fig. 4. JNK activation and tumor-like growth upon depletion of the myoblast cell population. (*A–F*) Larval wing primordia of the indicated genotypes stained for Ci (red) and Twist (cyan; *Left*) and DAPI (blue) and dMMP1 (green; *Right*). (*D–F*) Larvae expressed the proapoptotic gene *reaper* under the control of the *15B03-lexA* (*myo-lexA*) driver. Anterior (marked as "A") and posterior (marked as "P") compartments are marked. *hh-GAL4* drives expression to posterior cells, and Ci labels the anterior compartment. Arrows in *A* and *D* point to the endogenous expression of dMMP1 in the trachea of WT primordia. Note in *B*, *C*, *E*, *F* (*Right*) the ectopic expression of dMMP1 in the posterior compartment. Some background staining is observed in the folds of the anterior compartment in some discs (e.g., *E*). (*G*) Notum of a larval wing primordium expressing CD2-GFP (green) under the control of the *myo-lexA* driver and stained for DAPI (blue) and Twist (red). (Scale bars, *A–F*, 50 μm; *G*, 30 μm.) (*H*) Histogram plotting the ratio between the size of the posterior (marked as "P") compartment (labeled by the absence of Ci in *A–F*) and the total size (marked as "T") of wing discs of the indicated genotypes. Error bars indicate SD ($n > 6$ in all cases). No statistical difference (ns) in posterior compartment to total wing primordia (P/T) ratio was observed upon depletion of the myoblast population in the two tumor models [P(*rod-i, p35*) = 0.83, and P(*Ras-V12, dlg1-i*) = 0.1139].

15B03-lexA–driven *reaper* expression was able to deplete the whole myoblast population (Fig. 4 *D–F*). We observed that JNK activation and tumor size were both unaffected by the absence of myoblasts (Fig. 4 *A–F*; quantified in Fig. 4*H*). These results indicate that JNK-driven tumor-like overgrowth in CIN and polarity-impaired tumors is largely independent of the tumor-associated myoblasts. Interestingly, tumor growth and JNK activation were still observed upon simultaneous depletion of the myoblast and hemocyte cell populations (Fig. S2).

JNK Activation and Tumor Growth in the Absence of Eiger. Based on the aforementioned results indicating that TME cells—recruited hemocytes and resident myoblasts—do not have any impact on tumor initiation and JNK activation in CIN and polarity-impaired epithelial tumors, we next addressed the functional role of the ectopic expression of Eiger observed in epithelial cells (Fig. 2 *D–F* and Fig. S1). For this purpose, we depleted Eiger in CIN and polarity-impaired tumors by the use of an RNAi form against *eiger* or by inducing clones of cells homozygous for a null allele of *eiger* (*eiger*^{1}) (21). JNK activation, monitored by the expression of dMMP1, and the resulting tissue overgrowth were both largely unaffected by the coexpression of *eiger-RNAi* together with the tumor-inducing transgenes (Fig. 5 *A*, *B*, *F*, and *G*; quantified in Fig. 5 *C* and *H*). Consistent with these results, JNK activation was still observed in clones of cells mutant for *eiger* and expressing the CIN and polarity-impaired tumor-inducing transgenes (Fig. 5 *D*, *E*, *I*, and *J*). We next induced CIN and polarity-impaired tumors upon removal of Eiger in the whole animal by driving the tumor-inducing transgenes in *eiger*^{1} mutants (*eiger*^{1} is a null allele of *eiger*) (21). Complete loss of Eiger activity did not have any impact on JNK activation or tumor growth (Fig. 6 *A–D*; quantified in Fig. 6*O*). Eiger drives JNK activation in epithelial cells through its recently identified receptor Grnd (14). JNK activation and tumor growth were largely unaffected by targeted depletion of Grnd in epithelial cells with a *grnd-RNAi* form (Fig. 6 *E–H*; quantified in Fig. 6*P*) or by removal of Grnd in the whole animal by the use of a *grnd*^{MI05292} mutant allele (Fig. 6 *I–L*; quantified in Fig. 6*Q*). JNK activation in clones of cells expressing the tumor-inducing transgenes was also still observed upon *grnd* depletion, albeit at lower levels (Fig. 6 *M* and *N*, white arrows). We noticed that the capacity of *grnd* depletion to reduce the levels of JNK activation was stronger in clones of cells expressing the tumor-inducing transgenes in the eye primordia (Fig. S4) (14). The

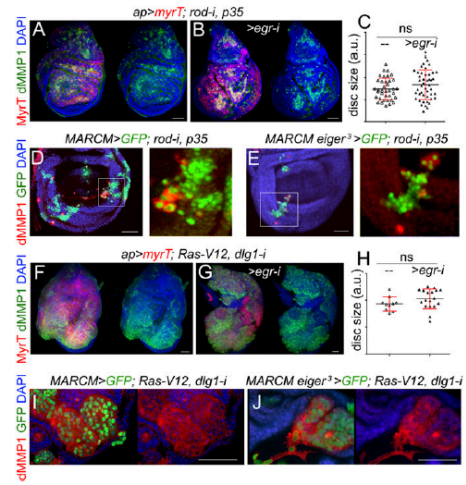

Fig. 5. Eiger is not required in epithelial cells to drive JNK activation and tumor-like growth. (*A*, *B*, *F*, and *G*) Larval wing primordia expressing the indicated transgenes under the control of the *ap-GAL4* driver and stained for DAPI (blue), MyrT (red), and dMMP1 (green). (*D*, *E*, *I*, and *J*) Larval wing primordia with clones of WT (*D* and *I*) or *eiger*^{3} mutant cells (*E* and *J*) induced by the mosaic analysis with a repressible cell marker (MARCM) technique and expressing the indicated transgenes. Clones were positively labeled by the expression of GFP (green), and the tissue was stained for dMMP1 (red) and DAPI (blue). (Scale bars, 50 μm.) (*C* and *H*) Histograms plotting the size [in arbitrary units (a.u.)] of larval wing primordia of the indicated genotypes. Error bars indicate SD ($n > 10$ in all cases). No statistical difference was observed between *eiger-RNAi* expressing and nonexpressing samples [P(*c*) = 0.1425 and P(h) = 0.1659].

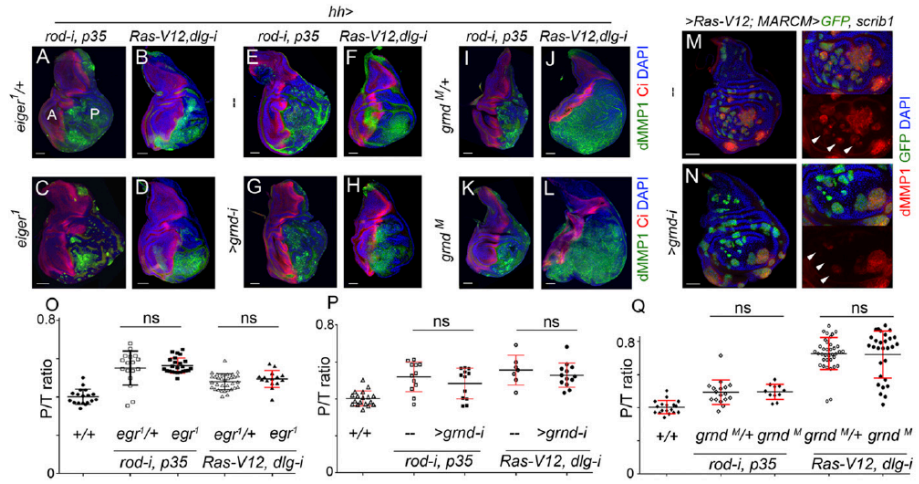

Fig. 6. JNK activation and tumor-like growth in the absence of Eiger and Grnd. (*A–L*) Larval wing primordia of the indicated genotypes and stained for DAPI (blue), Ci (red), and dMMP1 (green). *hh-GAL4* drives expression to posterior (marked as "P") cells, and Ci labels the anterior (marked as "A") compartment. In *C*, *D*, *G*, *H*, *K*, and *L*, larvae were homozygous mutant for *eiger* or *grnd* or expressing *grnd-i*. Larvae shown in *A*, *B*, *E*, *F*, *I*, and *J* served as controls. (*M* and *N*) Larval wing primordia with clones of cells induced by the MARCM technique and expressing the indicated transgenes. Clones were positively labeled by the expression of GFP (green), and the tissue was also stained for dMMP1 expression (red) and DAPI (blue). dMMP1 was cell-autonomously induced in WT and *grnd-i*–expressing cells (white arrows), albeit at lower levels in *grnd-i*–expressing cells. (Scale bars, 50 μm.) (*O–Q*) Histograms plotting the ratio between the size of the posterior compartment (labeled by the absence of Ci in *A–L*) and the total size (marked as "T") of wing discs of the indicated genotypes. Error bars indicate SD ($n > 7$ in all cases). No statistical difference (ns) in P/T ratio was observed between control wing discs and wing discs homozygous mutant for *egr* or *grnd* or expressing *grnd-i* [*O*: *P*(*Ras-V12, dlg1-i*) = 0.2743; *P*(*rod-i, p35*) = 0.5392]; *P*: *P*(*Ras-V12, dlg1-i*) = 0.4149; *P*(*rod-i, p35*) = 0.2906]; *Q*: *P*(*Ras-V12, dlg1-i*) = 0.8497; *P*(*rod-i, p35*) = 0.92].

mechanistic basis underlying the differential contribution of Grnd to JNK activation in eye and wing primordia is so far little understood. Altogether, these results indicate that JNK activation and growth of CIN and polarity-impaired epithelial tumors can

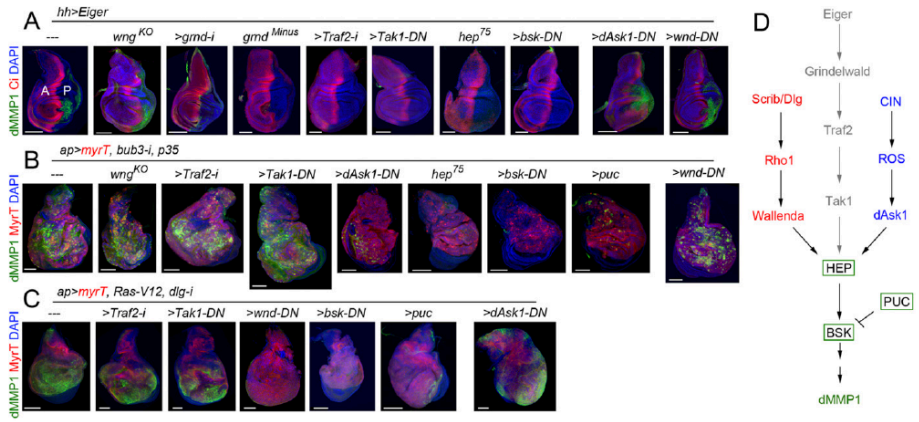

Fig. 7. Multiple Eiger-independent mechanisms to drive JNK activation in epithelial tumors. (*A–C*) Larval wing primordia of the indicated genotypes and stained for DAPI (blue), Ci (*A*, red), or MyrT (red, *B* and *C*) and dMMP1 (green). *hh-GAL4* drives expression to posterior (marked as "P") cells, and Ci labels the anterior (marked as "A") compartment. (Scale bars, 100 μm.) (*D*) Cartoon depicting three distinct molecular mechanisms driving JNK activation.

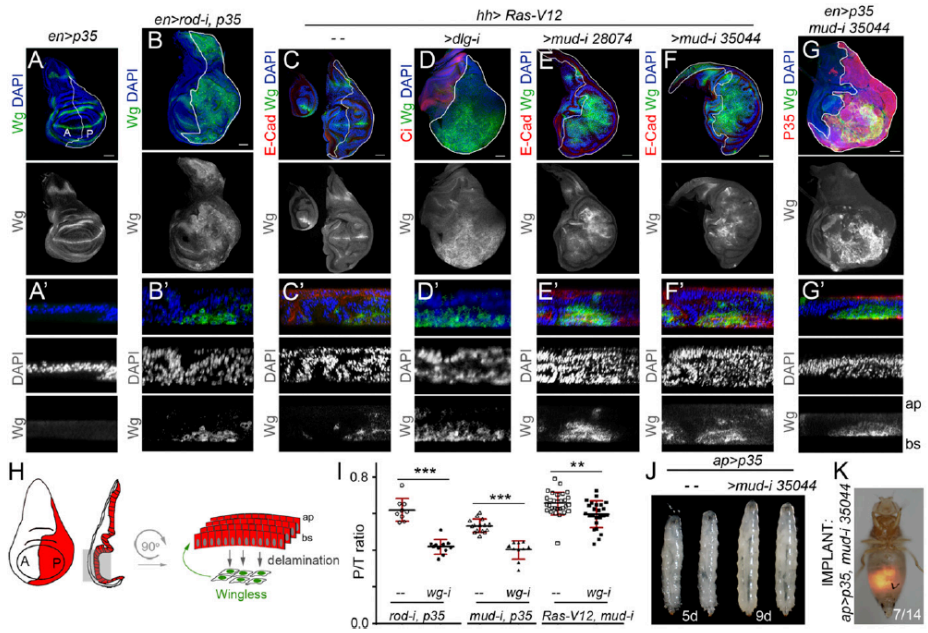

Fig. 8. Wg expression in delaminating cells drives growth in epithelial tumors. (*A–G′*) Larval wing primordia of the indicated genotypes and stained for DAPI (blue or white), Wg (green or white), and E-cadherin (E-Cad; red, *C–F′*) or P35 (*G*, red). *hh-GAL4* and *en-GAL4* drive expression to posterior (marked as "P") cells (marked by a white line or by the expression of P35). (Scale bars, 50 μm.) In *A′–G′*, cross-sections of larval wing primordia are shown to visualize delaminating cells expressing Wg in CIN (*B′*) and polarity-impaired (*D′*) tumor models or upon depletion of *mud* (*E′*, *F′*, and *G′*) compared with wing discs expressing P35 (*A′*) or Ras-V12 (*C′*). Apical (ap) and basal (bs) sides of the epithelium are marked, as are anterior (marked as "A") and posterior (marked as "P") compartments. (*H*) Cartoon depicting a wing disk in which cells in the posterior compartment (red) delaminate basally (bs) and express Wg (green), which drives the proliferation of nondelaminating cells (red). (*I*) Histogram plotting the ratio between the size of the posterior (marked as "P") compartment and the total size (marked as "T") of wing discs of the indicated genotypes. Error bars indicate SD ($n > 9$ in all cases; ***$P < 0.001$ and **$P < 0.01$). (*J*) Larvae expressing p35 alone [4 days after egg-laying (AEL)] or in combination with *mud-RNAi* (8 days AEL) under the control of the *ap-GAL4* driver. (*K*) Micrograph of an adult fly carrying a MyrT-labeled (red) implant of the indicated genotype. Image was taken 12 days after implantation; ratio indicates the reproducibility of the phenotype.

happen in the absence of Eiger and Grnd activities, and suggest that JNK activation in these tumors is most probably a cell-autonomous process.

Dissecting the Molecular Mechanisms Underlying JNK Activation. In vertebrate and invertebrate tissues, the conserved JNK pathway integrates signals from a diverse range of stimuli to elicit an appropriate physiological response. Within the *Drosophila* JNK cascade, JNKK/Hemipterous (Hep) phosphorylates JNK/Basket (Bsk) to activate, also by phosphorylation, the AP1 transcriptional complex. Upstream of Hep, different JNKK kinases have been identified in *Drosophila*, including Tak1, Ask1, and Wallenda (Wnd). Tak1 is involved in Eiger/Grnd-mediated JNK activation by binding to Traf2, a member of the TNF receptor-associated factor (TRAF) protein family (14). Consistent with these results, depletion of Grnd or Traf2 by RNAi, or expression of a kinase-dead isoform of Tak1 that acts as a dominant-negative version of the kinase (Tak1-DN) (35), in wing discs overexpressing Eiger rescued JNK activation, monitored by the expression of dMMP1 (Fig. 7*A*). By contrast, depletion of Traf2 or Tak1 activities did not reduce the levels of JNK activation of CIN and polarity-impaired tumors (Fig. 7 *B* and *C*), reinforcing our results unraveling the Eiger/Grnd-independent activation of JNK in these tumors. We observed that loss of Wengen (Wgn), which was identified as the first *Drosophila* TNF receptor (36) and was recently shown to be dispensable for Eiger-induced JNK activation in epithelial cells and RAS-induced tumorigenesis (14), did not rescue JNK activation in CIN tumors either (Fig. 7*B*). CIN tumors bear a large number of aneuploid cells, and the production of radical oxygen species (ROS) in these cells, most probably as a consequence of metabolic stress, contributes to JNK activation (25). A potential JNKK kinase able to phosphorylate Hep and activate Bsk in CIN-induced aneuploid cells is Ask1, as it is directly regulated by ROS through its binding to thioredoxin (37). Whereas the reduced version of thioredoxin binds Ask1 and suppresses its kinase activity, its ROS-induced oxidized version dissociates from Ask1, which becomes active. Interestingly, expression of a kinase-dead mutant form of Ask1, acting as a dominant-negative version of the kinase (Ask1-DN) (38), was able to rescue JNK activation in CIN tumors (Fig. 7*B*). The JNKK kinase Wnd has been identified as an important molecular link that mediates loss of cell polarity-triggered JNK activation (39). Expression of a kinase-dead form of Wnd (Wnd-DN) (40) largely rescued JNK activation in polarity-impaired tumors (Fig. 7*C*). Interestingly, a kinase-dead

version of Bsk (Bsk-DN) (41), a hypomorphic allele of *hep* (*hep*^{75}), or overexpression of Puckered, a phosphatase that inactivates Bsk, were all able to rescue JNK activation in wing discs overexpressing Eiger and in CIN and polarity-impaired tumors (Fig. 7 *A*–*C*) (8, 12, 23), implying that the core Hep/Bsk/Puc module integrates signals from different stimuli. By contrast, the JNKK kinases Tak1, Ask1, and Wnd are the ones sensing context-dependent stimuli, as the capacity of dominant-negative versions of these three kinases to block JNK activation was restricted to Eiger overexpression and CIN and polarity-impaired tumors, respectively (Fig. 7 *A*–*C*). All together, these results reinforce the tissue-autonomous character of JNK activation in CIN and polarity-impaired tumors and unravel different cell-autonomous routes to activate JNK in a tumor-specific manner (Fig. 7*D*).

A Tumor-Intrinsic Mechanism Confers Unlimited Growth Potential. We next characterized the mechanistic basis underlying the TME-independent growth potential of CIN and polarity-impaired tumors and the types of intratumor cell interactions involved. Remarkably, the gene-expression program promoting malignancy as well as the molecular and cellular mechanisms underlying CIN-induced tumor growth resemble those caused by the cooperative action of RAS oncogene activation and mutations in the *scrib* or *dlg1* tumor-suppressor genes (7–10, 12, 25, 26, 42, 43). Loss of cell-polarity determinants or CIN-induced aneuploidy induces cell delamination, and delaminating cells express mitogenic molecules like Wg (the *Drosophila* ortholog of mammalian Wnts) and IL-6–like Upd cytokines, which activate the JAK/STAT pathway (17, 23, 25, 42) (Fig. 8 *A*–*D* and *H* and Fig. S5). These two mitogenic molecules signal back to the tumor mass to drive growth, as depletion of JAK/STAT signaling or Wg reduced tumor growth (17, 23, 25) (Fig. 8*I*). These results highlight the nonautonomous and growth-promoting role of delaminating cells expressing Wg and Upd in CIN and polarity-impaired tumors. We then addressed whether the simple production of delaminating cells expressing mitogenic molecules was sufficient to drive tumor growth. Scrib or Dlg1 cell-polarity determinants have been shown to direct the planar orientation of the mitotic spindle, and failure to orient the mitotic spindle leads to cell delamination and JNK activation (44). Mitotic spindles are oriented by the dynein/dynactin motor complex, whose cortical localization depends on Mud/NUMA. Blocking the death of Mud-depleted misaligned cells by expressing p35 or Ras-V12 was sufficient to drive tumor-like structures formed by Wg- and Upd-expressing delaminating cells located on the basal side of the epithelium and epithelial cells actively proliferating (Fig. 8 *E*–*G* and Fig. S5) (44). Similarly to CIN and polarity-impaired tumors (23, 45, 46), larvae containing *mud/p35* tumors were developmentally delayed and became gigantic, and these tumors were malignant to the host and able to grow in allograft transplantations (Fig. 8 *J* and *K* and Fig. S5). Interestingly, depletion of Wg in *mud*-depleted tissues reduced tissue overgrowth (Fig. 8*I*). These results indicate that the simple production of delaminating cells expressing Wg, by means of compromising the planar orientation of the mitotic spindle, is sufficient to promote tumor-like overgrowths. As *scrib*- or *dlg1*-depleted tissues show defects in the planar orientation of the mitotic spindle (44), the observed ectopic expression of Wg in polarity-impaired tumors (Fig. 8*D* and Fig. S5) is also expected to contribute to their growth.

We noticed that mitotic activity in CIN and polarity-impaired tumors was highly increased in the cell population expressing the tumor-initiating transgenes (Fig. 9 *A*–*C*). Interestingly, mitotic activity was restricted to the nondelaminating cell population and absent in Wg-expressing cells (Fig. 9 *D* and *E*), suggesting that the latter cells are mitotically inactive. In CIN tumors, the Wg-dependent resulting hyperproliferation is expected to increase the chances of chromosome segregation errors and aneuploidy levels in the nondelaminating cell layer subject to CIN

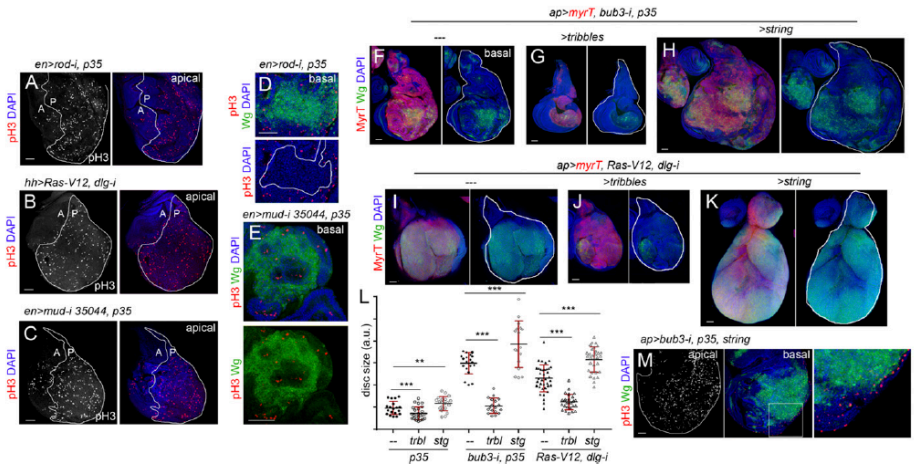

Fig. 9. Mitotic activity increases the number of delaminating cells expressing Wg. (*A*–*K* and *M*) Larval wing primordia of the indicated genotypes and stained for DAPI (blue), pH3 (red or white, *A*–*E* and *M*), Wg (green, *D*–*K*, *M*), and MyrT (red, *F*–*K*). *en-GAL4* drives expression to posterior (marked as "P") cells (marked by a white line in *A*–*C*), and *ap-GAL4* drives expression to dorsal (marked as "D") cells (marked by a white line in *F*–*K* and labeled by the expression of MyrT). Delaminating cells expressing Wg (*D*) or the contour of the disk (*M*) are marked by white lines. (*Right*) Higher magnification of the squared region. (Scale bars, 50 μm.) (*L*) Histogram plotting total size (marked as "T") of wing discs [in arbitrary units (a.u.)] of the indicated genotypes. Error bars indicate SD ($n > 17$ in all cases; $^{***}P < 0.001$ and $^{**}P < 0.01$).

and, consequently, to augment the number of aneuploidy-induced delaminated cells expressing Wg and Upd (47). In polarity-impaired tumors, the augmented cell proliferation in the epithelium, as a response to mitogenic molecules coming from delaminating cells, should also increase the chances of spindle misorientation and cell delamination, and, consequently, the pool of delaminating cells. We tested these proposals by manipulating the proliferating rates in CIN and polarity-impaired tumors and analyzing the impact on the production of Wg-expressing delaminating cells and on the size of the tumors. Overexpression of *Drosophila* Cdc25/String, which drives cells through the G2/M transition (48), or Tribbles, which arrests cells in G2 by ubiquitinating String and sending it to proteasome-mediated degradation (49), do not have a great impact on tissue size in otherwise WT tissues (Fig. 9*L*) (50). By contrast, overexpression of String in CIN and polarity-impaired tumors dramatically increased the number of Wg-expressing cells and tumor size, and Tribbles overexpression reduced the number of Wg-expressing cells and the size of the resulting tumors (Fig. 9 *F–K*; quantified in Fig. 9*L*). We noticed that only those cells remaining in the epithelium were mitotically active upon String overexpression (Fig. 9*M*), which is consistent with the proposal that the increase in the number of Wg-expressing cells is a consequence of augmented cell delamination. All together, these results indicate that a feedback amplification loop between delaminating cells expressing mitogenic molecules, which remain mitotically inactive, and the proliferative epithelium acting as source of delaminating cells drives growth and neoplastic transformation of CIN and polarity-impaired tumors in a TME-independent manner. Whether delaminating cells are arrested in G1, as occurs in senescent cells induced in fly epithelial tumors caused by the oncogenic cooperation between Ras-V12 and mitochondrial mutants (51, 52), is an interesting idea that needs to be elucidated but that could certainly explain their resistance to String overexpression.

Discussion

Tumor progression and metastatic colonization at distant sites rely on interactions with the surrounding TME (2, 53). The TME acts as a niche to provide secreted signaling molecules and growth factors that maintain the undifferentiated state of the tumor and promote its growth. Here we used two well-characterized and molecularly distinct JNK-driven epithelial tumors of *Drosophila*, the CIN and polarity-impaired models (23, 26), to unravel TME-independent mechanisms that contribute to the unlimited growth potential of these tumors. We used the *GAL4/UAS* system to drive tumorigenesis in large territories, thus reducing the amount of cell interactions with WT epithelial cells. We combined allograft transplantation experiments with the *GAL4/UAS* and *lexA/lexO* transactivation systems to ablate TME cells and analyzed the impact on tumor initiation and JNK activation. We present evidence that genetic ablation of resident myoblasts or recruited hemocytes, by means of expression of the proapoptotic gene *reaper*, does not prevent tumor formation or JNK activation in CIN or polarity-impaired models. Our results support the notion that, in the absence of a TME, the growth potential of these tumors is determined by interactions between functionally distinct cell populations within the tumors (Fig. 10*A*). It is interesting to note in this context that the two interacting cell populations within CIN tumors are clearly genetically distinct, as delaminating cells are highly aneuploid, whereas these two cell populations are genetically similar in RAS tumors. Cancer has been classically understood as a cell-autonomous process by which oncogenes and loss of tumor-suppressor genes drive clonal cell expansion. However, research in a variety of model organisms, including *Drosophila*, has unveiled the relevance of cell communication in tumor development (reviewed in refs. 3, 4). Interactions between tumor cells and the surrounding TME, and between clonally distinct cell populations,

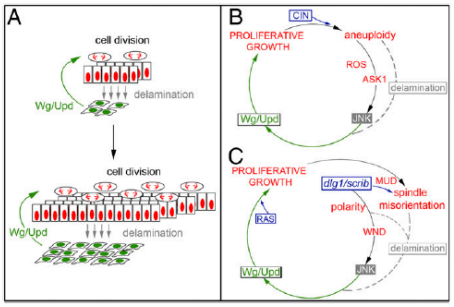

Fig. 10. A feedback amplification loop drives unlimited growth in epithelial tumors. (*A*) Cartoon depicting the cell populations and interactions responsible to the unlimited growth potential of epithelial tumors. While Wg and Upd emanating from basally delaminating cells (in green) promotes proliferative growth of the main epithelium (in red), the resulting increase in the number of mitotic events has a positive impact in the number of cells delaminating as a consequence of mistakes in the segregation of chromosomes or planar orientation of the mitotic spindle. (*B*) In CIN tumors, aneuploid cells activate in an ROS- and Ask1-dependent manner, JNK, which induces the expression of Wg and Upd. Those cells with the highest levels of aneuploidy delaminate basally and drive, through Wg and Upd, the proliferation of nondelaminating cells. Cell proliferation increases the chances of chromosome segregation errors and the levels of aneuploidy and, consequently, the pool of aneuploidy-induced delaminating cells. (*C*) In polarity-impaired tumors, loss of cell polarity determinants Scrib or Dlg1 activate, in a Wnd-dependent manner, JNK, which induces the expression of Wg and Upd. Defects in apicobasal polarity and planar orientation of the mitotic spindle as a consequence of loss of Scrib or Dlg1 induce cell delamination. Delaminating cells drive, through Wg and Upd, the proliferation of nondelaminating cells. Cell proliferation driven by the combined activities of Wg, Upd, and Ras increases the chances of defects in the planar orientation of the mitotic spindle and, consequently, augments the pool of Wg- and Upd-expressing delaminating cells.

have been shown to contribute to tumor progression and metastatic colonization. Our work supports the notion that intratumor communication also between genetically similar but functionally distinct cell populations can contribute to tumor growth. Remarkably, in all these relevant social interactions, secreted signaling molecules and growth factors play a similar role in driving proliferation and growth of tumor cells.

Interactions between tumor cells and the surrounding TME, and between clonally distinct cell populations, have been shown to be mediated by the TNF-α ligand Eiger and its receptor Grnd, which drive JNK activation, tumor growth, and invasive behavior (13–15). However, the conserved JNK pathway can also integrate signals from a diverse range of stimuli to elicit an appropriate physiological response in vertebrate and invertebrate tissues. Here we used CIN and polarity-impaired tumor models in which cell interactions with WT cells are being reduced to present evidence that different routes, sensing cell-autonomous stimuli, are used in a tumor-specific manner to activate a common JNKK/JNK core that induces a shared tumorigenic transcriptional program (Fig. 10 *B* and *C*). CIN tumors induce a large number of aneuploid cells, and the production of ROS in these cells contributes to JNK activation (25). We identified Ask1, which was shown to be directly regulated by ROS through its binding to thioredoxin (37), as the JNKK kinase driving JNK activation in CIN tumors. We present evidence that the JNKK kinase Wnd, which is activated by loss of cell polarity determinants (39), drives JNK activation in polarity-impaired tumors. These results, together with our experimental data ruling out any role of Eiger and Grnd in JNK activation, support the cell-autonomous

character of JNK activation in our CIN and polarity-impaired epithelial tumors and the TME-independent self-reinforcement mechanism that drives their unlimited growth potential.

Materials and Methods

Drosophila strains were obtained from Vienna *Drosophila* RNAi Center or the Bloomington Stock Center and are described in FlyBase. Antibodies were obtained from the Developmental Studies Hybridoma Bank or other private sources. These and other experimental details are described in *SI Materials and Methods*.

ACKNOWLEDGMENTS. We thank I. Ando, K. Basler, J. Colombani, H. Herranz, H. Jiang, P. Leopold, M. Leptin, M. Miura, and F. Serras; the Bloomington *Drosophila* Stock Center, the Vienna *Drosophila* RNAi Center, and the National Institute of Genetics (Japan) for flies; the Developmental Studies Hybridoma Bank for antibodies; and M. Clemente and other members of the laboratory for comments on the manuscript. This work was funded by a PhD fellowship from La Caixa (to L.M.), Ministerio de Economía, Industria y Competitividad (MINECO) (Government of Spain) Grants SIGNAGROWTH-BFU2013-44485 and INTERGROWTH-BFU2016-77587-P (to M. Milán), and Fondo Europeo de Desarrollo Regional (FEDER) "Una manera de hacer Europa" (M. Milán). Institute for Research in Biomedicine (IRB Barcelona) is the recipient of a Severo Ochoa Award of Excellence from MINECO. M. Milán is an Institució Catalana de Recerca i Estudis Avançats (ICREA) Research Professor.

1. Hanahan D, Weinberg RA (2011) Hallmarks of cancer: The next generation. *Cell* 144: 646–674.
2. Quail DF, Joyce JA (2013) Microenvironmental regulation of tumor progression and metastasis. *Nat Med* 19:1423–1437.
3. Tabassum DP, Polyak K (2015) Tumorigenesis: It takes a village. *Nat Rev Cancer* 15: 473–483.
4. Pastor-Pareja JC, Xu T (2013) Dissecting social cell biology and tumors using Drosophila genetics. *Annu Rev Genet* 47:51–74.
5. Cordero JB, et al. (2010) Oncogenic Ras diverts a host TNF tumor suppressor activity into tumor promoter. *Dev Cell* 18:999–1011.
6. Uhlirova M, Jasper H, Bohmann D (2005) Non-cell-autonomous induction of tissue overgrowth by JNK/Ras cooperation in a Drosophila tumor model. *Proc Natl Acad Sci USA* 102:13123–13128.
7. Brumby AM, Richardson HE (2003) scribble mutants cooperate with oncogenic Ras or Notch to cause neoplastic overgrowth in Drosophila. *EMBO J* 22:5769–5779.
8. Igaki T, Pagliarini RA, Xu T (2006) Loss of cell polarity drives tumor growth and invasion through JNK activation in Drosophila. *Curr Biol* 16:1139–1146.
9. Figueroa-Clarevega A, Bilder D (2015) Malignant Drosophila tumors interrupt insulin signaling to induce cachexia-like wasting. *Dev Cell* 33:47–55.
10. Külshammer E, et al. (2015) Interplay among Drosophila transcription factors Ets21c, Fos and Ftz-F1 drives JNK-mediated tumor malignancy. *Dis Model Mech* 8:1279–1293.
11. Külshammer E, Uhlirova M (2013) The actin cross-linker Filamin/Cheerio mediates tumor malignancy downstream of JNK signaling. *J Cell Sci* 126:927–938.
12. Uhlirova M, Bohmann D (2006) JNK- and Fos-regulated Mmp1 expression cooperates with Ras to induce invasive tumors in Drosophila. *EMBO J* 25:5294–5304.
13. Igaki T, Pastor-Pareja JC, Aonuma H, Miura M, Xu T (2009) Intrinsic tumor suppression and epithelial maintenance by endocytic activation of Eiger/TNF signaling in Drosophila. *Dev Cell* 16:458–465.
14. Andersen DS, et al. (2015) The Drosophila TNF receptor Grindelwald couples loss of cell polarity and neoplastic growth. *Nature* 522:482–486.
15. Ohsawa S, et al. (2011) Elimination of oncogenic neighbors by JNK-mediated engulfment in Drosophila. *Dev Cell* 20:315–328.
16. Katheder NS, et al. (2017) Microenvironmental autophagy promotes tumour growth. *Nature* 541:417–420.
17. Wu M, Pastor-Pareja JC, Xu T (2010) Interaction between Ras(V12) and scribbled clones induces tumour growth and invasion. *Nature* 463:545–548.
18. Pastor-Pareja JC, Wu M, Xu T (2008) An innate immune response of blood cells to tumors and tissue damage in Drosophila. *Dis Model Mech* 1:144–154, discussion 153.
19. Herranz H, Weng R, Cohen SM (2014) Crosstalk between epithelial and mesenchymal tissues in tumorigenesis and imaginal disc development. *Curr Biol* 24:1476–1484.
20. Moreno E, Yan M, Basler K (2002) Evolution of TNF signaling mechanisms: JNK-dependent apoptosis triggered by Eiger, the Drosophila homolog of the TNF superfamily. *Curr Biol* 12:1263–1268.
21. Igaki T, et al. (2002) Eiger, a TNF superfamily ligand that triggers the Drosophila JNK pathway. *EMBO J* 21:3009–3018.
22. Schvartzman JM, Sotillo R, Benezra R (2010) Mitotic chromosomal instability and cancer: Mouse modelling of the human disease. *Nat Rev Cancer* 10:102–115.
23. Dekanty A, Barrio L, Muzzopappa M, Auer H, Milán M (2012) Aneuploidy-induced delaminating cells drive tumorigenesis in Drosophila epithelia. *Proc Natl Acad Sci USA* 109:20549–20554.
24. Hay BA, Wolff T, Rubin GM (1994) Expression of baculovirus P35 prevents cell death in Drosophila. *Development* 120:2121–2129.
25. Clemente-Ruiz M, et al. (2016) Gene dosage imbalance contributes to chromosomal instability-induced tumorigenesis. *Dev Cell* 36:290–302.
26. Pagliarini RA, Xu T (2003) A genetic screen in Drosophila for metastatic behavior. *Science* 302:1227–1231.
27. Humbert PO, et al. (2008) Control of tumourigenesis by the Scribble/Dlg/Lgl polarity module. *Oncogene* 27:6888–6907.
28. Dow LE, et al. (2008) Loss of human Scribble cooperates with H-Ras to promote cell invasion through deregulation of MAPK signalling. *Oncogene* 27:5988–6001.
29. Dow LE, et al. (2003) hScrib is a functional homologue of the Drosophila tumour suppressor Scribble. *Oncogene* 22:9225–9230.
30. Prober DA, Edgar BA (2000) Ras1 promotes cellular growth in the Drosophila wing. *Cell* 100:435–446.
31. Blochlinger K, Jan LY, Jan YN (1993) Postembryonic patterns of expression of *cut*, a locus regulating sensory organ identity in *Drosophila*. *Development* 117:441–450.
32. Kurucz E, et al. (2007) Nimrod, a putative phagocytosis receptor with EGF repeats in Drosophila plasmatocytes. *Curr Biol* 17:649–654.
33. Kurucz E, et al. (2003) Hemese, a hemocyte-specific transmembrane protein, affects the cellular immune response in Drosophila. *Proc Natl Acad Sci USA* 100:2622–2627.
34. McGuire SE, Mao Z, Davis RL (2004) Spatiotemporal gene expression targeting with the TARGET and gene-switch systems in Drosophila. *Sci STKE* 2004:pl6.
35. Mihaly J, et al. (2001) The role of the Drosophila TAK homologue dTAK during development. *Mech Dev* 102:67–79.
36. Kanda H, Igaki T, Kanuka H, Yagi T, Miura M (2002) Wengen, a member of the Drosophila tumor necrosis factor receptor superfamily, is required for Eiger signaling. *J Biol Chem* 277:28372–28375.
37. Sekine Y, et al. (2012) The Kelch repeat protein KLHDC10 regulates oxidative stress-induced ASK1 activation by suppressing PP5. *Mol Cell* 48:692–704.
38. Kuranaga E, et al. (2002) Reaper-mediated inhibition of DIAP1-induced DTRAF1 degradation results in activation of JNK in Drosophila. *Nat Cell Biol* 4: 705–710.
39. Ma X, et al. (2016) Rho1-Wnd signaling regulates loss-of-cell polarity-induced cell invasion in Drosophila. *Oncogene* 35:846–855.
40. Collins CA, Wairkar YP, Johnson SL, DiAntonio A (2006) Highwire restrains synaptic growth by attenuating a MAP kinase signal. *Neuron* 51:57–69.
41. Weber U, Paricio N, Mlodzik M (2000) Jun mediates Frizzled-induced R3/R4 cell fate distinction and planar polarity determination in the Drosophila eye. *Development* 127:3619–3629.
42. Bunker BD, Nellimoottil TT, Boileau RM, Classen AK, Bilder D (2015) The transcriptional response to tumorigenic polarity loss in Drosophila. *eLife* 4:4.
43. Atkins M, et al. (2016) An ectopic network of transcription factors regulated by Hippo signaling drives growth and invasion of a malignant tumor model. *Curr Biol* 26: 2101–2113.
44. Nakajima Y, Meyer EJ, Kroesen A, McKinney SA, Gibson MC (2013) Epithelial junctions maintain tissue architecture by directing planar spindle orientation. *Nature* 500: 359–362.
45. Garelli A, Gontijo AM, Miguela V, Caparros E, Dominguez M (2012) Imaginal discs secrete insulin-like peptide 8 to mediate plasticity of growth and maturation. *Science* 336:579–582.
46. Colombani J, Andersen DS, Léopold P (2012) Secreted peptide Dilp8 coordinates Drosophila tissue growth with developmental timing. *Science* 336:582–585.
47. Milán M, Clemente-Ruiz M, Dekanty A, Muzzopappa M (2014) Aneuploidy and tumorigenesis in Drosophila. *Semin Cell Dev Biol* 28:110–115.
48. Edgar BA, O'Farrell PH (1990) The three postblastoderm cell cycles of Drosophila embryogenesis are regulated in G2 by string. *Cell* 62:469–480.
49. Mata J, Curado S, Ephrussi A, Rørth P (2000) Tribbles coordinates mitosis and morphogenesis in Drosophila by regulating string/CDC25 proteolysis. *Cell* 101:511–522.
50. Neufeld TP, de la Cruz AF, Johnston LA, Edgar BA (1998) Coordination of growth and cell division in the Drosophila wing. *Cell* 93:1183–1193.
51. Ohsawa S, et al. (2012) Mitochondrial defect drives non-autonomous tumour progression through Hippo signalling in Drosophila. *Nature* 490:547–551.
52. Nakamura M, Ohsawa S, Igaki T (2014) Mitochondrial defects trigger proliferation of neighbouring cells via a senescence-associated secretory phenotype in Drosophila. *Nat Commun* 5:5264.
53. Joyce JA, Pollard JW (2009) Microenvironmental regulation of metastasis. *Nat Rev Cancer* 9:239–252.
54. Evans CJ, et al. (2009) G-TRACE: Rapid Gal4-based cell lineage analysis in Drosophila. *Nat Methods* 6:603–605.
55. Bergmann A, Agapite J, McCall K, Steller H (1998) The Drosophila gene hid is a direct molecular target of Ras-dependent survival signaling. *Cell* 95:331–341.
56. Doggett K, Grusche FA, Richardson HE, Brumby AM (2011) Loss of the Drosophila cell polarity regulator Scribbled promotes epithelial tissue overgrowth and cooperation with oncogenic Ras-Raf through impaired Hippo pathway signaling. *BMC Dev Biol* 11: 57.
57. Zhang Y, You J, Ren W, Lin X (2013) Drosophila glypicans Dally and Dally-like are essential regulators for JAK/STAT signaling and Unpaired distribution in eye development. *Dev Biol* 375:23–32.
58. Martin-Blanco E, et al. (1998) puckered encodes a phosphatase that mediates a feedback loop regulating JNK activity during dorsal closure in Drosophila. *Genes Dev* 12:557–570.
59. Yagi R, Mayer F, Basler K (2010) Refined LexA transactivators and their use in combination with the Drosophila Gal4 system. *Proc Natl Acad Sci USA* 107:16166–16171.
60. Jiang H, Grenley MO, Bravo MJ, Blumhagen RZ, Edgar BA (2011) EGFR/Ras/MAPK signaling mediates adult midgut epithelial homeostasis and regeneration in Drosophila. *Cell Stem Cell* 8:84–95.
61. Leptin M (1991) twist and snail as positive and negative regulators during Drosophila mesoderm development. *Genes Dev* 5:1568–1576.
62. Ursprung H (1967) *In Vivo Culture of Drosophila Imaginal Discs* (T.Y. Crowell, New York), pp 485–492.